Propagation of solitary waves and undular bores over variable topography

by

Wei King Tiong

A Doctoral Thesis

Submitted in partial fulfilment of the requirements for the award of
Doctor of Philosophy of Loughborough University

October 2012

Abstract

Description of the interaction of a shallow-water wave with variable topography is a classical and fundamental problem of fluid mechanics. The behaviour of linear waves and isolated solitary waves propagating over an uneven bottom is well understood. Much less is known about the propagation of nonlinear wavetrains over obstacles. For shallow-water waves, the nonlinear wavetrains are often generated in the form of undular bores, connecting two different basic flow states and having the structure of a slowly modulated periodic wave with a solitary wave at the leading edge.

In this thesis, we examine the propagation of shallow-water undular bores over a nonuniform environment, and also subject to the effect of weak dissipation (turbulent bottom friction or volume viscosity). The study is performed in the framework of the variable-coefficient Korteweg-de Vries (vKdV) and variable-coefficient perturbed Korteweg-de Vries (vpKdV) equations. The behaviour of undular bores is compared with that of isolated solitary waves subject to the same external effects. We show that the interaction of the undular bore with variable topography can result in a number of adiabatic and non-adiabatic effects observed in different combinations depending on the specific bottom profile. The effects include: (i) the generation of a sequence of isolated solitons – an expanding large-amplitude modulated solitary wavetrain propagating ahead of the bore; (ii) the generation of an extended weakly nonlinear wavetrain behind the bore; (iii) the formation of a transient multi-phase region inside the bore; (iv) a nonlocal variation of the leading solitary wave amplitude; (v) the change of the characteristics wavelength in the bore; and (vi) occurrence of a "modulation phase shift" due to the interaction. The non-adiabatic effects (i) – (iii) are new and to the best of our knowledge, have not been reported in previous studies. We use a combination of nonlinear modulation theory and numerical simulations to analyse these effects. In our work, we consider four prototypical variable topography profiles in our study: a slowly decreasing depth, a slowly increasing depth , a smooth bump and a smooth hole, which leads to qualitatively different undular bore deformation depending on the geometry of the slope. Also, we consider (numerically) a rapidly varying depth topography, a counterpart of the "soliton fission" configuration. We show that all the effects mentioned above can also be observed when the undular bore propagates over a rapidly changing bottom .

We then consider the modification of the variable topography effects on the undular bore by considering weak dissipation due to turbulent bottom friction or volume viscosity. The dissipation is modelled by appropriate right-hand side terms in the vKdV equation.

The developed methods and results of our work can be extended to other problems involving the propagation of undular bores (dispersive shock waves in general) in variable media.

To my mother and father with deep respect and love.

The results of the thesis are partially summarised in two research papers:

G. A. El, R. H. J. Grimshaw and W. K. Tiong (2012) Transformation of a shoaling undular bore. *Journal of Fluid Mechanics*, Available on CJO doi:10.1017/jfm.2012.338

G.A. El, R.H.J. Grimshaw and W.K.Tiong, Propagation of dispersive shock waves in weakly inhomogeneous media – in progress.

Abbreviations

KdV – Korteweg-de Vries

vKdV – variable-coefficient Korteweg-de Vries

pKdV – perturbed Korteweg-de Vries

vpKdV – variable-coefficient perturbed Korteweg-de Vries

KdVB – Korteweg-de Vries-Burgers

vKdVB – variable-coefficient Korteweg-de Vries-Burgers

DSW – Dispersive shock waves

MOL – Method of Lines

ODEs – Ordinary differential equations

PDEs – Partial differential equations

Acknowledgement

Contents

Chapter 1

Introduction

The "great wave of translation" or solitary wave was first observed by John Scott Russell while he was riding on horseback along the Edinburgh-Glasgow canal. He observed that a smooth, bell shaped crest about half a meter high emerged at the front of a boat when the boat stopped suddenly after been hit by an underwater obstruction. He reported his observations to the British Association in his "Report on Waves" (Russell, 1845) and did extensive laboratory experiments to study this phenomenon more carefully (Miles, 1980, 1981).

The first mathematical theory to explain the observation by Russell was done by Boussinesq (1872) followed by Lord Rayleigh (1876). Later, Korteweg & de Vries (1895) derived a nonlinear evolution equation governing long one dimensional, small amplitude, surface gravity waves propagating in a shallow water channel of constant depth and found solitary wave solutions (Miles, 1980, 1981). This equation is now commonly known as the Korteweg-de Vries (KdV) equation although Boussinesq (1877) appeared to derive it first.

When Zabusky & Kruskal (1965) integrated the KdV equation numerically while they were investigating the Fermi, Pasta and Ulam (FPU) problem, they discovered that these solitary wave solutions have a remarkable property of retaining their shapes and speeds after the pairwise interaction, i.e. the interaction of the KdV solitary wave is elastic with some additional spatial phase shift. Therefore, they coined the term 'soliton' which is today used as a synonym for solitary wave in integrable model.

In real world problems, nonlinear waves are often propagating through a nonuniform environment, e.g. shallow water waves approaching a beach. The first notable experimental work on shoaling and breaking of solitary waves was done by Ippen & Kulin (1954) and numerical studies were performed by Peregrine (1967) and Madsen & Mei (1969). To derive the appropriate mathematical model for this type of problem, one has to take into account the effect of the varying depth. For surface water waves, the appropriate model was derived independently by Kakutani (1971) and Johnson (1973b) in the framework of the variable-coefficient KdV equation. The detailed analysis of the behaviour of solitary wave over variable topography was carried out by Grimshaw (1970, 1971); Johnson (1973b,a). Now, the theory behind the solitary waves propagation in uniform and nonuniform environments is well-developed and the effects of variable topography on the free-surface and

internal solitary waves evolution are well-understood (Grimshaw, 2004, 2005, 2007*a*).

However, the analogous theory for nonlinear wavetrain propagation in a variable environment is not so well-developed. In the context of water waves, nonlinear wavetrains are often generated in the form of undular bores, which connect two different basic flow states and exhibit solitary waves at one of the edges. Undular bores can be generated as the result of dispersive resolution of a shock or an initial discontinuity in fluid depth/ velocity (Smyth & Holloway, 1988; El *et al.*, 2006; Esler & Pearce, 2011). Another way to form an undular bore is through the resonant interaction of a fluid flow with variable topography (Grimshaw & Smyth, 1986; El *et al.*, 2009). *So, the principal aim of the thesis is to study the effects of variable topography and/ or bottom friction on the propagation of shallow-water undular bores.*

In a weakly nonlinear and weakly dispersive medium, a shallow-water undular bore is described by a slowly modulated periodic solution of the constant-coefficient KdV equation with solitary wave at the leading edge and linear sinusoidal wave at the trailing edge. The corresponding asymptotic solution was obtained and studied thoroughly by Gurevich & Pitaevskii (1973, 1974) using the Whitham modulation theory. It was shown in Khruslov (1976) (see also Claeys & Grava, 2010) that at large time, the leading solitary wave of undular bores represents asymptotically a genuine isolated KdV soliton, not constrained by the interaction with the remainder of the bore. However, in a variable environment, the evolution of the leading solitary wave in the undular bore could be strongly affected by the interaction with the wavetrain behind it. One of the objectives of this thesis is to study the behaviour of the leading solitary wave of undular bores when propagating over variable topography and to understand how it differs from the evolution of an isolated solitary wave propagating in the same environment. This is also relevant to many physical problems involving the propagation of dispersive shock waves/ undular bores in weakly inhomogeneous media, e.g. the modelling of near-shore tsunami propagation (Grue *et al.*, 2008; Madsen *et al.*, 2008) or the description of dispersive shock waves in expanding Bose-Einstein condensates (Hoefer *et al.*, 2006).

The structure of the thesis is as follows: first, in Chapter 2, we introduce the Whitham modulation theory, which will be our principal tool throughout the entire work. We describe briefly how the modulation equations for the KdV equation are derived by averaging the KdV conservation laws as originally proposed by Whitham (1965). In the same chapter, we also present a modern approach to derive the modulation equations based on the associated spectral problem. This approach was originally proposed by Flaschka *et al.* (1980) for multi-phase averaging of the KdV equation and then adapted by Kamchatnov (1997) for

single-phase averaging of integrable equation belonging to the AKNS hierarchy. We employ Kamchatnov's method to recover the Riemann invariant form of the KdV modulation system, originally developed by Whitham (1965). We then continue by discussing the classical Gurevich & Pitaevskii (1973, 1974) modulation solution describing the evolution of a dispersive shock wave (undular bore). This asymptotic result will be used extensively in our work.

Chapter 3 discusses the propagation of solitary waves over varying depth regions. We start, following Grimshaw (2007a), with a brief outline of the derivation of the governing equation, which is the variable-coefficient KdV equation. We then present a detailed analysis on how solitary waves behave when they propagate over various types of varying topography, e.g. rapidly changing bottoms and slowly varying slopes. The results are important for our work later.

The main results of the thesis are presented in Chapters 4 and 5. In Chapter 4, we consider the propagation of undular bores over variable topography using the mathematical model outlined in Chapter 3. However, now we shall consider our initial condition for the governing equation to be in the form of a smooth step, which leads to the generation of an undular bore. The initial step is placed far before the slope so that the generated undular bore is fully developed when it enters the sloping region. Using the modulation theory and detailed numerical simulations, we study the adiabatic and non-adiabatic deformations of the undular bore when propagating over slowly varying topography. We consider four prototypical configurations for variable topography region: slowly decreasing depth, slowly increasing depth, a smooth bump and a smooth hole. Also, we consider numerically the case when the undular bore propagates over a region of rapidly varying depth, an undular bore counterpart of the "soliton fissioning" setting. We are particularly interested in looking at how the behaviour of the leading solitary wave of the undular bore differs from that of an isolated single solitary wave described in Chapter 3.

In Chapter 5, we extend the problem considered in Chapter 4 by including the effects of weak dissipation (bottom friction or volume viscosity), which are modelled by the additional perturbation term in the variable-coefficient KdV equation. Here, we consider three different types of weak dissipation: (a) Chezy bottom friction, (b) linear bottom friction and (c) Burgers friction (volume viscosity), and examine the impact of these types of dissipation on the evolution of solitary waves and undular bores over the depth varying regions. Most of the results in this chapter are numerical, although we also use the analytical insights from the Chapter 4 to interpret the modifications of the wave structure due to the dissipative effects.

The final chapter provides the summary and reviews the main conclusions of the thesis. Here, we also give some insights on how our work can be extended for a future study.

The detailed description of the numerical method used throughout the entire work is included in the Appendix.

Chapter 2

Whitham modulation theory and undular bores

In this chapter, we will look at the Whitham modulation theory, which is the main analytical tool used in the thesis. We start by finding the periodic solution of the KdV equation. Next, we give a brief outline of the general procedure of obtaining the modulation equations as suggested by Whitham (1965). After that, we present an alternative approach for deriving the KdV-Whitham equations developed by Kamchatnov (1997, 2000). Then, we give a brief overview on dispersive shock waves, their occurrences in the natural world and the dispersive shock wave solution of the KdV equation as studied by Gurevich & Pitaevskii (1973, 1974). At the end of this chapter, we discuss briefly about the perturbed modulation equations as obtained by Kamchatnov (2004) when there is a small perturbation term in the KdV equation. Also, we show the two qualitatively different types of behaviour of the leading solitary wave of the undular bore as the result of the external perturbation in the KdV equation (El et al., 2007).

2.1   Periodic solution of the KdV equation

The KdV equation in the canonical form is

$$u_t + 6uu_x + u_{xxx} = 0. \tag{2.1}$$

To find the periodic solution, we seek the solution in the form of $u = u(\xi)$ where $\xi = x - Vt$ and V is the phase velocity. Hence (2.1) reduces to

$$u_{\xi\xi\xi} = Vu_\xi - 6uu_\xi. \tag{2.2}$$

After integrating twice, we obtain

$$\left.\begin{aligned}
\frac{1}{2}u_\xi^2 &= -A + Bu + \frac{1}{2}Vu^2 - u^3 \\
&\equiv f(u) = -(u - b_1)(u - b_2)(u - b_3),
\end{aligned}\right\} \tag{2.3}$$

where A and B are integration constants.

Equation (2.3) has real bounded solutions if $f(u)$ has three real roots denoted by $b_1 > b_2 > b_3$. The real oscillating solution corresponds to the motion of u between $b_2 \le u \le b_1$,

where $f(u) \geq 0$. Thus, the three constants, A, B and V are related to the three roots by

$$A = -b_1 b_2 b_3, \qquad -B = b_1 b_2 + b_2 b_3 + b_1 b_3, \qquad V = 2(b_1 + b_2 + b_3). \qquad (2.4)$$

We can rewrite equation (2.3) as

$$\frac{du}{d\xi} = \pm\sqrt{2(b_1 - u)(u - b_2)(u - b_3)}, \qquad (2.5)$$

so that the periodic solution of the KdV equation is given implicitly by

$$\sqrt{2}\xi = \int_u^{b_1} \frac{du'}{\sqrt{(b_1 - u')(u' - b_2)(u' - b_3)}}. \qquad (2.6)$$

By introducing new variables

$$u' = b_1 - (b_1 - b_2)\sin^2 \phi', \qquad \text{and} \qquad \sin\phi' = \sqrt{\frac{b_1 - u'}{b_1 - b_2}}, \qquad (2.7)$$

equation (2.6) becomes

$$\begin{aligned} \sqrt{2}\xi &= \frac{2}{\sqrt{b_1 - b_3}} \int_0^\phi \frac{d\phi'}{\sqrt{1 - m\sin^2 \phi'}}, \\ &= \frac{2}{\sqrt{b_1 - b_3}} F(\phi, m), \end{aligned} \qquad (2.8)$$

where

$$m = \frac{b_1 - b_2}{b_1 - b_3}, \qquad 0 \leq m \leq 1, \qquad (2.9)$$

is the modulus, and $F(\phi, m)$ is the incomplete elliptic integral of the first kind. As the result of these transformations, the periodic solution $u(\xi)$ of the KdV equation is given by

$$u(x, t) = b_2 + (b_1 - b_2)\text{cn}^2(\sqrt{2(b_1 - b_3)}(x - Vt), m), \qquad (2.10)$$

where $\text{cn}(\xi, m)$ is the Jacobi elliptic sine function. Equation (2.10) is known as cnoidal wave solution. The wavelength of the cnoidal wave (2.10) is given by

$$\begin{aligned} L = \int_0^L d\xi &= 2\int_{b_2}^{b_1} \frac{du'}{\sqrt{2(b_1 - u')(u' - b_2)(u' - b_3)}}, \\ &= \frac{2\sqrt{2}K(m)}{\sqrt{b_1 - b_3}}, \end{aligned} \qquad (2.11)$$

where $K(m)$ is the complete elliptic integral of the first kind. The waveform specified by equation (2.10) depends on the value of the modulus m (see Figure 2.1). When $m \to 0$ (i.e. $b_1 \to b_2$), equation (2.10) becomes a small-amplitude harmonic wave solution

$$u(x, t) = a\cos^2\left[2\sqrt{\frac{a}{m}}(x - Vt)\right] + b_2, \qquad (2.12)$$

propagating against the background b_2. On the other hand, when $m \to 1$ or $b_2 \to b_3$, we obtain a solitary wave solution

$$u(x, t) = 2a\,\text{sech}^2\left[\sqrt{a}(x - Vt)\right] + b_3, \qquad (2.13)$$

propagating on the background b_3.
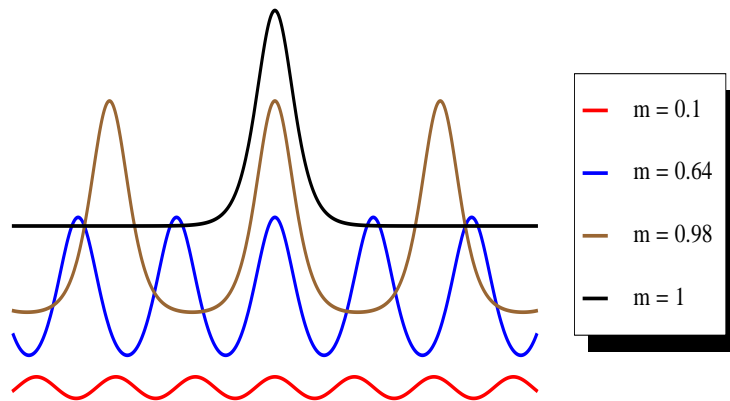
Figure 2.1: Periodic solution of the KdV equation with different values of m

2.2 Whitham method

If one allows the parameters b_1, b_2 and b_3 of the periodic solution of the KdV equation (2.1) to be functions of x and t on a large spatio-temporal scale, then the periodic solution (2.10) will be slowly modulated, i.e. these parameters change little in one wavelength. As a result, we have encountered the problem of deriving the equations describing the slow evolution of these parameters. Formally, we would write $b_i = b_i(X, T)$ where $X = \varepsilon x$, $T = \varepsilon t$ and $\varepsilon \ll 1$. However, we are not going to introduce the small parameter explicitly. Instead, we shall assume that x and t vary on a large scale in the modulation equations. These modulation equations are commonly known as the Whitham modulation equations. They can be obtained by using multiple-scale perturbation method, which involves some extensive calculations.

A more convenient formal approach was proposed by Whitham (1965) (see also Whitham, 1974; Kamchatnov, 2000). Whitham proposed simply to average conservation laws over the periodic family rather than derive the modulation equations via multiple-scale expansions. Later, the Whitham prescription was rigorously justified using formal perturbation theory (Luke, 1966; Dobrokhotov & Maslov, 1982) and also the inverse scattering transform (Lax *et al.*, 1994).

Generally, let us suppose that we have the evolution equation in the form

$$\Phi(u, u_t, u_x, u_{tt}, u_{tx}, u_{xx}, \ldots) = 0, \tag{2.14}$$

and we want to seek the periodic solution in the form of

$$u = u(\xi), \qquad \xi = x - Vt.$$

Assume that (2.14) can be reduced into

$$u_\xi^2 = F(u, V, A_i), \tag{2.15}$$

where $A_i = A_i(\mathbf{b}), \mathbf{b} = b_i$ are integration constants obtained when reducing (2.14) into (2.15). Let b_1 and b_2 denote the zeros of $F(u)$ where $F(u) \geq 0$. The periodic solution corresponds to oscillations of u between b_2 and b_1. The wavelength is given by

$$L = 2 \int_{b_2}^{b_1} \frac{du}{\sqrt{F(u; V, A_i)}}.$$

Suppose that we have a set of conservation laws for (2.14),

$$\frac{\partial P_i}{\partial t} + \frac{\partial Q_i}{\partial x} = 0, \qquad i = 1, 2, 3, \dots, N, \tag{2.16}$$

which, in general, can be deduced from the evolution equations. Equation (2.16) is then averaged over a period of the travelling wave solution according to the averaging formula

$$\langle F \rangle = \frac{1}{L} \int_0^L F \, d\xi,$$

so that the modulation equations are

$$\frac{\partial}{\partial t} \langle P_i \rangle + \frac{\partial}{\partial x} \langle Q_i \rangle = 0, \qquad i = 1, 2, 3, \dots, N. \tag{2.17}$$

Note that x and t in equation (2.17) vary on a much larger scale than in equation (2.16). If $\det[\partial \langle P_i \rangle / \partial b_j] \neq 0$, then equations (2.17) represent a hydrodynamic type system for $b_i(x, t)$. These equations can then be handled by the using general theory of hyperbolic quasi-linear systems and the theory of characteristics in particular.

For the KdV equation (2.1), we need to average any three independent conservation laws from the infinite set of conservations laws (Miura *et al.*, 1968). The first two conservation laws are (Drazin & Johnson, 1989)

$$u_t + (3u^2 + u_{xx})_x = 0,$$
$$\left(\frac{1}{2}u^2\right)_t + \left(2u^3 + uu_{xx} - \frac{1}{2}u_x^2\right)_x = 0.$$

For the third conservation law, the 'conservation of waves' equation, $k_t + \omega_x$, can be used to obtain the modulation equations. Whitham (1965) showed that by introducing symmetric combinations

$$\lambda_1 = -\frac{b_1 + b_2}{2}, \qquad \lambda_2 = -\frac{b_1 + b_3}{2} \qquad \text{and} \qquad \lambda_3 = -\frac{b_2 + b_3}{2}, \tag{2.18}$$

the modulation equations reduce to the diagonal form

$$\frac{\partial \lambda_i}{\partial t} + v_i \frac{\partial \lambda_i}{\partial x} = 0, \tag{2.19}$$

where

$$
\begin{aligned}
v_i &= -2(\lambda_1 + \lambda_2 + \lambda_3) + \frac{2L}{\partial L/\partial \lambda_i}, \\
&= \left(1 - \frac{L}{\partial_i L}\partial_i\right)V, \qquad \partial_i \equiv \frac{\partial}{\partial \lambda_i}, \qquad i = 1,2,3.
\end{aligned}
$$

λ_i are known as Riemann invariants and v_i are characteristics velocities, which can be expressed explicitly as

$$
\begin{aligned}
v_1 &= -2(\lambda_1 + \lambda_2 + \lambda_3) + \frac{4(\lambda_3 - \lambda_1)(1-m)K(m)}{E(m)}, \\
v_2 &= -2(\lambda_1 + \lambda_2 + \lambda_3) + \frac{4(\lambda_3 - \lambda_2)(1-m)K(m)}{E(m) - (1-m)K(m)}, \\
v_3 &= -2(\lambda_1 + \lambda_2 + \lambda_3) + \frac{4(\lambda_3 - \lambda_2)K(m)}{E(m) - K(m)},
\end{aligned}
$$

where $E(m)$ and $K(m)$ are the complete integrals of the first and second kind respectively. The modulus m is given by

$$
m = \frac{\lambda_3 - \lambda_2}{\lambda_3 - \lambda_1}.
$$

Generally, the Whitham method can be applied to any nonlinear wave equations, which has periodic traveling wave solutions, e.g. nonlinear Schrödinger equation (Kamchatnov *et al.*, 2002), Kaup-Boussinesq equation (El *et al.*, 2001, 2005) and Su-Gardner equation (El *et al.*, 2006). However, the Riemann invariant form can be obtained only in exceptional cases when the original equation is completely integrable.

2.3 Derivation of the Whitham equations for the KdV equation via spectral approach

The transformation of the KdV modulation system to the Riemann invariant form involves rather complicated and ingenious algebra (see Whitham, 1965; Kamchatnov, 2000). A simpler approach to derive Whitham modulation equations directly in Riemann invariants was proposed by Kamchatnov (1997) (see also Kamchatnov, 2000). His general method applies to the equations belonging to the AKNS hierarchy and makes essential use of the associated spectral problem. We shall use the Kamchatnov's method to recover the Riemann invariant form (2.19) of the KdV-Whitham equation.

The integrability of the equations of the AKNS hierarchy is based on the possibility of presenting the evolution equations as compatibility conditions of two linear systems with

2.3. DERIVATION OF THE WHITHAM EQUATIONS FOR THE KDV EQUATION VIA SPECTRAL APPROACH

spectral parameter. The 2×2 matrix form of the linear problem equivalent to the Lax pair is given by

$$\Psi_x = \mathbb{U}\Psi, \qquad \Psi_t = \mathbb{V}\Psi, \tag{2.20}$$

where

$$\Psi = \begin{pmatrix} \psi_1 \\ \psi_2 \end{pmatrix}, \qquad \mathbb{U} = \begin{pmatrix} F & G \\ H & -F \end{pmatrix}, \qquad \text{and} \qquad \mathbb{V} = \begin{pmatrix} A & B \\ C & -A \end{pmatrix}.$$

The matrix elements depend both on the field variable $u(x,t)$ of the equations under consideration and on the spectral parameter λ. The compatibility condition $\Psi_{xt} = \Psi_{tx}$ of the systems (2.20) yields at once the evolution equations in general form

$$\begin{aligned} F_t - A_x + CG - BH &= 0, \\ G_t - B_x + 2(BF - AG) &= 0, \\ H_t - C_x + 2(AH - CF) &= 0. \end{aligned}$$

Another common form of linear equations associated with nonlinear integrable equations can be written as

$$\psi_{xx} = \mathcal{A}\psi, \tag{2.21}$$
$$\psi_t = \frac{1}{2}\mathcal{B}_x\psi + \mathcal{B}\psi_x. \tag{2.22}$$

The coefficients $\mathcal{A}$ and $\mathcal{B}$ depend on the field variables and the spectral parameter λ. By applying the compatibility condition, $(\psi_{xx})_t = (\psi_t)_{xx}$ on both equations (2.21) and (2.22), we obtain

$$\mathcal{A}_t - 2\mathcal{B}_x\mathcal{A} - \mathcal{B}\mathcal{A}_x + \frac{1}{2}\mathcal{B}_{xxx} = 0. \tag{2.23}$$

We take two basis solutions ψ^+ and ψ^- of (2.21) and construct the so-called 'squared basis function' from them

$$g = \psi^+\psi^-.$$

It can be shown that it satisfies the equation

$$g_{xxx} - 2\mathcal{A}_x g - 4\mathcal{A}g_x = 0.$$

Multiplying the above equation by $g/2$ and integrating once yields

$$\frac{1}{2}gg_{xx} - \frac{1}{4}g_x^2 - \mathcal{A}g^2 = P(\lambda). \tag{2.24}$$

The dependence of g on time t is obtained from the equation

$$g_t = \mathcal{B}g_x - \mathcal{B}_x g, \tag{2.25}$$

which follows from (2.22)

For the KdV equation (2.1), there is only one field variable $u(x,t)$ and

$$\mathcal{A} = -(u + \lambda), \qquad \mathcal{B} = 4\lambda - 2u. \tag{2.26}$$

By substituting (2.26) into (2.23), we will have the KdV equation (2.1). Also, equation (2.24) becomes

$$\frac{1}{2}gg_{xx} - \frac{1}{4}g_x^2 + (u + \lambda)g^2 = P(\lambda), \tag{2.27}$$

where the integration constant denoted by $P(\lambda)$ can depend on spectral parameter λ. From the finite-gap integration theory (see Novikov *et al.*, 1984), it is known that periodic solutions are distinguished by the condition that $P(\lambda)$ be a polynomial in λ. For the KdV equation (2.1), it is a polynomial of third degree. Thus in our case, we take

$$\begin{aligned} P(\lambda) &= (\lambda - \lambda_1)(\lambda - \lambda_2)(\lambda - \lambda_3), \\ &= \lambda^3 - s_1\lambda^2 + s_2\lambda - s_3, \end{aligned}$$

where

$$\left.\begin{aligned} s_1 &= \lambda_1 + \lambda_2 + \lambda_3, \\ s_2 &= \lambda_1\lambda_2 + \lambda_1\lambda_3 + \lambda_2\lambda_3, \\ s_3 &= \lambda_1\lambda_2\lambda_3. \end{aligned}\right\} \tag{2.28}$$

The right-hand side of equation (2.27) contains only λ, so we have to look for g in the form of a polynomial in λ. The simplest nontrivial solution corresponding to the first degree polynomial is

$$g = \lambda - \mu(x,t), \tag{2.29}$$

where $\mu(x,t)$ is an unknown variable. On substitution (2.29) into (2.27), we obtain

$$-\frac{1}{2}(\lambda - \mu)\mu_{xx} - \frac{1}{4}\mu_x^2 + (u + \lambda)(\lambda - \mu)^2 = \lambda^3 - s_1\lambda^2 + s_2\lambda - s_3. \tag{2.30}$$

By equating the coefficient for λ^2, we have

$$\begin{aligned} u(x,t) &= 2\mu - s_1, \\ &= 2\mu - (\lambda_1 + \lambda_2 + \lambda_3). \end{aligned} \tag{2.31}$$

Next, after substitution of (2.26) and (2.29) into (2.25), we obtain

$$\mu_t = (4\lambda - 2u)\mu_x + 2(\mu - \lambda)u_x. \tag{2.32}$$

If we put the spectral parameter $\lambda = \mu$, equations (2.30) and (2.32) can be rewritten as

$$\mu_x = 2\sqrt{-P(\mu)}, \tag{2.33}$$

$$\mu_t = (4\mu - 2u)\mu_x = 2s_1\mu_x. \tag{2.34}$$

11

2.3. DERIVATION OF THE WHITHAM EQUATIONS FOR THE KDV EQUATION VIA SPECTRAL APPROACH

From (2.34), μ depends on x and t only in the combination $\xi = x + 2s_1 t$, that is the phase velocity V is connected with the zeros of the polynomial $P(\lambda)$ by the relation

$$\begin{aligned} V &= -2s_1, \\ &= -2(\lambda_1 + \lambda_2 + \lambda_3). \end{aligned} \tag{2.35}$$

From (2.33), we have the cnoidal wave solution of the KdV equation directly as a function of $\lambda_1, \lambda_2, \lambda_3$

$$u(\xi) = \lambda_3 - \lambda_1 - \lambda_2 - 2(\lambda_3 - \lambda_2)\operatorname{sn}^2(\sqrt{\lambda_3 - \lambda_1}\xi, m). \tag{2.36}$$

Both equations (2.35) and (2.36) coincide with (2.4) and (2.10) respectively if one introduces Riemann invariants $\lambda_1 \le \lambda_2 \le \lambda_3$ through the relations in (2.18).

Since the parameters defining the periodic solution are roots of the polynomial $P(\lambda)$, we can obtain the Whitham equations directly in the diagonal Riemann form. By dividing both sides by g^2, (2.25) can be rewritten as

$$\left(\frac{1}{g}\right)_t = \left(\frac{\mathcal{B}}{g}\right)_x.$$

This is the generating function for conservation laws. By making a change $g \to g/\sqrt{P(\lambda)}$, the above equation becomes

$$\frac{\partial}{\partial t}\left(\sqrt{P(\lambda)} \cdot \frac{1}{g}\right) = \frac{\partial}{\partial x}\left(\sqrt{P(\lambda)} \cdot \frac{2u - 4\lambda}{g}\right).$$

With the help of (2.29) and (2.31), we have

$$\frac{\partial}{\partial t}\left(\sqrt{P(\lambda)} \cdot \frac{1}{\lambda - \mu}\right) + \frac{\partial}{\partial x}\left[\sqrt{P(\lambda)} \cdot \left(-4 - \frac{2s_1}{\lambda - \mu}\right)\right] = 0.$$

On substitution of (2.30) and averaging over a period, the above equation becomes

$$\begin{aligned} &\frac{\partial}{\partial t}\left(\sqrt{P(\lambda)} \cdot \frac{1}{L}\oint \frac{d\mu}{2(\lambda - \mu)\sqrt{-P(\mu)}}\right) \\ &+ \frac{\partial}{\partial x}\left[\sqrt{P(\lambda)}\left(-4 - 2s_1 \cdot \frac{1}{L}\oint \frac{d\mu}{2(\lambda - \mu)\sqrt{-P(\mu)}}\right)\right] = 0, \end{aligned} \tag{2.37}$$

where the wavelength, L is equal to

$$L = \oint \frac{d\mu}{2\sqrt{-P(\mu)}}, \tag{2.38}$$

provided the integration is taken over the cycle around the gap $\lambda_2 \le \mu \le \lambda_3$. In (2.37), the zeros λ_i of the polynomial $P(\lambda)$ are slow functions of x and t, which have to be differentiated. Thus, we obtain terms with

$$\frac{1}{\sqrt{\lambda - \lambda_i}}\frac{\partial \lambda_i}{\partial t} \qquad \text{and} \qquad \frac{1}{\sqrt{\lambda - \lambda_i}}\frac{\partial \lambda_i}{\partial x},$$

which are singular as $\lambda \to \lambda_i$. As a result, for the equation (2.37) to be satisfied, the slow evolution of λ_i must obey the equations

$$\frac{1}{L} \oint \frac{d\mu}{2(\lambda_i - \mu)\sqrt{-P(\mu)}} \cdot \frac{\partial \lambda_i}{\partial t}$$
$$+ \left(-4 - 2s_1 \frac{1}{L} \oint \frac{d\mu}{2(\lambda_i - \mu)\sqrt{-P(\mu)}} \right) \cdot \frac{\partial \lambda_i}{\partial x} = 0. \tag{2.39}$$

From (2.38), we have

$$\frac{1}{2L} \oint \frac{d\mu}{(\lambda_i - \mu)\sqrt{-P(\mu)}} = -\frac{2}{L} \frac{\partial L}{\partial \lambda_i}.$$

Consequently, (2.39) becomes

$$\frac{\partial \lambda_i}{\partial t} + v_i \frac{\partial \lambda_i}{\partial x} = 0, \tag{2.40}$$

where

$$\left. \begin{aligned}
v_1 &= -2(\lambda_1 + \lambda_2 + \lambda_3) + \frac{4(\lambda_3 - \lambda_1)(1 - m)K(m)}{E(m)}, \\
v_2 &= -2(\lambda_1 + \lambda_2 + \lambda_3) + \frac{4(\lambda_3 - \lambda_2)(1 - m)K(m)}{E(m) - (1 - m)K(m)}, \\
v_3 &= -2(\lambda_1 + \lambda_2 + \lambda_3) + \frac{4(\lambda_3 - \lambda_2)K(m)}{E(m) - K(m)}.
\end{aligned} \right\} \tag{2.41}$$

To study the Whitham equations when $m \to 0$ and $m \to 1$, we need asymptotic formulae for the complete elliptic integrals (Gradshteyn & Ryzhik, 2007):

$$\begin{aligned}
m \ll 1 : K(m) &\cong \frac{\pi}{2}\left(1 + \frac{1}{4}m + \frac{9}{64}m^2 + \cdots \right), \\
E(m) &\cong \frac{\pi}{2}\left(1 - \frac{1}{4}m - \frac{3}{64}m^2 + \cdots \right), \\
(1 - m) \ll 1 : K(m) &\cong \frac{1}{2}\ln\frac{16}{1 - m}, \\
E(m) &\cong 1 + \frac{1}{4}(1 - m)\left(\ln\frac{16}{1 - m} - 1 \right).
\end{aligned}$$

When $m \to 0$ or $\lambda_2 = \lambda_3$, we have $v_1 = -6\lambda_1$ and $v_2 = v_3 = 6\lambda_1 - 12\lambda_3$. Thus the Whitham equations become

$$\left. \begin{aligned}
\frac{\partial \lambda_1}{\partial t} - 6\lambda_1 \frac{\partial \lambda_1}{\partial x} &= 0, \\
\frac{\partial \lambda_3}{\partial t} + 6(\lambda_1 - 12\lambda_3)\frac{\partial \lambda_3}{\partial x} &= 0.
\end{aligned} \right\} \tag{2.42}$$

On the other hand, we have $v_2 = v_1 = -(4\lambda_1 + 2\lambda_3)$ and $v_3 = -6\lambda_3$, when $m \to 1$ or $\lambda_2 = \lambda_1$. Hence the Whitham system reduces to

$$\left. \begin{aligned}
\frac{\partial \lambda_1}{\partial t} - (4\lambda_1 + 2\lambda_3)\frac{\partial \lambda_1}{\partial x} &= 0, \\
\frac{\partial \lambda_3}{\partial t} - 6\lambda_3 \frac{\partial \lambda_3}{\partial x} &= 0.
\end{aligned} \right\} \tag{2.43}$$

13
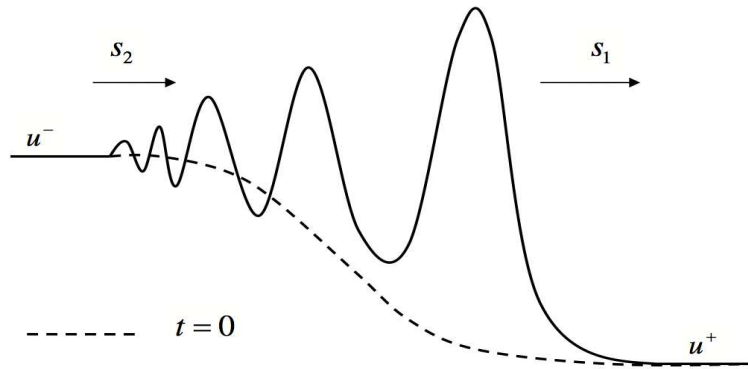
Figure 2.2: Structure of an undular bore

One can see that in both limits, one of the Whitham equations reduces to the Hopf equation which is also dispersionless limit of the KdV equation (2.1) and the remaining two merge into one Riemann invariant along a double characteristic.

2.4 Dispersive shock waves/ Undular bores

Dispersive shock waves (DSW) have been observed in many applications, e.g. plasma physics (Taylor *et al.*, 1970), nonlinear optics (Wan *et al.*, 2007), Bose-Einstein condensates (Hoefer *et al.*, 2006), morning glory atmospheric phenomena (Reeder *et al.*, 1995; Porter & Smyth, 2002), etc. In the context of water waves, they are commonly known as undular bores. An undular bore represents a slowly modulated nonlinear periodic wavetrain with a solitary wave at the leading edge and a linear wave packet at the trailing edge (see Figure 2.2). The leading solitary wave travels with velocity, s_1, while the velocity for the trailing edge is s_2. In general, $s_1 \neq s_2$. As a result, the structure of the undular bore will expand as time increases.

Examples of shallow-water undular bores include Severn bore in England (see Figure 2.3) and Dodgorne bore in France (see Figure 2.4). Also, there are some observations of undular bores made in certain tsunamis caused by earthquakes in deep ocean (see Figure 2.5). This may happen when the fronts of nonlinear long waves become very steep and turn into undular bores when propagating into shallow water, as was observed in the 1983 Nihonkai-Chubu tsunami (Shuto, 1985) and the 2004 Indian Ocean tsunami (Grue *et al.*, 2008; Madsen, 2010). In some cases, tsunami waves ascended into several rivers in the form of undular bores, as reported in Tsuji *et al.* (1991) (see Figure 2.6). In all these cases, the undular bore propagation occurs over variable topography.

Figure 2.3: Undular bore of the Severn River in England in April 2007. Courtesy of Mark Humpage.

Figure 2.4: Undular bore of the Dordogne River in France on 27 September 2008

Figure 2.5: Undular bore of the 2004 Indian Ocean tsunami reaching the island of Koh Jum, Thailand (Copyright Anders Grawin)

Figure 2.6: An undular bore ascended along the small channel in Noshiro Port, Akita Prefercture during 1983 Japan Sea tsunami (Tsuji *et al.*, 1991).

2.4.1 Gurevich-Pitaevskii problem and the matching conditions for the Whitham equations

To study the evolution of undular bores, let us consider a smooth large-scale initial distribution $u(x,0) = u_0(X)$ where $X = \varepsilon x, \varepsilon \ll 1$ for the KdV equation (2.1). At the early stage of wave evolution, $|u_x| \sim \varepsilon, |u_{xxx}| \sim \varepsilon^3$. Thus, $|u_{xxx}| \ll |uu_x|$. So, at this stage, the dispersive effect can be ignored as the nonlinear term has dominant role. Consequently, the KdV equation (2.1) reduces to the Hopf equation

$$u_t + 6uu_x = 0. \tag{2.44}$$

The smooth evolution of the initial profile governed by the Hopf equation (2.44) leads to the wave steepening due to the effects of nonlinearity. At some point x_b at time t_b, the distribution $u(x,t)$ has a vertical tangent line, that is $u_x \to -\infty, u_{xx} \to 0$. The point (x_b, t_b) is called the wave breaking point. At this stage of wave evolution, we can no longer ignore the dispersive term in the KdV equation. Thus, the steepening wave starts to oscillate due to the dispersive effect. Thus, an undular bore forms, which occupies an expanding region $x_-(t) < x < x_+(t)$ (see Figure 2.7).

According to Gurevich & Pitaevskii (1974), the solution $u(x,t)$ in the region $x_- < x < x_+$ is asymptotically described by the modulated cnoidal wave solution (2.36), which is considered to be locally periodic. The modulation provides a gradual change of the waveform from the linear wave ($m = 0$) at the trailing edge, $x = x_-(t)$, to the solitary wave at the leading edge, $x = x_+(t)$. At $x = x_\pm$, the solution (2.36) must match with the solution of the Hopf equation (2.44), which remains valid outside the oscillating region (see Figure 2.8).

2.4.1 Gurevich-Pitaevskii problem and the matching conditions for the Whitham equations
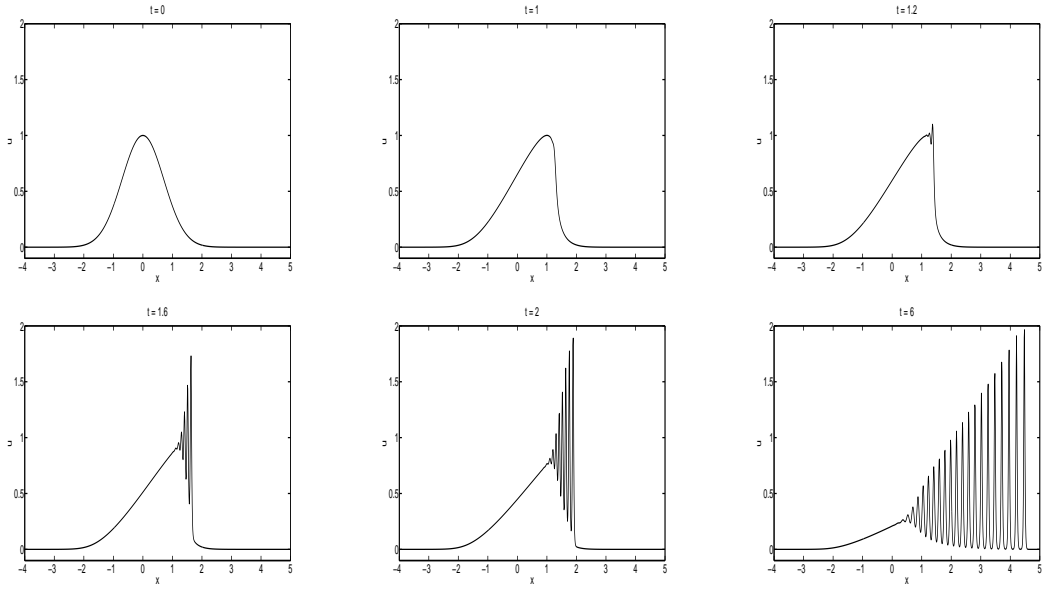
Figure 2.7: Evolution of a smooth initial condition.
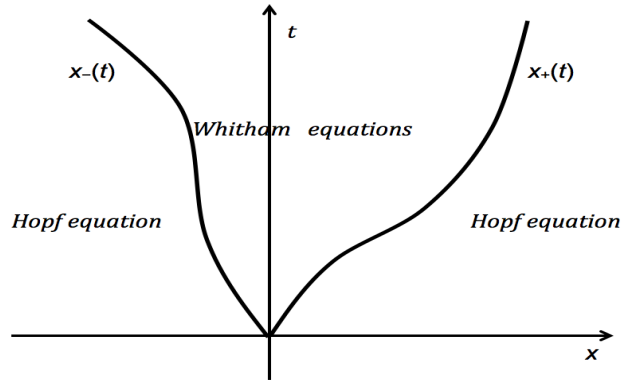
Figure 2.8: Splitting of the xt-plane in the Gurevich- Pitaevskii problem

The Whitham equations (2.40) were obtained for the "spectral" variables, λ_1, λ_2 and λ_3. Here, it is more convenient to introduce new Riemann invariants as follows:

$$r_3 = -\lambda_3, \quad r_2 = -\lambda_2, \quad r_1 = -\lambda_1, \quad r_3 \le r_2 \le r_1,$$

which will match the physical variable $u(x,t)$ at the edges $x_\pm$ of the undular bore. Therefore, the cnoidal wave solution (2.36) becomes

$$u(x,t) = r_1 + r_2 - r_3 - 2(r_2 - r_3)\text{sn}^2(\sqrt{r_1 - r_3}(x - Vt), m), \qquad (2.45)$$

where

$$V = 2(r_1 + r_2 + r_3), \qquad m = \frac{r_2 - r_3}{r_1 - r_3}.$$

The wavelength (2.38) in the new parameterisation is

$$L = \frac{2K(m)}{\sqrt{r_1 - r_3}}.$$

and the Whitham equations (2.40) assume the form

$$\frac{\partial r_i}{\partial t} + v_i \frac{\partial r_i}{\partial x} = 0, \tag{2.46}$$

where the characteristic velocities are given by

$$\left.\begin{aligned}
v_1(r_1, r_2, r_3) &= 2(r_1 + r_2 + r_3) + \frac{4(r_1 - r_3)(1 - m)K(m)}{E(m)}, \\
v_2(r_1, r_2, r_3) &= 2(r_1 + r_2 + r_3) - \frac{4(r_2 - r_3)(1 - m)K(m)}{E(m) - (1 - m)K(m)}, \\
v_3(r_1, r_2, r_3) &= 2(r_1 + r_2 + r_3) + \frac{4(r_2 - r_3)K(m)}{E(m) - K(m)}.
\end{aligned}\right\} \tag{2.47}$$

To describe the undular bore, Gurevich & Pitaevskii (1974) proposed special matching conditions for the Whitham equations

$$\begin{aligned}
\text{at the trailing edge,} \quad & x = x_- : \quad r_2 = r_3, \quad r_1 = r, \\
\text{at the leading edge,} \quad & x = x_+ : \quad r_2 = r_1, \quad r_3 = r,
\end{aligned} \tag{2.48}$$

where $r(x, t)$ satisfies the Hopf equation

$$r_t + 6rr_x = 0,$$

with the KdV initial condition $r(x, 0) = u_0(x)$. Conditions (2.48) ensure the continuous matching of the mean flow $\bar{u}$ in the undular bore region with the smooth, non-oscillating solution outside the undular bore.

2.4.2 Decay of an initial discontinuity

To illustrate the outlined theory, we consider the following initial-value problem for the KdV equation (2.1)

$$u(x, 0) = u_0(x) = \begin{cases} \Delta & : x < 0 \\ 0 & : x > 0 \end{cases}, \tag{2.49}$$

where $\Delta > 0$. Since the initial condition (2.49) and the Whitham equations (2.46) are invariant with respect to scaling transformation

$$x \to Cx, \qquad t \to Ct,$$

2.4.2 Decay of an initial discontinuity

where C is an arbitrary constant, then the solution of the Whitham equations must be self-similar, that is

$$r_i = r_i(s) \qquad \text{where} \qquad s = \frac{x}{t}.$$

Hence, the Whitham equations (2.46) reduce to a system of ordinary differential equations

$$\frac{dr_i}{ds}(v_i - s) = 0, \qquad i = 1, 2, 3. \tag{2.50}$$

Also, the Gurevich-Pitaevskii matching conditions become

$$\text{at the trailing edge,} \qquad s = s_- : \qquad r_2 = r_3, \qquad r_1 = \Delta,$$
$$\text{at the leading edge,} \qquad s = s_+ : \qquad r_2 = r_1, \qquad r_3 = 0.$$

The solution of equation (2.50) satisfying the above matching condition has the form

$$r_3 = 0, \qquad r_1 = \Delta, \qquad v_2(\Delta, r_2, 0) = s. \tag{2.51}$$

Using the explicit expression for $v_2(r_1, r_2, r_3)$, the last equation of (2.51) determines the dependence of the self-similar variable $s = x/t$

$$s = \frac{x}{t} = 2\Delta \left[1 + m - \frac{2m(1-m)K(m)}{E(m) - (1-m)K(m)} \right]. \tag{2.52}$$

The velocities, $s_\mp$ of the trailing and leading edges of the undular bore can be obtained by letting $m \to 0$ and $m \to 1$ respectively in the solution (2.52).

$$\frac{x_-}{t} = s_- = s(0) = -6\Delta, \qquad \frac{x_+}{t} = s_+ = s(1) = 4\Delta. \tag{2.53}$$

Therefore, the undular bore is confined to an expanding zone $-6\Delta t \leq x \leq 4\Delta t$. The amplitude of the solitary wave at the leading edge is $a = 2(r_1 - r_3) = 2\Delta$, which is twice of the initial jump. In Figure 2.9, we present the plot of an undular bore solution generated from an initial jump with $\Delta = 1$ together with the corresponding behaviour of the Riemann invariants. At the leading edge where we have solitary wave, $r_1 = r_2$ while at the trailing edge, $r_2 = r_3$.

If $\Delta < 0$, then the initial condition (2.49) will not generate an undular bore. Instead, it will produce a rarefaction wave (see Figure 2.10)

$$u(x,t) = \begin{cases} 0; & x > 0 \\ \dfrac{x}{6t}; & 6\Delta t < x < 0 \\ \Delta; & x < 6\Delta t \end{cases}. \tag{2.54}$$
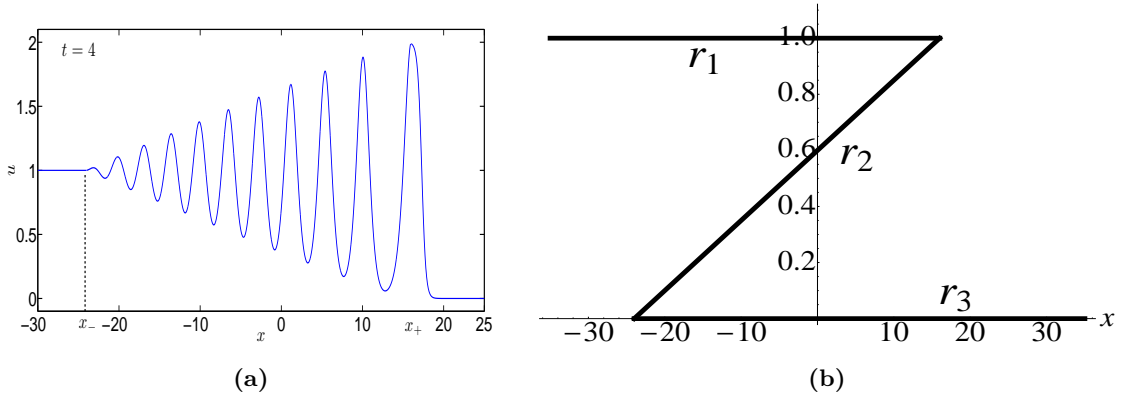
Figure 2.9: Left: Analytical solution for undular bore, $u(x,t)$ – modulation theory; Right: behaviour of the Riemann invariants, $r_1 \geq r_2 \geq r_3$.
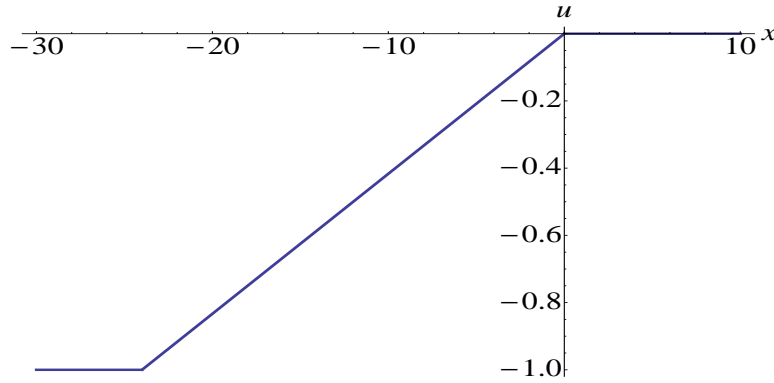
Figure 2.10: Analytical plot of a rarefaction wave where $\Delta = -1$ at $t = 4$

2.5 Perturbed modulation system

So far, we have only considered wave propagation over a flat bottom, which is governed by the constant-coefficient KdV equation (2.1), and the corresponding Whitham equations are given by (2.46). However, in the presence of slowly varying topography or/ and weak dissipation (i.e. bottom friction), the wave dynamics is generally governed by the perturbed KdV (pKdV) equation

$$u_t + 6uu_x + u_{xxx} = \sigma R(u, u_x, \cdots), \tag{2.55}$$

where $\sigma \ll 1$. We stress that the independent variables x and t in (2.55) are not necessarily physical space and time variables. For the wave propagation over variable topography without bottom friction, the term σR is given by $-\frac{9h_t}{4h}u$ (see equation (4.3) in Section 4.1), where the small parameter $\sigma \sim h_t$ is determined by the slow depth variations. The specific forms of the perturbation term in (2.55) when different types of dissipation are

taken into account will be presented in Chapter 5. The formal approach for perturbed modulation theory was proposed by Forest & McLaughlin (1984), where they suggested averaging the conservation laws for the perturbed KdV equation (2.55) over the (quasi-) periodic solution of the unperturbed equation. This procedure in general is quite technical, but for a single-phase (periodic) case, another, more convenient and effective method was proposed by Kamchatnov (2004), where he extended the spectral approach to the single-phase averaging described in Section 2.3 to the perturbed integrable equations belonging to the AKNS hierarchy. The corresponding perturbed Whitham equations for (2.55) have been obtained by Kamchatnov (2004) in terms of "spectral" variables, λ_i (see Section 2.3)

$$\frac{\partial \lambda_i}{\partial t} + v_i \frac{\partial \lambda_i}{\partial x} = \frac{\sigma L}{\partial L/\partial \lambda_i} \frac{\langle (2\lambda_i - s_1 - u)R \rangle}{4 \prod_{j \neq i}(\lambda_i - \lambda_j)}, \qquad i = 1, 2, 3, \tag{2.56}$$

where s_1, u, L and v_i are given by (2.28), (2.31), (2.38) and (2.41) respectively. When $R \equiv 0$, the system (2.56) transforms into the standard unperturbed Whitham system in the Riemann invariant form (2.40). Here, we present the explicit form of the perturbed Whitham system (2.56) for the waves propagating over an uneven bottom without bottom friction (El *et al.*, 2007)

$$\frac{\partial \lambda_i}{\partial t} + v_i \frac{\partial \lambda_i}{\partial x} = \sigma C_i A_i, \qquad i = 1, 2, 3, \tag{2.57}$$

where

$$\sigma = -\frac{9h_t}{4h}, \tag{2.58}$$

$$C_1 = \frac{1}{E(m)}, \qquad C_2 = \frac{1}{E(m) - (1 - m)K(m)}, \qquad C_3 = \frac{1}{E(m) - K(m)}; \tag{2.59}$$

and

$$\left.\begin{aligned}
A_1 &= \frac{1}{3}(5\lambda_1 - \lambda_2 - \lambda_3)E(m) + \frac{2}{3}(\lambda_2 - \lambda_1)K(m), \\
A_2 &= \frac{1}{3}(5\lambda_2 - \lambda_1 - \lambda_3)E(m) - (\lambda_2 - \lambda_1)\left(\frac{1}{3} + \frac{\lambda_2}{\lambda_3 - \lambda_1}\right)K(m), \\
A_3 &= \frac{1}{3}(5\lambda_3 - \lambda_1 - \lambda_2)E(m) - \left[\lambda_3 + \frac{1}{3}(\lambda_2 - \lambda_1)\right]K(m),
\end{aligned}\right\} \tag{2.60}$$

where $E(m)$ and $K(m)$ are the complete integrals of the first and second kind respectively. When $m = 0$ (linear waves), the perturbed modulation system reduces to

$$\left.\begin{aligned}
\lambda_2 &= \lambda_3, \\
\frac{\partial \lambda_1}{\partial t} - 6\lambda_1 \frac{\partial \lambda_1}{\partial x} &= \lambda_1 \sigma, \\
\frac{\partial \lambda_3}{\partial t} + (6\lambda_1 - 12\lambda_3)\frac{\partial \lambda_3}{\partial x} &= \frac{1}{3}(4\lambda_3 - \lambda_1)\sigma.
\end{aligned}\right\} \tag{2.61}$$

Figure 2.11: Behaviour of the Riemann invariants in the vicinity of the leading edge of the undular bore. (a) Weak soliton interaction (b) Strong soliton interaction

When $m = 1$ (soliton), we obtain from (2.57)

$$\left. \begin{array}{c} \lambda_2 = \lambda_1, \\[2mm] \dfrac{\partial \lambda_1}{\partial t} - (4\lambda_1 + 2\lambda_3)\dfrac{\partial \lambda_1}{\partial x} = \dfrac{1}{3}(4\lambda_1 - \lambda_3)\sigma, \\[2mm] \dfrac{\partial \lambda_3}{\partial t} - 6\lambda_3 \dfrac{\partial \lambda_3}{\partial x} = \lambda_3 \sigma. \end{array} \right\} \qquad (2.62)$$

Note that equations (2.61) and (2.62) reduce to (2.42) and (2.43) respectively when there is no perturbation term on the right-hand side.

2.6 Leading solitary wave: local vs. nonlocal behaviour

For flat bottom propagation, the leading edge of the undular bore is given by $x_+ = 4U_0 t$. The behaviour of the Riemann invariants, $r_i(x,t) = -\lambda_i(x,t), i = 1, 2, 3$, near the leading edge can be readily obtained from the modulation solution (2.52) by expanding it for $(1 - m) \ll 1$. The typical behaviour is shown in Figure 2.9b. In the presence of a small perturbation term due to external perturbation, e.g. variable topography and/ or bottom friction, the asymptotic analysis of the perturbed Whitham equations (2.56) for $(1-m) \ll 1$ reveals two qualitatively different possibilities for the behaviour of the Riemann invariants, r_1, r_2 near the leading edge (soliton), $x = x_+(t)$ (El *et al.*, 2007):

(a) "local (weak soliton interaction) scenario": if $\lim_{x \to x_+} |dr_i/dx| < \infty, i = 1, 2$, then the leading solitary wave in the undular bore behaves as an isolated, adiabatically varying solitary wave (see Figure 2.11a), and

(b) "nonlocal (strong soliton interaction) scenario": if $\lim_{x \to x_+} |dr_i/dx| = \infty, i = 1, 2$, then the evolution of the leading solitary wave is determined not only by the local variations

of the topography or/and the presence of bottom friction but also by the interaction with the entire nonlinear wavetrain behind it (see Figure 2.11b).

For the evolution of undular bores over variable topography, the threshold between the "weak interaction" and "strong interaction" scenarios can also be determined by the asymptotic behaviour of the wavenumber, k near the leading edge, $x = x_+$ implied by (4.9) and (4.11) of Gurevich & Pitaevskii (1974)

$$k \sim \frac{1}{\ln(1/\delta)}, \tag{2.63}$$

$$\text{where} \qquad \delta = \frac{x_+ - x}{x_+ - x_-} \ll 1, \tag{2.64}$$

x_- being the trailing edge of the undular bore. The formula (2.63) is obtained by expanding (2.9) and (2.11) for $(1-m) \ll 1$. If $k \lesssim 1/\ln(1/\delta)$, then the solitary wave interactions near the leading edge are weak, and the lead solitary wave of the undular bore behaves as an isolated soliton. However, if $k \gg 1/\ln(1/\delta)$ near the leading edge, then the propagation of the lead solitary wave is strongly affected by its interaction with the remainder of the wavetrain.

2.6.1   Behaviour of the leading solitary wave: an example

In order to illustrate the qualitatively different types of behaviour of the solitary wave near the leading edge of the undular bore in the two different scenarios mentioned above, let us consider the Korteweg-de Vries-Burgers (KdVB) equation

$$u_t + 6uu_x + u_{xxx} = \nu u_{xx}, \tag{2.65}$$

where $0 \leq \nu \ll 1$ is the viscosity coefficient.

Figure 2.12 shows the numerical plots of the solution to the KdVB equation (2.65) with the initial condition in the form of a step

$$u = (1 - \tanh(x/10))/4, \tag{2.66}$$

where the size of the step is $\Delta = 0.5$ for different values of ν. When there is no dissipation, i.e. when $\nu = 0$, equation (2.65) reduces to the KdV equation (2.1). Thus, we have an unsteady DSW or undular bore solution (dashed green line) of the KdV equation. The undular bore will continue to expand as time increases. The leading solitary wave has amplitude twice of the jump, 2Δ (see Section 2.4.2 for detailed explanation). The typical behaviour of the Riemann invariants, r_1, r_2, in the vicinity of the leading edge is shown

2.6.1 Behaviour of the leading solitary wave: an example
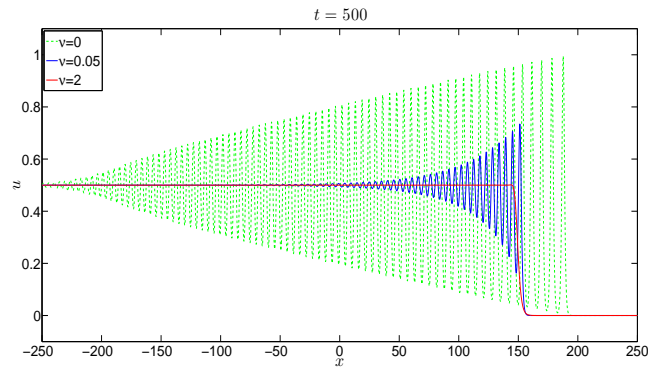
Figure 2.12: Comparison of the shock profile for the KdVB equation (2.65) for different values of ν: $\nu = 0$ – dashed green line, $\nu = 0.05$ – solid blue line and $\nu = 2$ – solid red line.

in Figure 2.9b, which corresponds to the local interaction scenario (see Figure 2.11a). Indeed, Khruslov (1976) and Claeys & Grava (2010) showed that the leading solitary wave of undular bore of the KdV equation at large time represents asymptotically a genuine isolated KdV soliton, not constrained by the interaction with the remainder of the bore.

When $\nu = 0.05$ (i.e. when (2.65) becomes the KdVB equation), we have weakly dissipative (or viscous) DSW (solid blue line). Unlike the undular bore solution of the KdV equation, the undular bore solution of the KdVB equation is asymptotically ($t \rightarrow \infty$) steady and propagates as a whole with the classical shock speed (cf. the smooth shock solution for $\nu = 2$ in Figure 2.12). The leading wave is asymptotically close to the solitary solution of the KdV equation (Johnson, 1970; Gurevich & Pitaevskii, 1987; Avilov *et al.*, 1987). However, in contrast to the inviscid, $\nu = 0$, case, the amplitude of the leading solitary wave is 1.5Δ, which is smaller than in the DSW solution of the KdV equation. This amplitude is constant in time (for $t \gg 1$).

One can see that the behaviour of the leading solitary wave in the undular bore solution of the KdVB equation is markedly different from the behaviour of an isolated solitary wave. The leading solitary wave amplitude of the undular bore solution for the KdVB equation stays constant at 1.5Δ. However, for an isolated solitary wave, its amplitude keeps decreasing over time (see Section 5.4.1.1) due to dissipation. The physical explanation of such drastic difference in the behaviour of an isolated solitary wave and a lead solitary wave in the undular bore for the same weakly dissipative KdVB equation is that the action of weak dissipation on an expanding undular bore is twofold: on the one hand, the dissipation tends to decrease the amplitude of the wave locally but, on the other hand, it 'squeezes' the undular bore so that the interaction (i.e momentum exchange) between separate solitary waves within the bore becomes stronger than in the absence of the dissipation and this acts
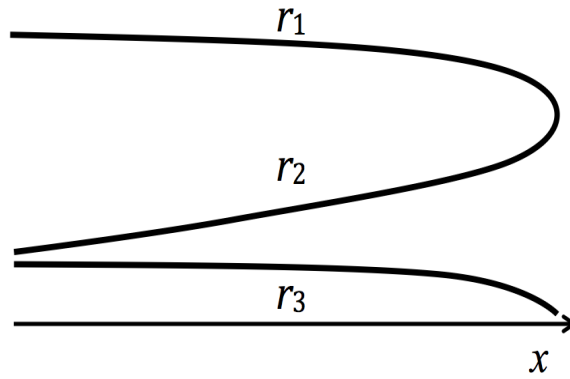
Figure 2.13: Schematic illustration of the behaviour of the Riemann invariants for the undular bore of the KdVB equation.

as the amplitude-increasing factor. This implies that we have a strong soliton interaction scenario in the vicinity of the leading edge (El *et al.*, 2007). The exact modulation solution for the steady undular bore of the KdVB equation was obtained by Gurevich & Pitaevskii (1987) and Avilov *et al.* (1987). The behaviour of the Riemann invariants in this solution is schematically shown in Figure 2.13. One can see that near the leading edge, the behaviour of the Riemann invariants indeed corresponds to the "strong interaction" scenario described in the previous subsection (see Figure 2.11b).

Finally, if we have strong dissipation, $\nu = 2$, we do not have an oscillatory structure at all. Instead, we have a steady monotonic shock transition (solid red line in Figure 2.12), also propagating with the classical shock speed.

2.7 Concluding remarks

In this chapter, we have discussed the general procedure for the derivation of the modulation equations as proposed by Whitham (1965). Then, we presented an alternative method by Kamchatnov (1997) to derive the Whitham equations via the spectral problem associated with the equations belonging to the AKNS hierarchy. Also, we have discussed the general idea of a dispersive shock wave (undular bore) in the context of water waves where an undular bore can be generated from an initial distribution in the form of sharp step. We have derived the classical Gurevich-Pitaevskii modulation solution (2.52) for the undular bore. Finally, we have described the qualitative behaviour of the leading solitary wave in the undular bore in two different scenarios as proposed by El *et al.* (2007). The Gurevich-Pitaevskii solution and the discussion of the solitary wave behaviour near the leading edge of the undular bore will be used extensively in the subsequent chapters of the thesis.

Chapter 3

Solitary wave propagation over variable topography

In this chapter, we first give a brief outline of the derivation of the variable-coefficient Korteweg-de Vries equation, which can be found in the literature. Next, we examine how solitary waves evolve when they propagate over different types of varying bottom profiles. Some numerical results will also be presented. The results of this chapter will be used later for comparison with corresponding results for undular bores propagating over variable topography.

3.1   Introduction

In many physical problems, waves propagate over variable depth regions. Therefore, the effect of varying depth has to be taken into consideration when deriving the appropriate mathematical model. Grimshaw (1970), Kakutani (1971) and Johnson (1973b) were among the first who derived the variable-coefficient Korteweg-de Vries (vKdV) equation to model the propagation of weakly nonlinear waves over an uneven bottom. There are many versions of the derivation of the vKdV equation given in the literature, depending on the physical problem under consideration. Here we give a brief outline of the derivation following Grimshaw (2007a).

3.2   Derivation of the variable-coefficient Korteweg-de Vries equation

Consider two-dimensional gravity waves, which propagate on the free-surface of a fluid layer with a variable bottom surface represented by $z = -h(x)$ (see Figure 3.1). We suppose that the fluid is inviscid and incompressible with constant density, ρ. The velocity field $\mathbf{u} = (u, w)$ is assumed to be irrotational so that $\mathbf{u} = \nabla\phi$, where $\phi(x, z, t)$ satisfies Laplace's equation

$$\phi_{xx} + \phi_{zz} = 0. \tag{3.1}$$

Since the fluid is assumed to be inviscid, the fluid can only flow parallel to the bottom

3.2. DERIVATION OF THE VARIABLE-COEFFICIENT KORTEWEG-DE VRIES EQUATION
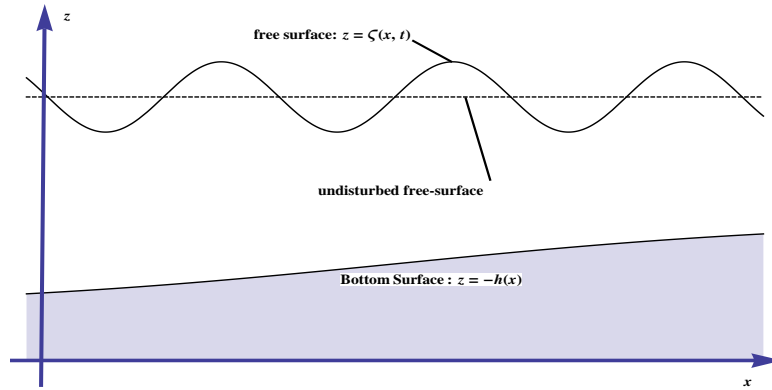
Figure 3.1: Geometrical configuration of the propagation of surface water waves over an uneven bottom

surface. Thus we have the boundary condition at the rigid bottom

$$\phi_z + h_x \phi_x = 0 \qquad \text{at} \qquad z = -h. \tag{3.2}$$

On the other hand, the boundary conditions at the free-surface are given by (Kawahara, 1975; Grimshaw, 2007a)

$$\phi_z = \zeta_t + \phi_x \zeta_x \qquad \text{at} \qquad z = \zeta, \tag{3.3}$$

$$\phi_t + \frac{1}{2}(\phi_x^2 + \phi_z^2) + g\zeta = 0 \qquad \text{at} \qquad z = \zeta, \tag{3.4}$$

Equation (3.3) is the kinematic condition, while (3.4) expresses the continuity of pressure at the free-surface, which arises from Bernoulli's theorem (the dynamic condition). The effect of surface tension is ignored since we consider waves of long wavelength.

To obtain the vKdV equation, we need to apply a multi-scale asymptotic expansion. Hence, a small parameter $\varepsilon \ll 1$ is introduced and we assume the usual KdV balance, where the amplitude scales with ε^2. Next, we rescale the horizontal coordinate and the time, so that

$$X = \varepsilon x, \qquad T = \varepsilon t. \tag{3.5}$$

We seek an asymptotic expansion of the form

$$\zeta = \varepsilon^2 \zeta^{(1)}(X, T) + \varepsilon^4 \zeta^{(2)}(X, T) + \cdots . \tag{3.6}$$

The depth is assumed to vary slowly on a spatial scale of ε^{-3}. Thus, we may formally write $h = h(\chi)$, where $\chi = \varepsilon^2 X$. For convenience, we define the depth-averaged mean flow

$$U(X, T) = \frac{1}{h + \zeta} \int_{-h}^{\zeta} u(X, T, z)\, dz. \tag{3.7}$$

The conservation of mass implies that

$$\zeta_T + (U(h + \zeta))_X = 0. \tag{3.8}$$

3.2. DERIVATION OF THE VARIABLE-COEFFICIENT KORTEWEG-DE VRIES EQUATION

Thus, at the leading order, we have

$$\zeta_T^{(1)} + hU_X^{(1)} = 0, \tag{3.9}$$

$$U_T^{(1)} + g\zeta_X^{(1)} = 0. \tag{3.10}$$

The general solution of this system is the sum of waves propagating in both directions, i.e. in the positive and negative X-direction with the phase speed for linear shallow water waves, $c = \sqrt{gh}$ which depends on the slow variable χ, $c = c(\chi)$.

We choose a wave propagating in the positive X-direction so that to leading order we have

$$\zeta^{(1)} = \frac{h}{c}U^{(1)} = A(\sigma, \theta), \tag{3.11}$$

where

$$T^* = \int^X \frac{dX}{c}, \qquad \theta = T^* - T, \qquad \sigma = \varepsilon^2 T^*. \tag{3.12}$$

Here, we have anticipated that, as the wave propagates to the right with speed c, it also evolves on the long spatial scale of ε^{-3}, and the slow variable σ is introduced. At the next order, we obtain

$$\zeta_T^{(2)} + hU_X^{(2)} = F^{(2)}, \tag{3.13}$$

$$U_T^{(2)} + g\zeta_X^{(2)} = G^{(2)}, \tag{3.14}$$

where

$$F^{(2)} = -\zeta_\sigma^{(1)} - \frac{1}{c}(U^{(1)}\zeta^{(1)})_\theta - \frac{c_\sigma}{c}\zeta^{(1)}, \tag{3.15}$$

$$G^{(2)} = -\frac{c}{h}\zeta_\sigma^{(1)} - \frac{1}{c}U^{(1)}U_\theta^{(1)} - \frac{h}{3c}\zeta_{\theta\theta\theta}^{(1)}. \tag{3.16}$$

Note that, to leading order, $\zeta_X^{(1)} = \zeta_\theta^{(1)}/c$. From (3.11), the inhomogeneous terms are functions of σ and θ. Thus, this system of equations reduces to

$$-c\zeta_\theta^{(2)} + hU_\theta^{(2)} = F^{(2)}, \tag{3.17}$$

$$-cU_\theta^{(2)} + g\zeta_\theta^{(2)} = G^{(2)}. \tag{3.18}$$

The homogeneous version of the above system has a non-trivial solution, namely the right-propagating wave $\zeta^{(1)}$ and $U^{(1)}$ given by (3.11). Hence, the inhomogeneous terms on the right-hand side must be orthogonal to the non-trivial solution of the homogeneous adjoint system to drop the secular terms. This is readily found to be (c, h) and so the required compatibility condition is

$$cF^{(2)} + hG^{(2)} = 0. \tag{3.19}$$

Next, we substitute the expressions (3.11) into (3.19) and after some simplifications and obtain

$$A_\sigma + \frac{c_\sigma}{2c}A + \frac{3}{2h}AA_\theta + \frac{h^2}{6c^2}A_{\theta\theta\theta} = 0. \tag{3.20}$$

Using the transformation (3.5) and (3.12) and replacing $\varepsilon^2 A$ with A this becomes

$$A_t + cA_x + \frac{c_x}{2}A + \frac{3c}{2h}AA_x + \frac{ch^2}{6}A_{xxx} = 0. \tag{3.21}$$

Equation (3.21) is the vKdV equation for water waves propagation over a variable depth.

3.3 Transformation of a solitary wave over variable topography

In this section, we will look at the evolution of solitary waves over two different types of varying topography, namely rapidly varying depth and slowly varying depth. So, the governing equation is the vKdV equation (3.21). The first two terms in (3.21) are the dominant terms, and by themselves describe the propagation of a linear long wave with speed c. The remaining terms represent, respectively, the effect of varying depth, weakly nonlinear effects and weak dispersion. As a reminder, equation (3.21) is derived using the usual KdV balance in which $\partial/\partial t \sim \partial/\partial x \sim \varepsilon \ll 1, A \sim \varepsilon^2$. Here, a weak inhomogeneity is added to this balance so that c_x/c scales as ε^3. Equation (3.21) can be asymptotically transformed into

$$A_\tau + \frac{h_\tau}{4h}A + \frac{3}{2h}AA_X + \frac{h}{6}A_{XXX} = 0, \tag{3.22}$$

where

$$\tau = \int_0^x \frac{dx'}{c(x')}, \qquad X = \tau - t. \tag{3.23}$$

Here $h = h(x(\tau))$ explicitly depends on the variable τ, which describes the evolution along the path of the wave. Formally, we write $A(x,t) = \tilde{A}(X,\tau)$ and $h(x) = \tilde{h}(\tau)$ but then omit the "tilde" in (3.22). The balance of terms in (3.22) is ensured by $\partial/\partial\tau \sim \varepsilon^3, \partial/\partial X \sim \varepsilon, A \sim \varepsilon^2$. So, unlike in the original vKdV equation (3.21), where both independent variables x and t vary on the same scale $\sim 1/\varepsilon$, in (3.22), the "time" τ is a slow variable relative to the "spatial" coordinate X. Equations (3.21) and (3.22) are *asymptotically* the same, but differ with respect to terms of $O(\varepsilon^7)$, which is the same as the error terms in both equations.

We shall suppose that the depth varies according to

$$h(x) = h_0 = 1 \text{ for } x < x_0, \qquad \text{and} \qquad h(x) = h_1 \text{ for } x > x_1,$$

3.3. TRANSFORMATION OF A SOLITARY WAVE OVER VARIABLE TOPOGRAPHY
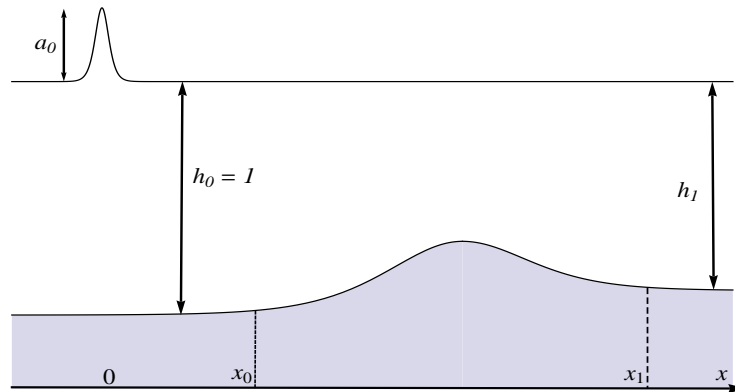
Figure 3.2: Schematic illustration for the solitary wave propagation over variable topography.

where h_0, h_1 are constant and varies monotonically in the region $x_0 \leq x \leq x_1$. We assume that $x_0 \geq 0$ and $x_1 - x_0 \gg 1$. In this chapter, we consider four different types of the variable topography regions in the interval $x_0 \leq x \leq x_1$:

(a) a gentle monotone slope where $h'(x) < 0$, $|h'(x)| \ll 1$ (slowly decreasing depth, $h_1 < 1$),

(b) a gentle monotone slope where $h'(x) > 0$, $|h'(x)| \ll 1$ (slowly increasing depth, $h_1 > 1$),

(c) a sharp step where $h'(x) = \infty$, $h_0 > h_1$ (rapidly decreasing depth, $h_1 < 1$), and

(d) a sharp step where $h'(x) = \infty$, $h_0 < h_1$ (rapidly increasing depth, $h_1 > 1$).

Note that in cases (c) and (d), $x_0 = x_1$.

An initial condition in the form of

$$A(x, t = 0) = A_0(x) = a_0 \operatorname{sech}^2(\gamma_0 x), \qquad 4\gamma_0^2 = 3a_0, \qquad (3.24)$$

for the vKdV equation (3.21) is placed at $x = 0$ so that initially, we have a solitary wave having an amplitude of a_0. Our aim is to look at how the solitary wave evolves as it moves through the varying depth region, $x > x_0$. A schematic of the problem is illustrated in Figure 3.2. In terms of new variables (3.23), the initial condition for equation (3.22) becomes

$$\widetilde{A}(X(t = 0) = \tau, \tau) = A_0(x),$$

where $x(\tau)$ is given by (3.23). However, because τ is a slow variable relative to X (recall that $\partial/\partial \tau \sim \varepsilon^3$ and $\partial/\partial X \sim \varepsilon$), we have $\widetilde{A}(X, \tau) = \widetilde{A}(X, 0) + O(\varepsilon^5)$. So, within the error inherent in the derivation of the original model (3.21), the initial condition for (3.22) is

$$A(X, \tau = 0) = A_0(X, 0),$$

where we have again omitted "tilde" for A. Equation (3.22) can be rewritten as the vKdV equation

$$B_\tau + \alpha(\tau)BB_X + \beta(\tau)B_{XXX} = 0, \tag{3.25}$$

$$\text{where} \qquad B = h^{1/4}A, \qquad \alpha(\tau) = \frac{3}{2h^{5/4}}, \qquad \beta(\tau) = \frac{h}{6}. \tag{3.26}$$

Equation (3.25) has two integrals of motion with the densities proportional to $B = h^{1/4}A$ and $B^2 = h^{1/2}A^2$, which commonly referred to conservation laws for "mass" and "momentum". Note that the equations (3.22) and (3.25) are exactly equivalent. The variable τ is referred as "time" even though it describes the evolution along the path of the wave. The initial condition for equation (3.25) is

$$B(X, \tau = 0) = B_0(X) = A_0(X).$$

In terms of the new variables $B(X, \tau)$, we will consider that $h(\tau) = 1$ for $0 < \tau < \tau_0$ and varies monotonically in the interval $\tau_0 < \tau < \tau_1$ to $h(\tau) = h_1$ when $\tau > \tau_1$.

3.3.1 Rapidly varying depth: soliton fission

When a solitary wave travels from a constant depth to another shallower constant depth, where the depth changes rapidly, it will disintegrate into several solitary waves of different sizes, followed by small radiation tail depending on the depth variation. This has been proven numerically and experimentally by Madsen & Mei (1969). The process of soliton disintegration is called soliton fission, analogous to nuclear fission. The analytical explanation was done by Tappert & Zabusky (1971) and Johnson (1973a).

To explain soliton fission, let us suppose that the coeficients $\alpha(\tau)$ and $\beta(\tau)$ in the vKdV equation (3.21) vary rapidly with respect to the wavelength of a solitary wave. So, we consider that these coefficients make a rapid transition from the values α_- and β_- in $\tau < \tau_0$ region to the values α_+ and β_+ in $\tau > \tau_0$ region. Thus, a solitary wave solution in the region $\tau < \tau_0$, is given by

$$B = b\,\mathrm{sech}^2(\gamma(X - W\tau)) \quad \text{where} \quad W = \frac{\alpha_- b}{3} = 4\beta_-\gamma^2. \tag{3.27}$$

The initial solitary wave will propagate through the transition zone $\tau \approx \tau_0$ without change. However, it is no longer a solution of (3.21) when it emerges onto another flat bottom at $\tau > \tau_0$, which now yields constant coefficients α_+ and β_+ in (3.21). Instead, (3.27) at $\tau = \tau_0$ becomes an initial condition for the new constant-coefficient KdV equation. The
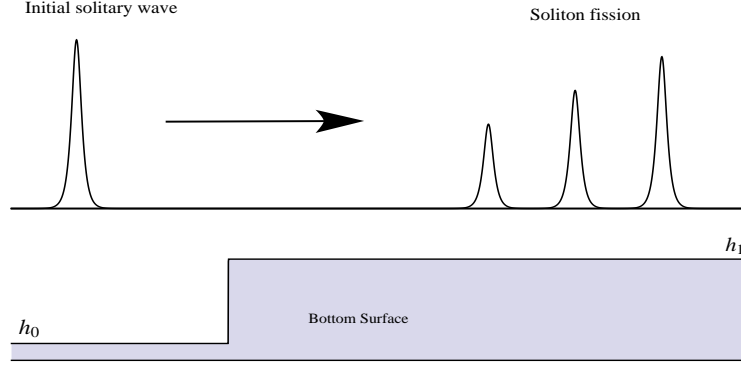
Figure 3.3: Soliton fission

new solution in $\tau > \tau_0$ region can be constructed using inverse scattering transform. The result is that the initial solitary wave fissions into N solitons, trailed by an oscillatory tail depending on the depth variation. The number of secondary solitary waves and the parameters of the oscillatory tail can be determined from the inverse scattering transform (Gardner *et al.*, 1967). The schematic illustration of soliton fission is shown in Figure 3.3

The number of N solitons produced is determined by the ratio of the coefficients

$$R = \frac{\alpha_+ \beta_-}{\alpha_- \beta_+}. \tag{3.28}$$

If there is no change in polarity of solitary waves, $R > 0$, then $N = 1 + [(\sqrt{8R+1} - 1)/2]$. When the polarity changes, then $R < 0$. In this case, no solitons are produced and the entire solitary wave decays into a radiation (see e.g. Johnson, 1997; Grimshaw, 2007a).

For water waves, where a solitary wave is propagating from constant depth h_0 into another constant depth h_1, the ratio of coefficients, R is given by

$$R = \left(\frac{h_0}{h_1}\right)^{9/4}. \tag{3.29}$$

Here $R > 0$. If $h_0 > h_1$, the solitary waves propagates over a decreasing depth, that is into a shallower water, $N \geq 2$, and at least one or more solitary waves are generated. On the other hand, if $h_1 > h_0$, then the solitary wave propagates over an increasing depth or into a deeper region, then $N = 1$ and no other solitons are produced.

3.3.1 Rapidly varying depth: soliton fission
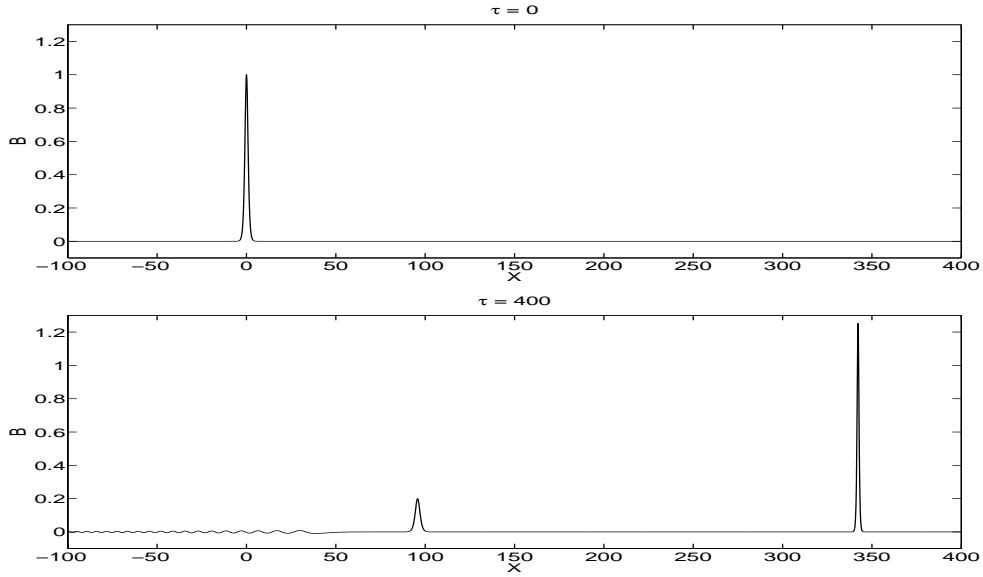
Figure 3.4: A soliton fissions into two solitons followed by an oscillatory tail when the depth decreases rapidly.

3.3.1.1   Numerical results

For numerical simulations, we will solve the vKdV equation (3.21) numerically using the method of lines (see Appendix A). First we consider the depth $h(\tau)$ decreases rapidly,

$$h(\tau) = \begin{cases} h_0 = 1.0 & : \tau < 100, \\ h_1 = 0.7 & : \tau > 100. \end{cases} \tag{3.30}$$

The initial condition is taken as

$$B(X,0) = \text{sech}^2(\gamma X), \qquad \gamma = (3/4)^{1/2}. \tag{3.31}$$

Figure 3.4 shows the numerical simulation of a soliton fissioning into two solitons followed by an oscillatory tail.

On the other hand, Figure 3.5 shows the evolution of a solitary wave over a rapidly increasing depth region. Here, no fission of solitary waves is observed. Instead, the solitary wave decays rapidly and produces a radiation tail. The depth profile is taken as

$$h(\tau) = \begin{cases} h_0 = 1.0 & : \tau < 100, \\ h_1 = 1.3 & : \tau > 100, \end{cases} \tag{3.32}$$

with the same initial data as in (3.31).
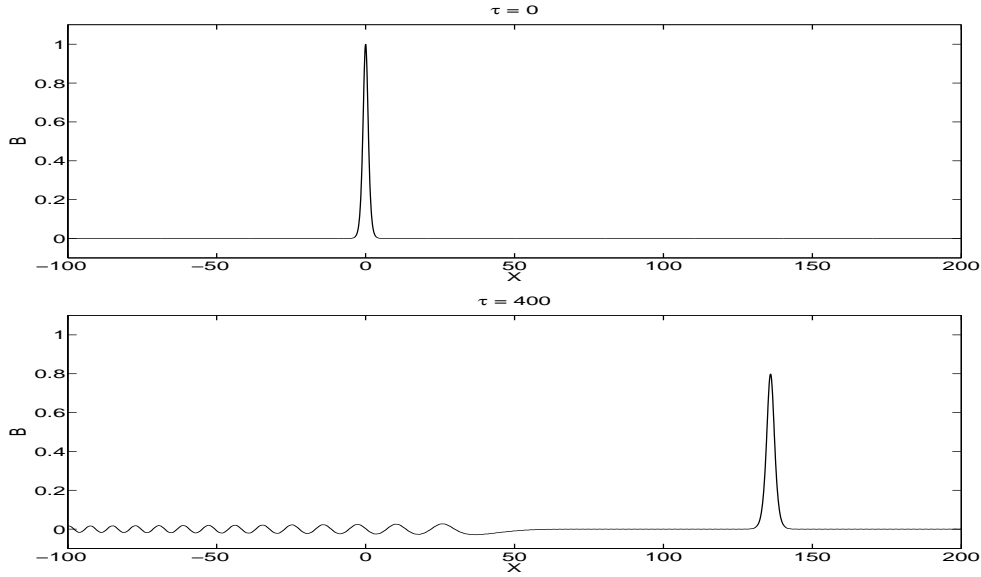
Figure 3.5: No soliton fission when a solitary wave propagates into deeper region where the depth changes rapidly

3.3.2 Slowly varying depth

Now we will consider the opposite situation, where the solitary wave is propagating over a slowly changing topography, i.e. when the coefficients $\alpha(\tau)$ and $\beta(\tau)$ in the vKdV equation (3.21) vary slowly with respect to the "wavelength" of a solitary wave. To find the slowly varying solitary wave solution, one has to use a multi-scale perturbation expansion with the leading term given by

$$B \sim b\,\mathrm{sech}^2\gamma(X - \int_{\tau_0}^{\tau} W\,d\tau), \qquad W = \frac{\alpha b}{3} = 4\beta\gamma^2. \qquad (3.33)$$

Here, the wave amplitude $b(\tau)$ and the coefficients $\alpha(\tau)$, $\beta(\tau)$ are slowly varying functions. Since the vKdV equation (3.21) possesses momentum (action flux) conservation law

$$\int_{-\infty}^{\infty} B^2\,dX = \text{constant}, \qquad (3.34)$$

we can determine the variations of the amplitude b with time τ. Substitution of (3.33) into (3.34) shows that

$$b = b_0 \left(\frac{h_0}{h(\tau)}\right)^{3/4}, \qquad (3.35)$$

where b_0 and h_0 are initial solitary wave amplitude and local depth respectively. Using (3.26), which provides the relationship between $B(X,\tau)$ and the physical surface elevation $A(x,t)$, we recover the classical Boussinesq result for the amplitude of the shallow-water solitary wave propagating over variable depth

$$a = \frac{a_0 h_0}{h(x)}. \qquad (3.36)$$

Figure 3.6: Initial solitary wave travelling into varying topography (top figure), formation of trailing shelf (middle figure) and generation of undular bore or secondary solitary wave on the shelf (bottom figure)
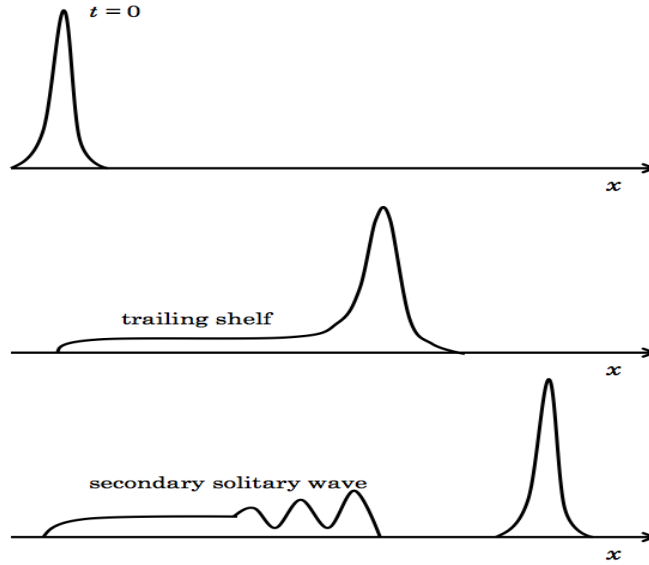
Although the momentum of the solitary wave is conserved, the mass of the wave is not conserved (Grimshaw, 1970, 1971; Knickerbocker & Newell, 1985). Thus, we need to introduce a trailing shelf behind the solitary wave. The trailing shelf, B_s, has a small amplitude, but long length scale. Since the vKdV equation (3.21) also has a conservation law for mass, we have

$$\int_{-\infty}^{\phi} B_s \, dX + \frac{2b}{\gamma} = \text{constant}, \tag{3.37}$$

where $\phi = \int_{x_0}^{x} W d\tau$ is the location of the solitary wave and the second term represents the mass of the solitary wave (3.33) (Knickerbocker & Newell, 1980; Grimshaw, 2005).

Therefore, under these circumstances, the solitary wave generally itself will deform adiabatically. At the same time, there is a non-adiabatic response in the form of an extended small-amplitude secondary structure or a shelf, which can have a positive or negative polarity and which will travel behind the solitary wave. This is shown schematically in Figure 3.6. Also, in a general two-wave setting, a reflected wave which travels away in the opposite direction to the solitary wave and the trailing shelf will be created. In this case, one needs to use the Boussinesq equation. However, in this thesis, the reflection wave is ignored so that we can use the uni-directional KdV equation (Miles, 1979; Knickerbocker & Newell, 1985).

On a very long time-scale, the trailing shelf leads to the generation of an undular bore. This is due to the nonlinear effects which eventually will lead to steepening and thus the dispersive effects will be invoked. The leading wave of the trailing shelf undular bore can be inter-

preted as a secondary solitary wave (El & Grimshaw, 2002; Grimshaw & Pudjaprasetya, 2004) reconciling thus this effect with the soliton fission described earlier.

3.3.2.1 Numerical results

In Figure 3.7, we present the numerical plot of a solitary wave propagating over a slowly increasing slope for the vKdV equation (3.21). The depth, $h(\tau)$ is described by

$$h(\tau) = \begin{cases} 1.0 & : \tau < 100 \\ (1 - \frac{\alpha(\tau - 100)}{2})^2 & : 100 < \tau < 766.67 \\ 0.64 & : \tau > 766.67 \end{cases} , \qquad \alpha = 0.0006. \qquad (3.38)$$

Figure 3.8 shows the generation of a small-amplitude trailing shelf behind the solitary wave as it propagates over the sloping region.

Figure 3.9 shows the comparison for the solitary wave amplitude adiabatic variation predicted by formula (3.35) (circles) and the numerical data (solid line). A good agreement is found between numerics and the analytical prediction.

Figure 3.7: A solitary wave propagating over a slowly increasing slope. Its amplitude increases adiabatically.

Figure 3.8: A trailing shelf of positive polarity is generated behind the solitary wave as it propagates over a slowly decreasing depth region.

Figure 3.9: Comparison for the amplitude of adiabatically changing solitary wave described by the formula (3.35) with $h_0 = 1$ and $a_0 = 1$ (solid line) and numerically obtained solitary wave amplitude (circles).
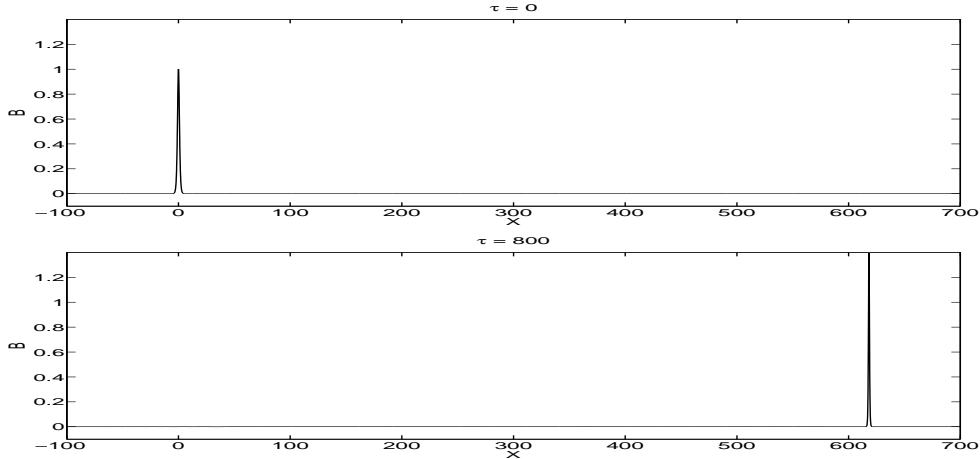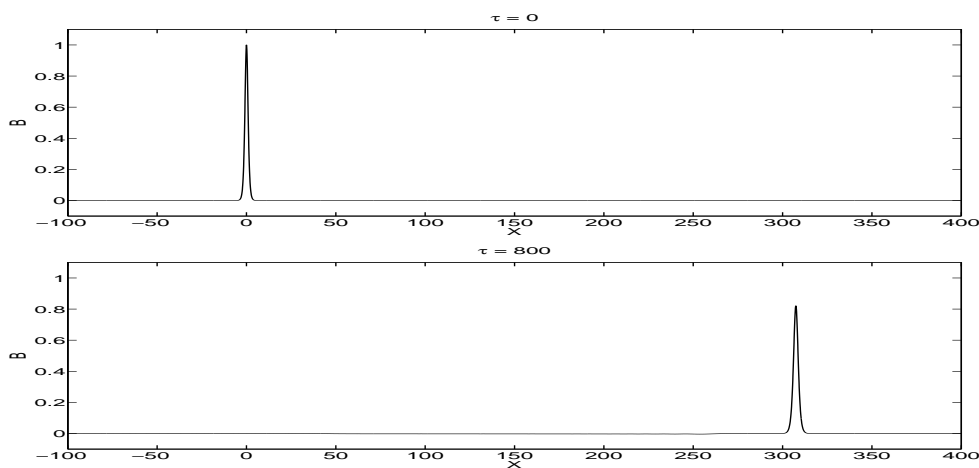

Figure 3.10: A solitary wave propagating over a slowly decreasing slope. Its amplitude decreases adiabatically
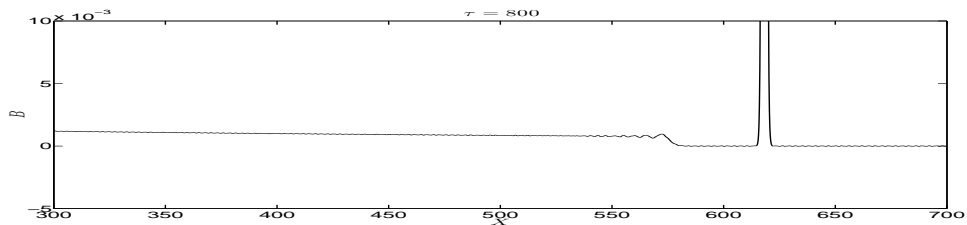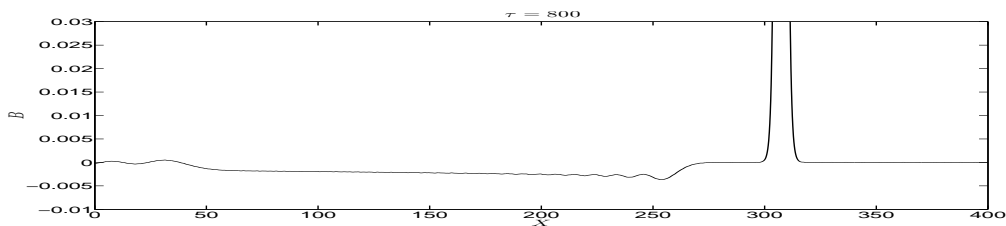

Figure 3.11: A trailing shelf of negative polarity is generated behind the solitary wave as it propagates over a slowly increasing depth region.

On the other hand, Figure 3.10 shows the numerical simulation of the propagation of

solitary wave into a deeper region. The depth profile, $h(\tau)$ is given by

$$h(\tau) = \begin{cases} 1.0 & : \tau < 100 \\ (1 + \frac{\alpha(\tau-100)}{2})^2 & : 100 < \tau < 660.7 \\ 1.3 & : \tau > 660.7 \end{cases} , \qquad \alpha = 0.0005. \qquad (3.39)$$

One can see the generation of a small-amplitude trailing shelf behind the solitary wave (see Figure 3.11).

The comparison for the amplitude of the solitary wave obtained numerically (circles) and from formula (3.35) (solid line) is shown in Figure 3.12. Again, there is an excellent agreement between numerics and formula (3.35).
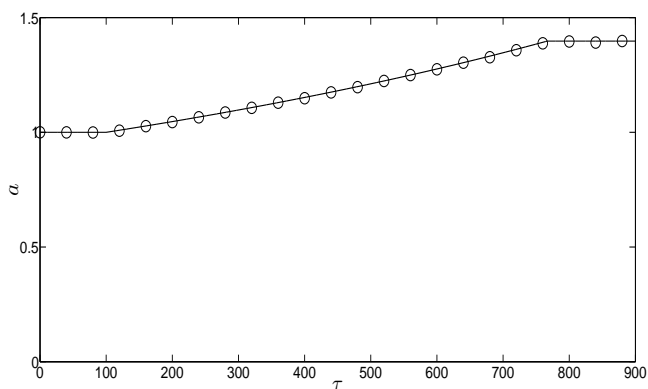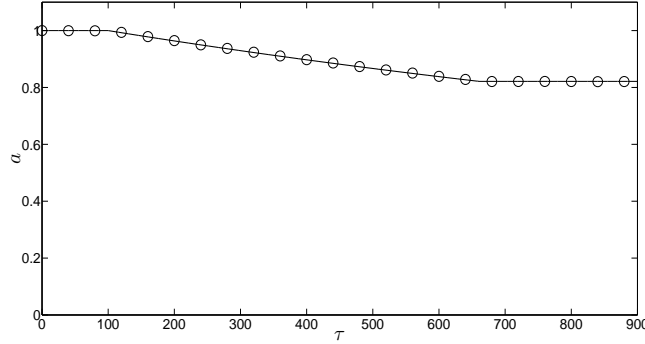

Figure 3.12: Comparison for the amplitude of adiabatically changing solitary wave described by the formula (3.35) with $h_0 = 1$ and $a_0 = 1$ (solid line) and numerically obtained solitary wave amplitude (circles).

3.4 Concluding remarks

In this chapter, we have looked into solitary wave propagation over a variable bottom surface. We have considered the configuration where the water depth changes rapidly and slowly. When the depth decreases rapidly, solitary wave can fission into few solitons followed by an oscillatory tail. On the contrary, no soliton fission is observed when the depth increases rapidly. Instead, solitary waves decay and produce linear radiation. If the bottom profile varies gradually, the solitary wave will deform adiabatically over the slope and a trailing shelf is formed. Its amplitude variation is given by (3.35). For a gradually decreasing depth, the trailing shelf will also decompose into secondary solitons, which is similar to the soliton fission scenario, albeit on a much larger temporal scale. Thus, the propagation of the solitary wave over slowly varying topography leads to a non-adiabatic response regardless of the smallness of the bottom slope variation.

Chapter 4

Undular bore propagation over variable topography

This chapter focuses on the propagation of an undular bore over variable topography. Here, we consider six different configurations for the varying depth regions: slowly decreasing depth, slowly increasing depth, a smooth hole, a smooth bump, rapidly decreasing depth and rapidly increasing depth. Using modulation theory and detailed numerical simulations, we study the effect of slowly varying depth on the evolution of an undular bore in a nonuniform environment. We show that a number of adiabatic and non-adiabatic deformations occur as the undular bore propagates over the sloping region.

4.1 Mathematical model

In this chapter, we concentrate on the transformation of undular bores under the effect of varying depth. The governing equation will be the same vKdV equation (3.21) with variable coefficients determined by the depth profile $h(x)$. However, in this chapter, instead of the initial condition (3.24) in the form of a solitary wave, we shall consider an initial condition in the form of a step,

$$A(x, t = 0) = A_0(x) \quad \text{for} \quad x < 0, \qquad A(x, t = 0) = 0 \quad \text{for} \quad x > 0. \tag{4.1}$$

We shall consider the same typical depth profiles as described in Section 3.3, so that the depth variations are confined to some interval $[x_0, x_1]$, where $x_0 > 0$. The step (4.1) is placed at $x = 0$, i.e. in the region of flat bottom, so that initially, it generates an undular bore solution of the constant-coefficient KdV equation. Our aim is to look at how the undular bore evolves as it moves through varying depth region, $x > x_0$. A schematic of the problem is illustrated in Figure 4.1.

In addition to the varying depth regions mentioned in Section 3.3, we will consider two more types of variable topography:

(a) a smooth hole where $h(x) \geq 1$, $(h_1 = h_0)$, and

(b) a smooth bump where $h(x) \leq 1$, $(h_1 = h_0)$,

Besides the vKdV equation (3.25), we can also recast equation (3.22) into the standard
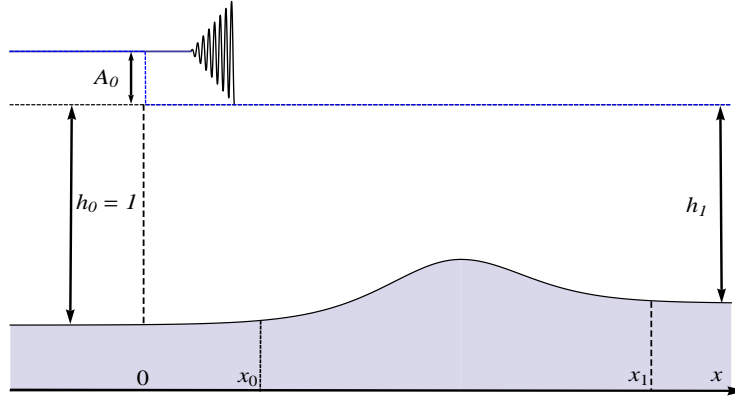
Figure 4.1: Schematic illustration for the undular bore propagation over variable topography.

constant-coefficient KdV equation form, modified by certain perturbation terms, by introducing new variables

$$u = \frac{3}{2h^2}A = \frac{3}{2h^{9/4}}B, \qquad S = \frac{1}{6}\int_0^\tau h(\tau')\,d\tau' = \frac{1}{6}\int_0^x h(x')^{1/2}\,dx', \qquad (4.2)$$

so that (3.22) becomes

$$u_S + 6uu_X + u_{XXX} = -\frac{9h_S}{4h}u. \qquad (4.3)$$

Equation (4.3) has the integrable KdV equation on the left-hand side while the term on right-hand side represents the effect of varying depth.

Yet another convenient form for equation (3.22) is given by

$$U_T + 6UU_X + \beta(T)U_{XXX} = 0, \qquad (4.4)$$

where

$$\beta(T) = h^{9/4}(T), \qquad (4.5)$$

by making transformation

$$U = \frac{3B}{2} \qquad \text{and} \qquad T = \frac{1}{6}\int_0^\tau \frac{d\tau'}{h^{5/4}(\tau')} = \frac{1}{6}\int_0^x \frac{dx'}{h^{7/4}(x')}. \qquad (4.6)$$

In this formulation, we will consider that $\beta(T) = 1$ for $0 < T < T_0$ and $\beta(T) = \beta_1$ for $T > T_1$ with a monotonic variation in the interval $T_0 < T < T_1$. Note that the equations (3.22), (3.25), (4.3) and (4.4) are exactly equivalent. The variables τ, S, T are referred as "time" even though they describe the evolution along the path of the wave.

The initial condition for equations (4.3) and (4.4) are

$$u(X, S = 0) = u_0(X) = U(X, T = 0) = U_0(X) = \frac{3}{2}A_0(X).$$

4.2 Transformation of an undular bore over slowly varying slope

4.2.1 Flat bottom

First, we consider the case when the bottom is flat, which is the case for the times before undular bore encounters the varying depth region. So, we let $\beta = 1$ in the vKdV equation (4.4). As was mentioned in Chapter 2, a discontinuous initial condition in the form of $U(X, 0) = U_0 H(-X)$, where $U_0 = 3A_0/2 > 0$, leads to the generation of an undular bore, which is described by the slowly modulated periodic solution (2.45) of (4.4). Here, we present this solution in a more physically transparent form

$$U = a \left\{ b(m) + \mathrm{cn}^2 \left(\frac{q}{\beta^{1/2}}(X - X_0 - VT); m \right) \right\} + d, \qquad (4.7)$$

where

$$b = \frac{1 - m}{m} - \frac{E(m)}{mK(m)}, \qquad a = 2mq^2,$$

and

$$V = 6d + 2a \left\{ \frac{2 - m}{m} - \frac{3E(m)}{mK(m)} \right\}.$$

Here, $\mathrm{cn}(x; m)$ is the Jacobi elliptic function of modulus m $(0 < m < 1)$ and $K(m), E(m)$ are the complete elliptic integrals of the first and second kind respectively; a is the wave amplitude, d is the mean level, V is the phase velocity, and X_0 is a constant defining the initial phase. The relationships between the parameters in (2.45) and (4.7) are:

$$\left.\begin{aligned}
a = 2(r_2 - r_3), \quad q = \sqrt{r_1 - r_3}, \quad V = 2(r_1 + r_2 + r_3), \\
d = r_3 + r_2 - r_1 + 4(r_1 - r_3)\frac{E(m)}{K(m)}.
\end{aligned}\right\} \qquad (4.8)$$

Note that equation (4.7) also enables one to include the case when $\beta \neq 1$. If the characteristic scale for slow variations of β with time is much greater than that of the modulation parameters in the undular bore, then the expression (4.7) remains asymptotically valid for $\beta_T \neq 0$. The value $\beta^{1/2}/q$ is the width of the wave humps, while their spatial period (wavelength) is given by

$$L = \frac{2\beta^{1/2}K(m)}{q}.$$

When $m \to 1$, the solution (4.7) becomes a solitary wave riding on a background level d. On the other hand, as $m \to 0$, $\mathrm{cn}(x, ; m) \to \cos x$. So in this case, the cnoidal wave (4.7) becomes a linear sinusoidal wave.

4.2.2 Slowly varying topography

From Section 2.4.2, we know that the similarity solution for the Whitham equations corresponding to the KdV equation (4.4) is given by (2.52) (Gurevich & Pitaevskii, 1973, 1974). In terms of the parameters used in (4.7), this solution assumes the form

$$
\frac{X}{T} = 2U_0 \left\{ 1 + m - \frac{2m(1-m)K(m)}{E(m) - (1-m)K(m)} \right\}
$$

$$
\text{for} \quad -6U_0 < \frac{X}{T} < 4U_0, \tag{4.9}
$$

$$
a = 2U_0 m, \quad d = U_0 \left\{ m - 1 + \frac{2E(m)}{K(m)} \right\}, \quad q = U_0^{1/2}. \tag{4.10}
$$

Note that the value of β does not affect the modulation solution (4.9) and affects only the wavelength of the underlying periodic wave (4.7). The wavenumber distribution in the undular bore is then given by

$$
k = \frac{2\pi}{L} = \frac{\pi U_0^{1/2}}{\beta^{1/2} K(m)}. \tag{4.11}
$$

The leading wave of the undular bore is a solitary wave of amplitude $2U_0$ relative to a mean level of 0. This solitary wave propagates with velocity $X/T = 4U_0$. Here, $m \to 1$, $a \to 2U_0$ and $d \to 0$. Ahead of the wavetrain where $X/T > 4U_0$, $U = 0$. At the trailing edge, the wavetrain is sinusoidal, propagating with the group velocity $X/T = -6U_0$. The wavelength at the trailing edge is $L = \pi(\beta/U_0)^{1/2}$, so all waves behind the undular bore have the same spatial wavelength for $\beta = $ const. Otherwise, the wavelength varies slowly with T. Also, behind the wavetrain where $X/T < -6U_0$, $U = U_0$ and at this end, $m \to 0$, $a \to 0$.

4.2.2   Slowly varying topography

First, the topography is assumed to be varying slowly, so that we consider a very gentle slope, $h_T \ll 1$ in the vKdV equation (4.4). Then, it is natural to expect the undular bore will change adiabatically and retain its structure as a slowly modulated nonlinear periodic wave train with a soliton at the leading edge and the linear wave at the trailing edge. As we shall see, this assumption implies that the amplitude of the leading solitary wave in the bore after the slope has the same value as in the initial bore. This conclusion, however, is in apparent contradiction with both local and nonlocal scenarios of the lead solitary wave propagation over uneven bottom (see Section 2.6). In the following subsections, we shall explore the implications of this contradiction.

4.2.2 Slowly varying topography

4.2.2.1 Jump conservation

One can infer from the vKdV equation (4.4) that depth variations would not affect the jump, $[U]$ across the undular bore after the slope. To show this, let us define the jump, $[U]$ as

$$[U] = \int_{X_a(T)}^{X_b(T)} U_X(X,T)\, dX, \tag{4.12}$$

and suppose that the undular bore is confined to the region $X_a(T) < X < X_b(T)$, so that $[U] = U(X_b) - U(X_a)$. Therefore from (4.12), the jump variation over time is given by

$$[U]_T = \frac{d}{dT} \int_{X_a}^{X_b} U_X\, dX. \tag{4.13}$$

From the vKdV equation (4.4), we have

$$\int_{X_a}^{X_b} U_{XT}\, dX + \int_{X_a}^{X_b} (3U^2 + U_{XX})_{XX}\, dX = 0. \tag{4.14}$$

Using the fact that

$$\frac{d}{dT} \int_{X_a}^{X_b} U_X\, dX = \int_{X_a}^{X_b} U_{XT}\, dX + U_X|_{X=X_b}\dot{X}_b - U_X|_{X=X_a}\dot{X}_a, \tag{4.15}$$

we obtain from (4.14) and (4.15)

$$[U]_T = 0,$$

provided $U_X = U_{XXX} = 0$ at $X = X_{a,b}(T)$. Since the undular bore propagates into the undisturbed depth region, $U(X_b) = 0$, we have

$$[U] = -U_0 \qquad \text{for all} \qquad T > 0. \tag{4.16}$$

Note that the result (4.16) is unaffected by the varying coefficient $\beta(T)$. Thus, once the undular bore emerges onto another constant depth with $\beta = \beta_1$, the jump, $[U]$, across the transformed bore remains the same. Therefore, assuming that the structure of the bore as a modulated wavetrain remains unchanged, the amplitude of the leading solitary wave of the transformed bore must be $2U_0$, i.e. unchanged from the incident bore. The modulation solution for the transformed undular bore will have the same form (4.9), but with X generally replaced by $X - \chi(m)$, where $\chi(m)$ is some function depending on the the variable coefficient $\beta(T)$ since it is no longer a centred fan but rather a more general simple-wave solution of the Whitham equations and can only be found from the full solution of the perturbed Whitham equations (2.57) (El *et al.*, 2007). The constant initial phase X_0 in the periodic wave solution (4.7) is then generally replaced by some function $X_0(m)$, which can be viewed as a "modulation phase shift" acquired by the undular bore due to its

interaction with variable topography. The functions $X_0(m)$ and $\chi(m)$ are related to each other. The calculation of the phase shift requires solution of the full perturbed Whitham system (2.57) and is beyond the scope of the thesis. We also note that a similar phase shift also arises in the interactions of dispersive shock waves with rarefaction waves (El *et al.*, 2012), which is to some degree analogous to the present problem of the transformation of the undular over sloping bottom.

4.2.2.2 Slowly decreasing depth

4.2.2.2.1 The leading edge

Now, we will look at the propagation of undular bores over a slowly decreasing depth topography, i.e. $\beta_T < 0$ in the vKdV equation (4.4). We first assume that the leading solitary wave of the undular bore evolves as an isolated soliton (the "weak soliton interaction" scenario) when the depth decreases slowly (this will be later confirmed by the analysis of the behaviour of the modulation Riemann invariants near the leading edge of the undular bore from numerical simulations). This assumption immediately implies that the amplitude of the leading solitary wave must vary adiabatically to conserve the action flux (momentum).

As was mentioned in Chapter 3, when a single soliton propagates over a slowly changing bottom surface, it deforms adiabatically such that its amplitude changes proportionally to h^{-1}. Here, it is instructive to derive the counterpart of this result for the vKdV equation (4.4), which possesses the conservation law of wave action flux

$$\frac{d}{dT} \int_{-\infty}^{\infty} U^2 \, dX = 0. \tag{4.17}$$

The slowly varying solitary wave solution for (4.4) is given by

$$U \sim a \operatorname{sech}^2(\gamma(X - \Phi(T))), \quad V = \Phi_T = 2a = 4\beta\gamma^2, \tag{4.18}$$

where the amplitude a etc. are slowly varying function of T. Substituting (4.18) into (4.17) yields

$$\frac{a^2}{\gamma} = 2\beta^2\gamma^3 = \text{constant}. \tag{4.19}$$

From the above equation, we have $\gamma \sim \beta^{-2/3}$ and $a \sim \beta^{-1/3}$. With the help of (4.5), we obtain $a \sim h^{-3/4}$. Since $U = h^{1/4}A$, so the result follows.

The amplitude of the leading solitary wave in the undular bore before the slope is $2U_0$. As it propagates over a slowly decreasing depth region, it will behave as if detached from the

undular bore. Thus, its amplitude must vary according to $a = 2U_0\beta^{-1/3}$ for $T_0 < T < T_1$. Once it emerges onto the shallower shelf, $T > T_1$, its amplitude is $a = 2U_0\beta_1^{-1/3} > 2U_0$. The trajectory of the solitary wave is

$$X = \Phi(T) = \int_0^T 4U_0\beta(T')^{-1/3}\, dT'. \qquad (4.20)$$

This clearly contradicts to our original assumption in the previous subsection that a single undular bore with the leading solitary wave having an amplitude of $2U_0$ will emerge onto the shelf after the slope. To resolve the above inconsistency, an additional solitary wavetrain should be added at the front of the undular bore to provide a gradual increase of the amplitude from $2U_0$ at the leading edge of the undular bore to the value of $2U_0\beta^{-1/3}$ implied by the momemtum conservation for an isolated solitary wave.

Thus, the propagation of an undular bore over a broad region of slowly decreasing depth would lead to a non-adiabatic effect: the generation of a solitary wavetrain in front of the bore. The adiabatic deformation of the bore itself is twofold:

(a) the change of the characteristic scale of the oscillations in the bore due to the change of the dispersion coefficient β in (4.4);

(b) the occurrence of the additional slow 'modulation phase shift' $X_0(m)$ throughout the bore so that the relevant modulation solution generally represents a non-centred simple wave of the Whitham equations.

All the described adiabatic and non-adiabatic deformations of the undular bore on a slope will be confirmed numerically.

4.2.2.2.2 The trailing edge

At the trailing edge of the undular bore, the amplitude of the modulated wave vanishes and it transforms into a linear wave packet. At the initial stage of the evolution (i.e. $0 < T < T_0$ for the vKdV equation (4.4)), the linear wave packet at the trailing edge of the undular bore propagates over the background, $U = U_0$ and the amplitude varies according to the Green's law. Thus, the linear dispersion relation for this wavepacket is given by

$$\omega = 6kU_0 - \beta(T)k^3\,, \qquad (4.21)$$

where $\beta(T) = 1$ for $0 < T < T_0$. The velocity of the trailing edge, $s_- = -6U_0$, following from the modulation solution (4.9), must coincide with the linear group velocity $\partial\omega/\partial k$.

Thus, we have

$$\frac{\partial \omega}{\partial k} = 6U_0 - 3k_0^2 = -6U_0, \tag{4.22}$$

which gives the value of the wavenumber at the trailing edge, $k_0 = 2U_0^{1/2}$. This is valid for the initial stage of the evolution, $0 < T < T_0$. Note that this result is in agreement with the modulation formula (4.11) when we consider $m \to 0$. As we have established in Section 4.2.2, the modulation solution (4.9) and the jump (4.16) across the bore are not influenced by the variations of $\beta(T)$. Therefore, if the structure of the bore is to remain unchanged, the velocity of the trailing edge must also remain the same, i.e. $-6U_0$ for $T > T_1$, i.e. when the bore emerges onto the constant shelf with $\beta = \beta_1 < 1$ (for the decreasing depth).

Now, we consider the equation for the conservation of waves

$$k_T + \omega_X = 0, \tag{4.23}$$

which is always valid for modulation dynamics (Whitham, 1974) and is consistent with the perturbed modulation system (2.56) regardless of the specific form of the perturbation term. On substitution of (4.21) into (4.23), we have

$$k_T + (6U_0 - 3\beta(T)k^2)k_X = 0. \tag{4.24}$$

Solving (4.24) using the method of characteristics, we obtain

$$k = k_0 \qquad \text{on} \qquad \frac{dX}{dT} = 6U_0 - 3\beta(T)k^2.$$

So, when the undular bore emerges onto the new shelf, $\beta(T) = \beta_1$, the group velocity of the trailing edge becomes

$$s_-^* = 6U_0 - 3\beta_1 k_0^2 = 6U_0(1 - 2\beta_1). \tag{4.25}$$

For slowly decreasing depth, $\beta_1 < \beta_0 = 1$ and (4.25) implies that $s_-^* > s_- = -6U_0$. Thus, the "new" trailing edge will be located *inside* the "main" undular bore restoring its original structure after the interaction with the sloping bottom. This implies the simultaneous occurrence of two waves in the region close to the trailing edge of the transformed bore. Hence, the splitting of the linear group velocity characteristic, shown in Figure 4.2, has an important implication in terms of the structure of the undular bore. Indeed, due to this splitting, one expects that the undular bore propagation over slowly decreasing depth region will exhibit a multi-phase (presumably two-phase) behaviour near the trailing edge. This will be confirmed by direct numerical simulations.
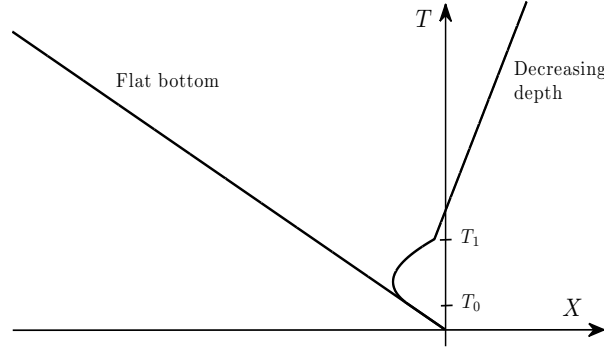
Figure 4.2: The linear group velocity characteristics plot for flat bottom and decreasing depth propagation.

4.2.2.2.3 Evolution of the undular bore over a region of slowly decreasing depth: numerical simulation

In the right panel of Figure 4.3, we present the evolution of an undular bore over a slowly decreasing depth region obtained from numerical simulations of the vKdV equation (3.25) (see Appendix A.2) with the following depth profile:

$$h(\tau) = \begin{cases} 1.0 & : \tau < 400 \\ \left(1 - \frac{\alpha(\tau - 400)}{2}\right)^2 & : 400 < \tau < 844.44 \\ 0.64 & : \tau > 844.44 \end{cases}, \qquad \alpha = 0.0009. \qquad (4.26)$$

The initial condition is taken as

$$B(X, 0) = \frac{1}{4}(1 - \tanh(\frac{X}{10})), \qquad (4.27)$$

so that an undular bore is fully developed before the slope, $\tau < 400$. As a comparison, the left panel of the Figure 4.3 shows the undular bore propagation over a flat bottom, $h(\tau) = 1$.

In plot 4 in the right panel of Figure 4.3, one can clearly see that there is a solitary wavetrain attached to the front of the undular bore when the transformed bore emerges onto a shallower shelf. The leading solitary wave of the undular bore itself has the same amplitude as in the incident bore, i.e. $2U_0$. One can also see the multi-phase behaviour at the rear part of the bore as shown in plot 3 in the right panel of Figure 4.3 (see also Figure 4.4 for a clearer illustration). This multi-phase behaviour continues for some time after the bore emerges onto the shelf. The bore will restore its single-phase slowly modulated wave behaviour throughout the entire bore at sufficiently large time. The multi-phase behaviour

4.2.2 Slowly varying topography

does not affect the front part of the bore, which retains its single-phase structure all the time.
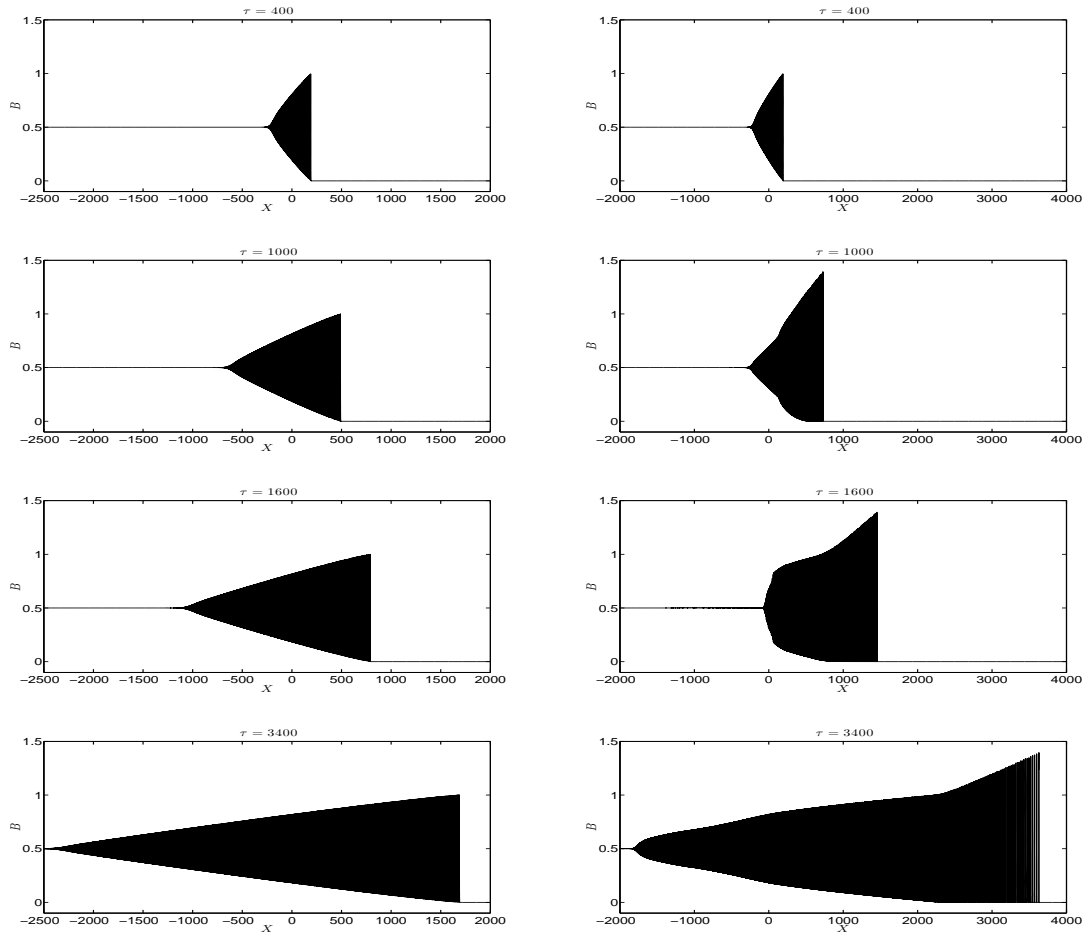
Figure 4.3: Numerical solution of the vKdV equation (3.25) with the initial condition (4.27). Left panel: propagation of an undular bore over a constant bottom; Right panel: propagation of an undular bore over a slowly decreasing depth topography with the profile $h(\tau)$ given by (4.26).
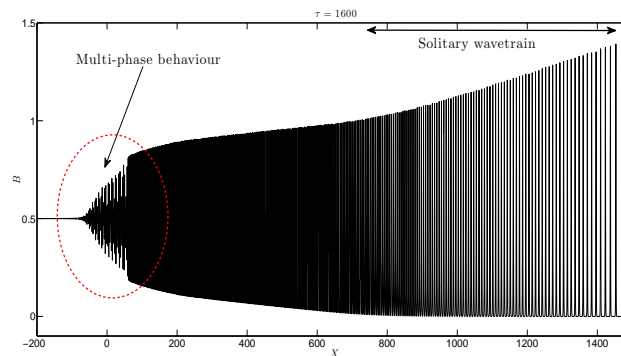

Figure 4.4: The occurrence of multi-phase behaviour at the rear part of the undular bore when the bore propagates over a slowly decreasing depth region.
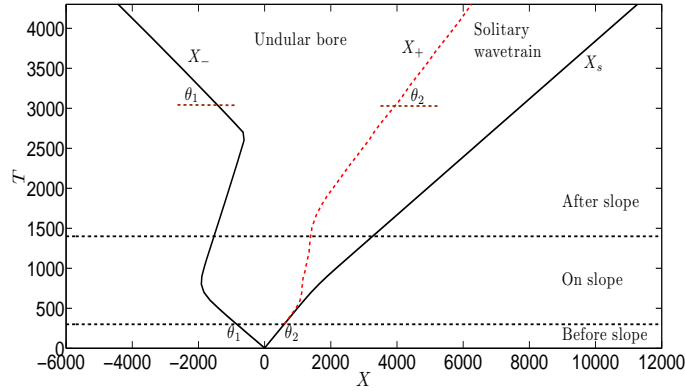
4.2.2 Slowly varying topography

Figure 4.5: X-T plane of the evolution of an undular bore over a slowly decreasing depth region according to the vKdV equation (4.4). The undular bore and the solitary wavetrain are confined to $[X_-(T), X_+(T)]$ and $[X_+(T), X_s(T)]$ respectively. One can see the spatial shift of $X_\pm(T)$ due to the interaction with the slope.

Figure 4.5 illustrates the boundaries of the undular bore, $X_\pm(T)$ obtained from the numerical simulation of the vKdV equation (4.4), which is exactly equivalent to (3.25), and will be used in our analytical construction below. The initial condition considered here is

$$U(X,0) = \frac{1}{4}\left(1 - \tanh\frac{x}{10}\right). \tag{4.28}$$

The depth profile is taken in the form of

$$h(T) = \frac{9}{50}\left(1 - \tanh\left(\frac{T - 450}{150}\right)\right) + 0.64,$$

so that the variable coefficient $\beta(T) = h^{9/4}$ will have a very smooth transition between $\beta = 1$ and $\beta \approx 0.367$ over the interval $\Delta T \approx 1100$. X_s is the position of the leading soliton in the solitary wavetrain, which was the leading solitary wave of the initial undular bore.

Figure 4.6 shows the comparison for the numerically obtained velocity of the linear wavepacket at the trailing edge of the undular bore and the linear group velocity predicted by formula (4.25). One can see that the velocity of the trailing edge of the incident bore increases due to the interaction of the linear wave packet with the slope as predicted by the linear wave group velocity (4.25) before it restores to the value of $-6U_0$. This non-monotonic behaviour of the trailing edge of the undular bore (see the curve $X_-(T)$ in Figure 4.5) is another feature of the propagation of undular bore over a slope besides the formation of the solitary wavetrain ahead of the bore. This behaviour is not clear in Figure 4.3.
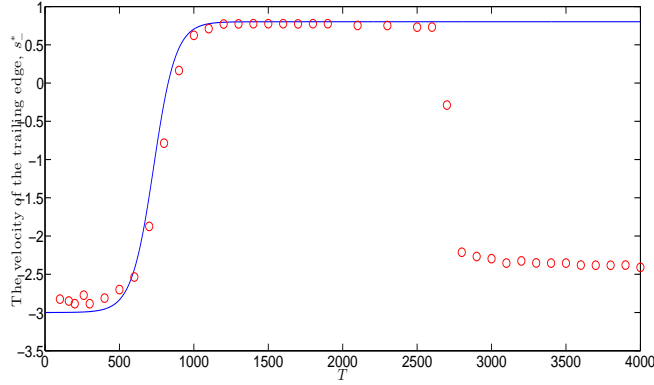
4.2.2 Slowly varying topography

Figure 4.6: Comparison for the numerically obtained velocity of the trailing edge of the undular bore propagating over a slowly decreasing depth region – circles; and the linear group velocity predicted by the formula (4.25) over the same slope – solid line.

So far, we can make three conclusions based on our analysis and confirmed by our numerics presented in Figures 4.3 – 4.5:

(a) the propagation of undular bore into the region of slowly decreasing depth leads to generation of a large-amplitude solitary wavetrain ahead of the bore,

(b) the asymptotic values of the velocities of the trailing and leading edges of the undular bore, $X'_-(T) = \cot(\theta_1)$ and $X'_+(T) = \cot(\theta_2)$ remain unchanged after the interaction with variable topography (see Figure 4.5),

(c) there are spatial shifts in the position of the trailing and leading edge of the transformed undular bore relative to the initial bore, and

(d) the occurrence of the multi-phase behaviour near the trailing edge.

We note that a similar observation to (a) was made by Ablowitz *et al.* (2009) in one of the cases where an undular bore interacts with a rarefaction wave, producing a soliton wavetrain in front of the undular bore. They also observed a transient multi-phase behaviour at the rear part of the undular bore. These similarities between two apparently different problems are not surprising when one observes that, in our present formulation, the undular bore essentially propagates through the "rarefaction region" of the decreasing depth. The essential difference is, of course, that in our problem the profile $h(x)$ of the "rarefaction region" is fixed and described by the variable coefficients in the vKdV equation, while the evolving profile of the hydrodynamic rarefaction wave in Ablowitz *et al.* (2009) is given by the relevant solution (2.10) of the constant-coefficient KdV equation.

4.2.2.2.4   Formation and evolution of the solitary wavetrain

Here, we will construct the asymptotic description for the solitary wavetrain generated in front of the undular bore when entering a slowly decreasing depth region. In general, the local solitary wavetrain can be described, up to a constant phase shift, by an asymptotic expression (Grimshaw, 1970; Whitham, 1974)

$$0 < X < 1/\kappa : \qquad U \sim a \operatorname{sech}^2(\gamma\Theta) , \quad \Theta_T = -\kappa V , \Theta_X = \kappa , \qquad (4.29)$$

$$\text{where} \quad V = 2a = 4\beta\gamma^2\kappa^2 ; \qquad (4.30)$$

$$U(\Theta + 1) = U(\Theta) .$$

The term "locally" here implies distances comparable with a single spatial period $L = 1/\kappa$. In a modulated solitary wavetrain, a and κ are slowly varying functions of X and T (i.e. they vary on the scale much larger than $1/\kappa$) so that (4.29) can be viewed as a natural extension of (4.18) for a single slowly varying soliton, and it reduces (within each period) to that expression when one sets $\kappa = 1$. Here, the initial phase is not fixed in (4.29) as we are only interested in the behaviour of slow modulations of $a(X,T)$, and $\kappa(X,T)$.

The modulation equations for the amplitude a and the soliton train wavenumber κ are given by

$$\left\{\frac{a^2}{\kappa\gamma}\right\}_T + V\left\{\frac{a^2}{\kappa\gamma}\right\}_X = 0 , \qquad (4.31)$$

$$\kappa_T + (V\kappa)_X = 0 . \qquad (4.32)$$

The system (4.31), (4.32) was obtained by Grimshaw (1979) using a multiple-scale expansion of the vKdV solution with the leading term in the form (4.29). The amplitude equation (4.31) can also be obtained directly, using averaging of the KdV 'mass' conservation law via the averaged Lagrangian approach (Whitham, 1974). It is not difficult to show that the amplitude equation (4.31) is consistent with the soliton limit ($m \to 1$) of the full perturbed Whitham modulation equations (2.62) derived in El *et al.* (2007) for the perturbed KdV equation (4.3) (note the change of independent variables). We also need to stress that equation (4.32) is valid only asymptotically for $1 - m \ll 1$, i.e. within the range of validity of the approximation (4.29).

Using the relation (4.30), we can rewrite equations (4.31) and (4.32) as

$$\mathcal{A}_\sigma + 2\mathcal{A}\mathcal{A}_X = 0 , \qquad (4.33)$$

$$\kappa_\sigma + (2\mathcal{A}\kappa)_X = 0 , \qquad (4.34)$$

4.2.2 Slowly varying topography

where

$$\sigma = \int_0^T \beta(T')^{-1/3} dT', \tag{4.35}$$

$$\mathcal{A} = \left\{ \frac{a^2}{\sqrt{2}\kappa\gamma} \right\}^{2/3} = a\beta^{1/3}. \tag{4.36}$$

The system (4.33) and (4.34) for $\mathcal{A}(X,\sigma)$ and $\kappa(X,\sigma)$ has the same form as the system (4.31, 4.32) for $a(X,T)$ and $\kappa(X,T)$ in the case when $\beta = \beta_0 = constant$ (and so $a = 4\beta_0\gamma^2\kappa^2$), i.e. for the constant-coefficient KdV equation.

$\mathcal{A}, \kappa$ are constants when there is no X-variation and we recover the result (4.19). By using the method of characteristics, the general solution for (4.33) and (4.34) is

$$\mathcal{A} = \text{constant}, \quad \text{on} \quad \frac{dX}{d\sigma} = 2\mathcal{A}, \tag{4.37}$$

$$\text{and} \quad \frac{d\kappa}{d\sigma} = -2\mathcal{A}_X \kappa = \frac{\mathcal{A}_\sigma}{\mathcal{A}}\kappa. \tag{4.38}$$

Note that the system (4.37), (4.38) has only one multiple characteristic family and all the characteristics are straight lines in the X-σ plane.

Now, let us define the position of the trailing edge of the solitary wavetrain as the line $X = X_+(T)$ where $a = 2U_0$. This definition is consistent with the location of the leading edge of the undular bore for the flat bottom propagation case. Let the initial velocities for both the trailing edge of the solitary wavetrain and the leading edge of the undular bore be $X'_+(T_0) = 4U_0$. In the current problem for the varying bottom case, the line $X = X_+(T)$ is not associated with the trajectory of a particular solitary wave. This is because the solitary waves must be allowed to cross this boundary to enable the formation of the advancing modulated solitary wavetrain. Thus we have

$$0 < X'_+(T) < 4U_0 \quad \text{for} \quad T_0 < T < T_1. \tag{4.39}$$

So the boundary condition for the solitary wavetrain amplitude equation (4.33) is

$$\mathcal{A} = 2U_0\beta^{1/3} \quad \text{on} \quad X = \bar{X}(\sigma), \tag{4.40}$$

where $\bar{X}(\sigma) = X_+(T(\sigma))$. $T(\sigma)$ is the inverse relation of (4.35), so that $\sigma(T(\sigma)) = \sigma$. The latter relationship requires that $\beta(T)$ varies monotonically from 1 at $T = T_0$ to β_1 at $T = T_1$.

The solution for $\mathcal{A}$ in (4.37) is

$$\mathcal{A} = \mathcal{A}_0(\sigma_0) = 2U_0\beta^{1/3}(T(\sigma_0)), \quad X - \bar{X}(\sigma_0) = 2\mathcal{A}_0 \cdot (\sigma - \sigma_0), \tag{4.41}$$

4.2.2 Slowly varying topography

$\sigma_0 \in [0, \sigma_1]$ is a parameter on the curve $X = \bar{X}(\sigma)$. Formally, elimination of the parameter σ_0 from (4.41) yields $\mathcal{A}$ as a function of X and σ. The solution (4.41) is defined for $\bar{X}(\sigma) < X < X_s$, where $X_s = 4U_0\sigma$ is the trajectory of the leading soliton in the solitary wavetrain (see (4.20)), having amplitude $a = 2U_0\beta^{-1/3}$, i.e. $\mathcal{A} = 2U_0$. Ahead of the solitary wavetrain, where $X > 4U_0\sigma$, we have $\mathcal{A} = 0$.

From the first equation in (4.41), the derivative $\mathcal{A}_X$ is given by

$$\mathcal{A}_X = \frac{d\mathcal{A}}{d\sigma_0}\frac{\partial \sigma_0}{\partial X} = \mathcal{A}_0'(\sigma_0)\frac{\partial \sigma_0}{\partial X}. \tag{4.42}$$

Note that $\mathcal{A}_X$ is a partial derivative. The expression $\frac{\partial \sigma_0}{\partial X}$ can be obtained from the second equation in (4.41) by implicit differentiation

$$1 - \bar{X}'(\sigma_0)\frac{\partial \sigma_0}{\partial X} = 2\mathcal{A}_0'(\sigma_0)\frac{\partial \sigma_0}{\partial X} \cdot (\sigma - \sigma_0) - 2\mathcal{A}_0(\sigma_0)\frac{\partial \sigma_0}{\partial X}. \tag{4.43}$$

Thus, from (4.42) and (4.43), the derivative $\mathcal{A}_X$ is

$$\mathcal{A}_X = \frac{\mathcal{A}_0'(\sigma_0)}{2\mathcal{A}_0'(\sigma_0)(\sigma - \sigma_0) + [\bar{X}'(\sigma_0) - 2\mathcal{A}_0(\sigma_0)]}. \tag{4.44}$$

With the help of (4.39), we have the relation $[\bar{X}'(\sigma_0) - 2\mathcal{A}_0(\sigma_0)] < 0$. Therefore, in order to guarantee the existence of the obtained solution for all X and σ, we must have $\mathcal{A}_0' < 0$. This implies that $\beta'(T) < 0$ from (4.35) and (4.41). Then our solution represents a rarefaction fan emanating from the curve $X = \bar{X}(\sigma_0)$. Therefore, the condition $\beta'(T) < 0$ (decreasing depth) can be viewed as the condition of the formation of an expanding solitary wavetrain in front of the bore. This confirms our initial assumption that the leading solitary wave of the undular bore behaves as an isolated solitary wave when the bore advances into the decreasing depth region.

The corresponding general solution for κ can be found by substituting (4.44) into (4.38), which gives

$$\frac{d\kappa}{d\sigma} = \frac{-2\kappa\mathcal{A}_0'(\sigma_0)}{2\mathcal{A}_0'(\sigma_0)(\sigma - \sigma_0) + [\bar{X}'(\sigma_0) - 2\mathcal{A}_0(\sigma_0)]}. \tag{4.45}$$

The above equation can be integrated to give

$$\kappa = \kappa_0\left\{1 + \frac{2\mathcal{A}_0'(\sigma_0)(\sigma - \sigma_0)}{\bar{X}'(\sigma_0) - 2\mathcal{A}_0(\sigma_0)}\right\}^{-1}, \tag{4.46}$$

where κ_0 is the value of κ on the curve $X = X_+(T(\sigma_0)) = \bar{X}(\sigma_0)$ and $\sigma_0(X, \sigma)$ is defined by (4.41).

To find the curve $X = X_+(T)$ for $T_0 < T < T_1$, it is instructive to assume that

$$X_+'(T) \ll 4U_0 \quad \text{for} \quad T_0 < T < T_1, \tag{4.47}$$

and thus $\bar{X}'(\sigma_0) \ll 2\mathcal{A}_0(\sigma_0)$. This behaviour can be formally justified for functions $\beta(T)$ varying sufficiently fast on a typical time scale of the solitary wavetrain modulations (but still being slow functions on the time scale of a single soliton). Indeed, since $X'_+(T_0) = 4U_0$, in order to satisfy (4.39), one must have $X''_+(T) < 0$ (it is clear that $\text{sign}\, X''_+(T) = \text{sign}\, \beta'(T)$). Then the result follows as an asymptotic behaviour of $X_+(T)$ for sufficiently large T. Thus we have

$$X_+(T) \simeq X_+(T_0) = 4U_0 T_0 \quad \text{for} \quad T_0 < T < T_1. \tag{4.48}$$

Our numerical simulations show that behaviour (4.48) establishes itself quite quickly even for rather slow functions $\beta(T)$. This is shown in Figure 4.5, which corresponds to $\beta_T \sim 5 \cdot 10^{-4}$. For larger values of β_T, say $\beta_T \sim 10^{-3} - 10^{-2}$, the boundary $X_+(T)$ becomes stationary almost immediately as variations of β begin at $T = T_0$. X_+ resumes its motion at $T = T_1$ and gradually restores its initial velocity $4U_0$. Thus (4.47) and (4.48) can be safely used in the solution (4.41), (4.46) for a broad range of the slope values specified in terms of $\beta(T)$. The schematic behaviour of the boundaries $X_+(T)$ and $X_s(T)$ illustrating the asymptotic formulation of the problem of the generation of the solitary wavetrain on the given boundary $X = X_+(T) = X_+(T_0)$ for $T_0 < T < T_1$ is shown in Figure 4.7.
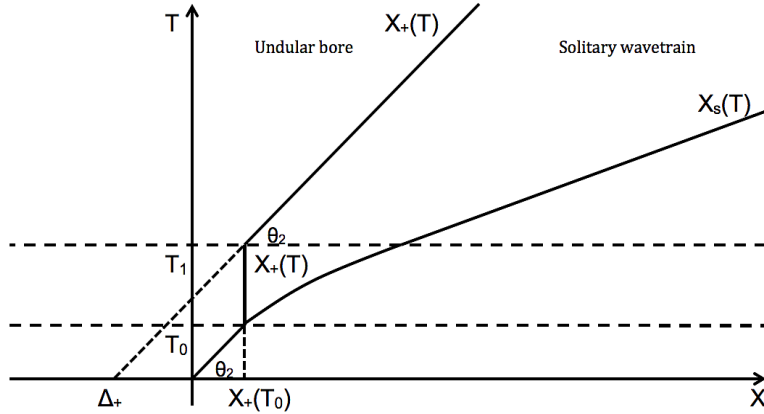

Figure 4.7: Schematic behaviour of the boundaries X_+ and X_s of the solitary wavetrain generated at the leading edge of the undular bore on a slope.

Thus, using (4.47), we have to leading order

$$\kappa \simeq \kappa_0 \left\{ 1 - \frac{\mathcal{A}'_0(\sigma_0)(\sigma - \sigma_0)}{\mathcal{A}_0(\sigma_0)} \right\}^{-1} = \kappa_0 \left\{ 1 - \frac{2}{3} \frac{\beta'(\sigma_0)}{\beta(\sigma_0)}(\sigma - \sigma_0) \right\}^{-1}, \tag{4.49}$$

where $\beta(\sigma_0) \equiv \beta(T(\sigma_0))$ so that $\beta'(\sigma_0) = \beta_T \beta^{1/3}(\sigma_0) < 0$ and therefore the solution (4.49) exists for all X and σ. Then the leading edge of the undular bore, that is also the trailing edge of the solitary wavetrain, emerging on the shelf is $X_+(T) \simeq 4U_0 T_0 + 4U_0(T - T_1)$ for

4.2.2 Slowly varying topography

$T > T_1$ and the phase shift $\Delta_+ = \chi(1)$ can be estimated as $\Delta_+ \simeq -4U_0(T_1 - T_0)$. Of course, one can guarantee the linear behaviour of $X_+(T) \sim 4U_0 T$ only for $T \gg T_1$ when the slowly modulated structure of the undular bore fully adjusts itself to the shelf region with $\beta = \beta_1$.

Let $\sigma_1 = \sigma(T_1)$. Then, on the shelf, where $T > T_1, \sigma > \sigma_1$, we have $\beta = \beta_1, \sigma = \sigma_1 + (T - T_1)\beta_1^{-1/3}$. The leading edge of the solitary wavetrain on the shelf is $X_s = 4U_0\sigma = 4U_0(\sigma_1 + (T - T_1)\beta_1^{-1/3})$. We note that for $T > T_1$, both boundaries $X_+(T)$ and $X_s(T)$ confining the expansion fan are characteristics and the total number of solitary waves in the train for $T > T_1$ does not change with time.

The wavenumber in the bore is given by the formula (4.11),

$$k = \frac{\pi U_0^{1/2}}{\beta^{1/2} K(m)} . \tag{4.50}$$

If we consider the solitary wavetrain as a small wavenumber asymptotic of the modulated cnoidal wave we must have (see Whitham, 1974)

$$1 - m \ll 1 : \qquad \kappa \simeq \frac{k}{2\pi} , \tag{4.51}$$

which suggests a continuous matching between $k/(2\pi)$ in the undular bore and $\kappa = \kappa_0$ in the solitary wavetrain at the leading edge $X_+(T)$ of the undular bore. This continuous matching, however, is not possible for the following reason.

The asymptotic behaviour of k in the modulation solution (4.9) near the leading edge $X = X_+(T)$ is (Gurevich & Pitaevskii, 1974)

$$k \sim \frac{2\pi}{\beta^{1/2}} \frac{U_0^{1/2}}{\ln(1/(s_+ - s))} , \tag{4.52}$$

where $s = X/T$, $s_+ = X_+/T = 4U_0$. This implies that $|k_X| \to \infty$ while $k \to 0$ when $X \to X_+$. Thus the wavenumber varies rapidly near $X = X_+$. On the other hand, the typical spatial scale of the variations of modulations in the advancing solitary wavetrain is much greater than that in the undular bore. Therefore, it is natural to require matching of κ with the *mean value* of $k/(2\pi)$ across the undular bore front, which one can naturally define as the (soliton) part of the bore propagating to the right, i.e. $0 < X < X_+$ (note that $X = 0$ is the characteristic of the modulation system separating the "rightward and leftwards propagating" parts of the characteristic fan (4.9)). The mean value of k across the bore front is then

$$\overline{k} = \frac{1}{X_+} \int_0^{X_+} k \, dX = \frac{1}{4U_0} \int_{m^*}^1 k(m) \cdot \left(\frac{ds}{dm}\right) dm , \tag{4.53}$$

4.2.2 Slowly varying topography

where $s(m)$ is given by the modulation solution (4.9) and $m^* \approx 0.6415$ — the value of m on the characteristic $X = 0$ — is the root of the equation $s(m) = 0$. Then, using (4.50) we obtain

$$\overline{k} = \frac{\pi U_0^{1/2}}{2\beta^{1/2}} I, \tag{4.54}$$

where

$$I = \int\limits_{m^*}^{1} \frac{W'(m)}{K(m)} dm \approx 0.6569, \tag{4.55}$$

$$W(m) = 1 + m - \frac{2m(1-m)K(m)}{E(m) - (1-m)K(m)}. \tag{4.56}$$

Thus we have

$$\kappa_0 = \frac{\overline{k}}{2\pi} = \frac{U_0^{1/2}}{4\beta^{1/2}} I, \quad \text{where} \quad I \approx 0.6569. \tag{4.57}$$

Now, from (4.30) and (4.36), we have $\gamma(X,T) = \kappa^{-1}\beta^{-1/3}(\mathcal{A}/2)^{1/2}$ and so the slowly varying solitary wavetrain (4.29) is fully defined. As $T \to \infty$, $\sigma \sim T\beta_1^{-1/3}$, $X_+ \sim 4U_0 T$, $X_s \sim 4U_0\beta_1^{-1/3}T$ and the asymptotic solution is,

$$4U_0 T < X < 4U_0\beta_1^{-1/3}T: \qquad \mathcal{A} \sim \frac{X}{2\sigma}, \quad \text{or} \quad a \sim \frac{X}{2T}, \tag{4.58}$$

$$\kappa \sim \frac{g(X/(2T))}{\sigma} \sim \frac{g(\mathcal{A})}{\sigma}, \quad \text{or} \quad \kappa \sim \frac{G(a)}{T}. \tag{4.59}$$

Here $g(\mathcal{A}) = 3\kappa_0\beta(\sigma_0)/(2\beta'(\sigma_0))$, where $\sigma_0(\mathcal{A})$ is found from the solution $\mathcal{A} = 2U_0\beta^{1/3}(\sigma_0)$ (see (4.41)). As a matter of fact, $g(\mathcal{A})$ is only defined for the variable coefficient region $0 < \sigma_0 < \sigma_1$, where $\beta'(\sigma) \neq 0$ and where the generation of the solitary wavetrain occurs. The function $G(a) = g(a\beta_1^{1/3})$ has the meaning of the distribution function over amplitude in the solitary wavetrain so that $G(a)da$ is the number of solitons with amplitudes in the interval $[a, a + da]$ (Whitham, 1974). Since the total number of solitons N in the train remains constant for $T > T_1$ it can be estimated by the formula

$$N \simeq \int_{2U_0}^{2U_0\beta_1^{-1/3}} G(a)\, da. \tag{4.60}$$

From our solution (4.49), when $\beta_T > 0$, the interaction of the solitary wavetrain with the increasing depth topography would increase the density of solitary waves. This will enhance their interaction and eventually rendering invalid the basic assumption about the isolated character of solitary waves in the wavetrain. Also, the amplitude profile specified by the solution (4.41) with $\beta'(T) > 0$ will develop a breaking singularity at some $\sigma = \sigma_c$ also making this solution physically invalid. All this suggests that one should not expect the generation of the chain of individual non-interacting solitons in front of the bore if
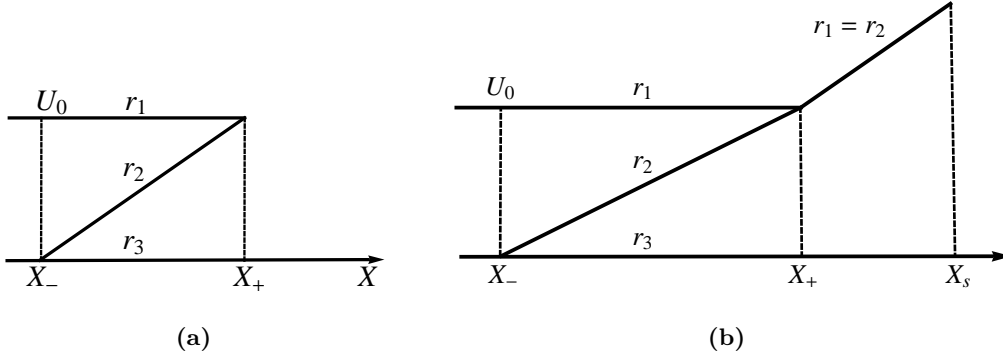
Figure 4.8: Schematic behaviour of the Riemann invariants in the modulation solution. (a) Regular undular bore (before the slope, $T < T_0$); (b) Undular bore with an advancing soliton train confined to $[X_+, X_s]$ (after the slope, $T \gg T_1$)

$\beta'(T) > 0$. Instead, this case appears to be relevant to the realisation of the second (nonlocal) "strong interaction" scenario of the undular bore evolution.

The transformation of an undular bore over a slowly decreasing depth region can be illustrated in terms of Riemann invariants, $r_j, j = 1, 2, 3$ of the Whitham equations. The schematic illustrations of the behaviour of the Riemann invariants before and after the slope are shown in Figure 4.8. In the solitary wavetrain region, we have $r_1 = r_2$. This behaviour will be confirmed by numerical results in the following section.

4.2.2.2.5   Numerical Results

Now, we will use numerical results to confirm our fundamental assumptions used in the modulation analysis in the previous subsections:

(a) an undular bore on a slope can be described by a slowly modulated periodic solution of the KdV equation,

(b) the leading solitary wave in the undular bore behaves as an isolated KdV soliton as described by the "weak interaction scenario", and

(c) a solitary wavetrain is formed at front of the undular bore.

For the numerical simulations, we will use the vKdV equation of the form (3.25). The depth profile, $h(\tau)$ is given by (4.26) and the initial condition is (4.27). As mentioned in the beginning of this chapter, the vKdV equation (3.25) is exactly equivalent to the vKdV

4.2.2 Slowly varying topography

equation (4.4), which was used for our asymptotic analysis. The present form (3.25) is slightly more convenient for numerical simulations as it produces fewer waves for the same running time interval. The initial condition is taken in the form of a smooth step (4.27).

The results of our numerical simulations are presented in Figures 4.9 – 4.13. Each of the Figures 4.9 – 4.12 corresponds to a particular value of time, $\tau = \tau_i$ and consists of three plots: the top plot shows the numerical solution for $B(X, \tau_i)$, the middle plot shows the spatial behaviour of the numerical "Riemann invariants" r_j and the bottom plot shows the behaviour of the numerically determined value of the modulus m.

The parameters r_1, r_2 and r_3 in the middle plots are found in the following way. Assume that a locally undular bore is described by the periodic solution (4.7) (assumption (a) above). Then, from the numerical data for $B(X, \tau_i)$, we can find the values of the basic wave parameters b_1, b_2 and b_3 (see Chapter 2)

$$b_1 \equiv B_{\mathrm{max}}, \qquad b_2 \equiv B_{\mathrm{min}}, \tag{4.61}$$

and the third parameter b_3 can be obtained from the numerical values of the local spatial period (wavelength) L, which for the vKdV equation (3.25) is given by the formula

$$L = \frac{4h^{9/8}K(m)}{\sqrt{3(b_1 - b_3)}} \quad \text{where} \quad m = \frac{b_1 - b_2}{b_1 - b_3}. \tag{4.62}$$

Using the values of b_1, b_2 and b_3, we construct

$$r_3 = \frac{b_2 + b_3}{2}, \qquad r_2 = \frac{b_1 + b_3}{2}, \qquad \text{and} \qquad r_1 = \frac{b_1 + b_2}{2}, \tag{4.63}$$

which would play the role of the modulation Riemann invariants in the perturbed Whitham system (2.56).

Now, if the "numerical" distributions of r_1, r_2 and r_3 qualitatively agree with those implied by our modulation analysis (in particular, for the shoaling bores, we would expect to obtain the distributions schematically shown in Figure 4.8), this would be a strong confirmation of our basic assumption that the transformed undular bore retains its structure as a slowly modulated single-phase wave, which can be described by the relevant solution of the Whitham equations.

The plot for the modulus m will then give a convenient information of the detailed waveform of the oscillatory structure, and, in particular, will allow one to identify the region of the solitary wavetrain where $m = 1$.

In Figure 4.9, we present the initial undular bore before the slope, $\tau = 400$. This agrees with the Gurevich-Pitaevskii solution (4.7) with $\beta = 1$ and the modulus m is in the range

of 0 to 1 (bottom plot). The distribution of the numerical values of the Riemann invariants agrees with Figure 4.8a.
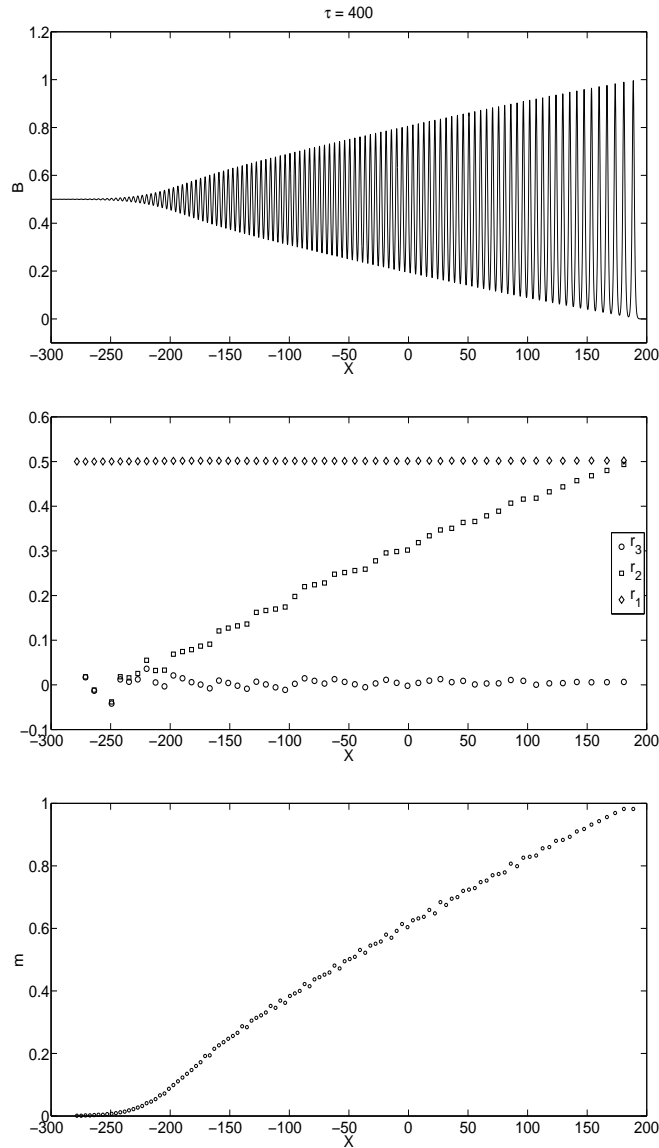

Figure 4.9: Initial undular bore (before the slope), $\tau = 400$. Upper plot: $B(X)$; Middle plot: the modulation Riemann variables $r_3 \leq r_2 \leq r_1$ obtained from the plot for $B(X)$ assuming a local representation of the wave in the form of a cnoidal periodic solution of the constant-coefficient KdV equation; Bottom plot: the modulus $m = (r_2 - r_3)/(r_1 - r_3)$ as function of X.

Figure 4.10 shows the evolution of the undular bore on the slope, $\tau = 800$. We can see the formation of the solitary wavetrain in front of the undular bore. This can be confirmed by the presence of the region where $r_1 = r_2$ or $m \rightarrow 1$.
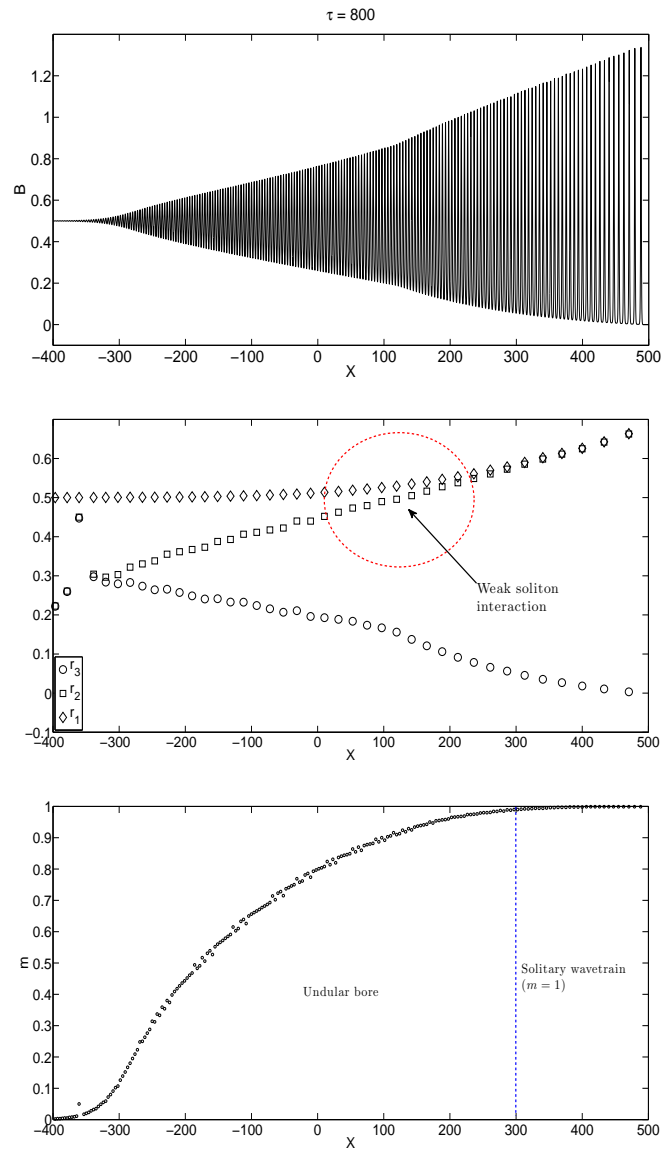
Figure 4.10: Same as in Figure 4.9 but for $\tau = 800$ (undular bore on the slope). One can see the solitary wavetrain ($m \to 1$ and $r_1 = r_2$) is formed between $X \approx 350$ and $X \approx 500$. The behaviour of the Riemann invariants near the leading edge is characteristics of the "weak interaction" (local) scenario (see Figure 2.11a).

In Figure 4.11, we present the plot of the undular bore "shortly" after the slope, $\tau = 1400$. We can observe that the solitary wavetrain retains its structure at the front part of the undular bore. Also, note the occurrence of the new multi-phase (presumably two-phase) region in the rear part of the undular bore. In this region, the modulus m is not defined (see the bottom plot).
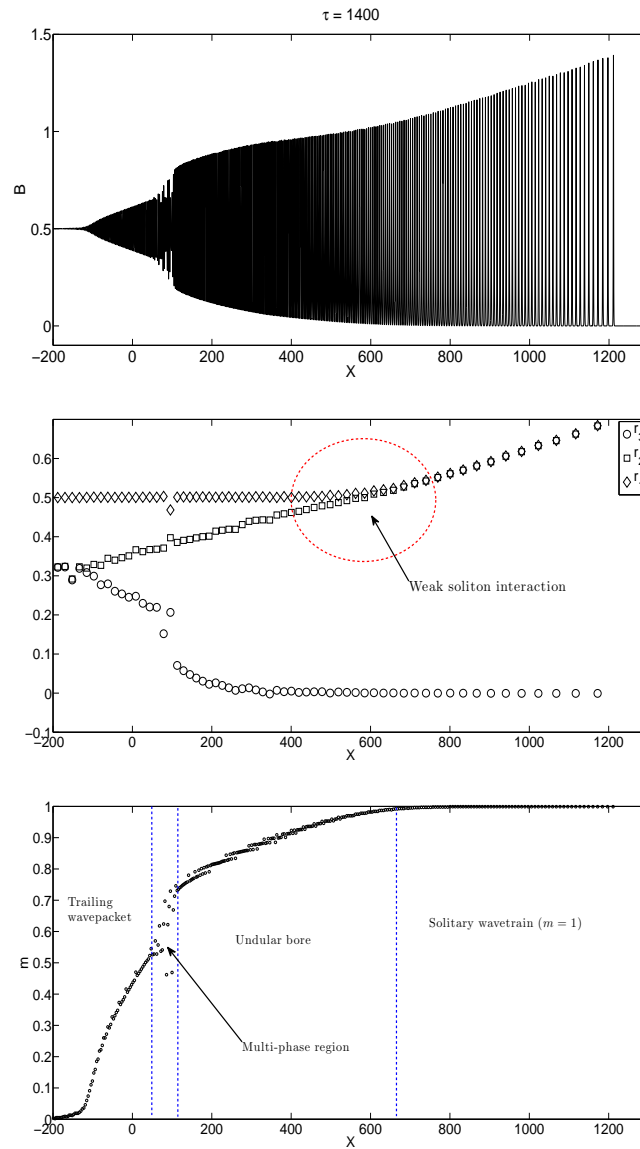
Figure 4.11: Same as in Figures 4.9, 4.10 but for $\tau = 1400$ (shortly after the slope). The solitary wave train is located between $X \approx 700$ and $X \approx 1200$. A multi-phase behaviour can be seen around $X = 100$.

Figure 4.12 corresponds to the long-time behaviour of the transformed bore after the slope. It is clear that we have a combination of two distinct wave structures in the transformed bore. At the front part, we have a solitary wavetrain joined by an undular bore behind it. The leading solitary wave amplitude of the undular bore has the same value as in the initial bore. The corresponding distribution of the Riemann invariants (the middle plot) agrees with our theoretical predictions as shown in Figure 4.8b.
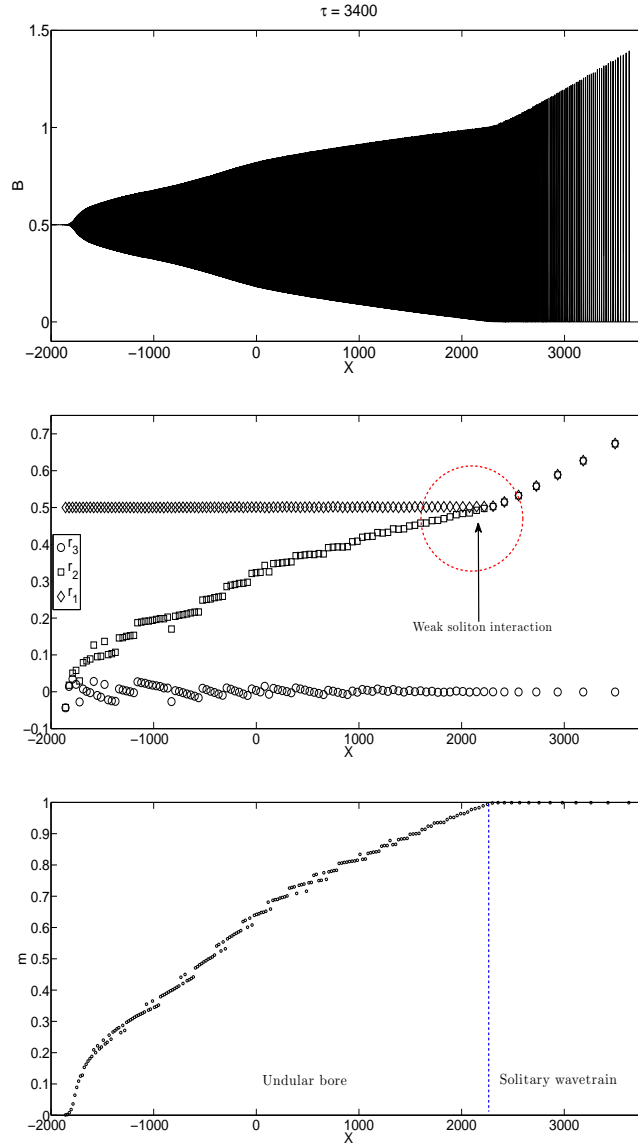
Figure 4.12: Same as in Figures 4.9, 4.10, 4.11 but for $\tau = 3400$ (long-time behaviour after the slope). The Riemann invariants distribution matches the schematic of the theoretical prediction in Figure 4.8b).

Note that the behaviour of the Riemann invariants near the leading edge of the bore in all the plots is similar to the diagram shown in Figure 2.11a, where $|dr_1/dX| < \infty$ and $|dr_2/dX| < \infty$. This confirms our assumption that the leading solitary wave of the undular bore behaves as an isolated soliton in the propagation over a decreasing depth region, which corresponds to the "weak soliton interaction" scenario. Therefore, the leading solitary wave must change adiabatically and behaves as a separate single soliton. The appearance of multi-valued regions in the distribution of modulus, m (the bottom plot), in Figures 4.9 – 4.12 are due to numerical artifact and it is not an indication of the presence of multi-phase interaction in the wavetrain. For the actual multi-phase interaction wavetrains, the
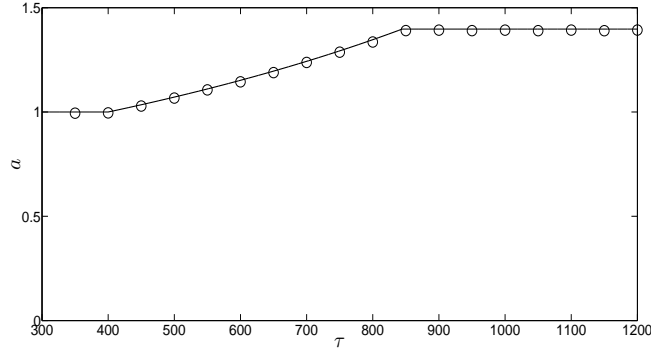
Figure 4.13: Comparison for the amplitude of the adiabatically varying solitary wave on a slowly decreasing depth region (formula (4.64) with $h_0 = 1$, $a_0 = 1$) – solid line; and the numerical data for the leading solitary wave in the modulated wavetrain (initially, a single undular bore on the same slope) – circles.

modulus, m is undefined, which is manifested in the numerical plots as chaotic collection of points. The same multi-valued regions of the same nature also present in the long-time numerical simulations for the flat-bottom propagation described by the constant-coefficient KdV equation. However, in this case an exact global single-phase modulation solution exists, which rules out the possibility of the multi-phase behaviour.

In Figure 4.13, we present a comparison for the amplitudes of the adiabatically varying isolated solitary wave on a slope with the numerical values of the leading solitary wave amplitude in the modulated wavetrain (initially a single undular bore) propagating over the same slope. In both cases, they have the same initial amplitude, $a = 1$.

Finally, we note that for the vKdV equation (3.25), the adiabatic variations of the solitary wave amplitude is given by the formula

$$a = a_0 \left(\frac{h_0}{h(\tau)} \right)^{3/4}, \qquad (4.64)$$

where h_0 and a_0 are the initial depth and the solitary wave amplitude respectively. Relationship (4.64) is an exact counterpart of the relationship (4.19) for the slowly varying solitary wave of the vKdV equation in the form (4.4). One can see that there is an excellent agreement between the numerics and formula (4.64). This provides direct quantitative confirmation of our assumption that the leading solitary wave of the undular bore evolves as an isolated solitary wave over the slowly decreasing depth region when $h'(\tau) < 0$.

4.2.2.3   Slowly increasing depth

4.2.2.3.1   The leading edge

Now, we will assume that the depth slowly increases, i.e. $\beta_T > 0$ in the vKdV equation (4.4). As our modulation analysis of the solitary wavetrain on a slope shows (see Section 4.2.2.2.4), the interaction of undular bores with slowly increasing depth topography must lead to the second interaction scenario described by El *et al.* (2007), which is "strong soliton interaction" (see Figure 2.11b). This will later be confirmed by the analysis of the Riemann invariants' behaviour obtained from the numerical simulations. Now, the evolution of the leading solitary wave cannot be found locally using the action wave conservation, as it was done in Section 4.2.2.2.1. In this case, in addition to local variations due to topography, one needs to take into account the interaction of the lead solitary wave with the wavetrain behind it. This would require the knowledge of the solution of the full perturbed Whitham system, which is generally unavailable at present. Thus, we only present some qualitative interpretation of the wave dynamics and perform numerical simulations to confirm our conclusions.

Because of the depth variations, the leading solitary wave amplitude of the initial undular bore decreases when it enters the variable topography region. Hence, in this case, there will be no formation of a solitary wavetrain ahead of the transformed bore. However, the nonlocal interaction near the leading edge will prevent the leading solitary wave diminishing further. Instead, it will cause the leading solitary wave to grow. Since the jump, $[U]$ across the bore remains unchanged (see (4.16)), the leading wave amplitude will eventually increase to the value of $2U_0$, which is the same as in the incident bore. Once this is achieved, the soliton interaction near the leading edge becomes weak again. This is because the leading solitary wave is now asymptotically close to the KdV soliton solution of the constant-coefficient KdV equation and is not constrained by the interaction of the wavetrain behind it (Khruslov, 1976; Claeys & Grava, 2010). The amplitude of the the leading solitary wave remains constant after that.

4.2.2.3.2   The trailing edge

When the depth is slowly increasing, $\beta_1 > \beta_0 = 1$, equation (4.25) implies that $s^*_- < s_- = -6U_0$. Therefore, the trailing edge of the incident bore with initial velocity $s_- = -6U_0$ would travel slower, $s^*_- < -6U_0$ when it advances through the slope. Since the bore restores
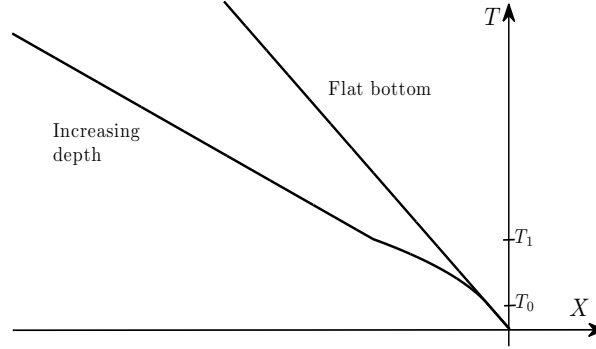
Figure 4.14: The linear group velocity characteristics plot for flat bottom and increasing depth propagation.

its structure when it emerges on a deeper shelf (an assumption to be confirmed by numerical simulation), the velocity of the trailing edge of the bore must remain $-6U_0$. Therefore, we need to insert an additional wave structure between the trailing edge of the undular bore travelling with velocity $s_- = -6U_0$ and the new trailing edge propagating with slower velocity $\tilde{s} < -6U_0$. The reasoning here is very similar to that used in Section 4.2.2.2.1, when we introduced solitary wavetrain ahead of the bore. Now, however, the required wave structure would be a weakly nonlinear wavetrain with the amplitude vanishing at the (new) trailing edge $\widetilde{X} = \tilde{s}T$ and stretching up to the point where its amplitude will match with the amplitude at some point near the trailing edge of the undular bore. The comparison for the behaviour of the linear group velocity over a slowly decreasing depth and that for a flat bottom is shown in Figure 4.14.

4.2.2.3.3   Evolution of the undular bore over a region of slowly increasing depth: numerical simulation

In the right panel of Figure 4.15, we present the evolution of an undular bore according to the vKdV equation (3.25) over a slowly increasing depth topography described by

$$h(\tau) = \begin{cases} 1.0 & : \tau < 400 \\ \left(1 + \frac{\alpha(\tau - 400)}{2}\right)^2 & : 400 < \tau < 960.7 \quad , \qquad \alpha = 0.0005. \\ 1.3 & : \tau > 960.7 \end{cases} \qquad (4.65)$$

The initial condition is given in (4.27) so that an undular bore is fully developed before the slope, $\tau < 400$. The left panel of the Figure 4.15 shows the same bore propagating over a flat bottom. When the undular bore is on the slope, the leading wave amplitude

decreases due to the depth variations (see plot 2 in the right panel of Figure 4.15). One can see the generation of new undular bore at the front part of the transformed bore in plot 3 in the right panel of Figure 4.15. In plot 4 in the right panel of the same figure, it is clear that the transformed bore consists of two distinct wave structures. At the front part of the transformed bore, we have an undular bore with the leading solitary wave of the undular bore is trying to reach the value of $2U_0$, and the rear part is a weakly nonlinear wave structure, which was part of the initial bore.
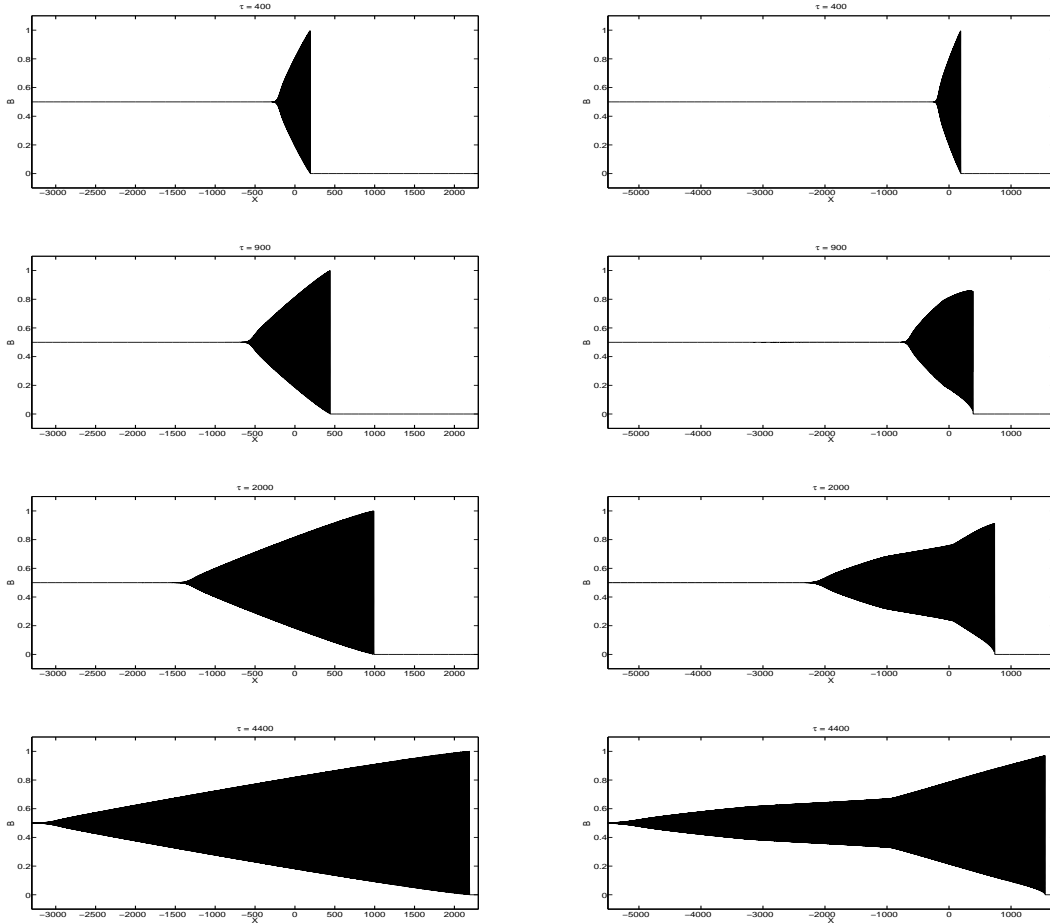

Figure 4.15: Numerical solution of the vKdV equation (3.25) with the initial condition (4.27). Left panel: propagation of an undular bore over a constant bottom; Right panel: propagation of an undular bore over a slowly increasing depth region with the profile $h(\tau)$ given by (4.65).

Figure 4.16 shows the boundaries of the undular bore obtained from the numerical simulations of the equivalent vKdV equation (4.4) used in our preliminary analysis in Section 4.2.2.3.2. The initial condition is taken in the form (4.28) and the depth profile is described

by

$$
h(T) = \begin{cases} 1 & : T < 300 \\ 1 + \alpha(T - 300) & : 300 < T < 1100 \\ 1.2 & : T > 1100 \end{cases} , \alpha = 0.00025.
$$

One can see that the leading solitary wave, X_+, of the undular bore, as was predicted, slows down after the slope (solid line) compared to the case when the bottom is flat (dashed blue line) due to the decrement in amplitude. Also, the velocity of the trailing edge of the initial bore decreases slowly on the slope as predicted by (4.25) (see also Figure 4.17).
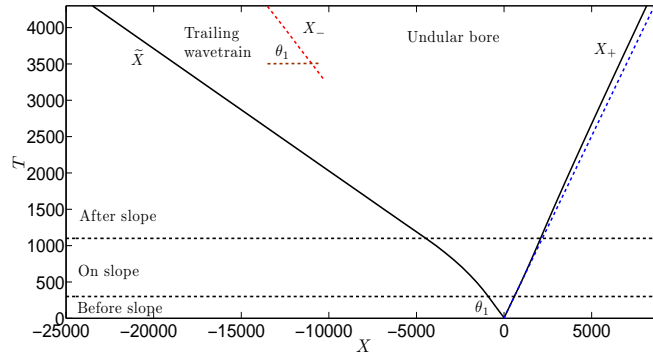

Figure 4.16: X-T plane of the evolution of an undular bore over a slowly increasing depth region according to the vKdV equation (4.4). The undular bore is confined to the region $[X_-(T), X_+(T)]$ while the trailing wavetrain is bounded in the region $[\widetilde{X}(T), X_-(T)]$.

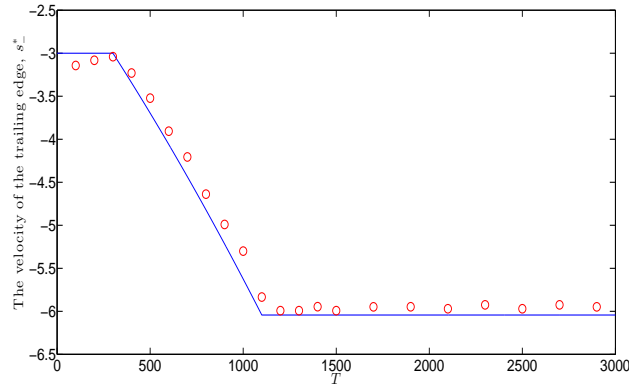**Figure 4.17:** Comparison for the numerically obtained velocity of the trailing edge of the undular bore propagating over a slowly increasing depth region – circles; and the linear group velocity predicted by the formula (4.25) over the same slope – solid line.

Thus far, based on our analysis, we can make three qualitative conclusions:

(a) the propagation of an undular bore over a broad range of slowly increasing depth

67

region leads to a non-adiabatic response, which is the generation of a weakly nonlinear wavetrain at the rear part of the bore,

(b) the asymptotic values of the velocities of the trailing and leading edges of the undular bore remain unchanged after the interaction with variable topography, and

(c) there are spatial shifts in the position of the trailing and leading edge of the transformed undular bore relative to the initial bore.

Again, similar observation to (a) was made in one of the cases studied by Ablowitz *et al.* (2009), where an undular bore interacts with a rarefaction wave producing a weakly non-linear trailing wavetrain behind the bore in the framework of constant-coefficient KdV equation. In our current problem setting, the undular bore is propagating through the "rarefaction region" of the increasing depth.

4.2.2.3.4   Numerical results

Now, we will use detailed numerical results to confirm our assumptions so far:

(a) the wave dynamics near the leading edge of the undular bore is governed by the "strong" (nonlocal) interaction scenario described by El *et al.* (2007), and

(b) a weakly nonlinear wavetrain is formed at the rear part of the transformed bore.

For numerical simulations, we will consider the vKdV equation (3.25). The depth profile is described by (4.65) and the initial condition is given by (4.27). The results are shown in Figures 4.18 – 4.21. The numerical result for the initial undular bore before the slope at $\tau = 400$, which agrees with the Gurevich-Pitaevskii solution, is similar to those presented in Figure 4.9.

Figure 4.18 corresponds to the undular bore propagation on the slope ($\tau = 900$). One can see that the amplitude of the leading wave decreases. However, it does not decrease as much as a single soliton, which is described by the formula (4.64). This is shown in Figure 4.21. Also, from the behaviour of the Riemann invariants (the middle plot), we have a nonlocal interaction scenario near the leading edge (see Figure 2.11b). Moreover, the distribution of the Riemann invariants shows that the structure is now a weakly nonlinear wavetrain. This also also be confirmed from the distribution of the modulus, m, where the modulus does not appear to approach 1 at the leading edge. This suggests that the wavetrain is not a classical bore structure.
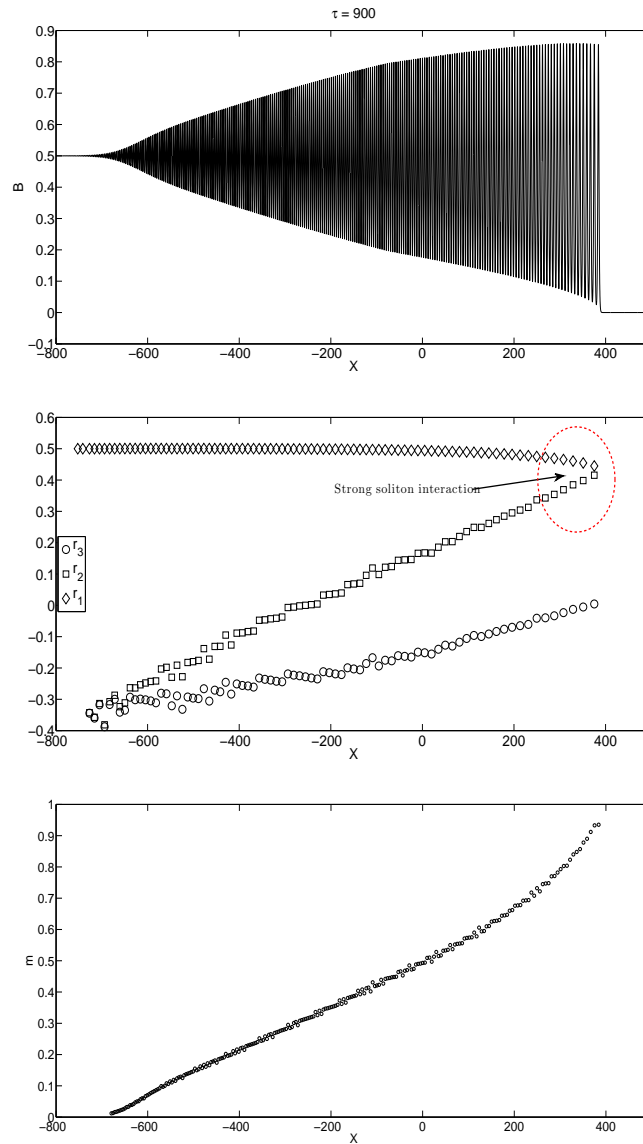
Figure 4.18: Undular bore on the slope, $\tau = 900$. One can see that the amplitude of the leading solitary wave decreases. The behaviour of the Riemann invariants near the leading edge is characteristics of the "strong interaction" (nonlocal) scenario (see Figure 2.11a).

In Figure 4.19, we present the evolution of the undular bore on a deeper shelf, $\beta(T) = \beta_1 > \beta_0$ at $\tau = 1400$. It is clear that the leading wave of the transformed bore is growing. At this moment, we still have "strong soliton interaction" scenario near the leading edge, where the lead wave is interacting 'strongly' with the rest of the nonlinear wavetrain (see the middle plot).

Figure 4.20 shows the plot for the transformed bore at $\tau = 9900$, which corresponds to the long-time behaviour after the slope. One can see clearly that the structure of the

69

transformed bore is a combination of two distinct wave structures. At the front part is the undular bore generated as the result of the nonlocal interaction at the leading edge when the bore is propagating over the slope. On the other hand, at the rear part, there is a weakly nonlinear trailing wavetrain, which was part of the incident bore. Also, the amplitude of the leading solitary wave in the transformed bore has reached the value of $2U_0$. Now, the soliton interaction at the leading edge has become weak again (compare the middle plot with Figure 2.11a). The multi-valued regions in the distribution of modulus, m (the bottom plot), in Figures 4.18 – 4.20 are due to numerics and it is not an indication that there is a multi-phase interaction in the bore.
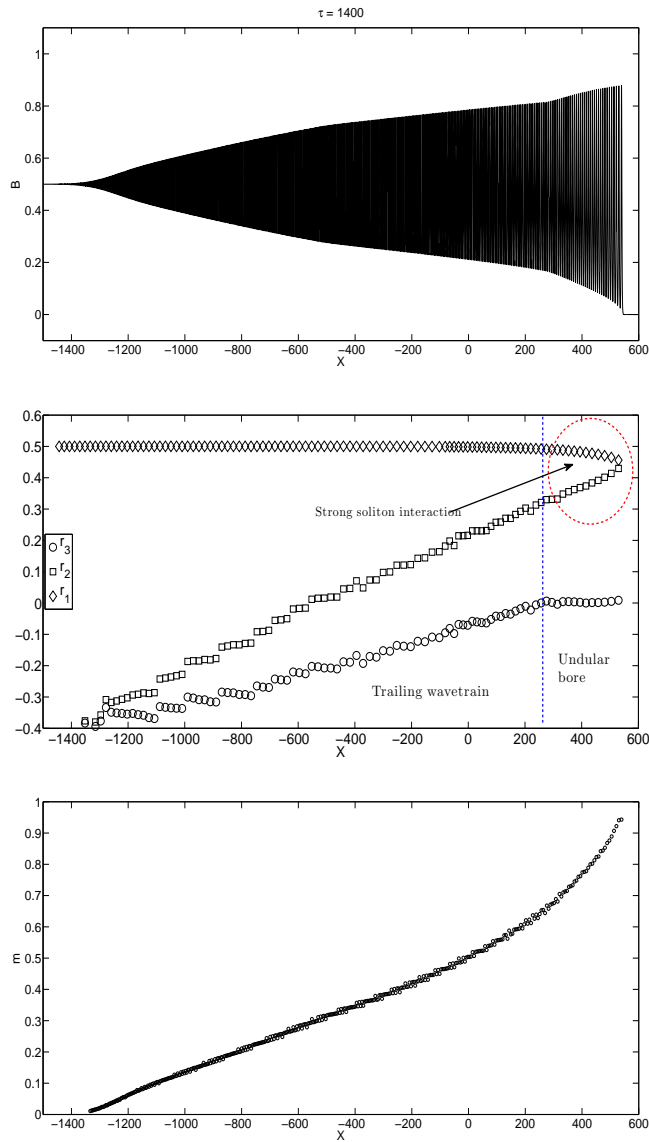

Figure 4.19: Undular bore after the slope at $\tau = 1400$. One can see that the leading wave is growing. The soliton behaviour at the leading edge is still governed by the "strong soliton interaction" scenario (see Figure 2.11b).
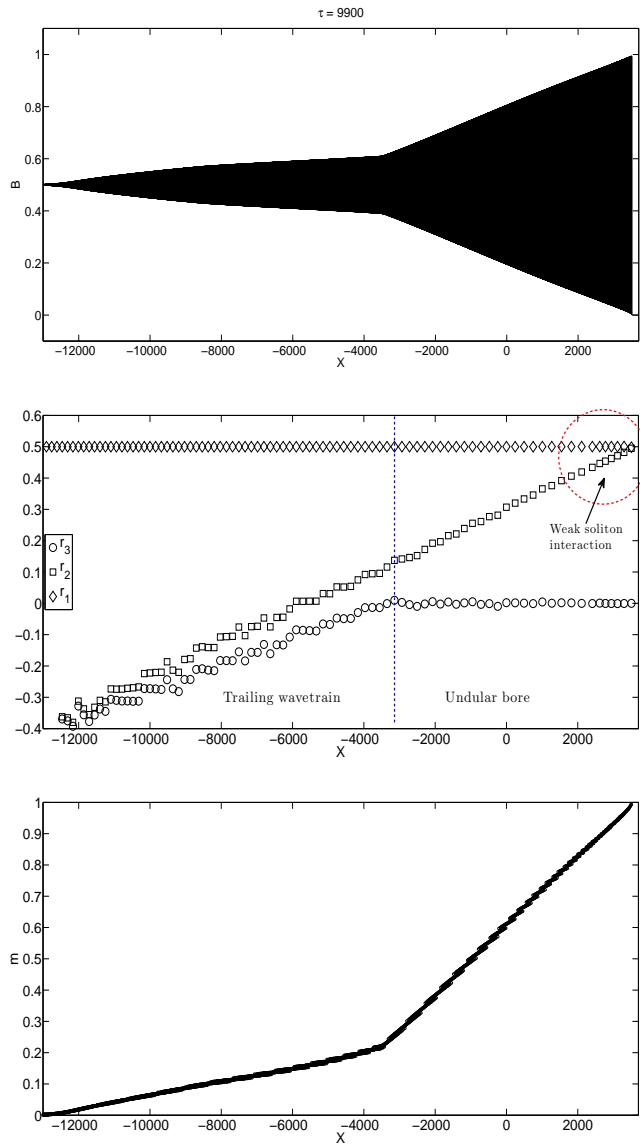
Figure 4.20: Long-time behaviour of the transformed bore after the slope at $\tau = 9900$. The leading solitary wave amplitude is twice of the initial jump, $2U_0$. One can observe two distinctive structures: an undular bore at the front part with trailing edge travelling with velocity, $s_= - 6U_0$ joined by a trailing wavetrain, where the velocity of the trailing edge is smaller than $\tilde{s} < -6U_0$.

Figure 4.21 is the comparison of the amplitudes for the adiabatically varying single solitary wave on a slope described by the formula (4.64) and the numerical values of the leading wave amplitude propagating over the same slope. At the initial stage, in both cases, they have the same amplitude. While on the slope, it is clear that the leading wave of the undular bore has greater amplitude compared to the isolated solitary wave, although both of them decrease. This validates our assumption that the "strong soliton interaction" scenario occurs near the leading edge. After some time, the amplitude of the leading wave
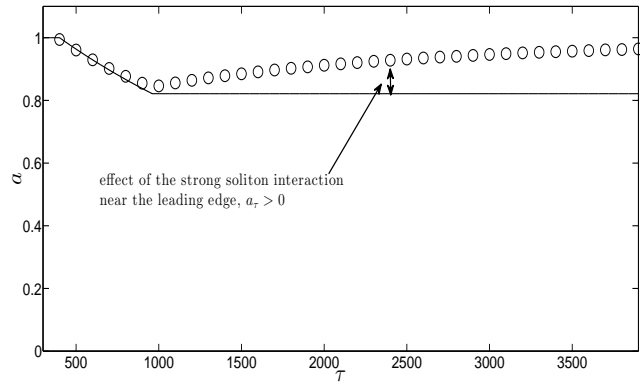
Figure 4.21: Comparison for the amplitudes of the adiabatically varying single solitary wave over a slowly increasing depth region described by formula (4.64) with $h_0 = 1, a_0 = 1$ – solid line, and the numerical data for the leading solitary wave in the undular bore – circles.

starts to increase and reaches the value of $a = 2U_0$. The amplitude of the lead wave stays constant afterwards. This is clearly different from the evolution of an isolated solitary wave over an increasing depth region, where the solitary wave decays on the slope and the amplitude of the solitary wave remains the same after that. Note that the behaviour of the Riemann invariants near the leading edge during the evolution corresponds to the second scenario described by El *et al.* (2007), which is "strong soliton interaction". This scenario continues for a significant amount of time after the slope until the amplitude of the leading solitary wave becomes twice of the jump, for which the soliton interaction near the leading edge becomes "weak" again.

4.2.2.4   Smooth hole

Now, we will look at the evolution of an undular bore over a hole with gently sloping walls and a wide bottom shelf on the bottom surface. Since a hole consists of both increasing and decreasing depth regions, we would expect to see all the effects discussed in Section 4.2.2.2 and 4.2.2.3. In this case, initially we have an increasing depth topography. Therefore, the leading solitary wave is expected to diminish initially before it grows again due to the strong soliton interaction at the leading edge. When the bore is on a deeper flat region, the leading wave continues to grow, asymptotically restoring its original amplitude $2U_0$. Before it happens, though, the undular bore encounters the opposite slope of the hole, i.e. the decreasing depth region. When the bore enters the decreasing depth region, the leading wave will behave as an isolated solitary wave and we, again, have the local interaction behaviour at the leading edge. Thus, after the hole, we would expect to see the formation

of a solitary wavetrain at the front of the transformed bore. The leading solitary wave amplitude of the undular bore after the slope remains the same as in the incident bore.
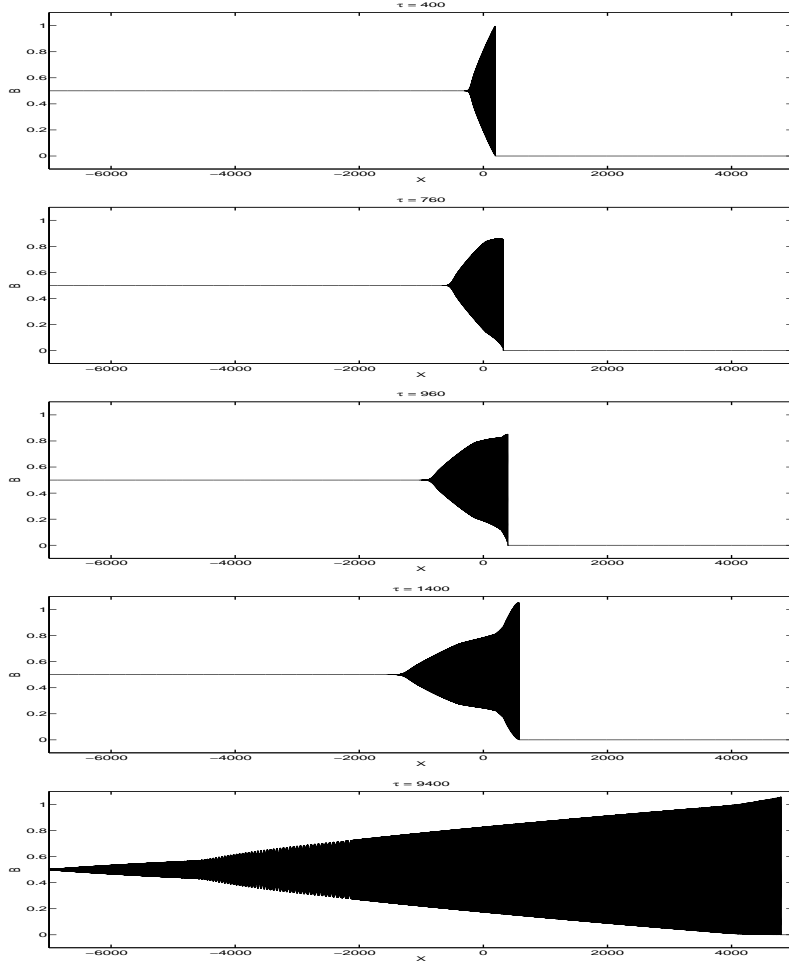
Figure 4.22: Propagation of an undular bore over a smooth hole described by (4.66) with initial condition (4.27)

In Figure 4.22, we present the evolution of an undular bore according to the vKdV equation (3.25) over a smooth hole given by

$$
h(\tau) = \begin{cases}
1 & : \tau < 400 \\
(1 + \alpha(\tau - 400)/2)^2 & : 400 < \tau < 773.80 \\
1.3 & : 773.80 < \tau < 973.80 \\
(\sqrt{1.3} - \alpha(\tau - 773.80)/2)^2 & : 973.80 < \tau < 1347.60 \\
1 & : \tau > 1347.60
\end{cases} , \qquad (4.66)
$$

where $\alpha = 0.00075$. The initial condition is given by (4.27). The evolution profile matches the description given earlier. In plot 5, one can see the formation of an advancing solitary

wavetrain ahead of the bore, multi-phase region and a trailing wavepacket (less pronounced) at the rear part of the bore.

4.2.2.4.1   Numerical results

Again, all numerical results are based on the vKdV equation (3.25) with initial condition and the hole description given by (4.27) and (4.66) respectively. All results are presented in Figures 4.23 – 4.26. The corresponding plot for the initial undular bore before the slope at $\tau = 400$ is the same as in Figure 4.9.
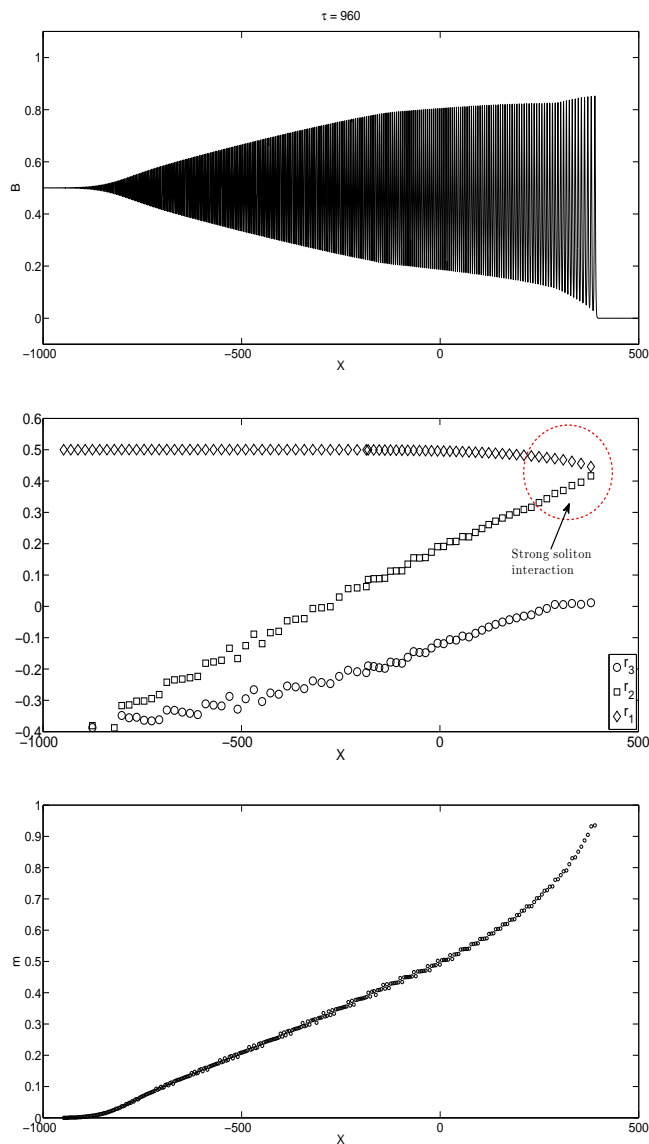

Figure 4.23: Undular bore on the deeper region of the hole at $\tau = 960$. Note that the leading wave is growing and nonlocal interaction at the leading edge of the bore (see Figure 2.11b).

4.2.2 Slowly varying topography

Figure 4.23 shows the undular bore on the deeper shelf of the hole. The amplitude of the leading solitary wave decreases but note the growth of the leading wave as predicted by the results in Section 4.2.2.3. Also, the behaviour of the Riemann invariants indicates that the soliton interaction near the leading edge is described by the nonlocal interaction (see Figure 2.11b).
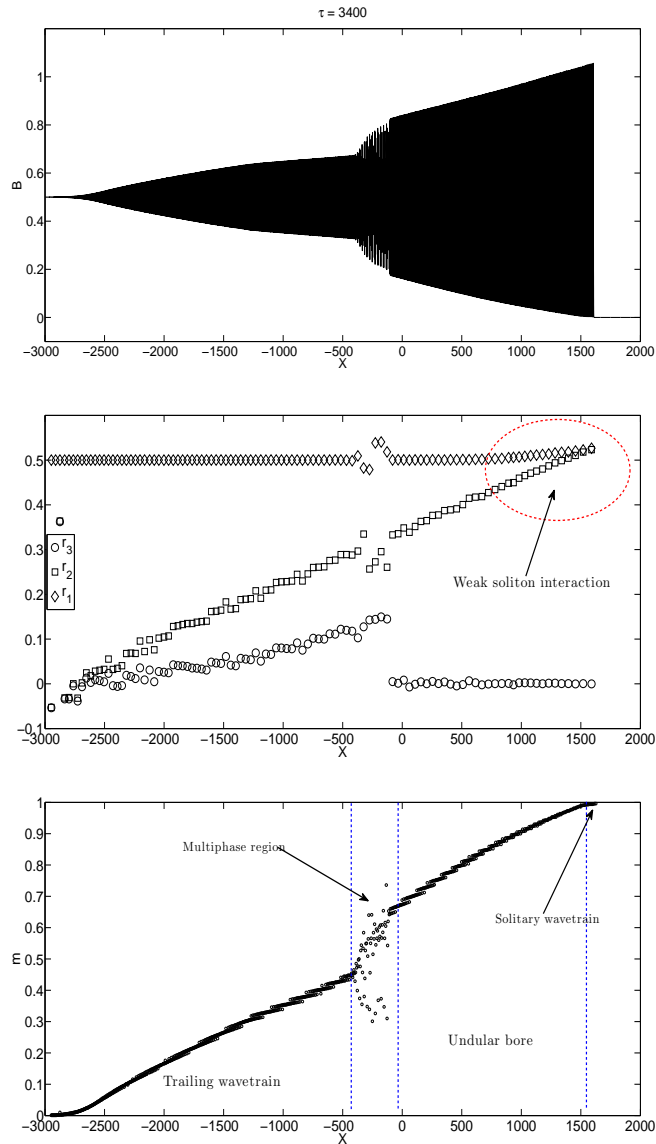
Figure 4.24: Undular bore after the hole at $\tau = 3400$. The multi-phase behaviour is present near $X \approx 400$. Also, the soliton interaction at the leading edge now follows the local interaction scenario (see Figure 2.11a) so that a solitary wavetrain is formed, where $r_1 = r_2$.

Figure 4.24 corresponds to the undular bore evolution after the hole at $\tau = 3400$. One can see the multi-phase behaviour around $X \approx -400$. The values for the Riemann invariants

and the modulus m are undefined in this region. Note that the behaviour of the Riemann invariants at the leading edge (see the middle plot) describes the weak soliton interaction scenario by El *et al.* (2007) (see Figure 2.11a). This is anticipated from our discussion in Section 4.2.2.2. Also, a solitary wavetrain is generated ahead of the bore ($r_1 = r_2$ in the middle plot).
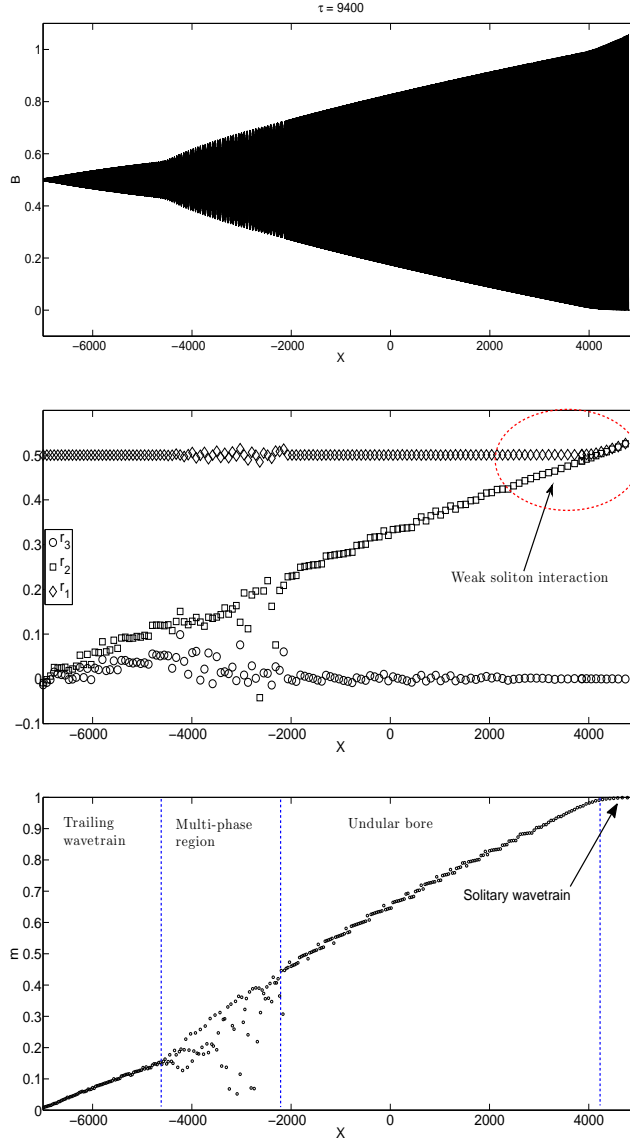
Figure 4.25: Long-time behaviour of the undular bore after the hole at $\tau = 9400$. Notice the formation of a solitary wavetrain ($m \to 1$ and $r_1 = r_2$) at the front of the undular bore and multi-phase behaviour at the rear part of the undular bore, $-4200 < X < -2000$.

In Figure 4.25, we present the plot of the transformed bore at a larger time after the hole, $\tau = 9400$. One can see that the multi-phase behaviour is still present at the rear part of

Figure 4.26: Comparison for the amplitudes for an adiabatically varying single solitary wave over a smooth hole given by the formula (4.64) with $h_0 = 1, a_0 = 1$ – solid line, and the numerical data for the amplitude of the leading solitary wave in the modulated wavetrain over the same hole – circles.

the transformed bore. We would expect the transformed bore to restore its single-phase interaction throughout the entire bore at larger time and then the Riemann invariants distribution will be similar to those illustrated in Figure 4.8b. Note that at the leading edge of the transformed bo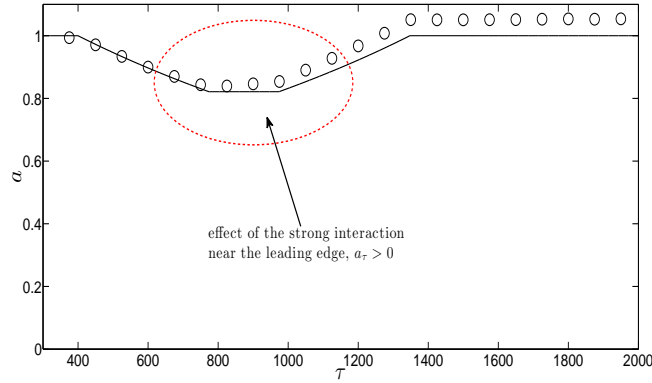re, the soliton interaction has changed from strong interaction scenario to weak interaction scenario. Also, from the values of Riemann invariants, the amplitude of the leading solitary wave in the bore is equivalent to those of the incident bore, $a = 2(r_1 - r_3)$.

Figure 4.26 shows the comparison for the amplitudes of the adiabatically varying isolated solitary wave over a hole predicted by the formula (4.64) with the numerical values of the leading wave amplitude propagating over the same hole. In both cases, the initial amplitude is the same. One can see that the leading solitary wave amplitude of the bore is greater than that of a solitary wave when the bore propagates over the increasing depth region of the hole. Then, the amplitude of the leading solitary wave continues to increase on the flat bottom of the hole. As the result, it is not surprising that the amplitude of the leading soliton in the solitary wavetrain is greater than that predicted by the (local) formula (4.64) although the leading solitary wave already behaves as an isolated soliton.

4.2.2.5 Smooth bump

In this section, we consider a smooth bump with gently sloping walls and wide bottom on the bottom surface. Again, a smooth bump is a combination of decreasing and increasing depth regions. Thus, we would expect to see all the transformations presented in Sections 4.2.2.2 and 4.2.2.3. The first part of the interaction of the undular bore with the bump

involves a slowly decreasing depth region. So, a sequence of an isolated solitary waves will be generated when the bore emerges onto a shallower shelf on the bump. The amplitude of the leading solitary wave in the undular bore remain the same as in the incident bore.

The second part of the evolution involves a slowly increasing depth region. All the solitons in the solitary wavetrain would deform adiabatically according to the formula (4.64) when the wavetrain propagates through the slope. After the bump, the amplitude of the leading soliton in the solitary wavetrain decreases to the value of $2U_0$. For the leading solitary wave of the undular bore behind the solitary wavetrain, the amplitude also decreases when it propagates through the increasing depth region. However, as was mentioned in Section 4.2.2.3, the leading wave in the bore will interact with the rest of the nonlinear wavetrain as the result of the interaction of the bore with the varying topography. Thus, the nonlocal interaction near the leading edge will push the leading solitary wave to grow until the amplitude reaches the value of $2U_0$. Because of the growth at the leading edge of the undular bore, which leads to the energy differences between the bore and solitons in the solitary wavetrain, the undular bore will start to overtake the solitons in the solitary wavetrain. Over time, we would expect the undular bore will overtake all the solitons in the solitary wavetrain except the leading soliton. This is because both the leading soliton in the solitary wavetrain and the leading solitary wave in the undular bore would have the same velocity.

Figure 4.27 illustrates the evolution of an undular bore over a smooth bump described by

$$
h(\tau) = \begin{cases} 1 & : \tau < 400 \\ (1 - \alpha(\tau - 400)/2)^2 & : 400 < \tau < 844.44 \\ 0.64 & : 844.44 < \tau < 1044.44 \\ (\sqrt{0.64} + \alpha(\tau - 1044.44)/2)^2 & : 1044.44 < \tau < 1488.88 \\ 1 & : \tau > 1488.88 \end{cases} , \qquad (4.67)
$$

where $\alpha = 0.0009$ according to the vKdV equation (3.25) with the initial condition (4.27). In plot 4 of the Figure 4.27, we can see a solitary wavetrain is formed ahead of the bore. At the same time, the leading wave of the undular bore behind the solitary wavetrain is growing. In plot 5 of the same figure, one can see clearly there are three wave structures in the transformed bore. At the front part, we have a solitary wavetrain, followed by an undular bore with the leading solitary wave having an amplitude of $2U_0$. The undular bore is seen to overtake solitons in the solitary wavetrain. At the rear part, we have a weakly nonlinear trailing wavetrain generated as the result of the interaction of the bore with increasing depth region as presented in Section 4.2.2.3.
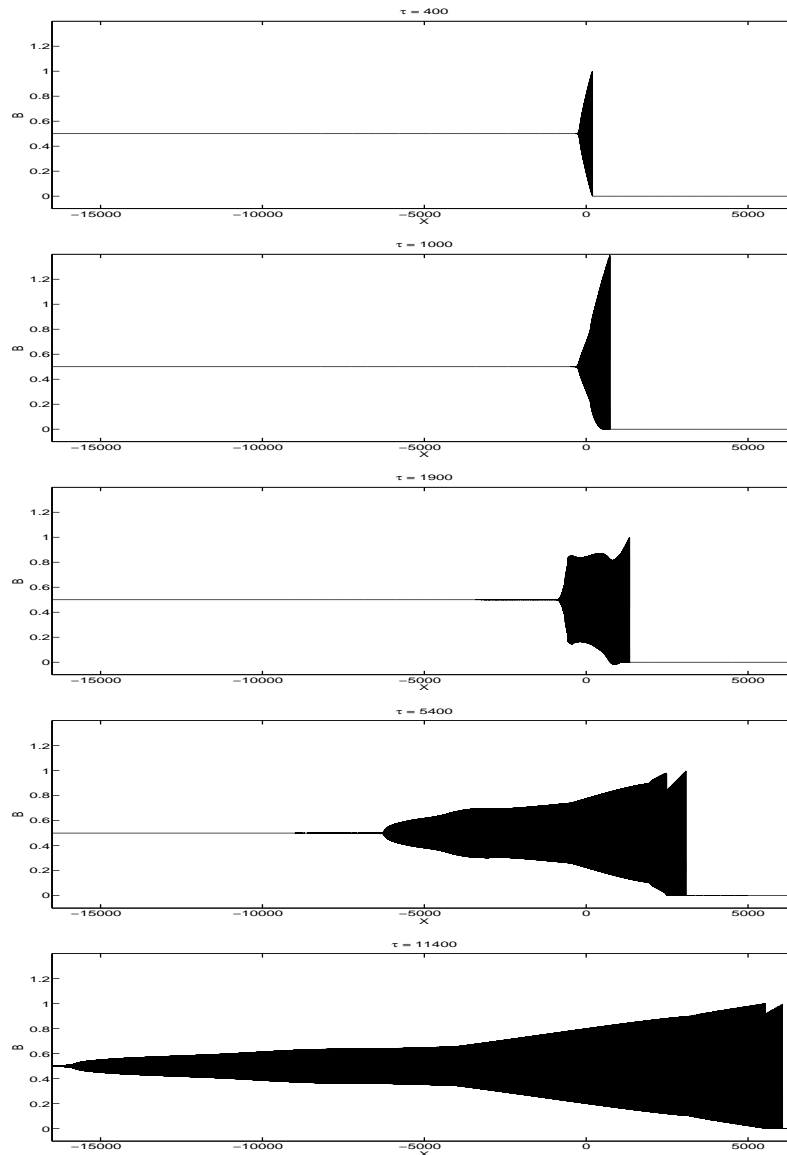
Figure 4.27: Propagation of an undular bore over a smooth bump described by (4.67) according to the vKdV equation (3.25).

4.2.2.5.1 Numerical results

For the numerical simulations, as usual, we consider the vKdV equation (3.25) with the bump described by (4.67) and the initial condition is taken as in (4.27). All numerical results are presented in Figures 4.28 – 4.32.

Figure 4.28 shows the transformation of the bore on the decreasing depth region of the bump ($\tau = 800$). Here, it is clear that there is a formation of solitary wavetrain at the

front of the bore. This is confirmed by the behaviour of the Riemann invariants, $r_1 = r_2$ or the modulus, $m \to 1$ as shown in the middle and bottom plots respectively.
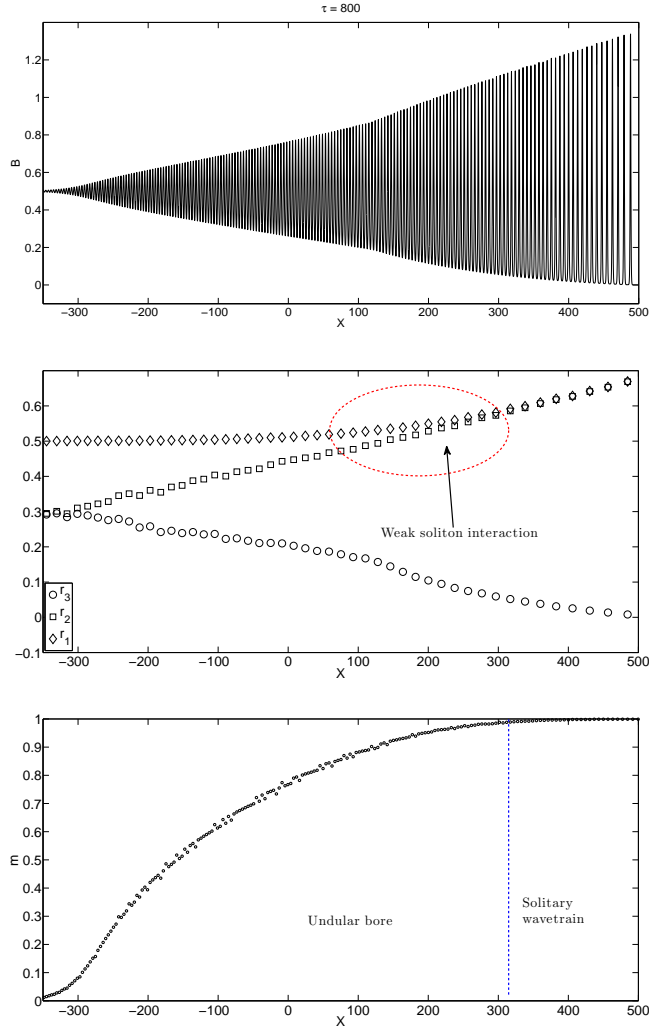
Figure 4.28: Undular bore on the decreasing depth region of the bump, $\tau = 800$. One can see the formation of the solitary wavetrain ($m \to 1, r_1 = r_2$) between $X \approx 350$ and $X \approx 500$.

On the other hand, we present the plot of the evolution of the bore over the increasing depth region of the bump ($\tau = 1400$) in Figure 4.29. Notice that the amplitude of the leading soliton in the solitary wavetrain decreases. Also, multi-phase interaction is observed at the rear part of the bore. Another interesting observation is that we still have "weak soliton interaction" scenario near the leading edge of the bore even though the bore is on the increasing depth region (see middle plot of Figure 4.29). We can see the effect of the increasing depth on the bore some time after the bump. At this moment, the soliton interaction near the leading edge is in the process of changing from the weak interaction scenario to the strong interaction scenario. Figure 4.30 shows the undular bore after the

bump at $\tau = 3400$. From the behaviour of the Riemann invariant, it is clear that there is a nonlocal interaction near the leading edge.
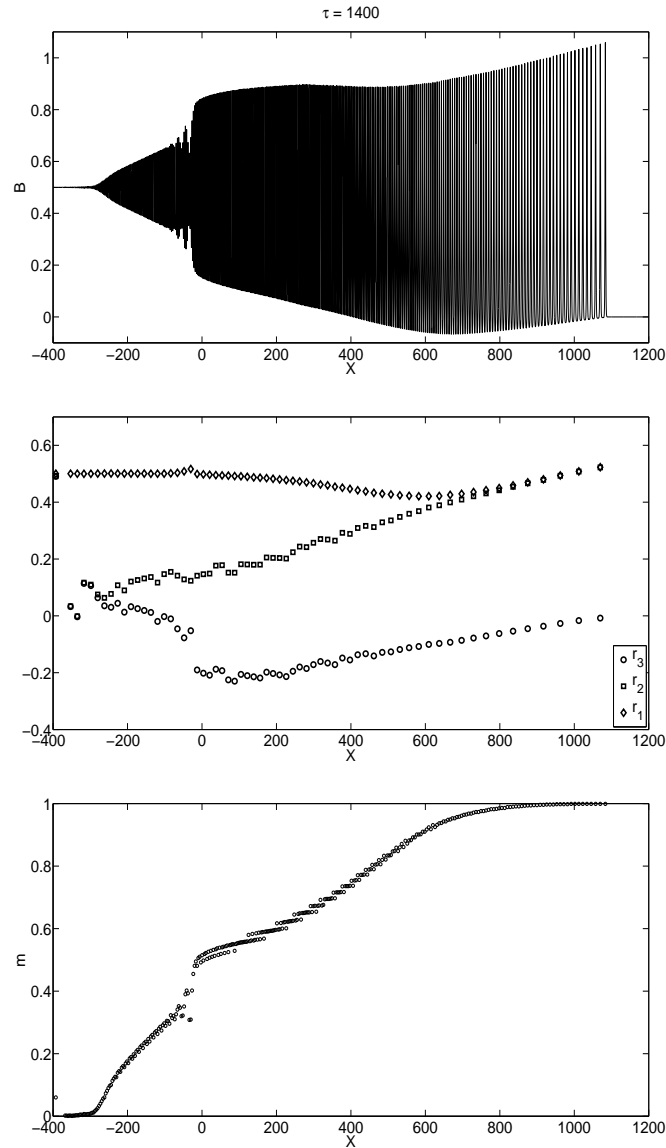
Figure 4.29: Undular bore on the increasing depth region of the bump, $\tau = 1400$. The solitary wavetrain is located at $X \approx 700$ and $X \approx 1100$. Notice that there is multi-phase behaviour around $X = -100$.

In Figure 4.31, we present the long-time evolution of the bore after the bump at $\tau = 15400$. Clearly, the leading solitary wave of the undular bore has the value of twice of the jump. At the front part of the undular bore, there is a multi-phase interaction region due to the interaction of the bore with the solitons in the solitary wavetrain. One can see that the number of solitons in the solitary wavetrain has reduced as the result of the bore overtaking the solitary wavetrain. As $\tau \to \infty$, we would expect that only the leading soliton in the

solitary wavetrain is left as the amplitude of the leading soliton in the solitary wavetrain has the same amplitude with the leading solitary wave of the undular bore. Again, the multi-valued regions in the distribution of modulus, m, in Figures 4.28 – 4.31 are not an indication that a multi-phase interaction present in the transformed bore.
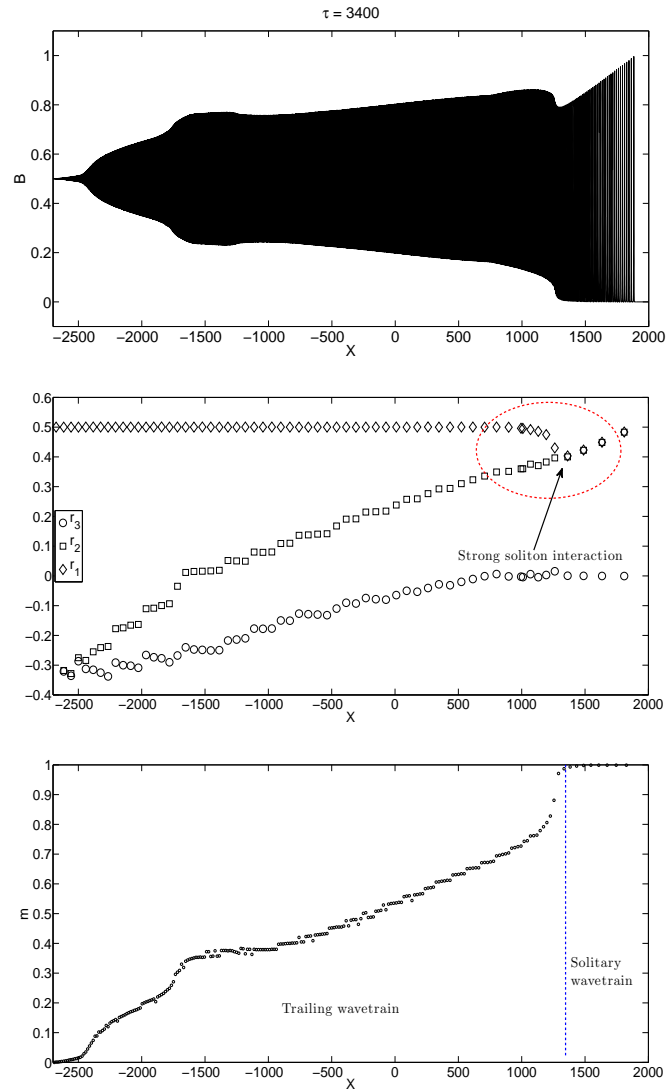
Figure 4.30: Undular bore after the bump at $\tau = 3400$. The solitary wavetrain is located at $X \approx 1300$ and $X \approx 1800$. Note that we have nonlocal interaction near the leading edge of the undular bore around $X \approx 1300$ (see Figure 2.11b).
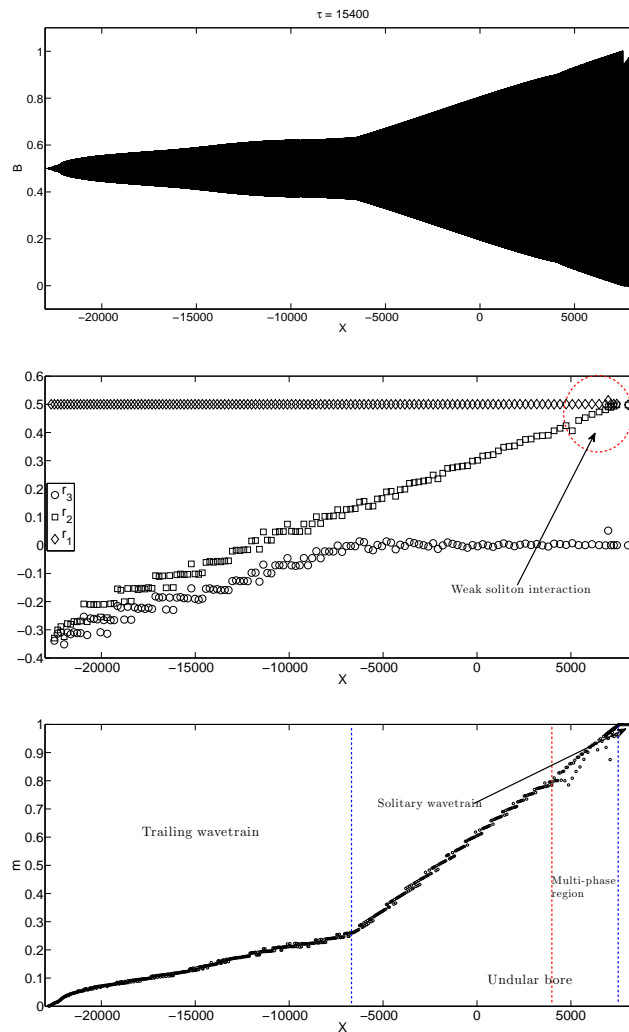
Figure 4.31: Long-time behaviour of the undular bore after the bump, $\tau = 15400$. One can see that the leading wave of the bore is slowly overtaking the solitary waves in the solitary wavetrain.

The comparison for the amplitudes for an isolated solitary wave and the leading solitary wave of the initial undular bore is shown in Figure 4.32. Clearly, there is an excellent agreement between the theoretical prediction and numerical data. This shows that the leading solitary wave of the incident bore behaves like a separate isolated soliton when the bore is propagating over a slowly decreasing depth region and continues to deform adiabatically according to the formula (4.64) afterwards.

Figure 4.32: Comparison for the amplitudes for an adiabatically varying solitary wave over a smooth bump (formula (4.64) with $h_0 = 1, a_0 = 1$) – solid line; and the numerical data for the leading solitary wave in the initial undular bore over the same bump – circles.

4.3 Transformation of an undular bore over rapidly varying slope

Now, we will focus on the transformations of the undular bore over a rapidly varying slope. This is an undular bore counterpart of the "soliton fissioning" setting (Johnson, 1973b). Due to the abrupt change in depth, the undular bore is not expected to deform adiabatically over the slope. Also, the sudden change in depth would cause some irregularities across the bore during the evolution. However, if the entire wave structure is allowed to 'sett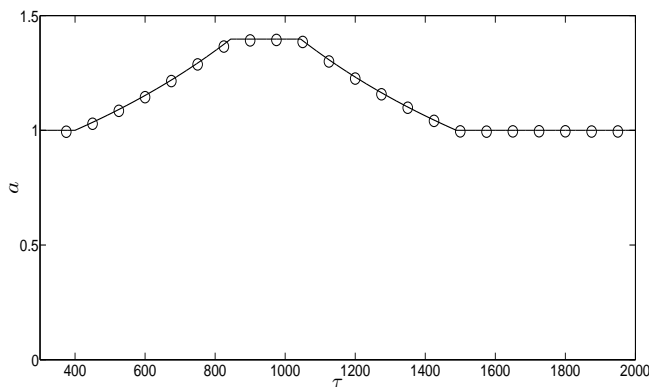le down', then we would still expect an undular bore described by the modulation solution (4.9) at large time. Since the depth variations have no influence on the jump, $[U]$, across the bore (see equation (4.16)), the amplitude of the leading solitary wave in the transformed bore is expected to be $2U_0$, i.e. twice of the jump across the bore. Since the Whitham modulation theory, which is our main analytical tool in the description of undular bores, is not applicable when rapid changes of the KdV coefficients are present, the problem will be investigated numerically. At the same time, as we shall see, our insights from the problem with slowly varying depth will be relevant.

4.3.1 Rapidly decreasing depth

As was shown in Section 4.2.2.2, the interaction of an undular bore with decreasing depth topography promotes the weak soliton interaction scenario near the leading edge where the leading solitary wave of the undular bore behaves as an isolated soliton. Therefore, for a rapidly decreasing depth region, the leading solitary wave is also expected to behave like a

single solitary wave. As mentioned in Section 3.3.1, when a single soliton advances through a rapidly decreasing depth region, it will disintegrate into a few solitons, i.e. soliton fission will occur depending on the depth variation. The same process would also happen to some part of the wavetrain at the leading edge as the wavetrain crosses the boundary to form a sequence of isolated solitary waves. However, a number of smaller solitons generated due to the fissioning process as the front part of the wavetrain of the undular bore crosses over the slope would interact with the remainder of the bore, causing it to form a multi-phase interaction region. If one allows the multi-phase behaviour to settle down at larger time, then the single-phase behaviour will persist and an undular bore solution of the constant-coefficient KdV equation, where $\beta = \beta_1 < \beta_0$ in the vKdV equation (3.25), will be established with the leading solitary wave having an amplitude of $2U_0$. The amplitude of the leading soliton in the solitary wavetrain (which was the leading solitary wave of the initial bore after the slope) must be equal to that of a single solitary wave, as presented in Section 3.3.1.

Therefore, the propagation of an undular bore over a broad range of rapidly decreasing depth region is also expected to lead to a long-time non-adiabatic deformation, similar to that in the slowly decreasing depth case, i.e. the generation of a solitary wavetrain in front of the undular bore.

In Figure 4.33, we present the evolution profile of an undular bore propagating over a rapidly decreasing depth region described by

$$h(\tau) = \left\{ \begin{array}{ll} 1.0 & : \tau < 400 \\ 0.7 & : \tau > 400 \end{array} \right. . \tag{4.68}$$

The initial condition is taken in the form of (4.27). In plots 3 and 4 of the figure, one can see the multi-phase interaction region at the rear part of the transformed bore caused by the sudden change in water depth. Clearly, there is a solitary wavetrain at the front of the transformed bore (see plot 5). Also, a small-amplitude wavetrain is found to be attached to the rear part of the transformed bore. Although the modulation theory is not applicable in this case, we will analyse the behaviour of the modulation Riemann invariants, r_j, in this region as a tool in order to determine the nature of this structure. This will be done in the following subsection.

4.3.1 Rapidly decreasing depth
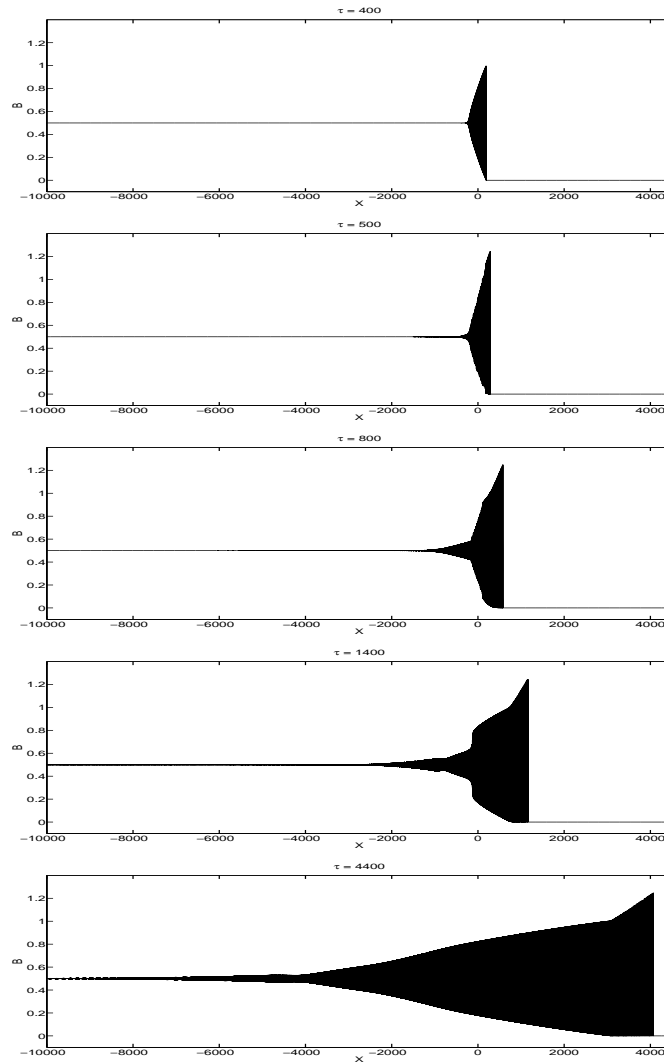
Figure 4.33: Propagation of an undular bore over a rapidly decreasing depth region described by (4.68).

4.3.1.1 Numerical results

We will use numerical results to confirm our assumptions as follows:

(a) the leading solitary wave in the undular bore behaves like a separate single solitary wave so that we have the weak interaction scenario at the leading edge, and

(b) there is a solitary wave train generated at the front of the undular bore as the result of the interaction of the undular bore with the decreasing depth topography.

All numerical results are based on the vKdV equation (3.25) and are presented in Figures 4.34 – 4.37. The plot for the initial undular bore before the slope is shown in Figure 4.9.
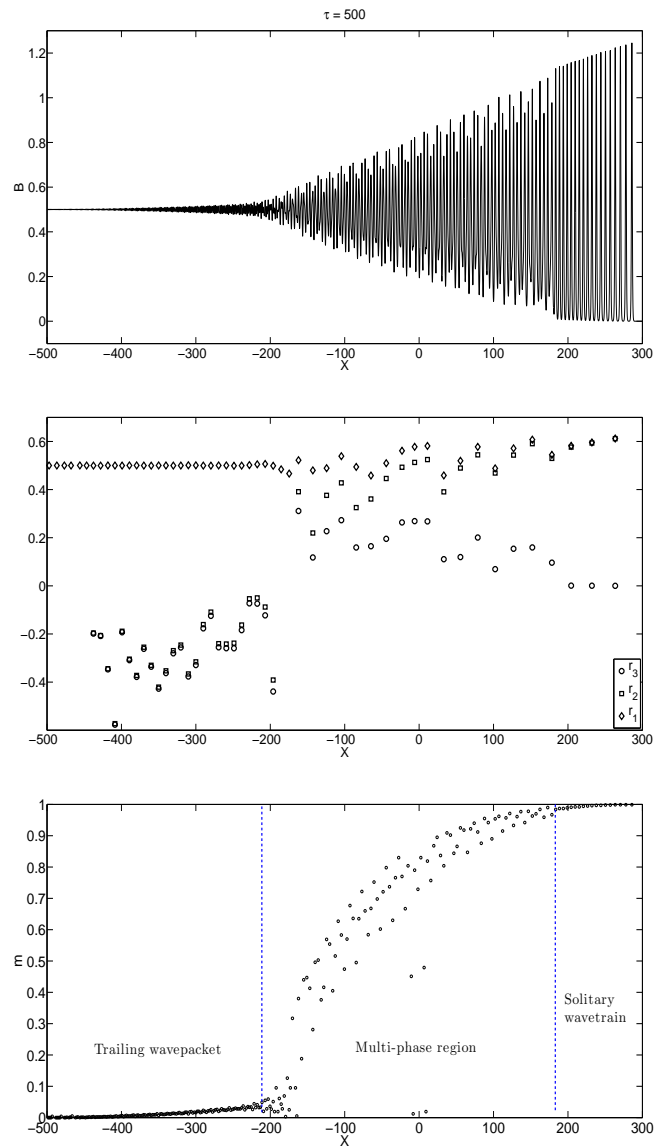
Figure 4.34: Undular bore after a rapidly varying slope at $\tau = 500$. A solitary wavetrain is generated ahead of the transformed bore. At the same time, we have multi-phase behaviour at the rear part of the transformed bore.

In Figure 4.34, we present the undular bore right after the slope at $\tau = 500$. One can see the formation of a solitary wavetrain between $X \approx 180$ and $X \approx 300$ ($r_1 = r_2$ and $m \to 1$). Note the occurrence of multi-phase behaviour behind the solitary wavetrain. In this region, the (single-phase) Riemann invariants and the modulus m are not defined.
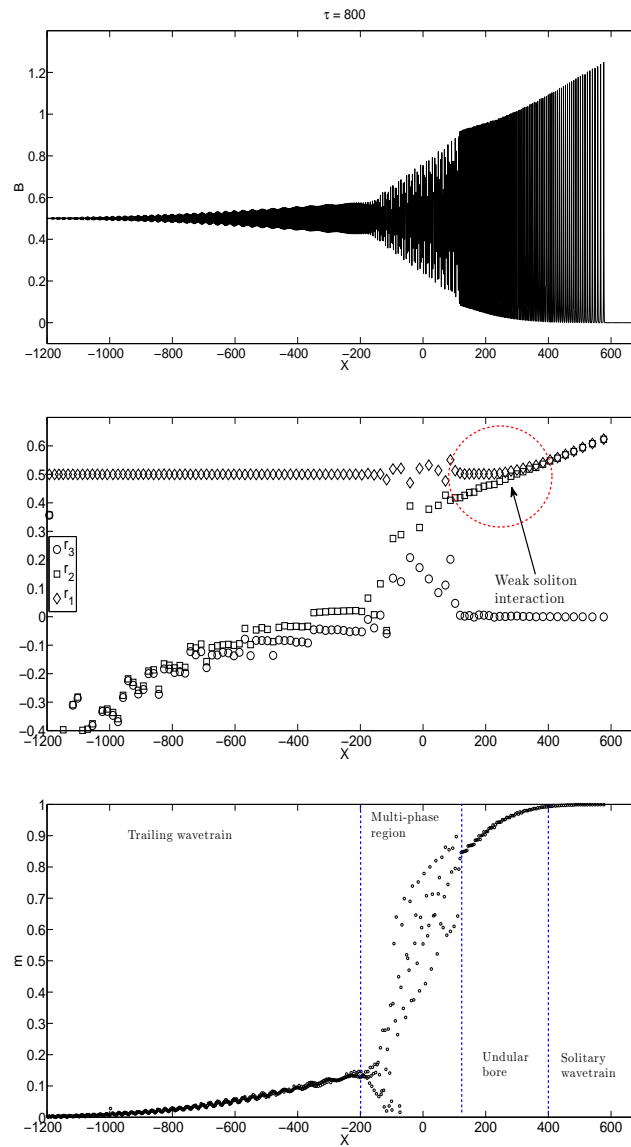
Figure 4.35: Undular bore after a rapidly varying slope at $\tau = 800$. The solitary wavetrain is located between $X \approx -300$ and $X \approx 600$.

Figure 4.35 shows the undular bore after the slope at $\tau = 800$. The solitary wavetrain is located between $X \approx 400$ and $X \approx 600$. The amplitude of the leading solitary wave of the undular bore is twice of the jump, $2U_0$ (i.e. $2(r_1 - r_3)$), as predicted. Note the multi-phase behaviour between $X \approx -200$ and $X \approx 100$. Also, there is a weakly nonlinear wavetrain at the rear part of the transformed bore.
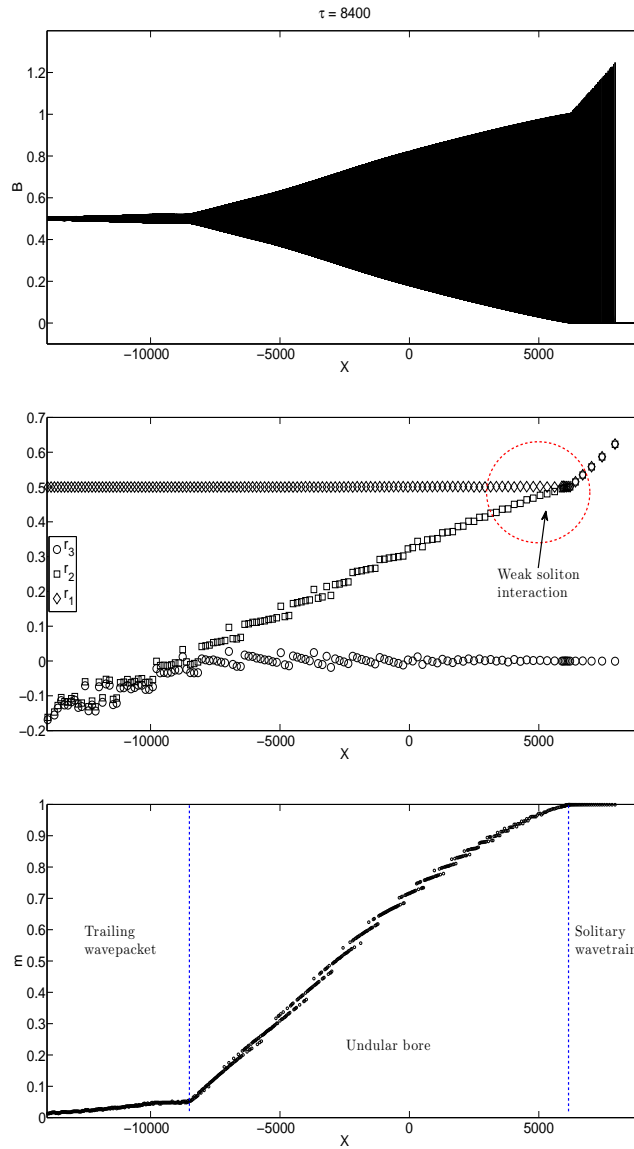
Figure 4.36: Undular bore after a rapidly varying slope at $\tau = 8400$. The transformed bore has restored its single-phase dynamics throughout the entire bore.

Figure 4.36 corresponds to the long-time behaviour of the undular bore after the slope at $\tau = 8400$. Ahead of the transformed bore, we have a solitary wavetrain $(r_1 = r_2, m \to 1)$ followed by an undular bore, and at the rear part, we have a linear wavetrain, $r_2 = r_3$. This is another non-adiabatic effect of the propagation of the undular bore over a rapidly decreasing depth region, an analogue to the oscillatory tail when soliton fission occurs for a single solitary wave. Note that at this moment, the transformed bore has restored its single phase structure throughout the entire bore. Also, the transformed bore is not an multi-phase wavetrain although there are multi-valued regions in the distribution of modulus, m, in Figure 4.36.
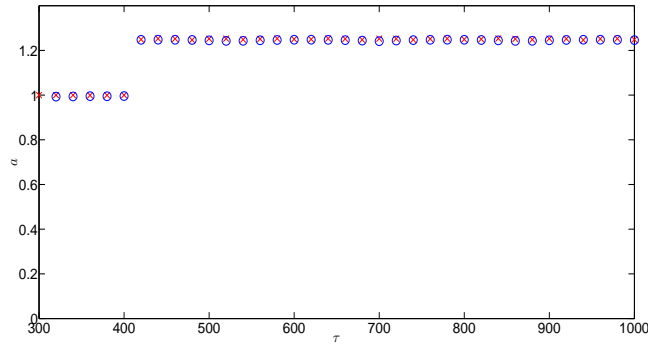
Figure 4.37: Comparison for the amplitudes for the leading solitary wave of the initial bore (blue circles) and an isolated solitary wave (red crosses).

The comparison for the numerically obtained amplitudes for the leading solitary wave of the initial bore and an isolated single solitary wave is shown in Figure 4.37. In both cases, the initial amplitude is the same. Clearly, in both cases, we have a very good agreement. This confirms our assumption that the leading solitary wave of the initial bore was indeed behaving like a separate isolated solitary wave when propagating over a region of rapidly decreasing depth.

4.3.2   Rapidly increasing depth

Now, we will consider the opposite case where the depth is increasing rapidly. Then the leading solitary wave and some part of the wavetrain of the undular bore will decay immediately when it emerges onto a deeper shelf. Unlike the case for a slowly increasing depth where the nonlocal interaction scenario is slowly achieved, in this case, however, the rapid change in the amplitude of the leading wave and also the wavetrain behind it leads to the nonlocal interaction scenario near the leading edge almost immediately after the slope. Therefore, the strong interaction at the leading edge will push the leading wave to grow until the amplitude reaches the value of $2U_0$. At the trailing edge, we would expect to see a nonlinear trailing wavetrain generated (which was part of the initial bore) and to be attached to the rear part of the transformed bore, similar to our results presented in Section 4.2.2.3 for the slowly increasing depth case. The sudden change of the depth would also cause some irregularities across the bore during the evolution.

In Figure 4.38, we present the evolution profile of an undular bore propagating over a

rapidly increasing depth region described by

$$h(\tau) = \begin{cases} 1.0 & : \tau < 400 \\ 1.3 & : \tau > 400 \end{cases}, \tag{4.69}$$

and the initial condition is given by (4.27). In plot 2 of the figure, we can see clearly the irregularities in the undular bore. Also, one can see that the amplitude of the leading wave decreases. In plot 3, the leading wave is growing and its amplitude will reach the value of $2U_0$ (see plot 5). At larger time, we have an undular bore generated due to the nonlocal interaction at the leading edge while at the rear part, we have a trailing wavetrain similar to those presented in Section 4.2.2.3.
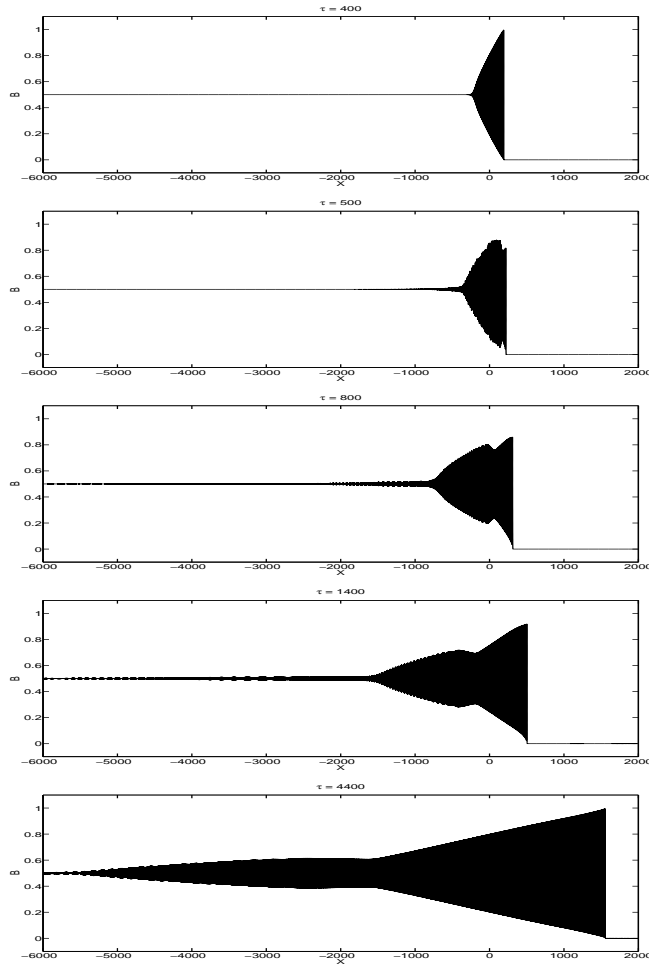
Figure 4.38: Propagation of an undular bore over a rapidly increasing depth region described by (4.69).

4.3.2.1   Numerical results

In a similar manner to those described in previous sections, we will use numerical results to confirm our description mentioned above, which was based on the following assumptions:

4.3.2 Rapidly increasing depth

(a) the soliton interaction near the leading edge of the undular bore is described by the nonlocal interaction scenario, and

(b) a nonlinear trailing wavetrain is generated at the rear part of the transformed bore.

Again, all the numerical results are obtained from numerical simulations of the vKdV equation (3.25). The depth profile and the initial condition are given by (4.69) and (4.27) respectively. The results for the undular bore after the slope are presented in Figure 4.39 – 4.42.
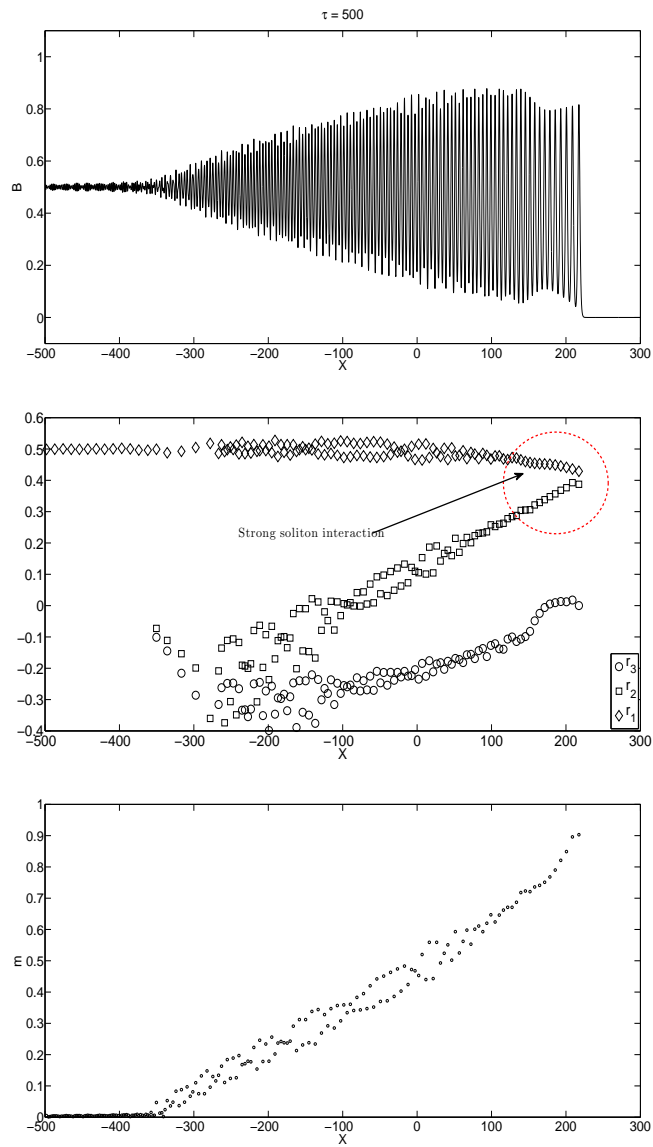
Figure 4.39: Undular bore after the slope at $\tau = 500$. The amplitude of the leading wave decreases.

Figure 4.39 shows the undular bore after the slope at $\tau = 500$. Clearly, the amplitude of the leading wave decreases. One can see that the behaviour of the Riemann invariants near the leading edge indicates the strong interaction scenario (see Figure 2.11b). Note the multi-phase behaviour across the bore during the evolution, which is caused by the abrupt change in depth. In this region, the Riemann invariants and the modulus, m are not defined.
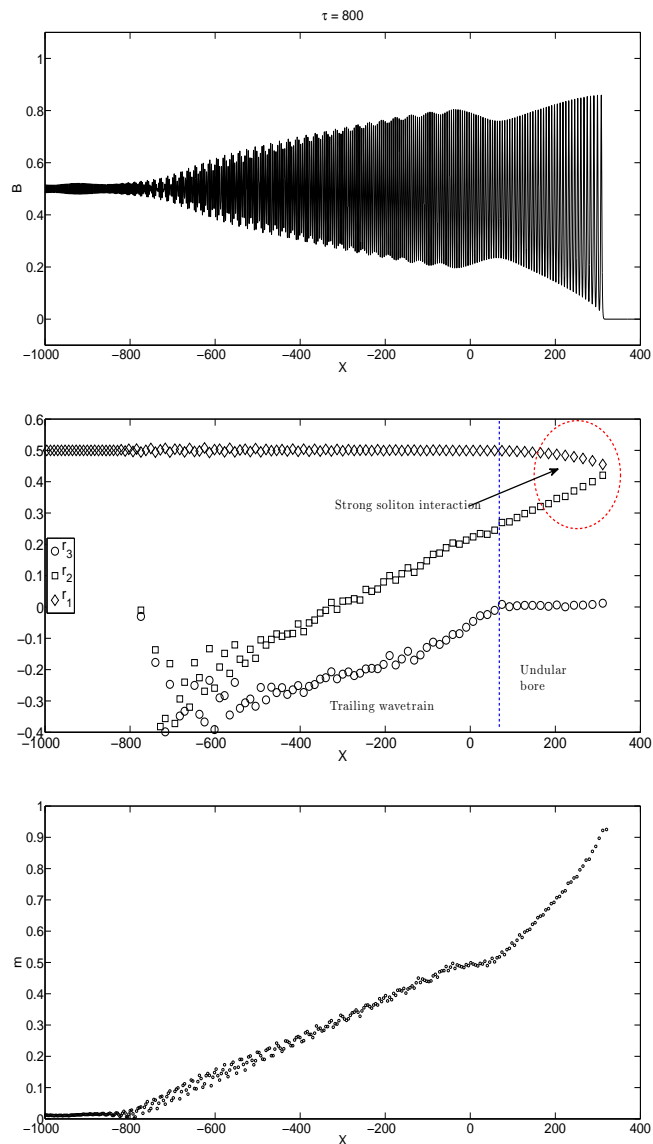
Figure 4.40: Undular bore after the slope at $\tau = 800$. Clearly, the leading wave near the leading edge is growing.

Figure 4.40 presents the undular bore after the slope at $\tau = 800$. The leading wave of the transformed bore is growing. From the behaviour of the Riemann invariants, we have a

nonlinear trailing wavetrain at the rear part of the transformed bore, similar to our results in Section 4.2.2.3. Also, the distribution of the Riemann invariants indicates that we still have the nonlocal interaction scenario at the leading edge.
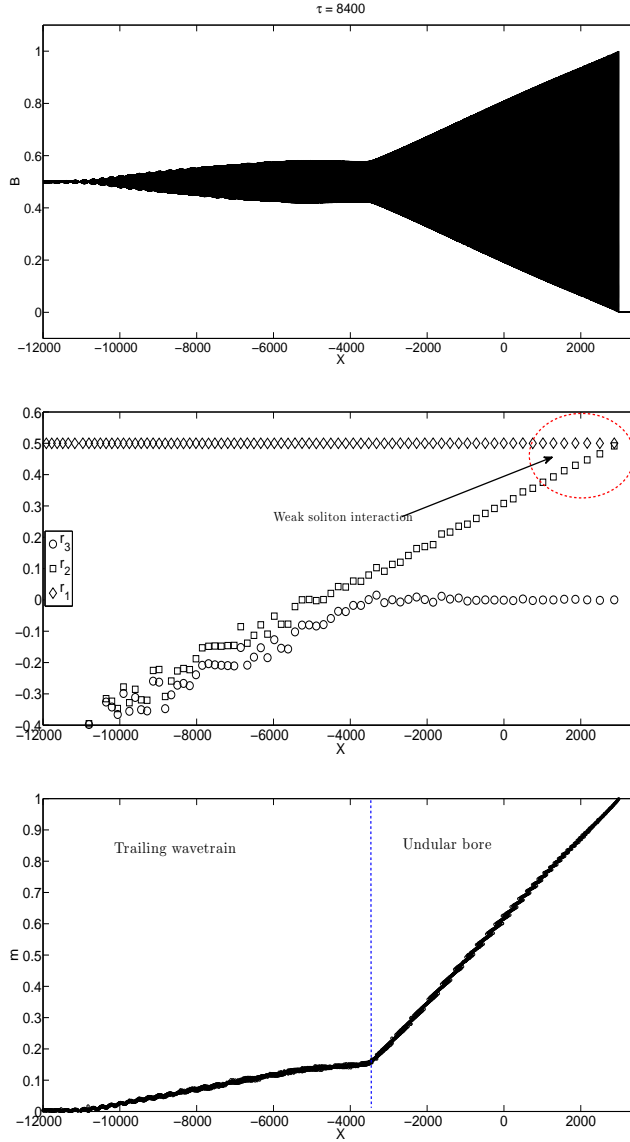
Figure 4.41: Long-time behaviour of the undular bore after the slope at $\tau = 8400$. The structure of the transformed bore is similar to those presented in Section 4.2.2.3.

In Figure 4.41, we present the long-time behaviour of the transformed bore at $\tau = 8400$. Clearly, the structure of the transformed bore is similar to those presented in Section 4.2.2.3. At the front, we have an undular bore with the leading solitary wave having an amplitude of $2U_0$, and a nonlinear trailing wavetrain at the rear part. Now, the soliton interaction at the leading edge is considered to be weak (see Figure 2.11a).

Figure 4.42 shows the comparison for the amplitudes of the leading solitary wave of the initial bore and an isolated solitary wave. One can see that the amplitude of the leading solitary wave of the initial bore right after the slope is the same as in the case for a single solitary wave . However, unlike the case for a single solitary wave, the amplitude of the leading wave of the transformed bore will increase over time until it reaches the value of $2U_0$.
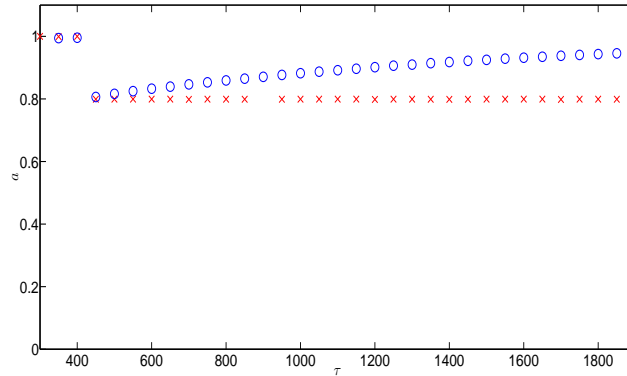
Figure 4.42: Comparison for the amplitudes for the leading solitary wave of the initial bore (blue circles) and an isolated solitary wave (red crosses).

4.4   Discussion

In this chapter, we have looked at the transformations of fully developed undular bores over different types of varying regions, i.e. a slowly decreasing depth, a slowly increasing depth, a smooth hole, a smooth bump, a rapidly decreasing depth and a rapidly increasing depth in the framework of the vKdV equation. It was shown that the propagation of undular bores over variable topography leads to a number of adiabatic and non-adiabatic effects:

(a) the generation of an advancing solitary wavetrain in front of the bore,

(b) the generation of a weakly nonlinear trailing wavetrain behind the bore,

(c) the occurrence of transient multi-phase behaviour,

(d) the occurrence of a modulation phase shift, and

(e) the change of the characteristic wavelength in the bore,

depending on the geometry of the slope. The non-adiabatic effects (a) – (c) are new results.

First, we have demonstrated that when an undular bore propagates over a broad range of slowly decreasing depth regions, the leading solitary wave will behave as an isolated solitary wave, which is described by the local interaction scenario (El *et al.*, 2007) (see Figure 2.11a). As a result, a sequence of isolated solitary waves, which is an expanding modulated solitary wavetrain is formed which propagates ahead of the bore. All solitons in the solitary wavetrain have amplitudes greater than the leading solitary wave in the undular bore. During the propagation of the bore over the slope, transient multi-phase behaviour is observed at the rear part of the bore. This is due to the increment in velocity of the linear wave packet at the rear part of the bore when propagating over the slope, which 'pushes' the linear wave packet to move forward, and thus interact with the wavetrain in front of it. The transformed bore will restore its single-phase behaviour throughout itself at a larger time. Also, there are spatial shifts in the position of the trailing and leading edges, $X_{\pm}$, of the transformed bore relative to the incident bore. The velocities of the leading and trailing edges of the undular bore after the slope remain the same as in the incident bore before the slope.

On the other hand, when an undular bore advances into a slowly increasing depth region, the evolution of the leading solitary wave is determined not only by the local variations of the topography, but also the interaction with the entire nonlinear wavetrain behind it, i.e. nonlocal interaction scenario (see Figure 2.11b) (El *et al.*, 2007). As for the linear wave packet at the trailing edge of the incident bore, it will evolve adiabatically on the slope and the velocity decreases, $\tilde{s} < -6U_0$. However, the velocity of the trailing edge of the undular bore must be $s_- = -6U_0$. Consequently, the incident bore becomes a nonlinear trailing wavetrain, attached to the rear part of the new undular bore generated by the nonlocal interaction in the transformed bore. Note that the leading and trailing edges of the transformed bore also experience some spatial shift compared to the incident bore.

The propagation of an undular bore over a smooth hole or a smooth bump is much more complicated because the evolution involves the adiabatic and non-adiabatic effects mentioned above. The final outcome of the structure of the transformed bore depends very much on the interaction of the bore with the final part of the topography. If the last section of the bottom surface is a slowly decreasing depth region, then we would expect a solitary wavetrain to be generated. Otherwise, a trailing wavetrain would be formed.

For the case where the depth changes rapidly, all the non-adiabatic effects of the interaction of the undular bore with slowly varying topography are also observed. In addition to that, a small amplitude linear wavetrain appeared to be attached to the rear part of the transformed bore when the undular bore propagates over a rapidly decreasing depth region

So far, in this chapter, we have only considered the incoming undular bore as fully developed at the moment it enters the slowly varying sloping region. However, this is not a pre-requisite to see all the adiabatic and non-adiabatic effects exhibited by the interaction of fully developed undular bores with slowly varying topography. Our numerical simulations show that all the key features presented in this chapter can be seen even for the case where the initial discontinuity is placed right before the slope, in which case the generation of the undular bore and the interaction of the bore with variable topography occurs simultaneously.

Chapter 5

Weak dissipation effects

In this chapter, we extend the problem considered in previous chapters by taking into consideration the effects of weak dissipation induced by various types of bottom friction or by volume viscosity. Here, we consider three different types of dissipative terms in the variable-coefficient KdV equation and examine the impact of weak dissipation (bottom friction in particular) on the propagation of solitary waves and undular bores over variable topography. Here, we only consider slowly varying topography. Using numerical simulations, we show that when an undular bore propagates over a gently sloping region, it also exhibits the non-adiabatic deformations mentioned in the previous chapter, depending on the parameter values of the topography and dissipation.

5.1   Mathematical model

We now consider an extension to the problem considered in the previous chapters by including the effects of weak dissipation, which can be modelled by additional perturbation terms in the vKdV equation (3.21). Thus, the suitable mathematical model to model the propagation of weakly nonlinear waves over a gradual varying slope, simultaneously subject to friction is the variable-coefficient perturbed Korteweg-de Vries (vpKdV) equation (Grimshaw, 2007b; El $et\ al.$, 2007)

$$A_t + cA_x + \frac{c_x}{2}A + \frac{3c}{2h}AA_x + \frac{ch^2}{6}A_{xxx} = F(A), \tag{5.1}$$

where $F(A)$ is generally a functional of $A(x, t)$. Of particular interest here are

(a) Chezy friction: $F(A) = -C_D\frac{c}{h^2}|A|A$,

(b) linear friction: $F(A) = -C_D\frac{c}{h}A$, and

(c) volume viscosity (Burgers' friction): $F(A) = C_D chA_{xx}$.

Here, C_D is a non-dimensional drag coefficient, which is different for different types of friction. The Chezy friction (Miles, 1983a,b; El $et\ al.$, 2007) and the linear friction (Brink, 1988; Myint & Grimshaw, 1995; Grimshaw $et\ al.$, 2003) terms have been derived to model

the turbulent bottom boundary layer, while the Burgers friction term was derived by Johnson (1970, 1972) to model the effects induced by volume viscosity. For convenience, we shall refer to "the dissipative terms" in all three cases as to friction terms.

In this chapter, we only consider the depth topography to be slowly varying. In a similar manner to those described in Chapters 3 and 4, we consider two different types of initial-value problem for the vpKdV equation (5.1).

(a) A solitary wave of a given amplitude a_0 initially propagating over a flat bottom without friction. Thus we specify

$$A_0(x) = a_0 \operatorname{sech}^2(\gamma_0 x), \qquad 4\gamma_0^2 = 3a_0.$$

So, at the initial stage, we have a soliton described by the unperturbed constant-coefficient KdV equation.

(b) An undular bore with the leading solitary wave of a given amplitude a_0 initially propagating over a flat bottom without friction. Therefore, we specify

$$A(x, t = 0) = A_0(x) \quad \text{for} \quad x < 0, \qquad A(x, t = 0) = 0 \quad \text{for} \quad x > 0.$$

Hence, at the initial stage of evolution, an undular bore solution of the constant-coefficient unperturbed KdV equation is generated.

Our main interest is to look at the impact of bottom and volume friction on the propagation of solitary waves and undular bores by comparing the results obtained numerically with the results presented in Chapters 3 and 4.

5.2 Chezy friction

First, we consider our friction term to be Chezy friction. So, our governing equation is (Miles, 1983a,b; El et al., 2007)

$$A_t + cA_x + \frac{c_x}{2}A + \frac{3c}{2h}AA_x + \frac{ch^2}{6}A_{xxx} = -C_D\frac{c}{h^2}|A|A. \tag{5.2}$$

By following similar transformation procedures mentioned in Sections 3.2 and 4.1, equation (5.2) can be asymptotically recast into the following vpKdV equations:

$$B_\tau + \frac{3}{2h^{5/4}}BB_X + \frac{h}{6}B_{XXX} = -\frac{C_D}{h^{7/4}}|B|B, \tag{5.3}$$

$$u_S + 6uu_X + u_{XXX} = F(S)u - G(S)|u|u, \tag{5.4}$$

$$\text{where} \quad F(S) = -\frac{9h_S}{4h} \quad \text{and} \quad G(S) = \frac{4C_D}{h^{1/2}}, \tag{5.5}$$

$$U_T + 6UU_X + \beta(T)U_{XXX} = -4\frac{C_D}{h^{1/2}}|U|U, \tag{5.6}$$

$$\text{where} \quad \beta(T) = h^{9/4}(T), \tag{5.7}$$

when one introduces the new variables $B(X,\tau), u(X,S)$ and $U(X,T)$ through (3.23), (3.26), (4.2), (4.6). Note that equations (5.3), (5.4) and (5.6) are exactly equivalent.

5.2.1   Adiabatic deformation of a solitary wave

First, we look at the adiabatic transformation of a solitary wave propagating over variable topography with Chezy bottom friction. One can obtain the slowly varying solitary wave solution by a multiple-scale perturbation expansion. Now, suppose that we have a very gentle slope, $h_S << 1$ and small friction coefficient, $C_D << 1$ in the vpKdV equation (5.4). Then the slowly varying solitary wave solution at the leading order is given by

$$u(X,S) = 2\gamma^2 \text{sech}^2[\gamma(X - \phi(S))], \tag{5.8}$$

where

$$\frac{d\phi}{dS} = V_s = 4\gamma^2. \tag{5.9}$$

We can derive the "momentum" balance equation for the vpKdV equation (5.4)

$$P_S = 2F(S)P - G(S)Q, \tag{5.10}$$

where

$$P = \int_{-\infty}^{\infty} \frac{u^2}{2}dX \quad \text{and} \quad Q = \int_{-\infty}^{\infty} |u|^3 dX. \tag{5.11}$$

Substituting (5.8) into (5.10) yields a first-order differential equation for $\gamma(S)$,

$$\frac{d\gamma}{dS} = \frac{2}{3}F(S)\gamma - \frac{16}{15}G(S)\gamma^3, \tag{5.12}$$

which can be integrated to give

$$\frac{1}{\gamma^2} = h^3 \left(C_0 + \frac{64}{45}C_D \int_0^x \frac{dx'}{h^3} \right), \tag{5.13}$$

where C_0 is an integration constant. By picking a reference point at $x = 0$ where $h = h_0$ and $a = a_0$, the constant of integration is given by $C_0 = 4/(3a_0h_0)$. From (5.8), the amplitude of the solitary wave is $2\gamma^2$ and with the help of (5.13), we obtain the formula

5.2.1 Adiabatic deformation of a solitary wave
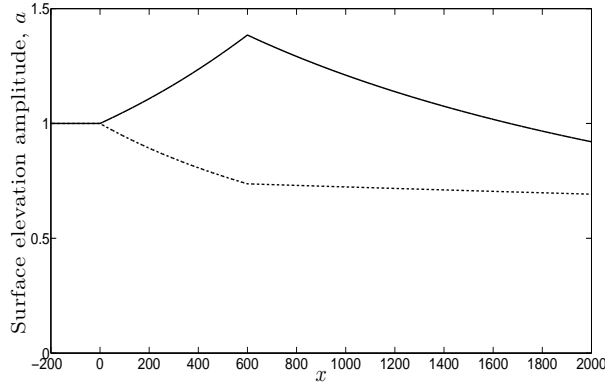
Figure 5.1: Surface elevation amplitude of the solitary wave described by formula (5.14) where $a_0 = 1, h_0 = 1, C_D = 0.0001$ for different kinds of topography: slowly decreasing depth – solid line, slowly increasing depth – dashed line.

describing the amplitude variations of slowly varying solitary waves over an uneven bottom with Chezy friction

$$a = a_0 \left(\frac{h_0}{h}\right) \left[1 + \frac{16}{15} C_D a_0 h_0 \int_0^x \frac{dx'}{h^3}\right]^{-1}, \tag{5.14}$$

where a_0 and h_0 are the initial solitary wave amplitude and local depth respectively. The formula in (5.14) was obtained by a different method in Miles (1983a,b) and then in El *et al.* (2007). Note that the factor $16C_D/15$ in El *et al.* (2007) is different from Miles (1983a,b) due to different definition of C_D used in their work. When $C_D = 0$, this reduces to $a \sim h^{-1}$. The amplitude variations for the solitary wave for different types of varying slopes are shown in Figure 5.1. The trajectory of the solitary wave is obtained from (5.9) and (5.13)

$$X_s = \frac{a_0 h_0}{2} \int_0^x dx' \, h^{-5/2}(x') \left[1 + \frac{16}{15} C_D a_0 h_0 \int_0^{x'} \frac{dz}{h^3(z)}\right]^{-1}. \tag{5.15}$$

5.2.1.1   Numerical results

In this section, we compare the analytical results for solitary wave propagation over different types of slowly varying slopes with Chezy friction with those obtained from direct numerical simulations.

5.2.1 Adiabatic deformation of a solitary wave
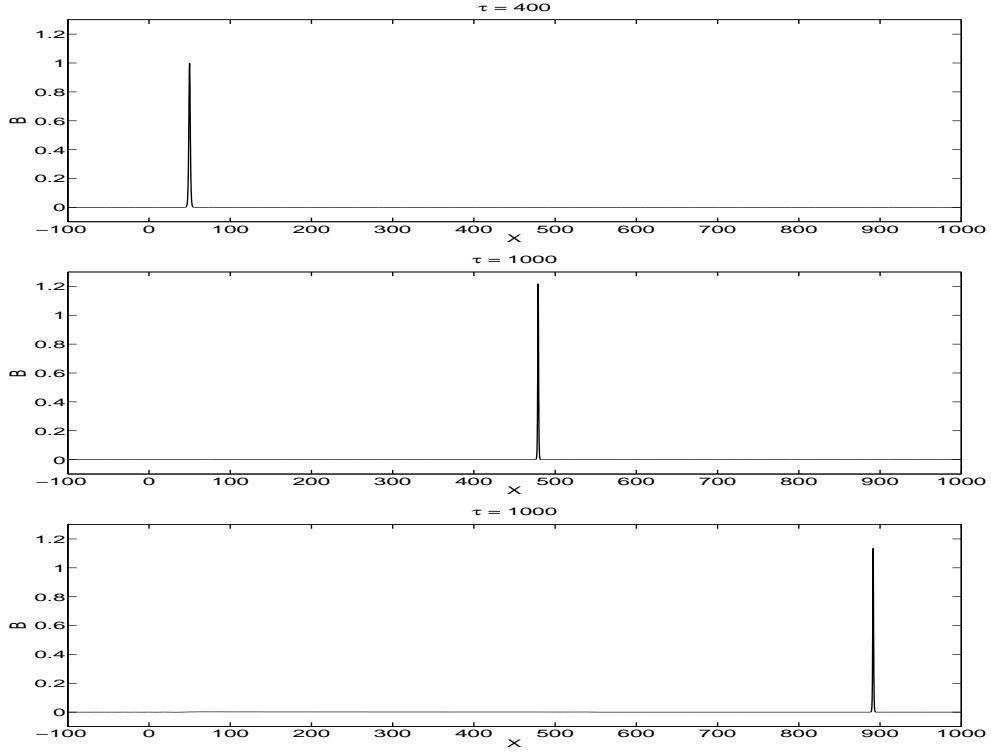
Figure 5.2: Propagation of a solitary wave over a slowly decreasing depth region described by (5.16) with Chezy friction.

5.2.1.1.1 Slowly decreasing depth

First, we consider that a solitary wave is propagating over a slowly decreasing depth region. Thus, we would expect the solitary wave to grow due to the decreasing depth topography. However, the friction has an opposite effect to the amplitude variation. The outcome depends on the relative magnitude of the slope and friction terms in the vpKdV equation.

In Figure 5.2, we present the numerical simulations for the evolution of a solitary wave according to the vpKdV equation (5.3) (see Appendix A.4.1) over a slope described by

$$h(\tau) = \begin{cases} 1.0 & : \tau < 400 \\ \left(1 - \frac{\alpha(\tau-400)}{2}\right)^2 & : 400 < \tau < 1066.67 \quad , \qquad \alpha = 0.0006. \\ 0.64 & : \tau > 1066.67 \end{cases} \qquad (5.16)$$

The initial condition is

$$B(X,0) = \operatorname{sech}^2(\gamma X) \qquad \text{where} \qquad \gamma = (3/4)^{1/2}. \qquad (5.17)$$

102

5.2.1 Adiabatic deformation of a solitary wave

Figure 5.3: Comparison for the amplitudes for the solitary wave propagating over a slowly decreasing depth region with Chezy friction: formula (5.19) with $h_0 = 1, a_0 = 1, C_D = 0.0001$ – red line, formula (5.19) with $h_0 = 1, a_0 = 1, C_D = 0.0005$ – blue line; numerical data with $C_D = 0.0001$ – diamonds; numerical data with $C_D = 0.0005$ – circles; numerical data with $C_D = 0$ – dashed line.

The drag coefficient, C_D is given by

$$C_D = \begin{cases} 0 & : \tau < 400 \\ 0.0001 & : \tau > 400 \end{cases},$$ (5.18)

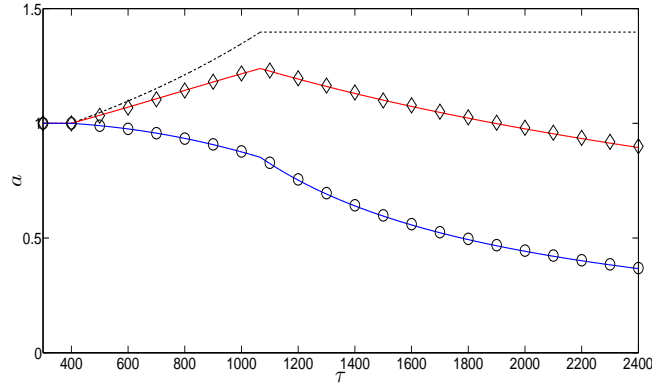i.e. the bottom friction "switches on" when the solitary wave reaches the variable region. The drag coefficient is chosen in this form so that the bottom friction would not dominate the undular bore propagation.

Figure 5.3 shows the comparison for the amplitudes of the solitary wave obtained numerically with the theoretical prediction given by the formula

$$a = a_0 \left(\frac{h_0}{h(\tau)} \right)^{3/4} \left[1 + \frac{16}{15} C_D a_0 h_0^{3/4} \int_0^\tau \frac{d\tau}{h^{5/2}} \right]^{-1}.$$ (5.19)

Here, a_0 and h_0 are the initial amplitude and depth respectively. The formula (5.19) is the exact counterpart of (5.14) for the vpKdV equation (5.3). Clearly, the amplitude growth of the solitary wave in the shoaling region is less than the case when there is no friction (dashed line). After reaching the flat bottom region at $\tau = 1066.67$, the amplitude decays under the sole effect of bottom friction. If $C_D > 0.0001$, say $C_D = 0.0005$, then the solitary wave will not grow at all despite the decreasing depth (circles). In general, whether or not the amplitude increases is determined by the combination of the effects of the slope, the depth and the bottom friction.

5.2.1 Adiabatic deformation of a solitary wave

5.2.1.1.2 Slowly increasing depth

Now, we consider the depth to be slowly increasing. In this case, the solitary wave amplitude will decrease when it encounters the varying depth region. However, due to the effect of friction, the decrement of the solitary wave amplitude is much higher than the case when $C_D = 0$.

In Figure 5.4, we present the numerical simulations for the propagation of a solitary wave over a slowly increasing depth region. The numerical solution is obtained for the vpKdV equation (5.3). The $h(\tau)$ profile is given by

$$h(\tau) = \begin{cases} 1.0 & : \tau < 400 \\ \left(1 + \frac{\alpha(\tau-400)}{2}\right)^2 & : 400 < \tau < 960.7 \\ 1.3 & : \tau > 960.7 \end{cases}, \qquad \alpha = 0.0005. \qquad (5.20)$$

The initial data and the drag coefficient are given by (5.17) and (5.18) respectively.
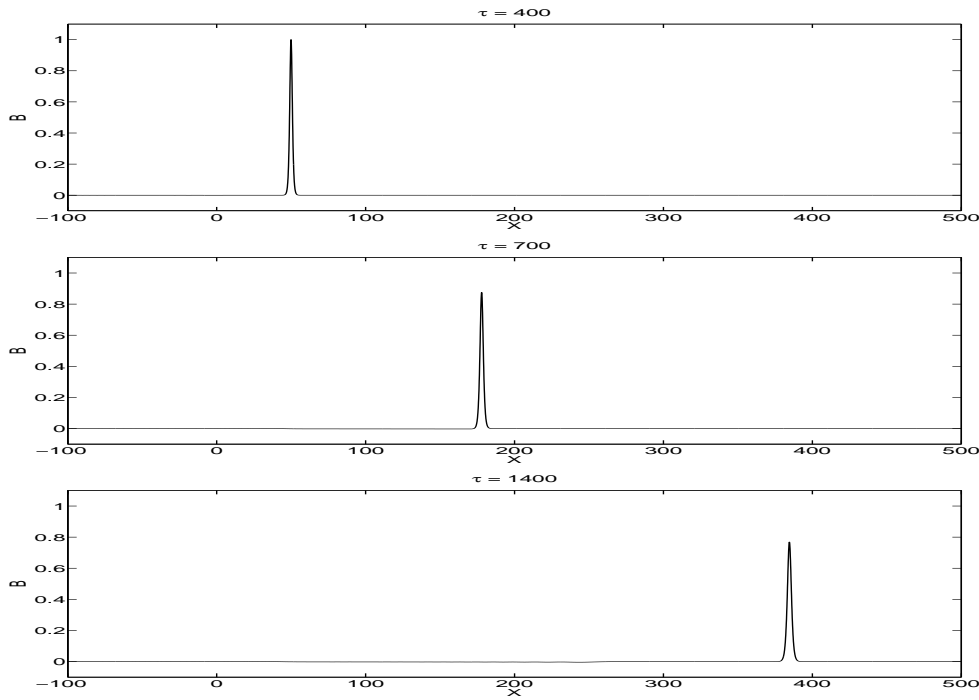
Figure 5.4: Propagation of a solitary wave over a slowly increasing depth topography described by (5.16) with Chezy friction.

Figure 5.5 shows the comparison for the numerically found amplitude of the solitary wave propagating over an increasing depth region with formula (5.19). Diamonds are the solitary wave amplitude over the slope with $C_D = 0.0001$, while circles are for the case when $C_D = 0.0005$. Again, we have excellent agreement between the numerical simulations

(diamonds, circles) and the corresponding theoretical prediction (solid lines). The dashed line shows the propagation of solitary waves over the same slope without friction. In both decreasing and increasing depth cases, the solitary wave amplitude continues to decrease on the shelf after the slope due to the presence of bottom friction.
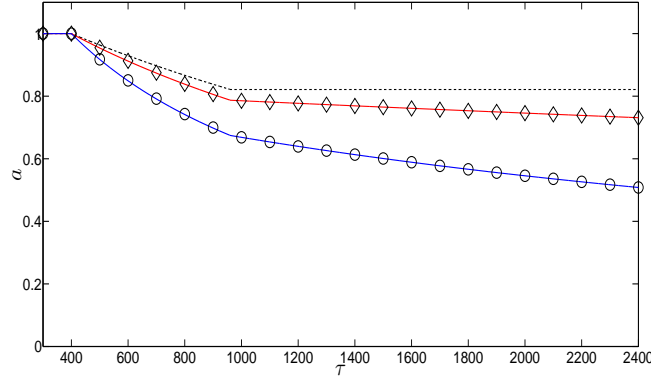
Figure 5.5: Comparison for the amplitudes for the solitary wave propagating over a slowly increasing depth region with Chezy friction: formula (5.19) with $h_0 = 1, a_0 = 1, C_D = 0.0001$ – red line, formula (5.19) with $h_0 = 1, a_0 = 1, C_D = 0.0005$ – blue line; numerical data with $C_D = 0.0001$ – diamonds; numerical data with $C_D = 0.0005$ – circles; numerical data with $C_D = 0$ – dashed line.

5.2.2 Transformation of an undular bore over variable topography with Chezy friction

In this subsection, we will look at the simultaneous effects of varying slope and bottom friction on the evolution of undular bores. In the previous chapter, where the effect of bottom friction was ignored, the interaction between undular bores and the varying topography had no impact on the jump, $[U]$, across the bore. However, this is not true when friction is present. To illustrate this, let us use the same definition of the jump, i.e.

$$[U] = \int_{X_a(T)}^{X_b(T)} U_X(X, T)\, dX \,, \tag{5.21}$$

$$= U(X_b) - U(X_a), \tag{5.22}$$

where the undular bore is confined in the region $X_a(T) < X < X_b(T)$. From the vpKdV equation (5.6), we have

$$[U]_T = \frac{\partial}{\partial T} \int_{X_a(T)}^{X_b(T)} U_X\, dX, \tag{5.23}$$

$$= \frac{4C_D}{h^{1/2}(T)} U_0^2, \tag{5.24}$$

5.2.2 Transformation of an undular bore over variable topography with Chezy friction

where $U_X = U_{XXX} = 0$ at $X = X_{a,b}(T)$. Here, we have assumed that the undular bore propagates into the undisturbed depth region, $U(X_b) = 0$. Thus, we obtain

$$[U] = -U_0 \left[1 - 4C_D U_0 \int_{T_0}^{T} h^{-1/2}(T') \, dT' \right] \qquad \text{for all} \qquad T > 0. \qquad (5.25)$$

We can see that the jump, $[U]$, varies with time. This will later be confirmed by direct numerical simulations. Since the jump, $[U]$, does not remain the same, this implies that the amplitude of the leading solitary wave of the undular bore is changing with time and no longer has the same value as in the incident bore, $2U_0$. Instead, we would generally expect that the leading solitary wave amplitude of the bore will decrease as time increases.

5.2.2.1 Slowly decreasing depth

First, we assume that the depth decreases slowly, $\beta_T < 0$ in the vpKdV equation (5.3). In the previous chapter, we have shown that the leading solitary wave of the undular bore behaves as a separate, isolated, adiabatically varying solitary wave when the bore interacts with a shoaling slope. The interaction between the undular bore and the decreasing depth region generates a train of solitary waves ahead of the bore. The leading solitary wave amplitude in the soliton wavetrain will be proportional to the inverse of the local depth.

Thus, in the current problem, we would expect to see the formation of a soliton train as well as the result of the interaction of the bore with the slope, provided the friction effect is smaller than the effect of the slope. However, the amplitude of the leading solitary wave in the solitary wavetrain will no longer be proportional to the inverse of the water depth. Instead, it will vary according to the formula

$$a = a_0 \left(\frac{h_0}{h(T)} \right)^{3/4} \left[1 + \frac{64}{15} C_D a_0 h_0^{3/4} \int_0^T \frac{dT}{h^{5/4}} \right]^{-1} \qquad (5.26)$$

due to the friction effect. Here, again, h_0 and a_0 are the initial depth and solitary wave amplitude respectively. Equation (5.26) is the exact counterpart of equation (5.14) for the vpKdV equation (5.6).

In Figure 5.6, we present the profile of the evolution of an undular bore over a slowly decreasing depth region with bottom friction obtained by solving the vpKdV equation (5.3) numerically. The depth profile is described by (5.16). The initial condition is taken as in (4.27). Also, the drag coefficient, C_D is given by (5.18) so that an undular bore is fully developed before the slope, $\tau < 400$. In plot 3 of the Figure 5.6, one can see the formation of a solitary wavetrain ahead of the bore. The effect of bottom friction still has impact on the propagation of the transformed bore after the slope. Thus, all the solitary

5.2.2 Transformation of an undular bore over variable topography with Chezy friction

waves in the soliton wavetrain will continue to decay after the slope. Similarly, the bottom friction also affects the entire structure of the undular bore, which leads to the strong interaction scenario at the leading edge. Consequently, the nonlocal interaction near the leading edge will push the leading wave to grow (El *et al.*, 2007). However, the growth will not last since the mean level across the bore is decreasing over time. Due to the difference between the amplitude of the leading wave in the transformed bore and solitons in the solitary wavetrain, the bore will overtake the solitary wavetrain. This process is shown in plots 4 and 5 of the Figure 5.6. Strictly speaking, at large time, the transformed bore is no longer an undular bore but a nonlinear wavetrain. However, for convenience, we still refer to it as a bore.

At the trailing edge of the bore, the linear wave packet at the trailing edge travels faster once it enters the sloping region as described by (4.25) and will restore to the value of $-6U_0$ again, similar to our discussion in Chapter 4. At larger time, the entire structure of the transformed bore will transform into a small-amplitude nonlinear wavetrain before the wave structure collapses entirely.

Figure 5.7 shows the characteristic plots for the leading soliton in the solitary wavetrain, $X_s(T)$, and the trailing edge of the transformed bore, $X_-(T)$, obtained by solving numerically the vpKdV equation (5.6). The slope profile is given by

$$h(T) = \begin{cases} 1.0 & : T < 300 \\ (1 - \alpha(T - 300)) & : 300 < T < 800 \\ 0.64 & : T > 800 \end{cases}, \qquad \alpha = 0.00072. \qquad (5.27)$$

The initial condition is taken as in (4.28) and the drag coefficient, C_D is given by (5.18). One can see that the leading soliton in the solitary wavetrain continue to slow down due to the bottom friction.

5.2.2 Transformation of an undular bore over variable topography with Chezy friction
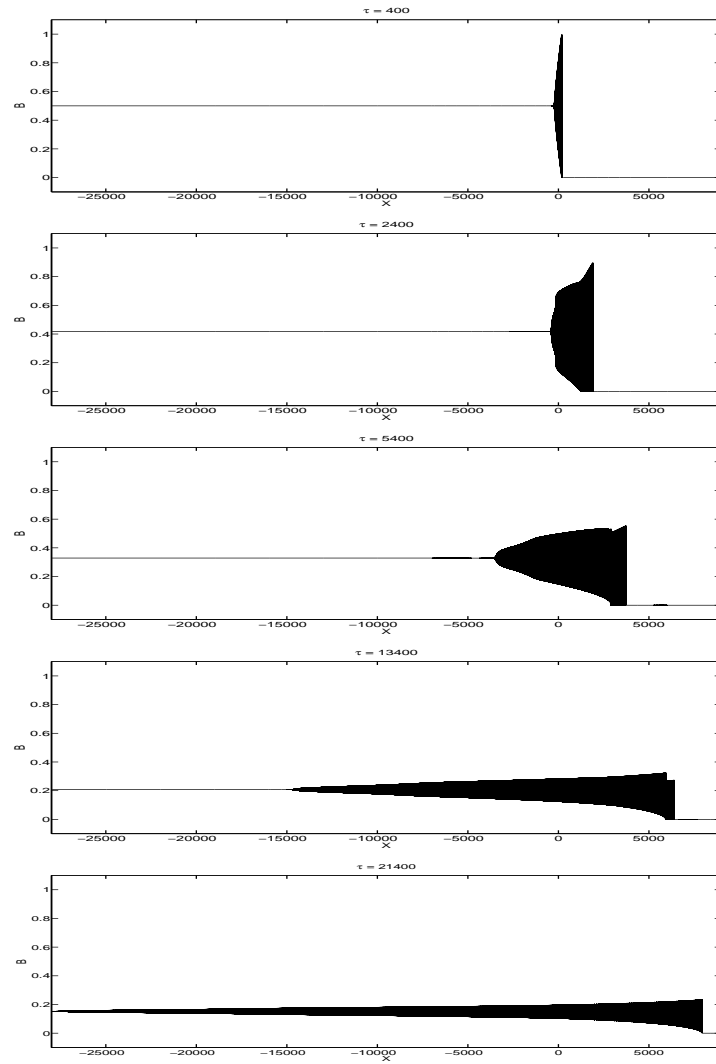

Figure 5.6: Propagation of an undular bore over a slowly decreasing depth region with Chezy friction, where the profile $h(\tau)$ is given by (5.16).
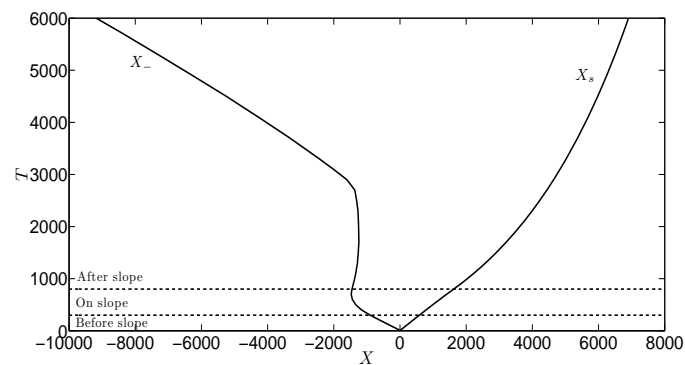

Figure 5.7: The characteristics plots for the leading soliton in solitary wavetrain, $X_s(T)$ and the trailing edge of the bore, $X_-(T)$.

5.2.2 Transformation of an undular bore over variable topography with Chezy friction

5.2.2.1.1   Numerical results

In this section, we will look at the numerical results for the vpKdV equation (5.3) where the variable topography and the friction coefficient, C_D are given by (5.16) and (5.18) respectively in order to confirm our assumptions:

(a) the wave dynamics near the leading edge of the undular bore on the slope is governed by the weak soliton interaction scenario (El *et al.*, 2007),

(b) there is a formation of a solitary wavetrain ahead of the undular bore after the slope due to the interaction of the undular bore with the shoaling region,

(c) the amplitude of the leading soliton in the solitary wavetrain is smaller than the case when there is no friction during the entire evolution process,

(d) the occurrence of a transient multi-phase behaviour at the rear part of the undular bore during the evolution,

(e) the jump, $[U]$, across the bore is changing with time after the slope is encountered, and

(f) at large time, the entire structure of the transformed bore is a small-amplitude non-linear wavetrain.

All the numerical results are illustrated in Figures 5.8 – 5.13. In each of the Figures 5.8 – 5.12, we have three plots at a particular value of time, $\tau = \tau_i$: the top plot shows the numerical solution for $B(X, \tau_i)$, the middle plot shows the behaviour of the Riemann invariants, r_j corresponding to the top plot and the bottom plot correspond to the value of the modulus, m, obtained numerically.

Figure 5.8 shows the initial bore before the slope, $\tau = 400$. As expected, both the Riemann invariants behaviour and the distribution of the modulus m agree with the Gurevich-Pitaevskii solution.

5.2.2 Transformation of an undular bore over variable topography with Chezy friction
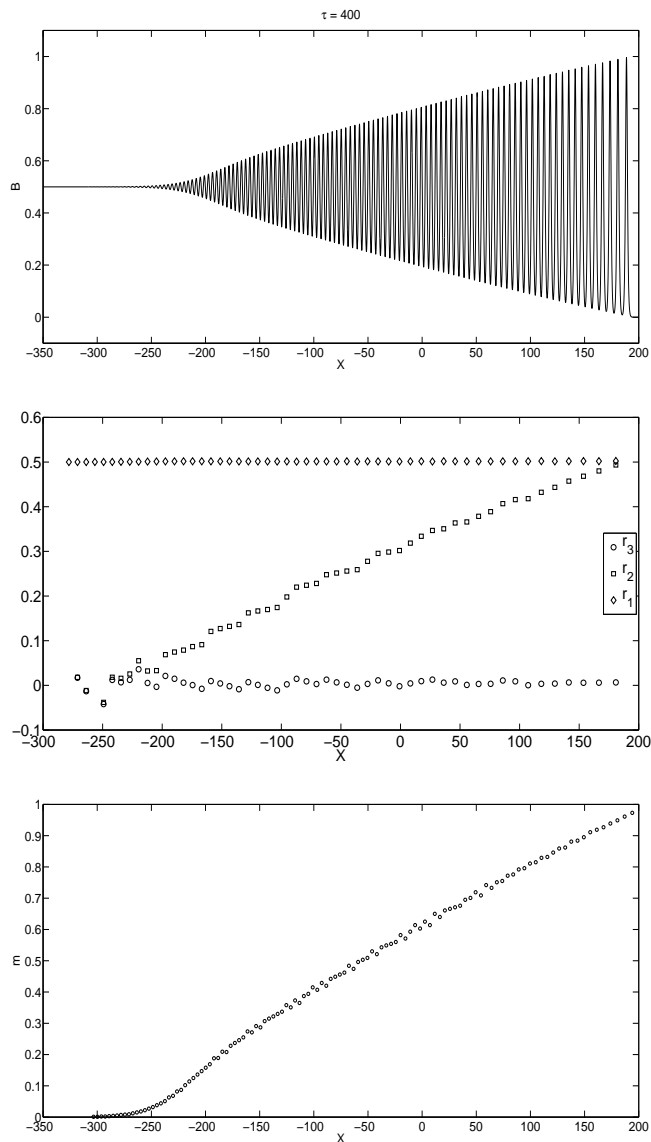
Figure 5.8: Initial undular bore before slope, $\tau = 400$. Upper plot: $B(X)$; Middle plot: the modulation of Riemann variables, $r_3 \leq r_2 \leq r_1$ obtained from the plot for $B(X)$; Bottom plot: the distribution of the modulus m.

Figure 5.9 corresponds to the undular bore propagation "shortly" after the slope, $\tau = 2400$. Clearly, there is a solitary wavetrain in front of the bore since $r_1 = r_2$ (the middle plot) and $m \to 1$ (the bottom plot) in that region. Note that at this moment, we have the "weak soliton interaction" scenario near the leading edge of the bore (see Figure 2.11a). Also present is the multi-phase behaviour near the trailing edge of the bore. In this region, the modulus m is not defined. All these observations are similar to and coincide with the results discussed in Chapter 4 when friction effect was neglected. In this case, the amplitudes of the leading soliton in the solitary wavetrain and the leading solitary wave of

5.2.2 Transformation of an undular bore over variable topography with Chezy friction

the bore after the slope continue to decrease due to the sole effect of the bottom friction.
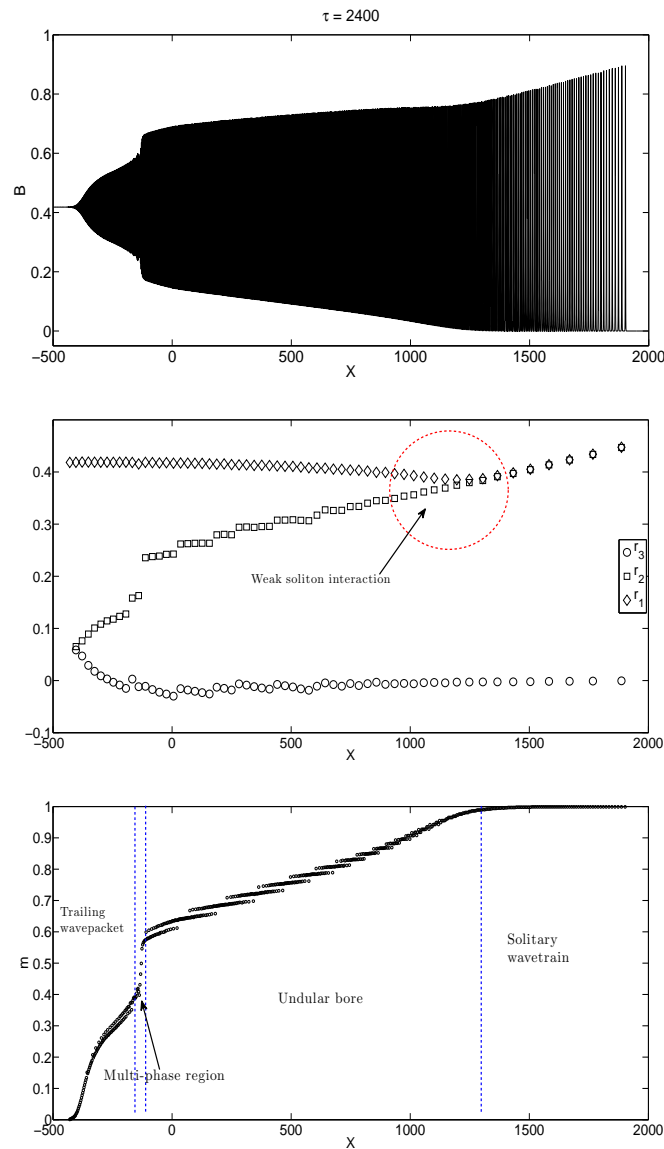
Figure 5.9: Same as Figure 5.8 but for $\tau = 2400$ (after the slope). One can see the solitary wavetrain ($m \to 1$ and $r_1 = r_2$) forming between $X \approx 1300$ and $X \approx 1900$. Also, multi-phase interaction is observed at $X \approx -200$.

In Figure 5.10, we have the plot of the bore after the slope, $\tau = 5400$. Here, the soliton interaction near the leading edge is starting to change from the "weak interaction" scenario to the "strong interaction" scenario due to the frictional effect. This is clear from the plot of the Riemann invariants distribution (the middle plot). The amplitudes of all the solitons in the solitary wavetrain continue to decrease due to bottom friction. Note that the transformed bore has restored its single-phase interaction throughout the bore at this

5.2.2 Transformation of an undular bore over variable topography with Chezy friction

moment.
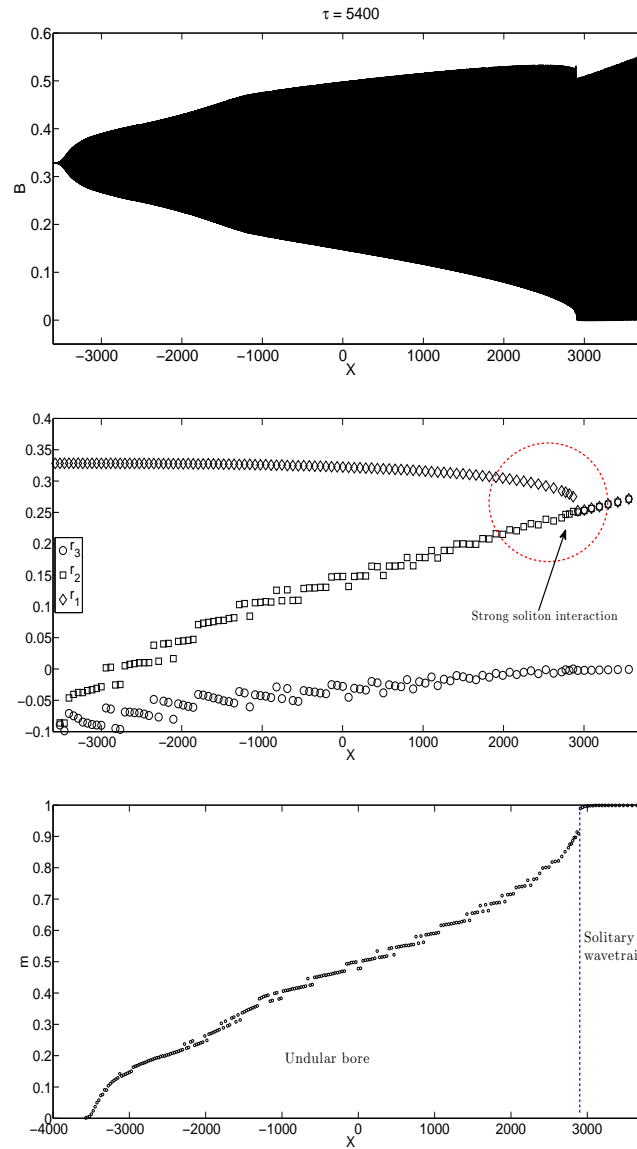
Figure 5.10: Same as Figures 5.8, 5.9 but for $\tau = 5400$ (after the slope). One can see "strong soliton interaction" near the leading edge, $X \approx 2900$ and formation of solitary wavetrain between $X \approx 2900$ and $X \approx 3600$.

Figure 5.11 shows the long-time behaviour of the bore after the slope, $\tau = 13400$. We can see that the leading wave of the bore is growing due to the nonlocal interaction near the leading edge. Since the leading wave amplitude of the bore is greater than all solitons in the solitary wavetrain, we expect the bore to overtake the solitary wavetrain. From the behaviour of the Riemann invariants, we can see that the bore behind the solitary wave is actually a nonlinear wavetrain.

5.2.2 Transformation of an undular bore over variable topography with Chezy friction
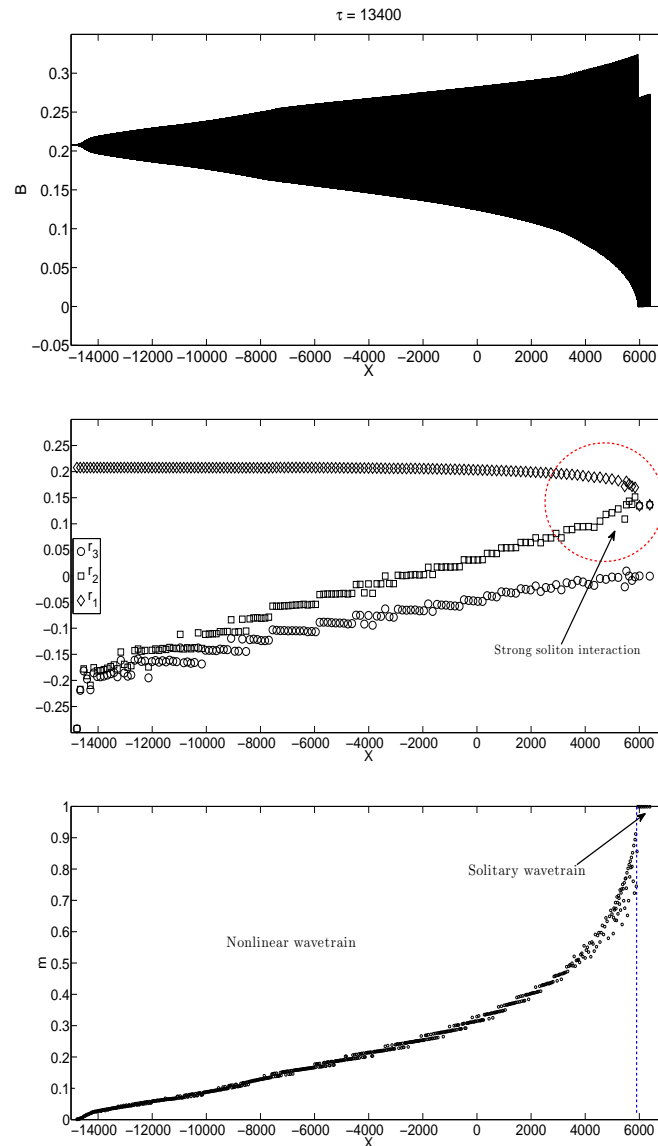
Figure 5.11: Same as Figures 5.8, 5.9, 5.10 but for $\tau = 13400$ (long-time after the slope). One can see the bore is overtaking the solitary wavetrain.

In Figure 5.12, we present another plot for the long-time behaviour of the bore after the slope, $\tau = 23400$. Here it is clear that the nonlinear wavetrain has overtaken the soliton wavetrain. Also, we still have the "strong interaction" scenario near the leading edge of the bore (see the middle plot). Despite the nonlocal interaction near the leading edge, the entire bore is decaying due to the collapse of the jump, $[U]$, across the bore. The entire wave structure is now a nonlinear wavetrain as indicated by the behaviour of the Riemann invariants. The presence of the multi-valued regions in the distribution of the modulus, m, in Figures 5.8 – 5.12 does not indicate that the transformed bore is a multi-phase wavetrain. These regions are due to numerical artifact.

5.2.2 Transformation of an undular bore over variable topography with Chezy friction
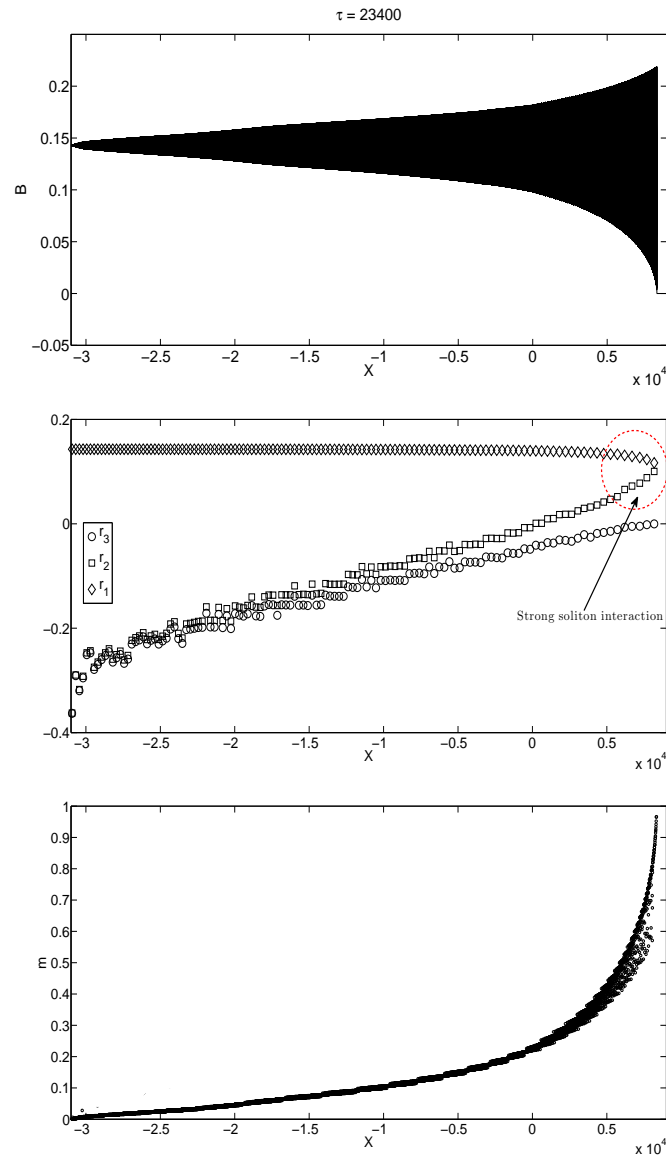
Figure 5.12: Same as Figures 5.8, 5.9, 5.10, 5.11 but for $\tau = 23400$ (long-time after the slope). The entire structure now represents a small-amplitude nonlinear wavetrain.

Figure 5.13 shows the comparison of the amplitudes for the leading soliton in the solitary wavetrain, which was part of the initial undular bore, for different values of the friction coefficient. It is clear that without the frictional effect, the leading soliton in the solitary wavetrain grows more compared to the case when friction is present. With a stronger friction coefficient, the leading wave amplitude of the bore decreases on the slope despite the decreasing depth topography. We can see that the numerical data matches well with the theoretical prediction (5.19), proving that the leading solitary wave of the initial bore is behaving like a single soliton, as described by the weak interaction scenario (El *et al.*, 2007) when advancing in the direction of decreasing depth topography (see Section 4.2.2.2).

5.2.2 Transformation of an undular bore over variable topography with Chezy friction
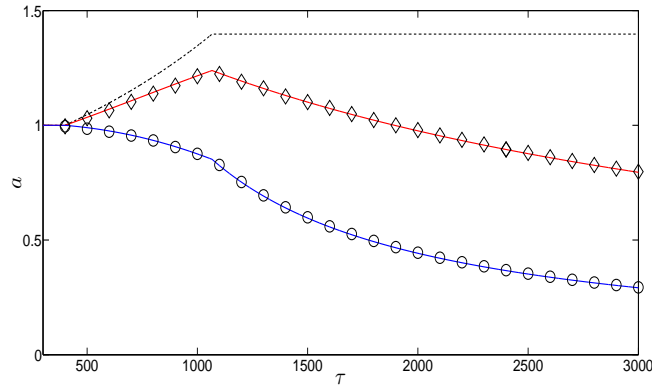
Figure 5.13: Comparison for the amplitudes for the leading solitary wave of the undular bore propagating over a slowly decreasing depth region with Chezy friction: formula (5.19) with $h_0 = 1, a_0 = 1, C_D = 0.0001$ – red line, formula (5.19) with $h_0 = 1, a_0 = 1, C_D = 0.0005$ – blue line; numerical data with $C_D = 0.0001$ – diamonds; numerical data with $C_D = 0.0005$ – circles; numerical data with $C_D = 0$ – dashed line.
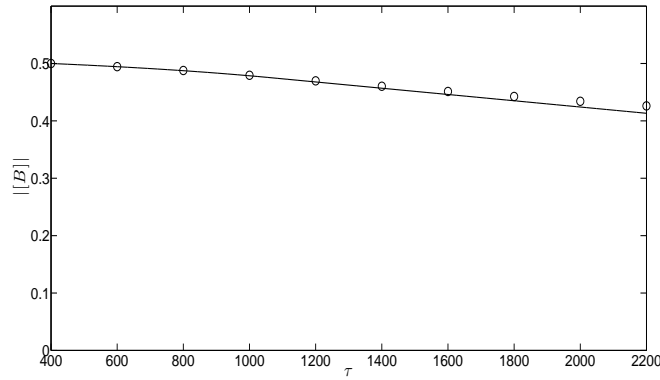
Figure 5.14: Comparison for the variations of the absolute value of jump, $|[B]|$ across the undular bore. Circles corresponds to the numerical data and the solid line to the analytical prediction (5.28).

Figure 5.14 shows the comparison for the variations of the absolute value of the jump, $|[B]|$, across the undular bore. For the vpKdV equation (5.3), the jump, $[B]$, across the bore is given by

$$[B] = -B_0 \left[1 - C_D B_0 \int_{\tau_0}^{\tau} h^{-7/4}(\tau') \, d\tau' \right] \qquad \text{for all} \qquad \tau > 0. \tag{5.28}$$

Here, B_0 is the initial jump across the bore before the slope. Note that equations (5.25) and (5.28) are exactly equivalent. One can see that there is a good agreement between the numerical simulation and analytical prediction. This confirms our result that the bottom friction will influence the jump across the bore.

5.2.2 Transformation of an undular bore over variable topography with Chezy friction

5.2.2.2   Slowly increasing depth

Now, we consider the propagation of an undular bore over a slowly increasing depth to-pography with Chezy friction. From our discussions in the previous chapter, no solitary wavetrain would be generated in this case. Instead, the amplitude of the leading solitary wave starts to decrease after it enters the negative slope region. This leads to wave de-celeration and, therefore, enhancedx interaction with the rest of the nonlinear wavetrain. Consequently, the leading wave starts to grow. However, the growth of the leading wave would be smaller than the case when $C_D = 0$. Since the bottom friction is still in force, the bore will start to decay again after some growth.

For the rest of the propagation, the leading edge would be in the "strong soliton interaction" scenario due to the frictional effect. However, this does not lead to more growth at the leading edge as the mean flow across the bore is collapsing.

As mentioned earlier in Section 4.2.2.3, the linear wave packet at the trailing edge of the incident bore travels slower when it advances through the slope. Therefore, part of the initial bore will now become a nonlinear trailing wavetrain and it will attach to the trailing edge of the new undular bore generated due to the strong interaction near the leading edge.

In Figure 5.15, we present the evolution profile of an undular bore propagating over a slowly increasing depth region with Chezy friction. The $h(\tau)$ profile is described by (5.20) while the initial data is given by (4.27). In plot 4, one can see clearly that the transformed bore consists of an undular bore at the front part and nonlinear trailing wavetrain at the rear part, which is similar to our observation made in Section 4.2.2.3.

Figure 5.16 shows the characteristic plots for the leading and trailing edges of the undular bore propagating over the topography described by

$$
h(T) = \begin{cases} 1.0 & : T < 300 \\ (1 + \alpha(T - 300)) & : 300 < T < 800 \\ 1.2 & : T > 800 \end{cases}, \qquad \alpha = 0.0004, \qquad (5.29)
$$

according to the vpKdV equation (5.6). One can see that the key features of the interaction of an undular bore with a slowly increasing depth topography is preserved as well in this case. The velocity of the leading edge continues to decrease over time due to the effect of bottom friction.

5.2.2 Transformation of an undular bore over variable topography with Chezy friction
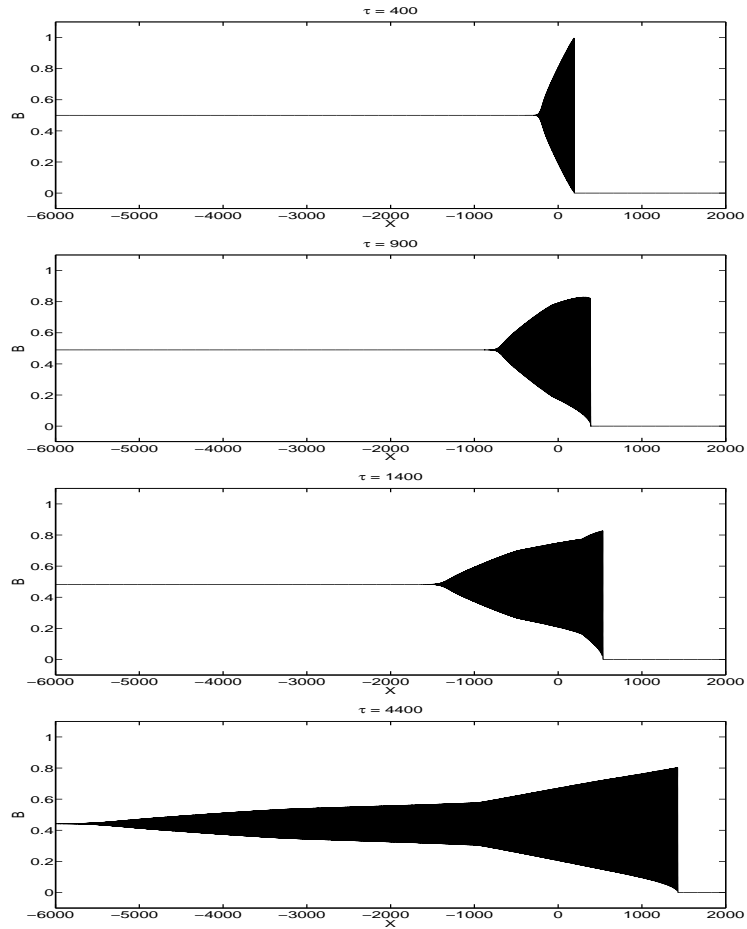
Figure 5.15: Propagation of an undular bore over a slowly increasing depth region with Chezy friction, where the profile $h(\tau)$ is given by (5.20)
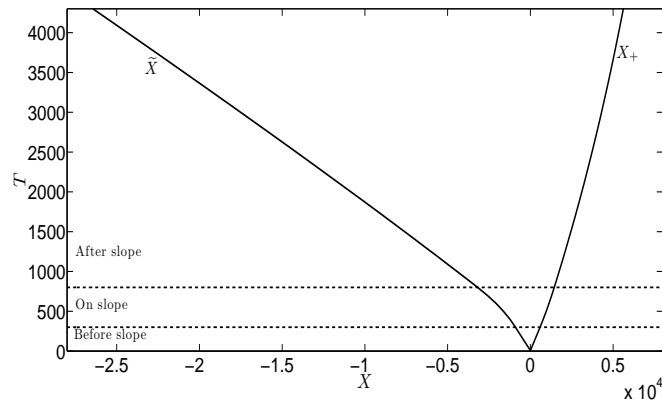
Figure 5.16: Characteristics plots for the leading and trailing edges of an undular bore propagating over a slowly increasing depth topography with Chezy friction, $C_D = 0.0001$.

5.2.2 Transformation of an undular bore over variable topography with Chezy friction

5.2.2.2.1 Numerical results

Now, we will use numerical results to confirm the evolution scenario described earlier, which was based on the following assumptions:

(a) the evolution of the undular bore is influenced not only by local variations of the topography or/ and bottom friction, but also by the nonlocal interaction at the leading edge, which is the description of the strong soliton interaction scenario mentioned in El *et al.* (2007),

(b) the mean flow across the bore decreases over time,

(c) there is a nonlinear trailing wavetrain generated at the rear part of the transformed bore after the slope, and

(d) at larger time, the transformed bore becomes a weakly nonlinear wavetrain.

All numerical results are based on the numerical solution of the vpKdV equation (5.3) where the depth profile and initial condition are given by (5.20) and (4.27) respectively. The results are presented in Figures 5.17 – 5.21. The plot for the initial bore before the slope is the same as in Figure 5.8.

Figure 5.17 shows the undular bore on the slope with friction at $\tau = 900$. The leading wave amplitude of the bore decreases once it enters the varying region. Note that the behaviour of the Riemann invariants near the leading edge in the middle plot indicates the presence of strong interaction scenario (see Figure 2.11b).

5.2.2 Transformation of an undular bore over variable topography with Chezy friction
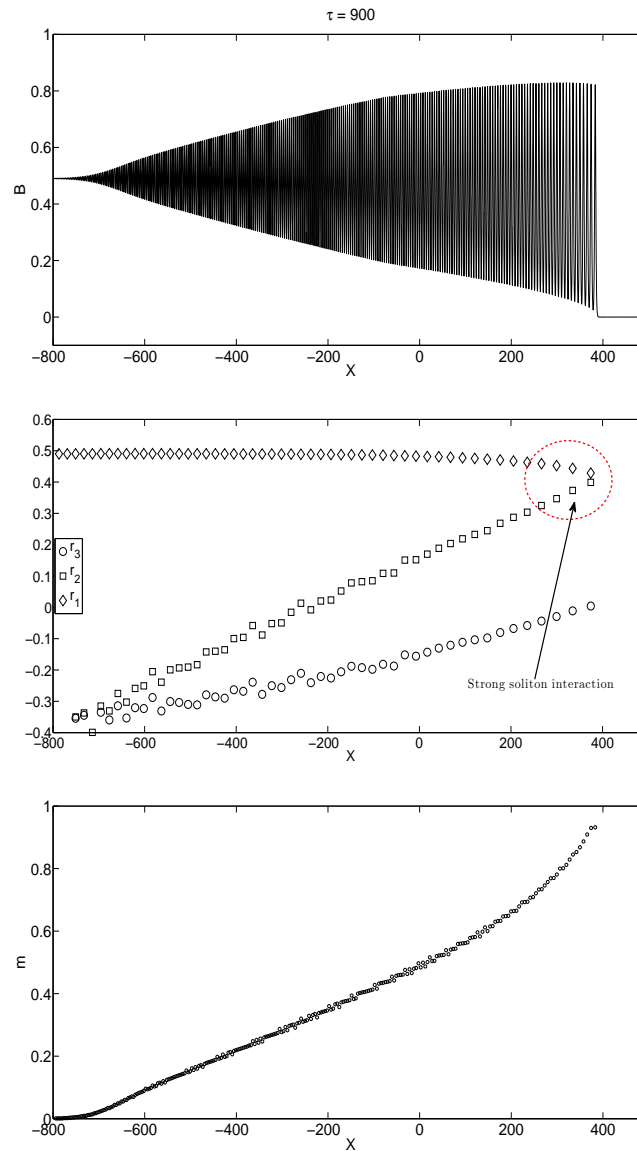
Figure 5.17: Undular bore after the slope at $\tau = 900$. The amplitude of the leading wave is decreasing. Note the strong soliton interaction near the leading edge.

Figure 5.18 corresponds to the bore "shortly" after the slope, $\tau = 1400$. Again, the behaviour of the Riemann invariants indicates that we have strong interaction scenario near the leading edge (see Figure 2.11b). One can see that the nonlocal interaction near the leading edge pushes the leading wave to grow.

5.2.2 Transformation of an undular bore over variable topography with Chezy friction
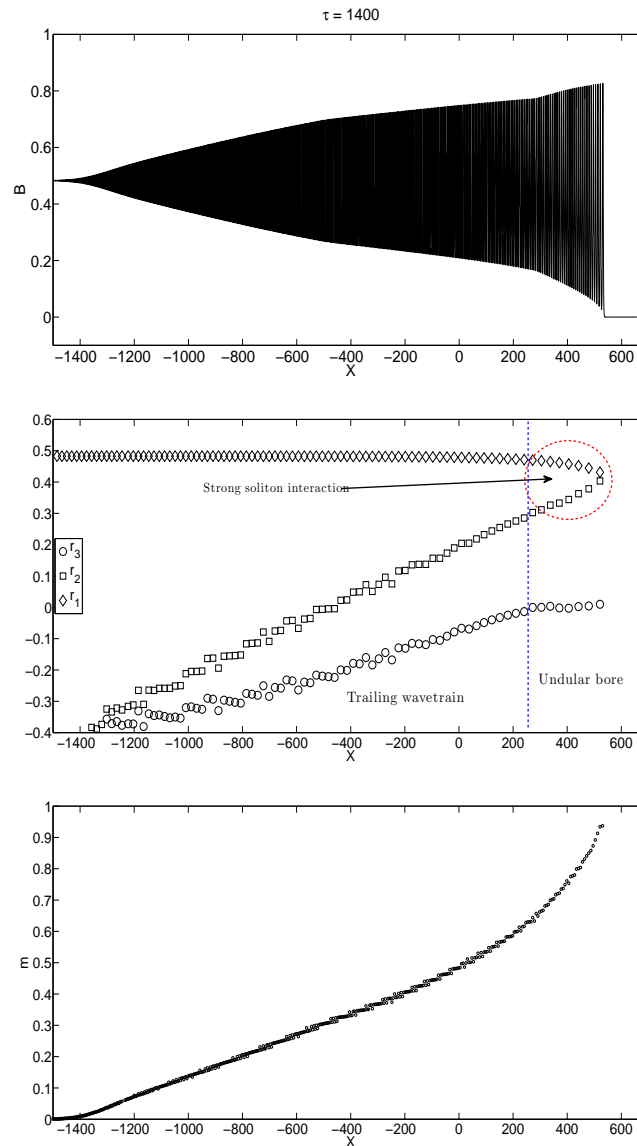
Figure 5.18: Undular bore after the slope at $\tau = 1400$. The leading wave starts to grow due to the strong interaction in the vicinity of the leading edge.

In Figure 5.19, we present the long-time behaviour of the transformed bore after the slope, $\tau = 8400$. Clearly, there are two distinct wave structures in the bore. At the front part of the transformed bore, we have an undular bore, followed by a trailing wavetrain at the rear part of the bore. Note that the amplitude of the leading wave in the bore is still decreasing due to the presence of friction.

5.2.2 Transformation of an undular bore over variable topography with Chezy friction
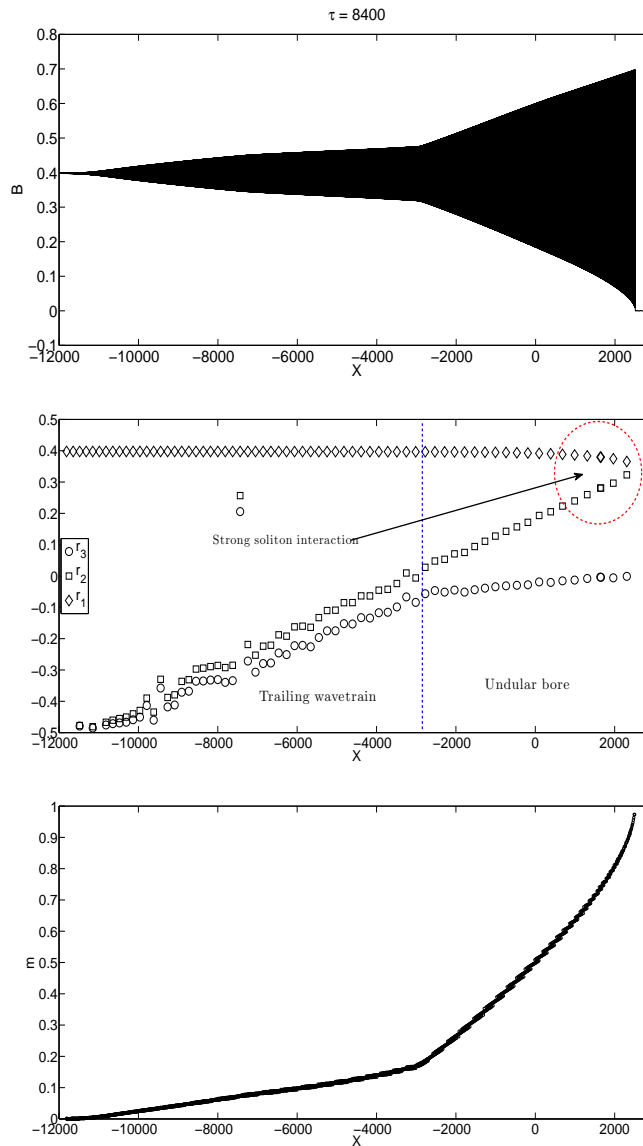
Figure 5.19: Long-time behaviour of the transformed bore after the slope at $\tau = 8400$. Two distinctive wave structures are observed here.

Figure 5.20 shows another plot for the long-time behaviour of the undular bore after the slope at $\tau = 16400$. Even though the shape of the transformed bore (the top plot) is similar to the one shown in Figure 5.19, from the behaviour of the Riemann invariants we can see that the undular bore at the front is slowly becoming a nonlinear wavetrain, which confirms our assumption. On the other hand, the wave structure at the rear part of the transformed bore is a linear wavetrain. This can be confirmed by the behaviour of the Riemann invariants where $r_2 = r_3$ in this region.

5.2.2 Transformation of an undular bore over variable topography with Chezy friction
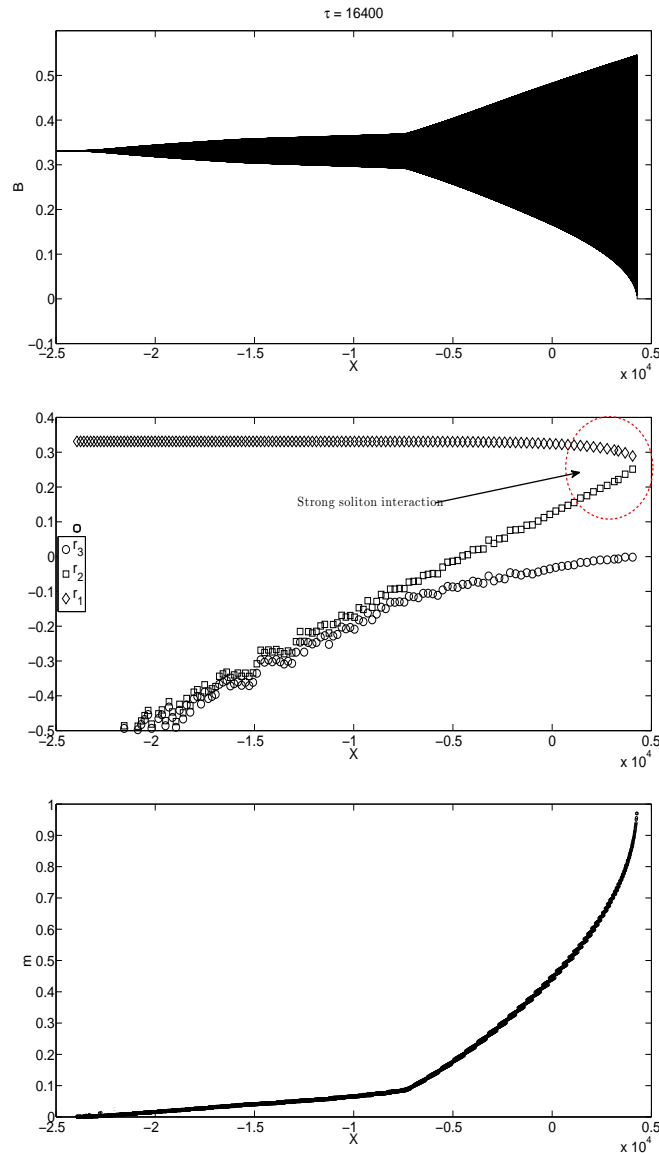
Figure 5.20: Long-time behaviour of the transformed bore after the slope at $\tau = 16400$. The behaviour of the Riemann invariants indicates that the wave structure now is slowly becoming a nonlinear wavetrain.

Figure 5.21 shows the comparison for the amplitudes for the leading solitary wave in the initial bore propagating over a slowly increasing depth region with different values of the friction coefficient and formula (5.19) for an isolated solitary wave. One can see that the leading wave of the bore can have some growth before it starts to decay again compared to the propagation of a single solitary wave where its amplitude decreases for all time. If there is no friction after the slope, the leading wave will continue to grow until it reaches the same amplitude as the incident bore.
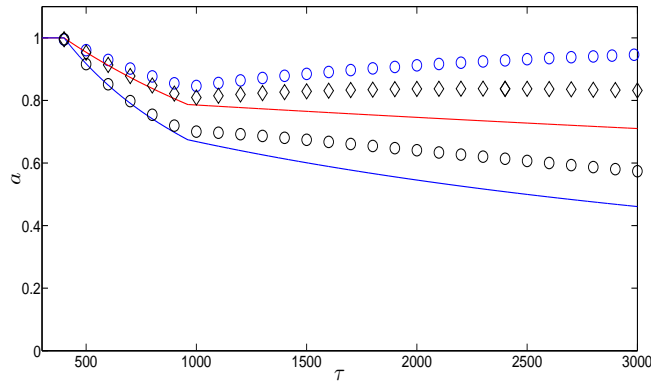
Figure 5.21: Comparison for the amplitudes for the leading solitary wave of the undular bore propagating over a slowly increasing depth region with Chezy friction: formula (5.19) with $h_0 = 1, a_0 = 1, C_D = 0.0001$ – red line, formula (5.19) with $h_0 = 1, a_0 = 1, C_D = 0.0005$ – blue line; numerical data with $C_D = 0.0001$ – diamonds; numerical data with $C_D = 0.0005$ – black circles; numerical data with $C_D = 0$ – blue cirlces.

Figure 5.22 presents the comparison for the variations of the absolute value of the jump, $|[B]|$, across the undular bore. One can see that the numerical data agrees with the theoretical prediction given by equation (5.28). Again, this confirms our assumption that the bottom friction will influence the jump across the bore.
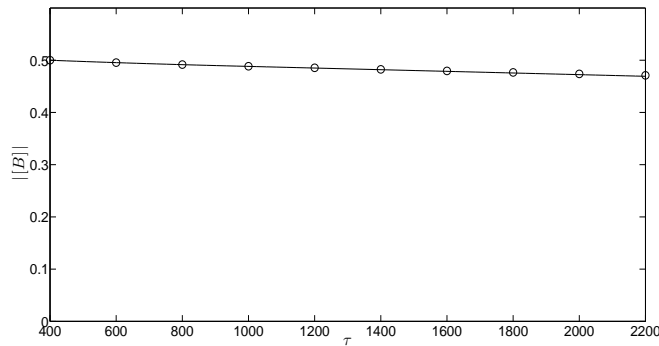
Figure 5.22: Comparison for the variations of the absolute value of jump, $|[B]|$ across the undular bore. Circles corresponds to the numerical data and the solid line to the analytical prediction (5.28).

5.3 Linear friction

Another relevant type of bottom friction is described by a linear perturbation term in the vpKdV equation (5.1) (Brink, 1988; Myint & Grimshaw, 1995; Grimshaw *et al.*, 2003). Linear friction is justified as a linearization for some nonlinear friction when the system

being studied has small amplitudes. So, now our governing equation is

$$A_t + cA_x + \frac{c_x}{2}A + \frac{3c}{2h}AA_x + \frac{ch^2}{6}A_{xxx} = -C_D\frac{c}{h}A. \tag{5.30}$$

The linear friction term is chosen to contain c, h so that C_D is dimensionless in order for us to use the same value (5.18) for C_D as for the Chezy friction. By following similar steps to those described in Sections 4.1 and 5.2, equation (5.30) can be recast asymptotically into several forms equivalent to (5.30):

$$B_\tau + \frac{3}{2h^{5/4}}BB_X + \frac{h}{6}B_{XXX} = -C_D\frac{c}{h}B, \tag{5.31}$$

$$u_S + 6uu_X + u_{XXX} = F(S)u, \tag{5.32}$$

$$\text{where} \qquad F(S) = -\frac{9h_S}{4h} - 6\frac{C_D}{h^{3/2}}, \tag{5.33}$$

$$U_T + 6UU_X + \beta(T)U_{XXX} = -6C_Dh^{3/4}U, \tag{5.34}$$

$$\text{where} \qquad \beta(T) = h^{9/4}(T), \tag{5.35}$$

by introducing the new variables $B(X, \tau), u(X, S)$ and $U(X, T)$ through (3.23), (3.26), (4.2), (4.6). One should bear in mind that equations (5.31), (5.32) and (5.34) are exactly equivalent.

5.3.1   Adiabatic deformation of a solitary wave

If the slope is slowly varying, $h_S << 1$, and the friction coefficient is small, $C_D << 1$, in the vpKdV equation (5.32), then to leading order, the slowly varying solitary wave solution is given by (5.8) and the velocity of the solitary wave is (5.9). Proceeding now in a similar manner to Section 5.2.1, but for the vpKdV equation (5.32), the adiabatic variation of the solitary wave amplitude over a varying slope with linear friction is given by

$$a = a_0 \left(\frac{h_0}{h(x)}\right) \exp\left[-\frac{4}{3}C_D \int_0^x \frac{dx'}{h(x')}\right]. \tag{5.36}$$

The amplitude variations of a solitary wave propagating over different types of slopes with linear friction is shown in Figure 5.23. The trajectory of the solitary wave can be found as

$$X_s = \frac{a_0h_0}{2} \int_0^x dx'\, h^{-5/2}(x') \exp\left[-\frac{4}{3}C_D \int_0^{x'} \frac{dz}{h(z)}\right]. \tag{5.37}$$

Similar to (5.14), when $C_D = 0$, the solitary wave amplitude varies proportionally to the inverse of the local depth.

5.3.1 Adiabatic deformation of a solitary wave
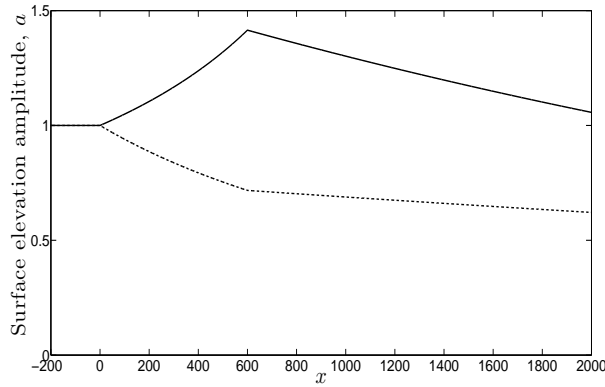
Figure 5.23: Surface elevation amplitude of the solitary wave described by formula (5.36) where $a_0 = 1, h_0 = 1, C_D = 0.0001$ for different kinds of topography: slowly decreasing depth – solid line, slowly increasing depth – dashed line.

5.3.1.1   Numerical results

All numerical results for the propagation of solitary wave over varying depth region with linear friction are presented in this section.

5.3.1.1.1   Slowly decreasing depth

First we consider the case of slowly decreasing depth. Following the description similar to that presented in Section 5.2.1.1.1, in this case, a solitary wave is expected to deform adiabatically according to the formula (5.36). Hence, the solitary wave will initially grow once it enters the shoaling region. The growth, however, depends on the relative magnitude of the effects of the slope and bottom friction. After the slope, the solitary wave continues to diminish due to the presence of bottom friction.

In Figure 5.24, we present the plot of the evolution of a solitary wave over a slowly decreasing depth topography with linear friction. The results are based of the numerical simulations of the vpKdV equation (5.31) (see Appendix A.4.2). The depth profile $h(\tau)$ and the drag coefficient, C_D are given by (5.16) and (5.18) respectively.

Figure 5.25 shows the comparison for the solitary wave amplitude variations over the slope with different values of C_D. For the vpKdV equation (5.31), the solitary wave amplitude variation is given by

$$a = a_0 \left(\frac{h_0}{h(\tau)} \right)^{3/4} \exp \left(-\frac{4}{3} C_D \int_0^\tau \frac{d\tau'}{h^{1/2}(\tau')} \right), \tag{5.38}$$

5.3.1 Adiabatic deformation of a solitary wave
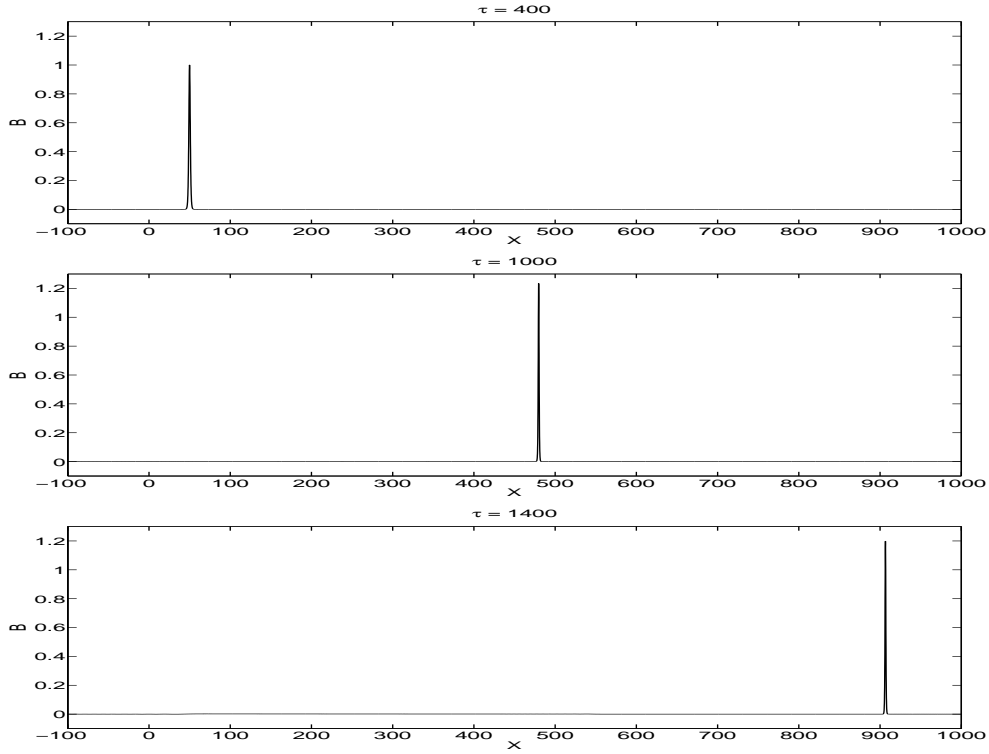
Figure 5.24: Propagation of a solitary wave over a slowly decreasing depth region described by (5.16) with linear friction given by (5.18)

Figure 5.25: Comparison for the amplitudes for the solitary wave propagating over a slowly decreasing depth region with linear friction: formula (5.38) with $h_0 = 1, a_0 = 1, C_D = 0.0001$ – red line; formula (5.38) with $h_0 = 1, a_0 = 1, C_D = 0.0005$ – blue line; numerical data with $C_D = 0.0001$ – diamonds; numerical data with $C_D = 0.0005$ – circles; numerical data with $C_D = 0$ – dashed line.

where a_0 and h_0 are the amplitude and local depth before the slope. The relationship (5.38) is the exact counterpart of (5.36) for the vpKdV equation (5.31). We can see there is an excellent agreement between the analytical predictions and the numerical data. The dashed line shows the amplitude of the solitary wave over the same slope without friction obtained from numerical simulations.
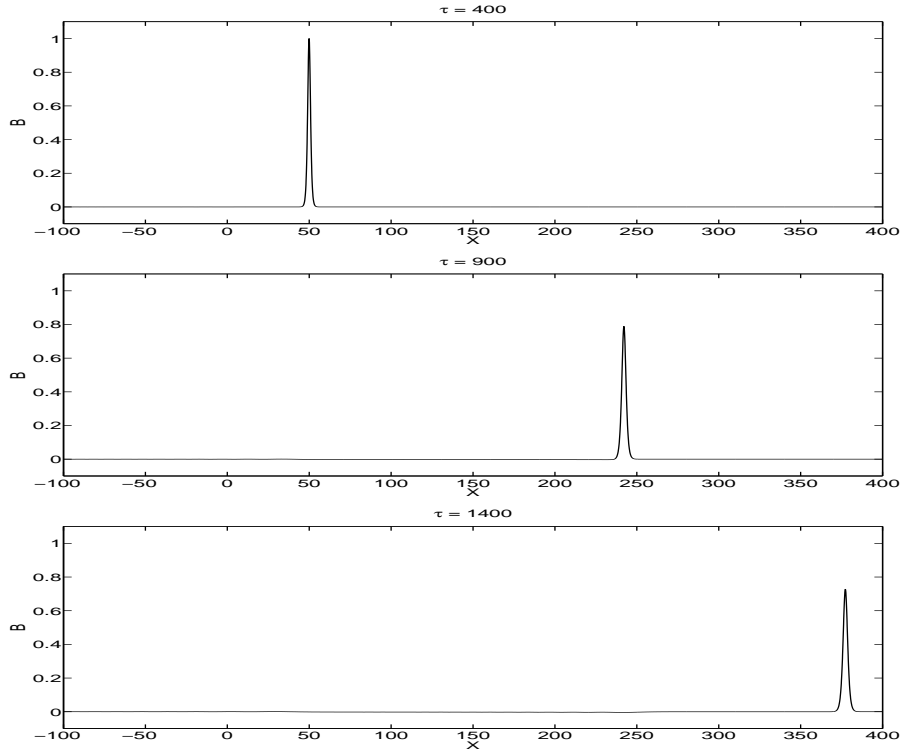
Figure 5.26: Propagation of a solitary wave over a slowly increasing depth region described by (5.20) where linear friction given by (5.18)

5.3.1.1.2 Slowly increasing depth

When the depth is slowly increasing, then the solitary wave will not grow at all. Instead, it will diminish once it moves into the deeper region and continue to decay henceforth. Similarly, the solitary wave amplitude varies adiabatically according to the formula (5.36).

The evolution profile of the solitary wave propagating over a slowly increasing depth region with linear friction according to the vpKdV equation (5.31) is illustrated in Figure 5.26. The variable topography is described by (5.20) while the friction coefficient, C_D, is given by (5.18).

The comparison for the surface elevation between the analytical formula (5.38) and numerical data for different values of C_D is shown in Figure 5.27. Again, there is excellent between the numerical data and the analytical predictions. The dashed line corresponds to the amplitude variation for solitary wave propagatiio over the same slope without friction. When friction is absent, the solitary wave amplitude is greater than in the case when friction is present.
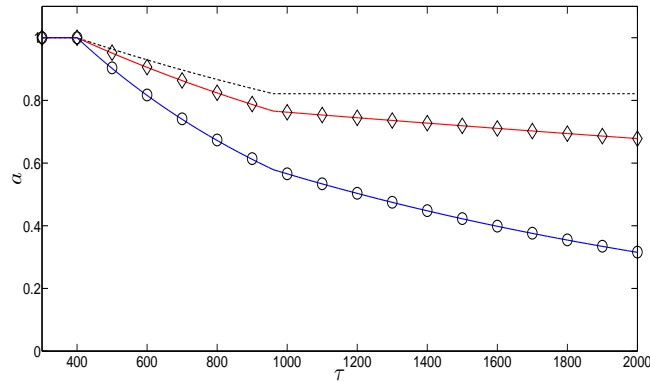
Figure 5.27: Comparison for the amplitudes for the solitary wave propagating over a slowly increasing depth region with linear friction: formula (5.38) with $h_0 = 1, a_0 = 1, C_D = 0.0001$ – red li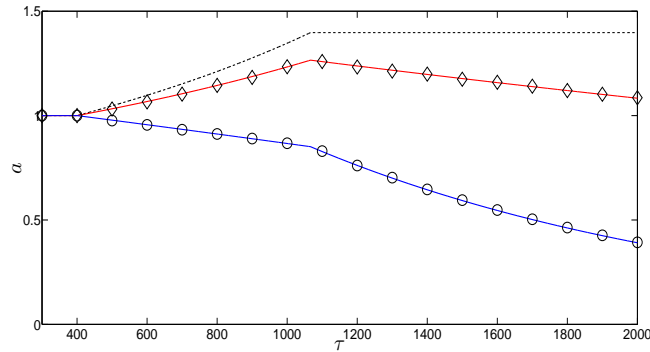ne; formula (5.38) with $h_0 = 1, a_0 = 1, C_D = 0.0005$ – blue line; numerical data with $C_D = 0.0001$ – diamonds; numerical data with $C_D = 0.0005$ – circles; numerical data with $C_D = 0$ – dashed line.

5.3.2 Transformation of an undular bore over variable topography with linear friction

In this section, we will look at the impact of linear friction on the undular bores propagation in a nonuniform environment. Previously in Section 5.2.2, we have shown that the Chezy friction would affect the mean level across the bore during the evolution. In a similar manner, we can show that the linear friction will have a similar effect on the jump, $[U]$ across the bore. Indeed, this can be shown from the vpKdV equation (5.34) and the definition (5.21), we obtain

$$[U]_T = \frac{\partial}{\partial T} \int_{X_a(T)}^{X_b(T)} U_X \, dX, \tag{5.39}$$

$$= 6C_D h^{3/4} U_0, \tag{5.40}$$

where $U_X = U_{XXX} = 0$ at $X = X_{a,b}(T)$. Again, we have assumed that undular bore propagates into an undisturbed depth region, $U(X_b) = 0$, so that

$$[U] = -U_0 \left[1 - 6C_D \int_{T_0}^{T} h^{3/4}(T) \, dT \right] \qquad \text{for all} \qquad T > 0. \tag{5.41}$$

Clearly, the jump, $[U]$, across the bore varies over time. Again, this will later be confirmed by direct numerical simulations. Thus, the leading wave amplitude of the undular bore after the slope would continue to change as time increases.

5.3.2 Transformation of an undular bore over variable topography with linear friction

5.3.2.1   Slowly decreasing depth

First, we let the depth to be slowly decreasing. By following the descriptions and results presented in Sections 4.2.2.2 and 5.2.2.1, the leading solitary wave of the incident bore should behave as separate isolated solitary wave when the bore interacts with the slope, and thus forms a train of solitary waves ahead of the bore, provided the slope a has more dominant effect compared with the bottom friction. The leading soliton in the solitary wavetrain, which is the leading solitary wave of the initial bore should deform adiabatically on the slope according to formula (5.38).
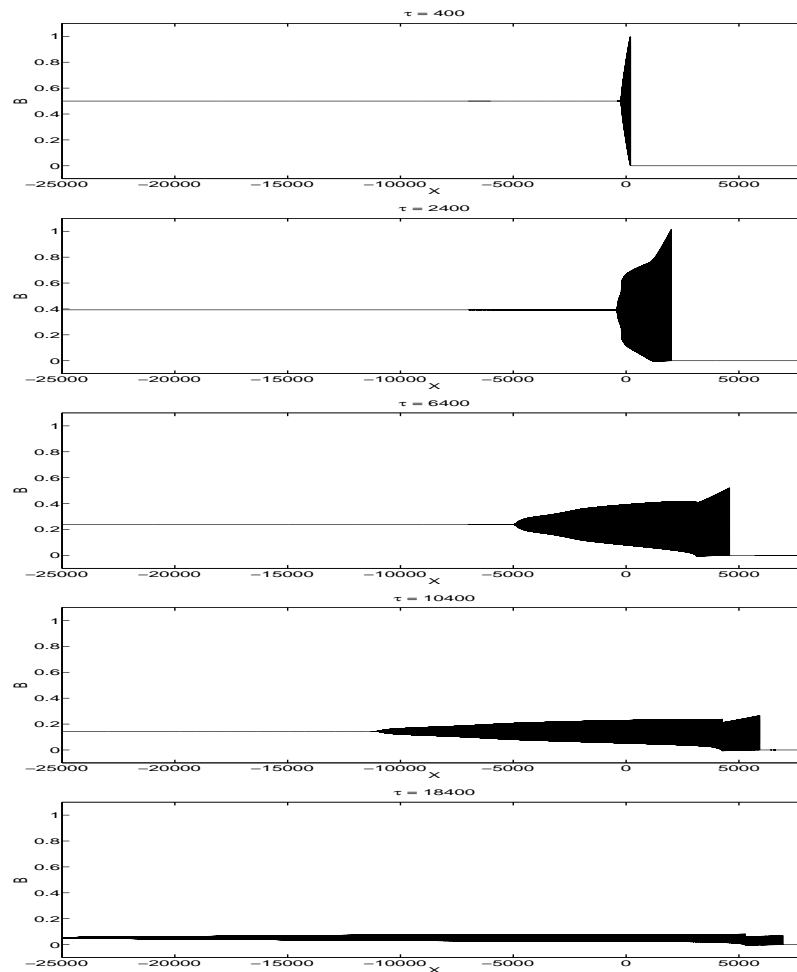
Figure 5.28: Propagation of an undular bore over a slowly decreasing depth region with linear friction where the profile $h(\tau)$ is given by (5.16)

In Figure 5.28, we present the evolution profile of an undular bore propagating over a slowly increasing slope described by (5.16) with linear friction, where the drag coefficient, C_D is given by (5.18). In plot 3 of the Figure 5.28, one can see that a sequence of isolated solitary waves is generated, similar to plot 4 of the Figure 4.3. Next, in plot 4 of the same

5.3.2 Transformation of an undular bore over variable topography with linear friction
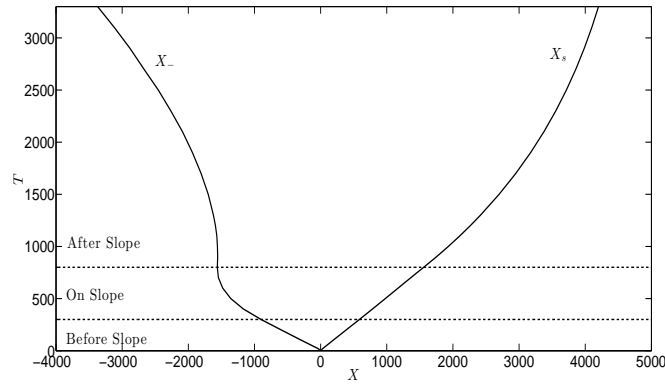
Figure 5.29: Characteristics plots for the leading soliton, X_s in the solitary wavetrain and the trailing edge of the transformed bore, X_-.

figure, it can be seen clearly that the leading wave in the transformed bore is growing. Moreover, note that the transformed bore and the solitary wavetrain are diminishing due to the sole effect of bottom friction. However, unlike the results presented in Figure 5.6 for Chezy friction, in this case, the leading wave in the transformed bore apparently does not have enough time to overtake the solitary wavetrain before the entire structure of the bore and solitary wavetrain collapses. This is shown in plot 5 of the same figure.

On the other hand, Figure 5.29 shows the characteristic plots for the trailing edge, X_- of the transformed bore and the leading soliton, X_s in the solitary wavetrain, which was the leading solitary wave of the initial bore. The numerical data was obtained by solving the vpKdV equation (5.34). The variable topography is described by (5.27) and the initial condition is given by (4.28). Clearly, the leading soliton in the solitary wavetrain, X_s decelerates over time. As for the trailing edge, X_-, it travels faster when it encounters the shoaling region as discussed in section 4.2.2.2.

5.3.2.1.1   Numerical results

Again, we use numerical results to confirm our theoretical description discussed in Section 5.3.2.1, which were based on assumptions similar to those used in Section 5.2.2.1.1. For the numerical simulations, we will use the vpKdV equation (5.31). The function describing the depth variations is given in (5.16) and the drag coefficient, C_D, is described by (5.18). The initial condition is taken in the form (4.27). One should bear in mind that the bottom friction only "switches on" on the slope. All numerical results are presented in Figures 5.30 – 5.33. The plot for the initial bore before the slope at $\tau = 400$ is similar to that in Figure

5.3.2 Transformation of an undular bore over variable topography with linear friction

5.8, which agrees with the solution obtained by Gurevich & Pitaevskii (1973, 1974).
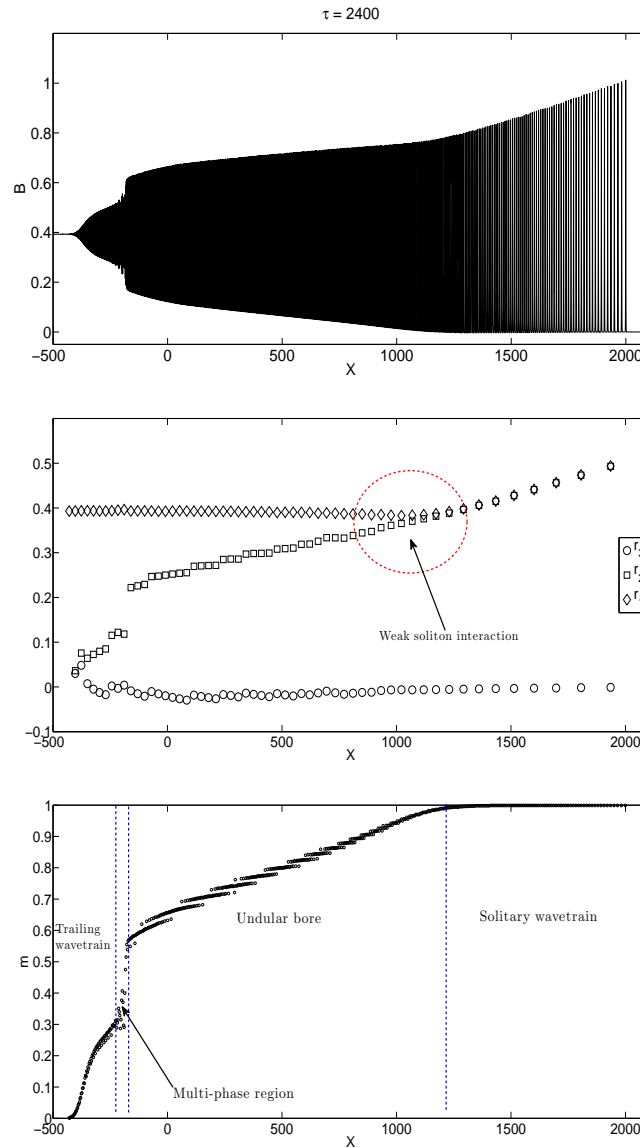
Figure 5.30: Undular bore after the slope at $\tau = 2400$. A train of solitary waves is generated at the front of the undular bore between $X \approx 1100$ and $X \approx 2000$. Multi-phase behaviour at the rear part of the bore.

Figure 5.30 shows the undular bore "shortly" after the slope, $\tau = 2400$. It is clear that a train of solitary waves is formed in front of the transformed bore. This is confirmed by the existence of the region $r_1 = r_2$ (the middle plot) or $m \rightarrow 1$ (the bottom plot). Also, multi-phase behaviour is observed at the rear part of the bore. In this region, the modulus, m is undefined. Note that we have the weak soliton interaction scenario near the leading edge of the undular bore(see the middle plot), as predicted by our discussion in Section 4.2.2.2.

5.3.2 Transformation of an undular bore over variable topography with linear friction
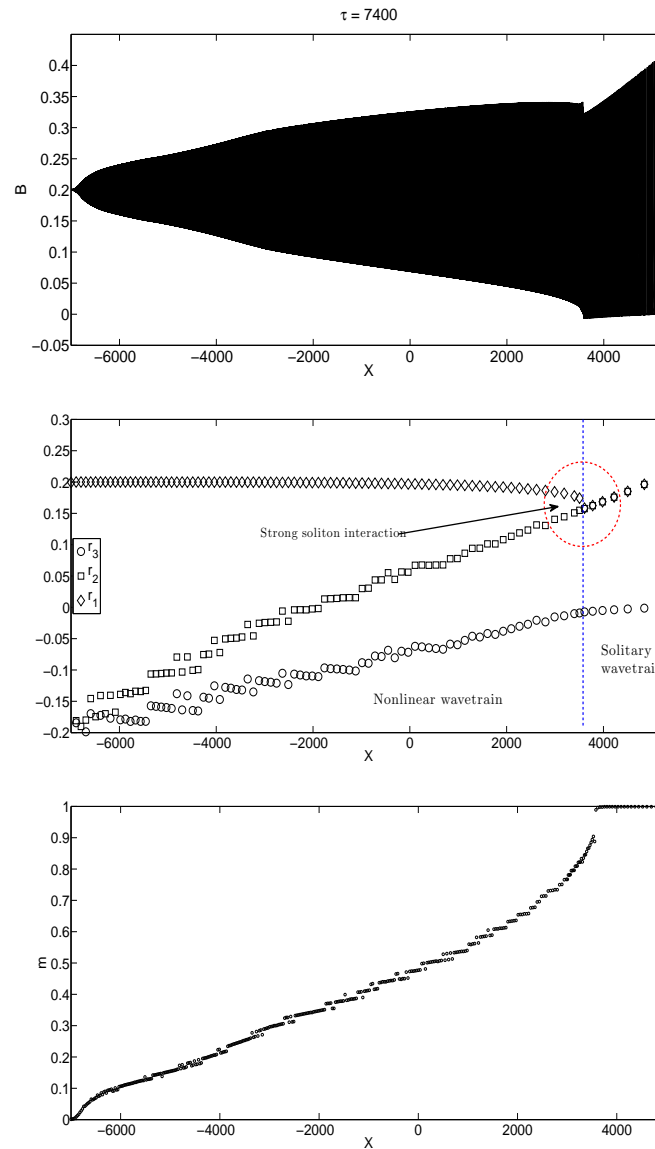
Figure 5.31: Undular bore after the slope at $\tau = 7400$. A solitary wavetrain is formed between $X \approx 3500$ and $X \approx 5000$.

Figure 5.31 is the plot for the undular bore after the slope at $\tau = 7400$. Notice that the amplitude of all solitons in the solitary wavetrain and the leading wave of the bore are decreasing as the result of the bottom friction effect. Also, at this moment, the solitary wave at the leading edge of the bore starts to interact strongly with the wavetrain behind it (see the middle plot and Figure 2.11b). Again, for convenience, we refer the nonlinear wavetrain as a bore. Note that the bore has restored its single-phase behaviour throughout the structure.

5.3.2 Transformation of an undular bore over variable topography with linear friction
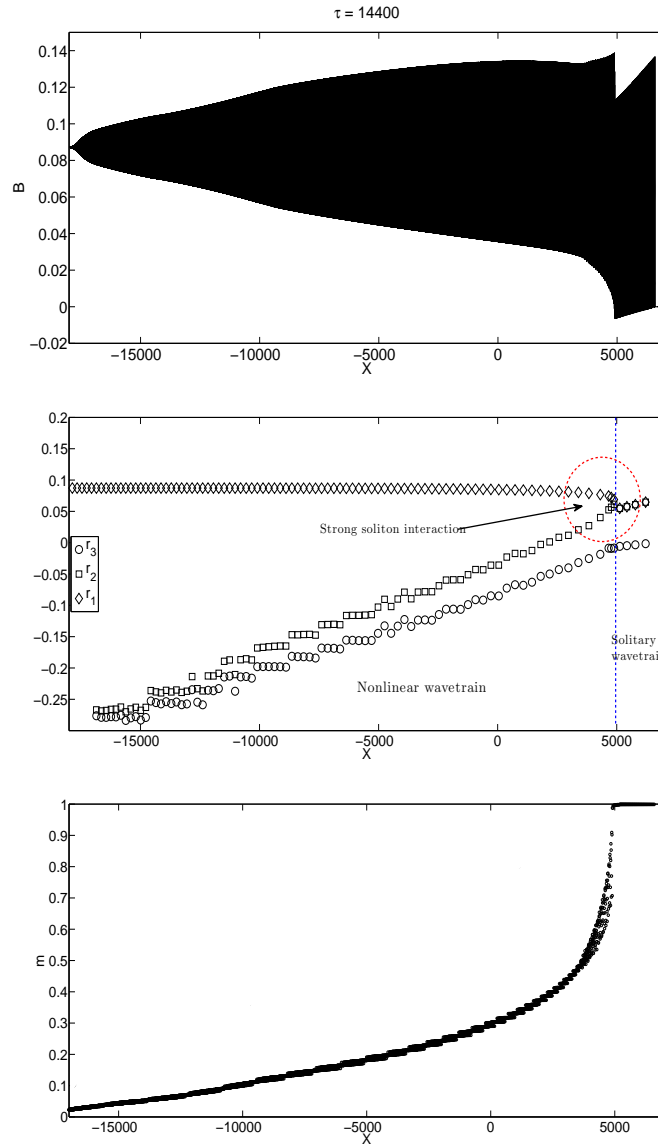
Figure 5.32: Long-time behaviour of the undular bore after the slope at $\tau = 14400$. The undular bore is seen to be overtaking the solitary wavetrain.

Figure 5.32 corresponds to the long-time behaviour of the undular bore after the slope at $\tau = 14400$. Here, we can see that the bore is overtaking the soliton wavetrain slowly. Whether the bore can successfully overtaken all solitons in the solitary wavetrain depends on the amount of time it has before the entire structure collapses. In this simulation, the bore apparently does not have sufficient time to overtake the entire solitary wavetrain before the whole structure collapses. Again, the multi-valued regions in the distribution of modulus in Figures 5.30 – 5.32 are due to numerical artifact.

5.3.2 Transformation of an undular bore over variable topography with linear friction
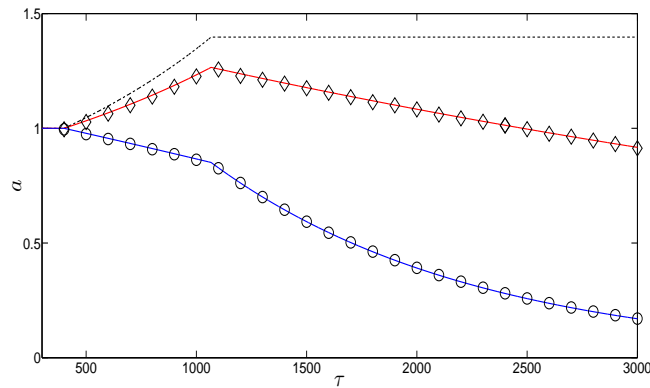
Figure 5.33: Comparison for the amplitudes for the leading solitary wave of the undular bore propagating over a slowly decreasing depth region with linear friction: formula (5.38) with $h_0 = 1, a_0 = 1, C_D = 0.0001$ – red line; formula (5.38) with $h_0 = 1, a_0 = 1, C_D = 0.0005$ – blue line; the numerical data with $C_D = 0.0001$ – diamonds; the numerical data with $C_D = 0.0005$ – circles; the numerical data with $C_D = 0$ – dashed line.

Figure 5.33 shows the comparison for the surface elevations for the leading wave in the incident bore for different values of C_D over the same slope. Again, we have excellent agreement between the numerical data and the formula (5.38). This confirms our assumption that the leading solitary wave in the initial bore is not influenced by interaction with the nonlinear wavetrain behind it, i.e. it behaves as a separate single solitary wave when it propagates over the slope.
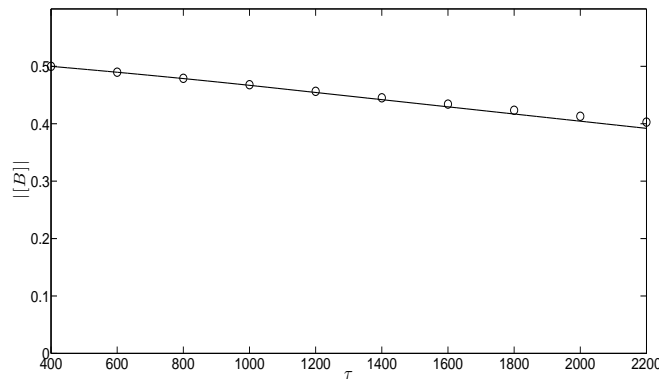
Figure 5.34: Comparison for the variations of the absolute value of jump, $|[B]|$ across the undular bore. Circles corresponds to the numerical data and the solid line to the analytical prediction (5.42).

Figure 5.34 shows comparisons for the variations of the absolute value of the jump, $|[B]|$, across the undular bore. For the vpKdV equation (5.31), the jump, $[B]$, across the bore is

5.3.2 Transformation of an undular bore over variable topography with linear friction

given by

$$[B] = -B_0 \left[1 - C_D \int_{\tau_0}^{\tau} h^{-1/2}(\tau') \, d\tau' \right] \qquad \text{for all} \qquad \tau > 0, \qquad (5.42)$$

where B_0 is the initial jump across the bore before the slope. One should bear in mind that equations (5.41) and (5.42) are exactly equivalent. Note that there is good agreement between the numerical simulations and the analytical prediction. Similar to the results presented for the Chezy friction, this confirms our assumption that the linear friction term also influences the jump across the bore.

5.3.2.2   Slowly increasing depth

When the depth is slowly increasing, we have shown in Sections 4.2.2.3 and 5.2.2.2 that no solitary wavetrain is generated ahead of the transformed bore. Instead, a nonlinear trailing wavetrain, which was part of the initial bore is generated. So, in this case, we expect to see the same behaviour. Due to the presence of the bottom friction, the jump of the mean flow across the bore decreases over time. Therefore, the growth at the leading edge will not last despite the nonlocal interaction scenario near the leading edge. The amplitude of the leading wave of the bore decreases over time after experiencing some growth for a short time-span.

In Figure 5.35, we present the evolution of an undular bore for the vpKdV equation (5.31) over a slowly increasing depth region described by (5.16). The drag coefficient, C_D and the initial condition are given by (5.18) and (4.27) respectively. In plot 2 of the same figure, one can see that the amplitude of the leading wave decreases. Also, we can see that there is some growth at the leading edge of the bore in plot 3 in the same figure.

Figure 5.36 shows the characteristics plot for the leading wave, X_+, of the transformed bore and the trailing edge, $\widetilde{X}$, of the trailing wavetrain. One can see that all the features in the interaction of the undular bore with the slowly increasing depth region as discussed in Section 4.2.2.3 are preserved. The leading wave continues to decelerate due to the continuous presence of the bottom friction.

5.3.2.2.1   Numerical results

The undular bore evolution scenario mentioned earlier was based on assumptions similar to those listed in Section 5.2.2.2.1. Thus, in order to confirm our assumptions, we turn to numerical simulations of the vpKdV equation (5.31). The depth profile is described

5.3.2 Transformation of an undular bore over variable topography with linear friction

by (5.20) and the initial distribution is given by (4.27). The drag coefficient, C_D is taken in the form (5.18). All numerical results are presented in Figures 5.37 – 5.39. Again, the plot for the initial undular bore before the slope at $\tau = 400$, which is described the Gurevich-Pitaevskii solution, is shown in Figure 5.8.
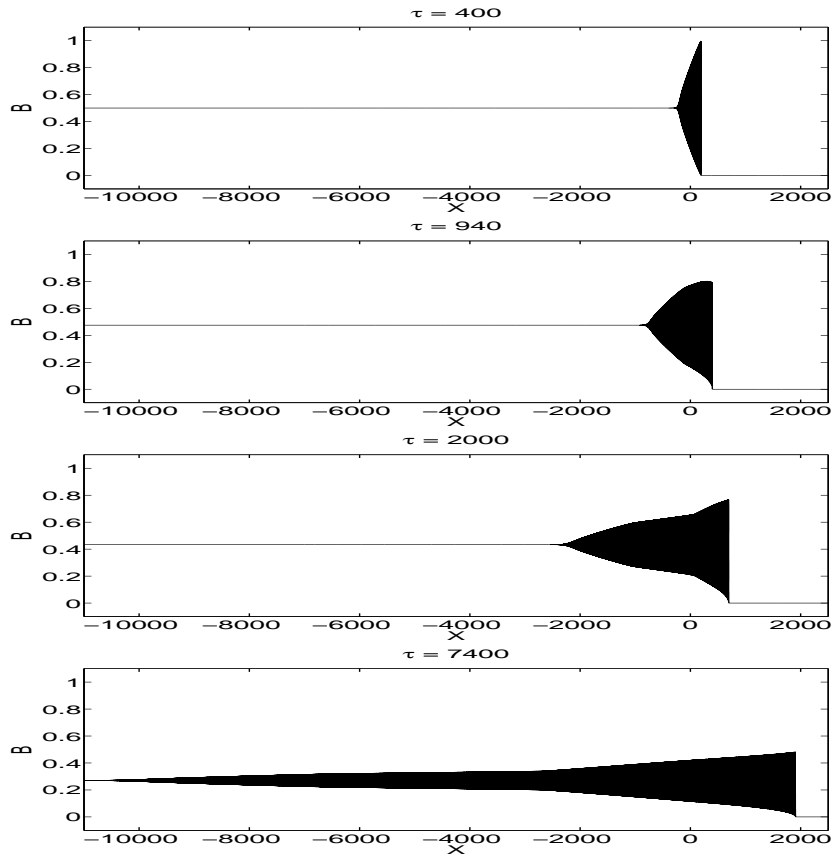
Figure 5.35: Propagation of an undular bore over a slowly increasing depth region with linear friction where the profile $h(\tau)$ is given by (5.20)
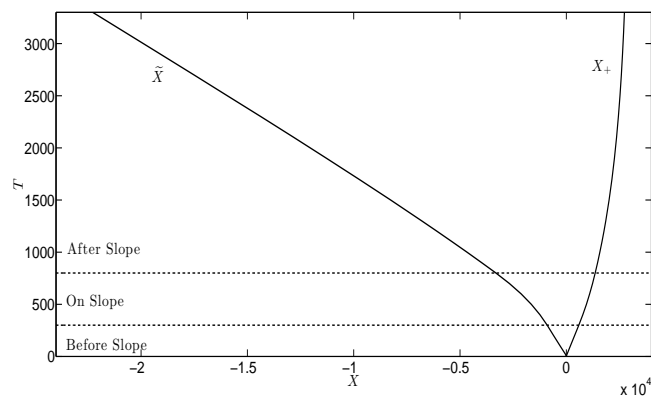
Figure 5.36: Characteristics plots for the leading wave, X_+ and the tailing edge of the trailing wavetrain, $\widetilde{X}$.

5.3.2 Transformation of an undular bore over variable topography with linear friction
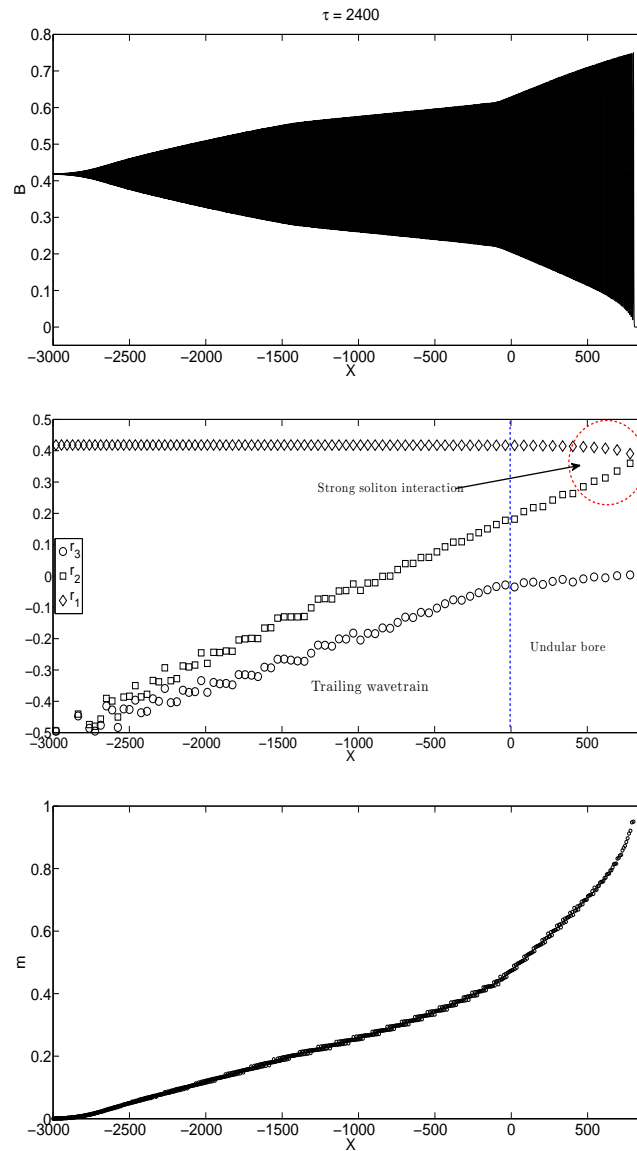
Figure 5.37: Undular bore after the slope at $\tau = 2400$. Note the growth near the leading edge.

Figure 5.37 shows the undular bore "shortly" after the slope, $\tau = 2400$. From the behaviour of the Riemann invariants (the middle plot), we can confirm that the wave dynamics near the leading edge is dominated by the strong (nonlocal) interaction scenario El *et al.* (2007) (see Figure 2.11b). Consequently, the leading wave of the bore is growing. At the rear part, we have a trailing wavetrain as the result of the interaction of the undular bore with the slowly increasing topography.

5.3.2 Transformation of an undular bore over variable topography with linear friction
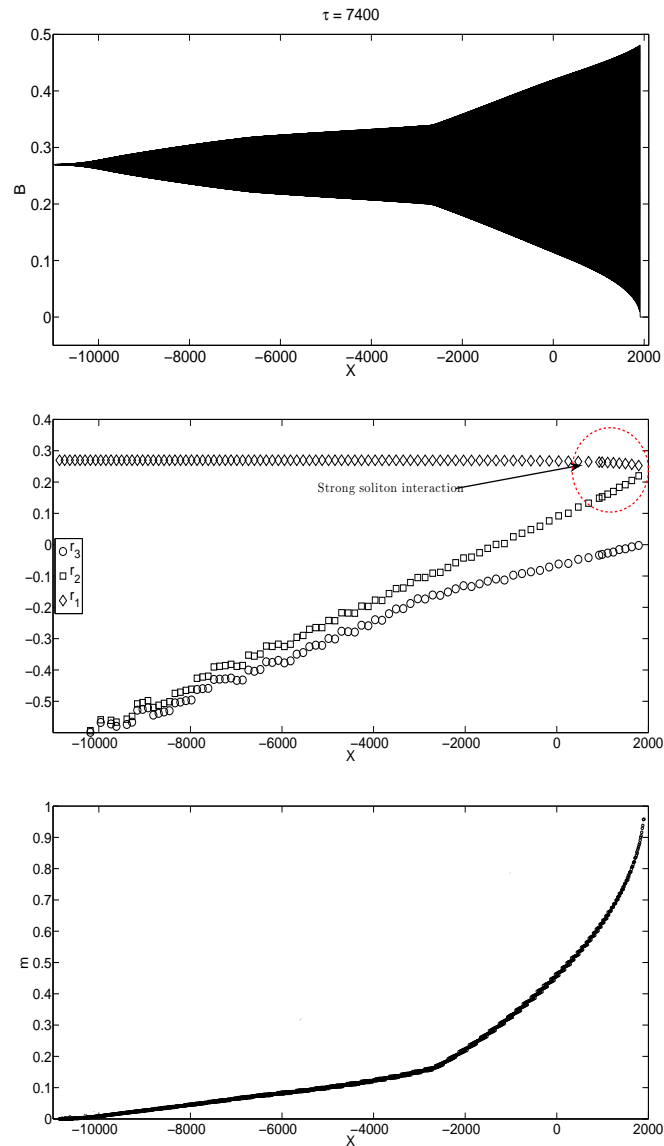
Figure 5.38: Undular bore after the slope at $\tau = 7400$. One can see clearly two distinctive structures in the transformed bore: undular bore at the front part and nonlinear wavetrain at the rear part. Note that the jump, $[U]$, of the bore is decreasing.

Figure 5.38 corresponds to the long-time behaviour of the undular bore after the slope at $\tau = 7400$. Even though the nonlocal interaction at the leading edge contributes to some growth in amplitude, this tendency will not last due to the fact that the jump across the bore is decaying. Note that, from the behaviour of the Riemann invariants, the entire structure of the transformed bore is slowly becoming a nonlinear wavetrain.

5.3.2 Transformation of an undular bore over variable topography with linear friction
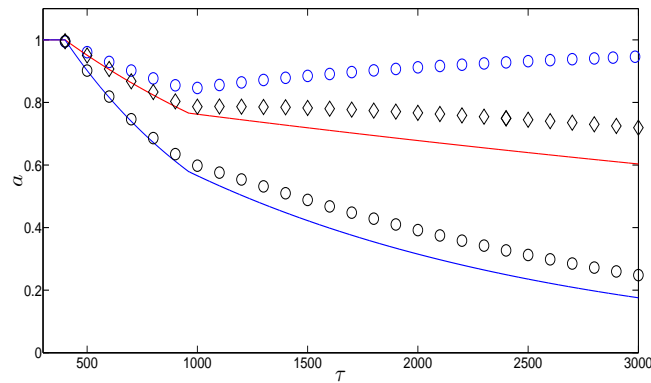
Figure 5.39: Comparison for the amplitudes for the leading solitary wave of the undular bore propagating over a slowly increasing depth region with linear friction: formula (5.38) with $h_0 = 1, a_0 = 1, C_D = 0.0001$ – red line; formula (5.38) with $h_0 = 1, a_0 = 1, C_D = 0.0005$ – blue line; the numerical data with $C_D = 0.0001$ – diamonds; the numerical data with $C_D = 0.0005$ – black circles; the numerical data with $C_D = 0$ – blue circles.

The comparison for the amplitude variations is shown in Figure 5.39. One can see that for each different value of C_D, the amplitude of the leading wave in the undular bore is greater than those of the single solitary wave described by formula (5.38). This is due to the growth gained by the leading wave as the result of the strong interaction near the leading edge. When friction is present, clearly the amplitude is smaller than the case when friction is absent.

Figure 5.40 corresponds to the comparison for the variations of the absolute value of the jump, $|[B]|$, across the undular bore. Again, there is an excellent agreement between the numerical simulations and analytical prediction (5.42). As expected, the jump across the bore decreases over time due to the effect of bottom friction.
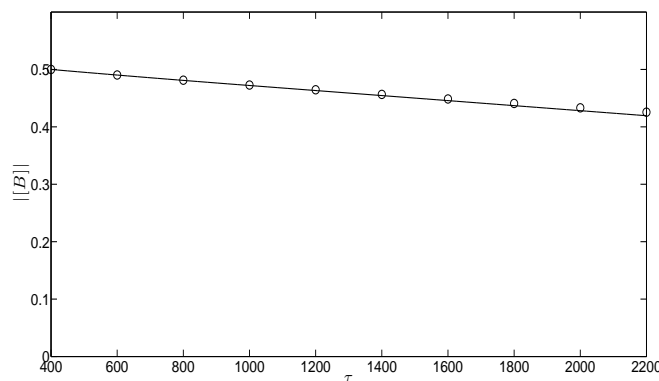
Figure 5.40: Comparison for the variations of the absolute value of jump, $|[B]|$ across the undular bore. Circles corresponds to the numerical data and the solid line to the analytical prediction (5.42).

139

5.4 Burgers' friction

Finally, we consider the last form of the dissipative term mentioned in Section 5.1, which describes volume viscosity or, for convenience, we call it Burgers' friction, so that our governing equation now becomes the variable coefficient KdV-Burgers (vKdVB) equation

$$A_t + cA_x + \frac{c_x}{2}A + \frac{3c}{2h}AA_x + \frac{ch^2}{6}A_{xxx} = C_D chA_{xx}. \tag{5.43}$$

Again, the Burgers friction term is chosen to contain c, h so that C_D is dimensionless in order for us to use the same value (5.18) for C_D as for the Chezy friction. By following a similar course as in Sections 4.1, 5.2 and 5.3, equation (5.43) can be asymptotically recast into the following vKdVB equations:

$$B_\tau + \frac{3}{2h^{5/4}}BB_X + \frac{h}{6}B_{XXX} = C_D\frac{h}{c}B_{XX}. \tag{5.44}$$

$$u_S + 6uu_X + u_{XXX} = F(S)u + G(S)u_{XX}, \tag{5.45}$$

$$\text{where} \quad F(S) = -\frac{9h_S}{4h} \quad \text{and} \quad G(S) = C_D\frac{6}{h^{1/2}}, \tag{5.46}$$

$$U_T + 6UU_X + \beta(T)U_{XXX} = 6C_D h^{7/4}U_{XX} \tag{5.47}$$

$$\text{where} \quad \beta(T) = h^{9/4}(T), \tag{5.48}$$

when, as earlier, one introduces the new variables $B(X, \tau), u(X, S)$ and $U(X, T)$ through (3.23), (3.26), (4.2), (4.6). Again, equations (5.44), (5.45) and (5.47) are exactly equivalent.

5.4.1 Adiabatic deformation of a solitary wave

Assuming that $h_S << 1$ and $C_D << 1$ in the vKdVB equation (5.45), the slowly varying solitary wave solution at the leading edge is given by (5.8), with the velocity given by (5.9). By repeating the same procedures as in Sections 5.2.1 and 5.3.1, we obtain a formula describing the amplitude variation $A(x, t)$ of the solitary wave

$$a = a_0 \left(\frac{h_0}{h}\right) \left[1 + \frac{4}{5}C_D a_0 h_0 \int_0^x \frac{dx'}{h^3(x')}\right]^{-1}, \tag{5.49}$$

where a_0 and h_0 are the initial solitary wave amplitude and local depth. Figure 5.41 shows the surface elevation of the solitary wave propagating over different types of sloping bottom with Burgers' friction. The trajectory of the solitary wave is given by

$$X_s = \frac{a_0 h_0}{2}\int_0^x dx' \, h^{-5/2}(x') \left[1 + \frac{4}{5}C_D a_0 h_0 \int_0^{x'} \frac{dz}{h^3(z)}\right]^{-1}. \tag{5.50}$$
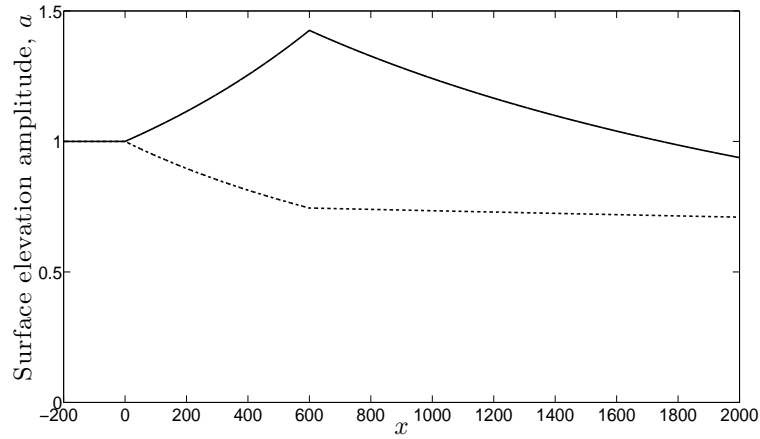
Figure 5.41: Surface elevation amplitude of the solitary wave described by formula (5.49) where $a_0 = 1, h_0 = 1, C_D = 0.0001$ for different kinds of topography: slowly decreasing depth – solid line, slowly increasing depth – dashed line.

5.4.1.1 Numerical results

This section is devoted to the numerical results for the solitary wave propagation over different types of varying regions with Burgers' friction.

5.4.1.1.1 Slowly decreasing depth

First we consider slowly decreasing depth. Similar to our previous discussions so far, a solitary wave will grow when it propagates over a slowly decreasing depth region with small friction. However, the growth magnitude is smaller compared with the frictionless case. Also, the strength of the friction will influence the growth of the solitary wave.

We present the numerical simulations for the transformation of a solitary wave over slowly decreasing depth according to the vKdVB equation (5.44) (see Appendix A.4.3) in Figure 5.42. The variable topography is given by (5.16) and the initial condition by (5.17). The Burgers' friction coefficient is described by (5.18).

5.4.1 Adiabatic deformation of a solitary wave

Figure 5.42: Propagation of a solitary wave over a slowly decreasing depth region described by (5.16) with Burgers' friction given by (5.18)

Figure 5.43: Comparison for the amplitudes for the solitary wave propagating over a slowly decreasing depth region with Burgers' friction: formula (5.51) with $h_0 = 1, a_0 = 1, C_D = 0.0001$ – red line; formula (5.51) with $h_0 = 1, a_0 = 1, C_D = 0.0005$ – blue line; numerical data with $C_D = 0.0001$ – diamonds; numerical data with $C_D = 0.0005$ – circles; numerical data with $C_D = 0$ – dashed line.

The comparison for the solitary wave amplitude for propagation over a slowly decreasing depth region with different values of C_D is presented in Figure 5.43. For the vKdVB equation (5.44), the amplitude variation of a solitary wave is given by

$$a = a_0 \left(\frac{h_0}{h(\tau)} \right)^{3/4} \left[1 + \frac{4}{5} C_D b_0 h_0^{3/4} \int_0^\tau \frac{d\tau'}{h^{5/2}(\tau')} \right]^{-1}. \qquad (5.51)$$

The formula (5.51) is the exact counterpart of (5.49) for the vKdVB equation (5.44).

5.4.1 Adiabatic deformation of a solitary wave

Clearly, the numerical simulations agree with the analytical formula (5.51) and the behaviour of the solitary wave matches with our theoretical description in Section 5.4.1.

5.4.1.1.2   Slowly increasing depth

Now, we consider the depth increasing gradually. So the solitary wave will start losing its amplitude from the moment it enters the varying region. This is clearly seen in Figure 5.44, which corresponds to numerical simulations for a solitary wave propagating over slowly increasing depth (5.20) for the KdVB equation (5.44). The initial condition and the drag coefficient, C_D considered here are (5.17) and (5.18) respectively.
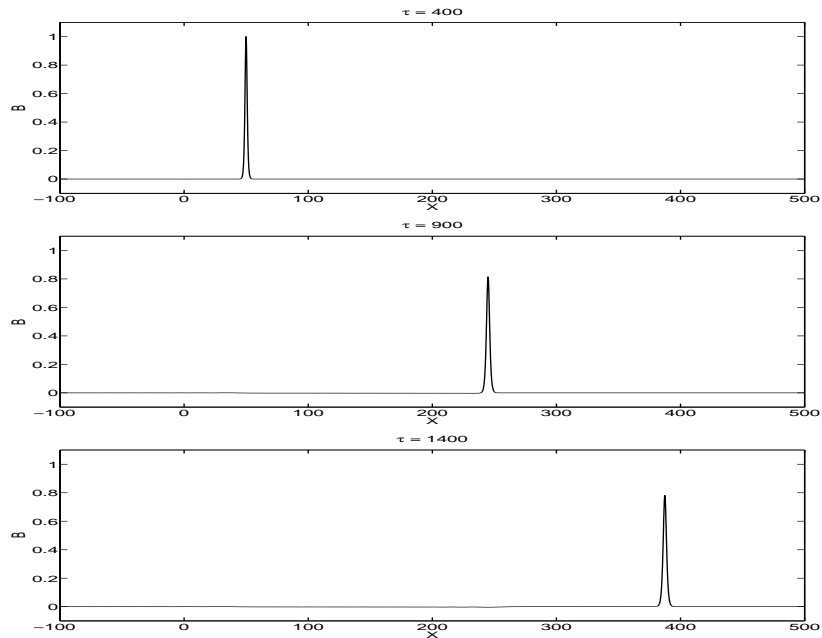
Figure 5.44: Propagation of a solitary wave over a slowly increasing depth region described by (5.16) with Burgers' friction given by (5.18)

In Figure 5.45, we present the comparison for the amplitude variations between the analytical predictions described by the formula (5.51) and the numerical data for different values of C_D. The dashed line shows the solitary wave amplitude when the friction effect is ignored.
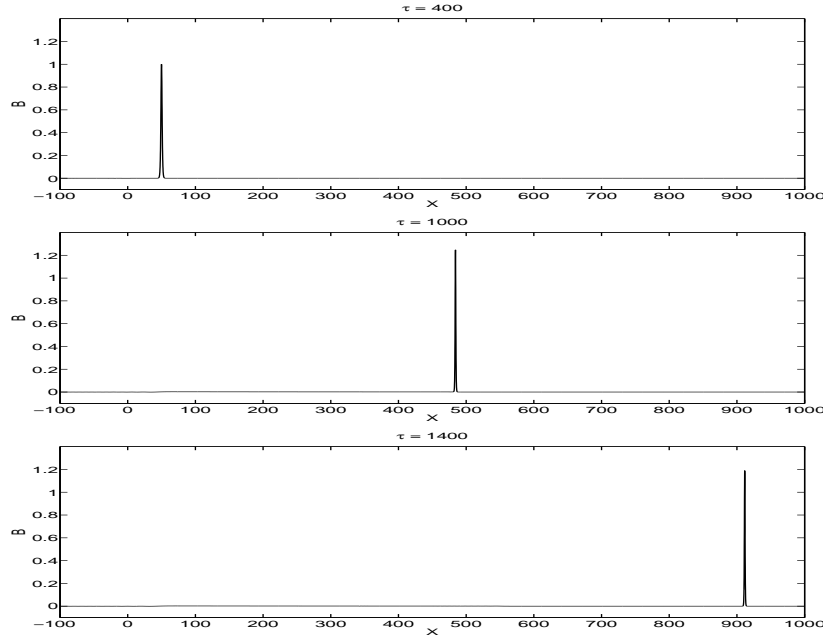
5.4.2 Transformation of an undular bore over variable topography with Burgers' friction
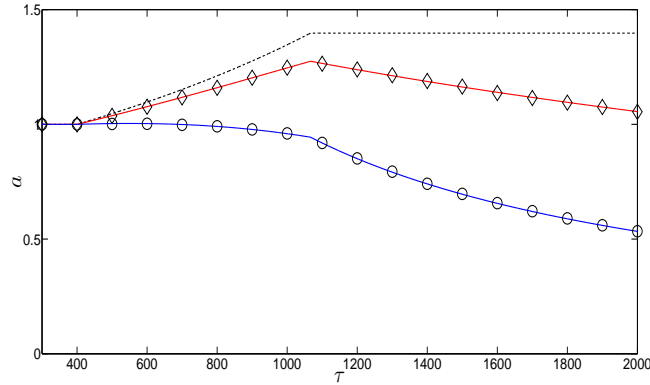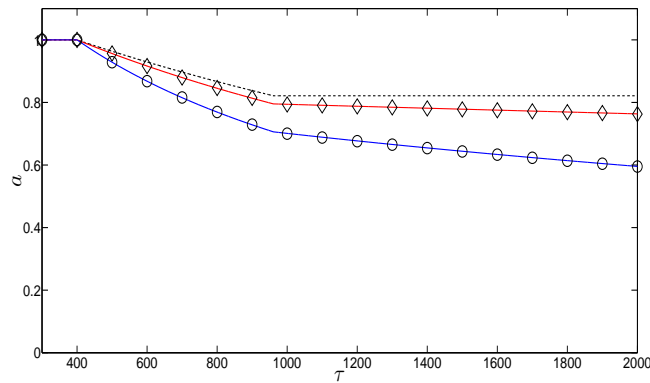

Figure 5.45: Comparison for the amplitudes for the solitary wave propagating over a slowly increasing depth region with Burgers' friction: formula (5.51) with $h_0 = 1, a_0 = 1, C_D = 0.0001$ – red line; formula (5.51) with $h_0 = 1, a_0 = 1, C_D = 0.0005$ – blue line; numerical data with $C_D = 0.0001$ – diamonds; numerical data with $C_D = 0.0005$ – circles; numerical data with $C_D = 0$ – dashed line.

5.4.2 Transformation of an undular bore over variable topography with Burgers' friction

So far, we have seen that the presence of Chezy friction and linear friction terms affects the jump, $[U]$, across the bore. Now, we would like to see whether Burgers' friction term has a similar effect on $[U]$. By following similar steps to those described in Sections 4.2.2, 5.2.2 and 5.3.2, we obtain

$$[U]_T = \frac{\partial}{\partial T} \int_{X_a(T)}^{X_b(T)} U_X(X, T)\, dX = 0, \tag{5.52}$$

provided $U_X = U_{XX} = U_{XXX} = 0$ at $X = X_{a,b}(T)$. Therefore, we have

$$[U] = -U_0 \qquad \text{for all} \qquad T > 0, \tag{5.53}$$

since the undular bore is propagating into undisturbed depth. Thus, we have shown that from the vKdVB equation (5.47), Burgers' friction has no influence on the jump, $[U]$, of the mean level across the bore. Again, this will be confirmed later by direct numerical simulations.

One should bear in mind that the friction term only comes into effect on the slope. So, the entire evolution of undular bore can be divided into two parts: (a) the undular bore is described by the solution of the unperturbed constant-coefficient KdV equation before the slope, and (b) after the slope, the transformed bore will asymptotically become the well-known steady undular bore solution of the constant-coefficient KdVB equation with the leading solitary wave having an amplitude of $1.5U_0$ (see Section 2.6.1).

144

5.4.2 Transformation of an undular bore over variable topography with Burgers' friction

5.4.2.1 Slowly decreasing depth

When the depth is slowly decreasing, the interaction of the bore with the slope is bound to produce a solitary wavetrain, provided the effects of friction are small enough. All solitons in the solitary wavetrain will deform adiabatically according to the formula (5.51). In a similar manner to those described in Sections 5.2.2.1 and 5.3.2.1, after the slope the effect of friction leads to the nonlocal interaction scenario at the leading edge of the undular bore and consequently the lead wave grows. However, unlike previous cases where the leading wave will decay after some growth, in this case, the leading wave amplitude will reach the value of $1.5U_0$ and remain constant after that. Since it is propagating over a flat bottom after the slope, it is expected that the solution will asymptotically become the steady undular bore solution of the KdVB equation (Gurevich & Pitaevskii, 1987; Avilov *et al.*, 1987).
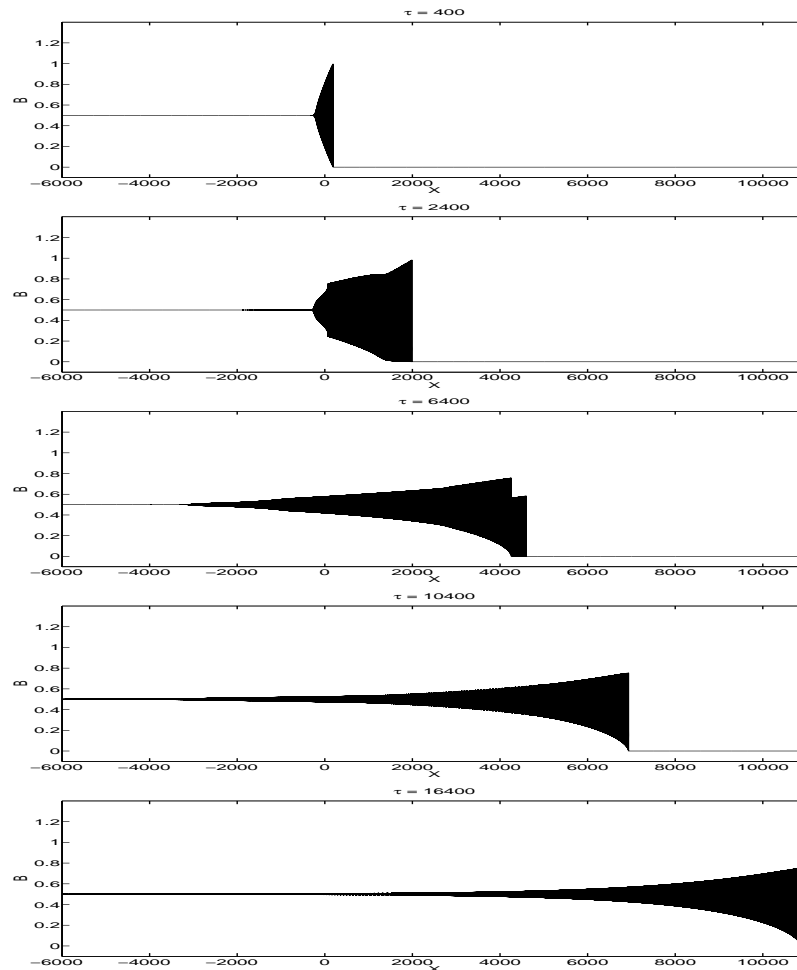
Figure 5.46: Propagation of an undular bore over a slowly decreasing depth topography with Burgers' friction where the profile $h(\tau)$ is given by (5.20)

145

5.4.2 Transformation of an undular bore over variable topography with Burgers' friction

In Figure 5.46, we present the evolution profile of an undular bore propagating over a slowly decreasing depth region with Burgers' friction. The topography is described by (5.16) and the friction drag coefficient is given by (5.18). The initial condition is taken as (4.27). In plot 2 of the Figure 5.46, one can see the formation of the solitary wavetrain ahead of the transformed bore. The leading solitary wave of the undular bore is growing, whilst the solitons in the solitary wavetrain are decaying. Thus, the bore will overtake the solitary wavetrain (see plot 3). In plot 4, it is clear that the undular bore has overtaken the solitary wavetrain.
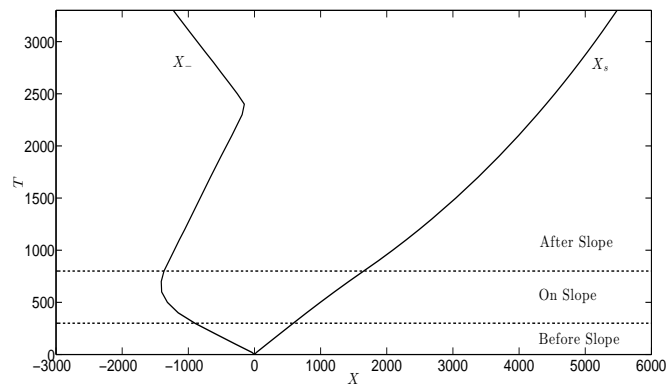
Figure 5.47: Characteristics plots for the leading soliton, X_s in the solitary wavetrain, which was part of the initial undular bore and the trailing edge, X_- of the transformed bore.

Figure 5.47 shows the characteristic plots for the leading soliton, X_s, in the solitary wavetrain, which is the leading solitary wave of the initial bore, and the trailing edge of the transformed bore for the vKdVB equation (5.47). The depth profile is given by (5.27). The initial condition and the drag-coefficient, C_D are described by (4.28) and (5.18) respectively. One can see that the key features of the interaction of the undular bore over a slowly decreasing depth are preserved. Note that the leading soliton, X_s, in the solitary wavetrain is decelerating due to the effect of the bottom friction.

5.4.2 Transformation of an undular bore over variable topography with Burgers' friction

5.4.2.1.1 Numerical results

This section is devoted to numerical simulations of the undular bore propagating over a slowly decreasing depth with Burgers' friction based on the vKdVB equation (5.44). The depth profile and drag coefficient are given by (5.16) and (5.18) respectively. The numerical results are used to confirm the following assumptions made to describe the evolution of an undular bore over a slowly decreasing depth region with Burgers' friction:

(a) the wave dynamics of the undular bore near the leading edge is governed by the weak soliton interaction scenario (El *et al.*, 2007),

(b) a sequence of solitary waves will be formed ahead of the bore after the slope,

(c) the occurrence of transient multi-phase behaviour at the rear part of the bore as the result of the undular bore propagating over slowly decreasing topography,

(d) at large time, the transformed bore after the slope will asymptotically become the steady undular bore solution of the constant-coefficient KdVB equation with the leading solitary wave amplitude $1.5U_0$. The behaviour of the corresponding Riemann invariants is similar to the description given by Avilov *et al.* (1987), and

(e) the Burgers friction has no influence on the jump, $[U]$ across the bore, i.e. $[U]$ remains the same for all time.

All results are presented in Figures 5.48 – 5.51. The plot for the initial bore before the slope, $\tau = 400$ is the same as in Figure 5.8.

5.4.2 Transformation of an undular bore over variable topography with Burgers' friction
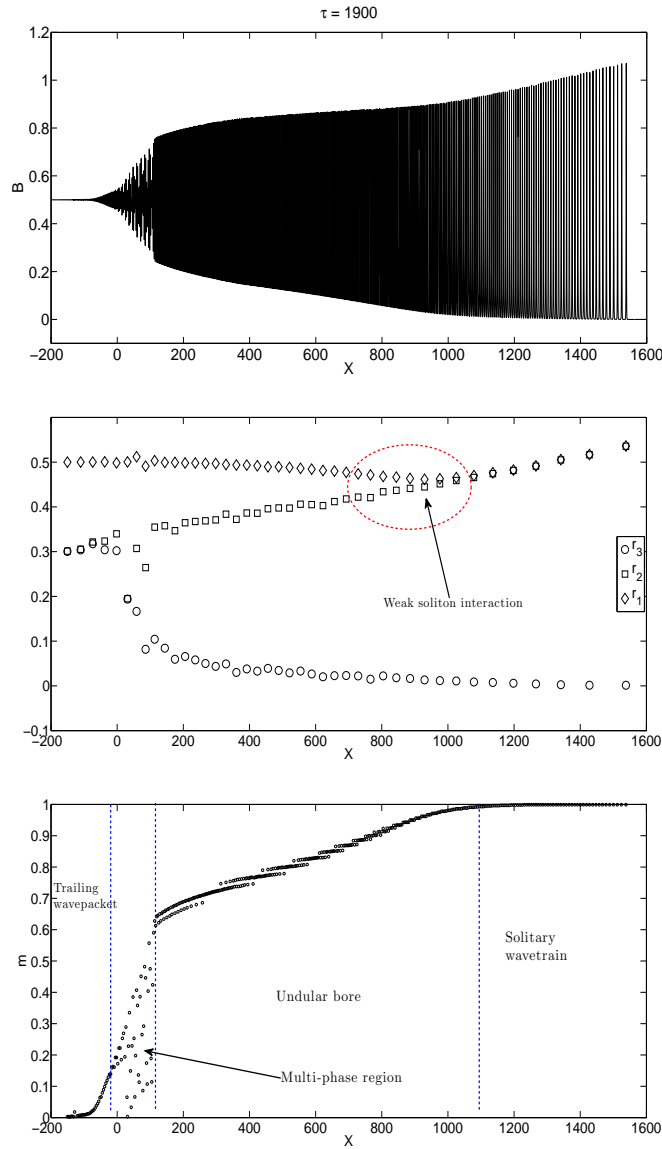
Figure 5.48: Undular bore after the slope at $\tau = 1900$. Note the generation of solitary wavetrain ($r_1 = r_2$ and $m \to 1$) ahead of the bore between $X \approx 1000$ and $X \approx 1550$. Multi-phase behaviour is observed at the rear part of the bore between $X \approx 0$ and $X \approx 100$.

In Figure 5.48, we present the plot for the undular bore after the slope, $\tau = 1900$. Clearly, there is a solitary wavetrain generated at the front of the bore, which is confirmed by the existence of the region $r_1 = r_2$ (the middle plot) and $m \to 1$ (the bottom plot) at the front of the bore. Also present is multi-phase behaviour at the rear of the bore. Note that at this moment, we have the weak soliton interaction scenario near the leading edge of the bore (see Figure 2.11a), as predicted by our discussion in Section 4.2.2.2.

5.4.2 Transformation of an undular bore over variable topography with Burgers' friction
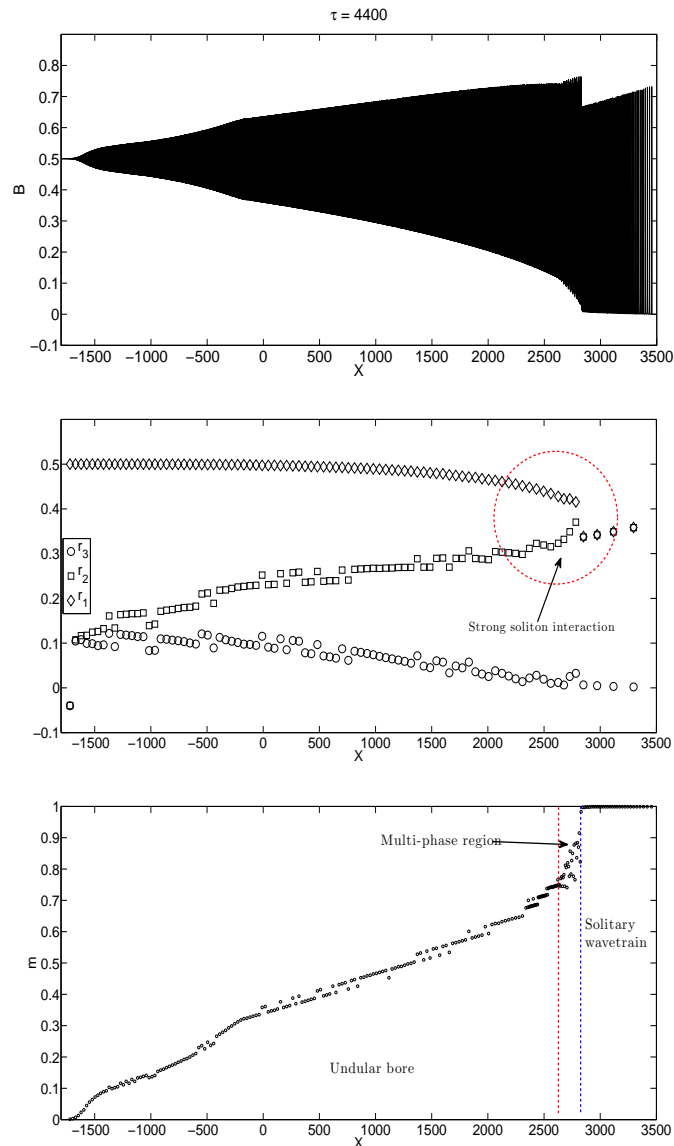
Figure 5.49: Undular bore after the slope at $\tau = 4400$. The leading wave of the transformed bore is growing and overtaking solitons in solitary wavetrain.

Figure 5.49 shows the undular bore after the slope at $\tau = 4400$. From the behaviour of the Riemann invariants, clearly, we have the strong soliton interaction scenario near the leading edge (see Figure 2.11b). Thus, the leading wave in the bore is growing again due to the nonlocal interaction near the leading edge. Also, there is multi-phase behaviour at the leading edge due to the interaction between the bore and the solitons in the solitary wavetrain when the bore is overtaking the solitary wavetrain. In this region, the modulus m is not defined. At larger time, the transformed bore is expected to overtake the entire solitary wavetrain due to velocity differences between the leading wave of the bore and solitons in the solitary wavetrain.

5.4.2 Transformation of an undular bore over variable topography with Burgers' friction
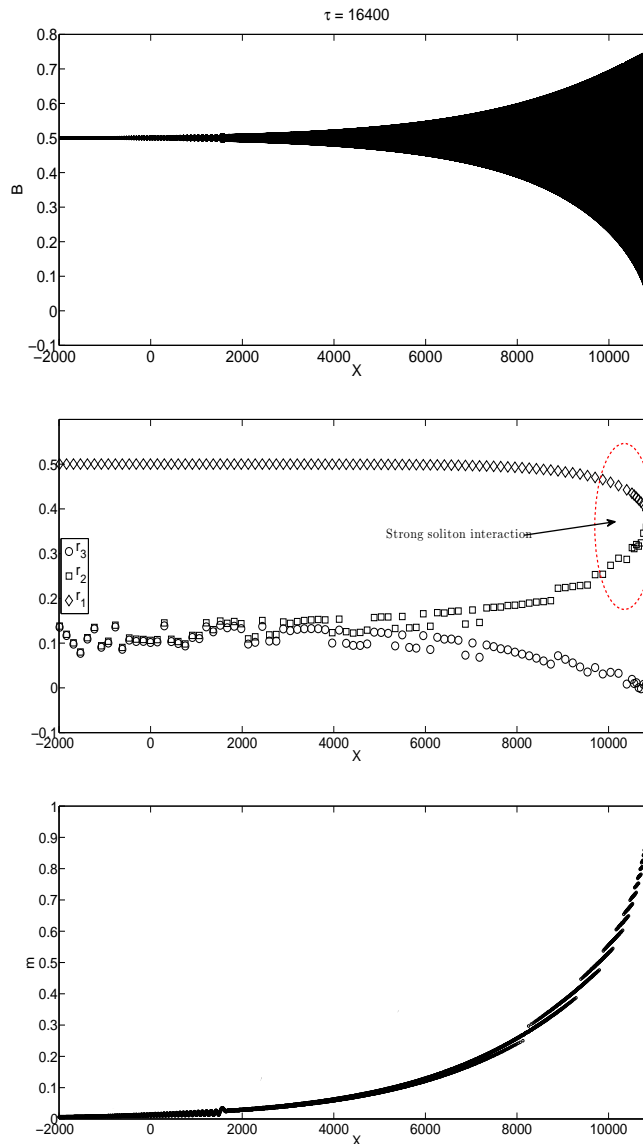
Figure 5.50: Long-time behaviour of the undular bore after the slope at $\tau = 1900$. The undular bore has transformed into the undular bore solution of the constant-coefficient KdVB equation.

Figure 5.50 presents the long-time behaviour for the undular bore after the slope, $\tau = 16400$. Here, it is clear that the undular bore has overtaken the solitary wavetrain. Since it is now propagating over a flat bottom, it is expected that the solution will asymptotically become the steady solution of the constant-coefficient KdVB equation. Indeed, one can see that the amplitude of the leading wave matches the analytical prediction, which is $1.5U_0$ (Gurevich & Pitaevskii, 1987; Avilov *et al.*, 1987). The qualitative behaviour of the Riemann invariants also agrees with the analytical results of Gurevich & Pitaevskii (1987) and Avilov *et al.* (1987) (see Figure 2.13). Similarly to the results presented in the previous sections, the multi-valued regions in the distribution of modulus in Figures 5.48 – 5.50 are

150

5.4.2 Transformation of an undular bore over variable topography with Burgers' friction

due to numerics and it is not an indication that the transformed wavetrain is a multi-phase wavetrain.

Figure 5.51 shows the comparison for the amplitude variations of the leading wave in the initial bore for different values of C_D. When the bore is on the slope, it behaves as a separate isolated solitary wave. So its amplitude varies according to the formula (5.51). Due to the friction effect, the leading wave in the transformed bore will grow or decay until it reaches the value of $1.5U_0$ and thus, it will overtake the solitary wavetrain. With stronger friction, the transformed bore only needs a shorter time span to overtake the solitary wavetrain (circles).
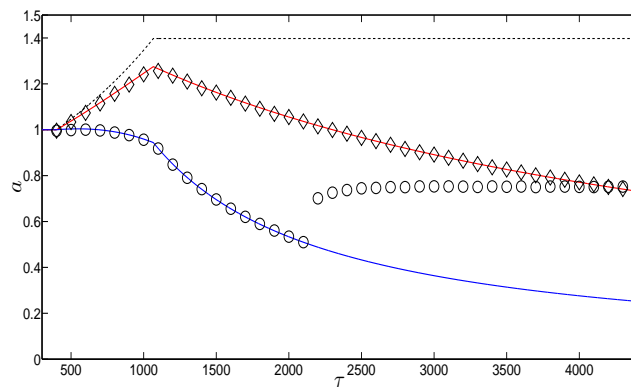
Figure 5.51: Comparison for the amplitudes for the leading solitary wave of the undular bore propagating over a slowly decreasing depth region with Burgers friction: formula (5.51) with $h_0 = 1, a_0 = 1, C_D = 0.0001$ – red line; formula (5.51) with $h_0 = 1, a_0 = 1, C_D = 0.0005$ – blue line; numerical data with $C_D = 0.0001$ – diamonds; numerical data with $C_D = 0.0005$ – circles; numerical data with $C_D = 0$ – dashed line.
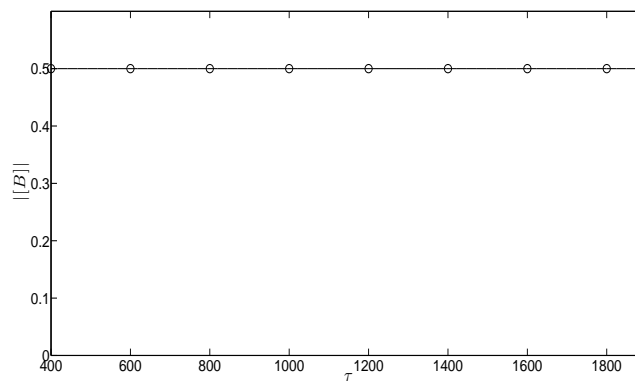
Figure 5.52: Comparison for the variations of the absolute value of jump, $\|[B]\|$ across the undular bore. Circles corresponds to the numerical data and the solid line to the analytical prediction.

5.4.2 Transformation of an undular bore over variable topography with Burgers' friction

Figure 5.52 shows comparisons for the variations of the absolute value of the jump, $|[B]|$, across the bore. One can see that there is good agreement between the numerical simulations and the analytical prediction. This confirms our assumption that the Burgers friction has no impact on the jump across the undular bore.

5.4.2.2   Slowly increasing depth

Finally, we consider the case where the depth is slowly increasing. In this case, the description of the undular bore evolution is similar to our discussion in Sections 5.2.2.2 and 5.3.2.2, i.e. a weakly nonlinear trailing wavetrain will be generated after the slope. The only difference in this case is that the leading solitary wave amplitude after the slope will reach the value of $1.5U_0$ and remain constant after that. The structure of the transformed bore will asymptotically become the steady undular bore solution of the KdVB equation.
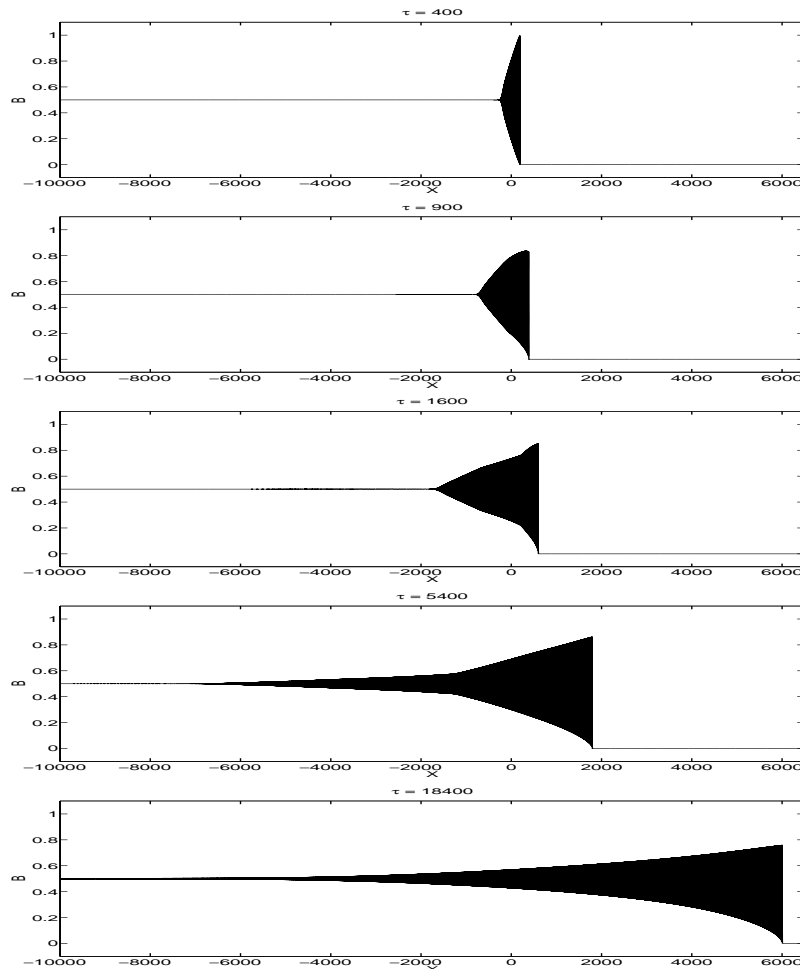
Figure 5.53: Propagation of an undular bore over a slowly increasing depth region with Burgers' friction where the profile $h(\tau)$ is given by (5.20)

5.4.2 Transformation of an undular bore over variable topography with Burgers' friction

In Figure 5.53, we present the evolution profile of an undular bore propagating over a slowly increasing depth region described by (5.20) with the initial condition (4.27). The drag coefficient, C_D is given by (5.18). In plot 4, one can see clearly the generation of a small-amplitude nonlinear wavetrain. At larger time, the undular bore is described by the solution of the KdVB equation.
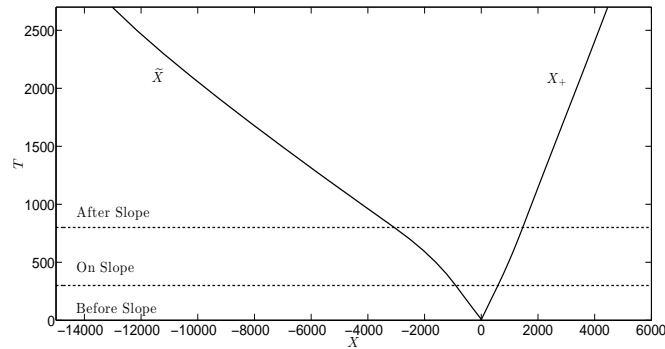
Figure 5.54: Characteristics plots for the leading edge, X_+, and the trailing edge, $\widetilde{X}$ of the undular bore.

Figure 5.54 shows the characteristic plots for the leading edge, X_+, and the trailing edge, $\widetilde{X}$ of the transformed bore. The numerical data was based on the numerical solution of the vKdVB equation (5.47) with the depth profile given by (5.29). Again, all the features of the interaction of the undular bore are preserved in this case.

5.4.2.2.1   Numerical results

Numerical results are, again, used to confirm the following assumptions made earlier to describe the evolution of an undular bore over a slowly increasing depth region with Burgers' friction:

(a) the interaction of the undular bore with the increasing depth topography leads to the strong soliton interaction scenario described by El *et al.* (2007),

(b) the mean flow across the bore remains constant for all time,

(c) a weakly trailing wavetrain is generated after the slope, and

(d) at large time, the transformed bore after the slope will asymptotically become the steady undular bore solution of the constant-coefficient KdVB equation.

5.4.2 Transformation of an undular bore over variable topography with Burgers' friction

All numerical results are based on the numerical solution of the vKdVB equation (5.44) and are presented in Figures 5.55 – 5.58. The variable topography is given by (5.20) with the same initial condition (4.27) as considered before. Again, the drag coefficient is given by (5.18). The plot for the initial bore, which matches the Gurevich-Pitaevskii solution, is again similar to Figure 5.8.
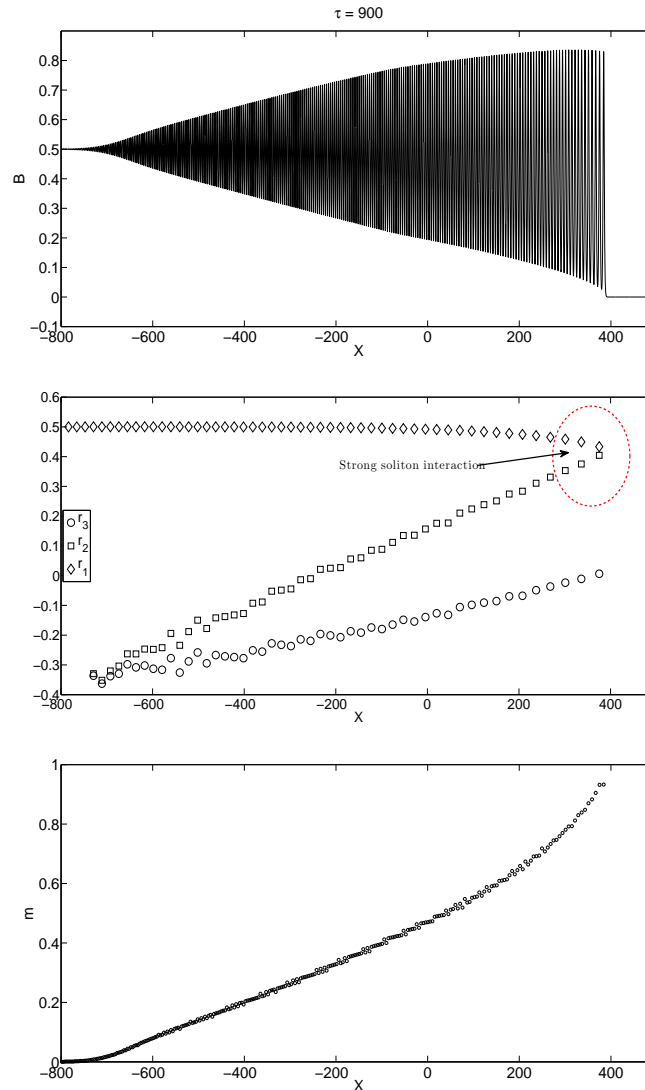
Figure 5.55: Undular bore on the slope at $\tau = 900$. One can see that the amplitude of the leading wave decreases.

Figure 5.55 shows the undular bore on the slope, $\tau = 900$. Clearly, the amplitude of the leading wave decreases, which leads to the strong soliton interaction scenario near the leading edge, as indicated by the distribution of the Riemann invariants in the middle plot (cf. Figure 2.11b).

5.4.2 Transformation of an undular bore over variable topography with Burgers' friction
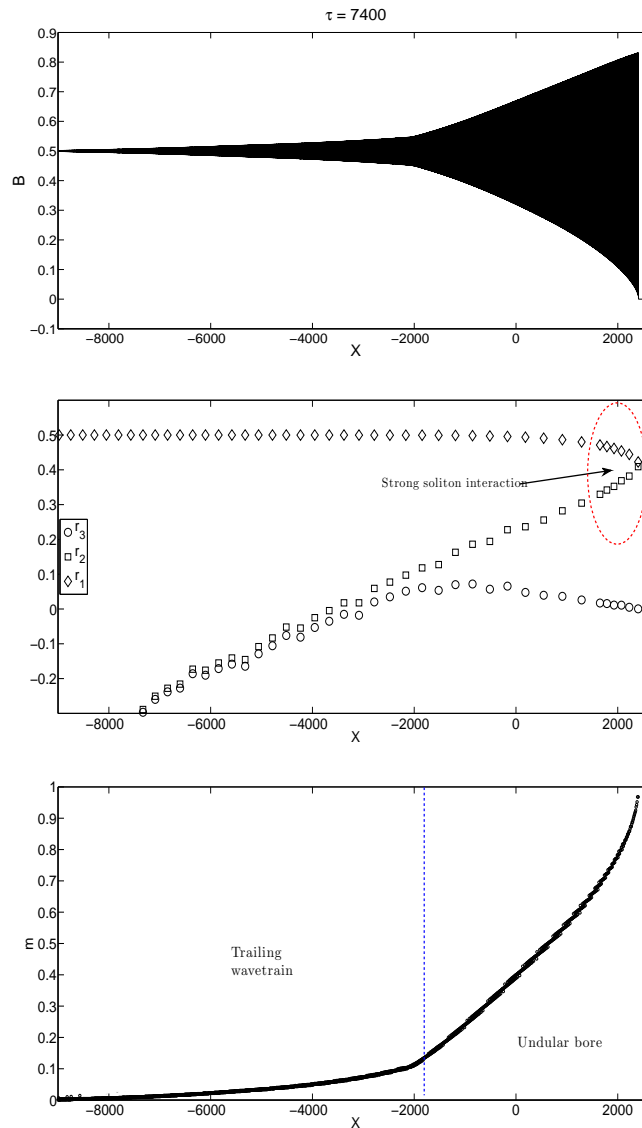
Figure 5.56: Undular bore after the slope at $\tau = 7400$. Note that there is strong interaction scenario near the leading edge (see Figure 2.11b).

In Figure 5.56, we present the transformed bore after the slope at $\tau = 7400$. The behaviour of the Riemann invariant (middle plot) near the leading edge indicates the presence of the strong soliton interaction scenario as described by El *et al.* (2007) (see Figure 2.11b). Notice that we have a small-amplitude nonlinear trailing wavetrain at the rear part of the bore.

5.4.2 Transformation of an undular bore over variable topography with Burgers' friction
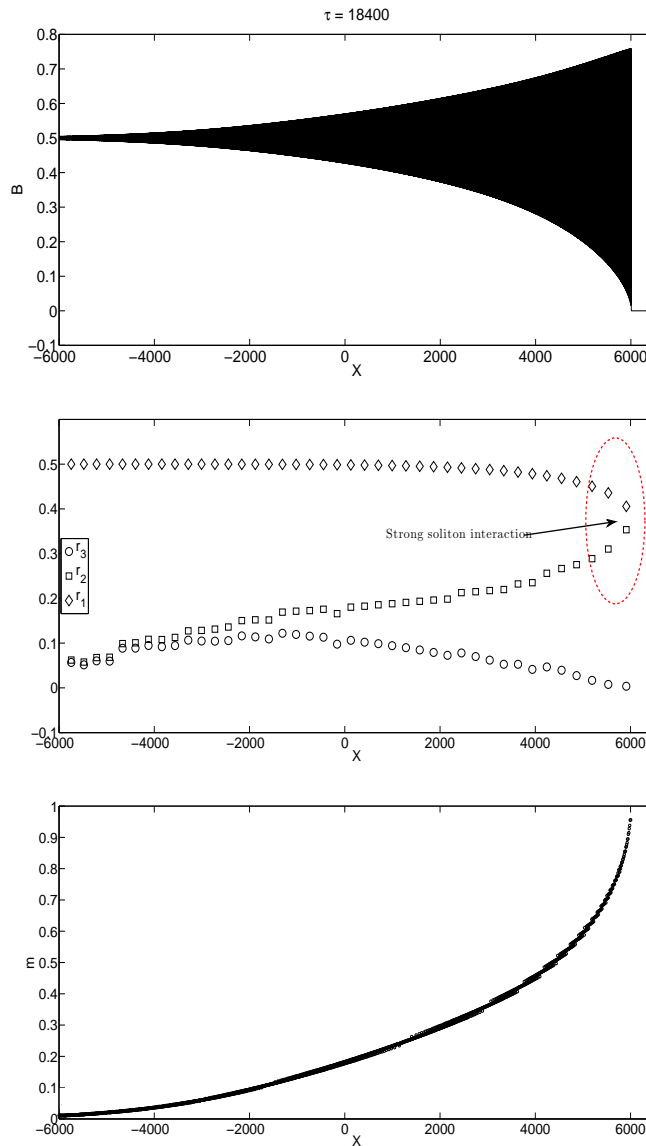
Figure 5.57: Long time behaviour of the transformed bore at $\tau = 18400$. The numerical solution, $B(X)$ represents undular bore solution for the KdVB equation. The behaviour of the Riemann invariants matches the description given by Avilov *et al.* (1987).

Figure 5.57 corresponds to the long-time behaviour of the transformed bore after the slope at $\tau = 18400$. One can see that the transformed bore is now asymptotically a steady undular bore solution of the constant-coefficient KdVB equation. Indeed, one can see that the leading solitary wave has amplitude $1.5U_0$, as predicted by the analytical solution (Gurevich & Pitaevskii, 1987; Avilov *et al.*, 1987). The qualitative behaviour of the Riemann invariants (the middle plot) also agrees with the analytical description given by Gurevich & Pitaevskii (1987) and Avilov *et al.* (1987) (see Figure 2.13).

5.4.2 Transformation of an undular bore over variable topography with Burgers' friction

Figure 5.58 shows the comparison for the amplitude variations for the leading solitary wave in the initial bore with the formula (5.51) with different values of C_D. For every value of C_D considered, one can see that the leading wave of the transformed bore after the slope continues to grow, unlike the results presented for Chezy and linear frictions. At larger time, the amplitude of the leading solitary of the transformed bore for both $C_D = 0.0001$ and $C_D = 0.0005$ will reduce to 0.75 or $1.5U_0$. This is shown in Figure 5.58 for $C_D = 0.005$ (black circles) but not for $C_D = 0.001$ (black diamonds) as it takes much longer time before the lead soliton amplitude reaches 0.75.
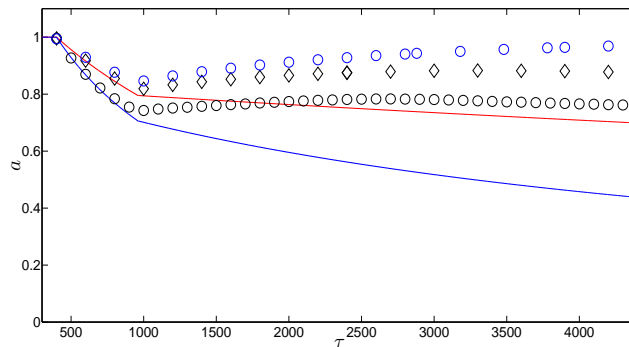
Figure 5.58: Comparison for the amplitudes for the leading solitary wave of the undular bore propagating over a slowly increasing depth region with Burgers friction: formula (5.51) with $h_0 = 1, a_0 = 1, C_D = 0.0001$ – red line; formula (5.51) with $h_0 = 1, a_0 = 1, C_D = 0.0005$ – blue line; numerical data with $C_D = 0.0001$ – diamonds; numerical data with $C_D = 0.0005$ – black circles; numerical data with $C_D = 0$ – blue circles.

Figure 5.59 shows comparisons for the variations of the absolute value of the jump, $|[B]|$, across the bore. One can see that there is good agreement between the numerical simulations and the analytical prediction. This confirms our assumption that Burgers' friction has no impact on the jump across the undular bore.
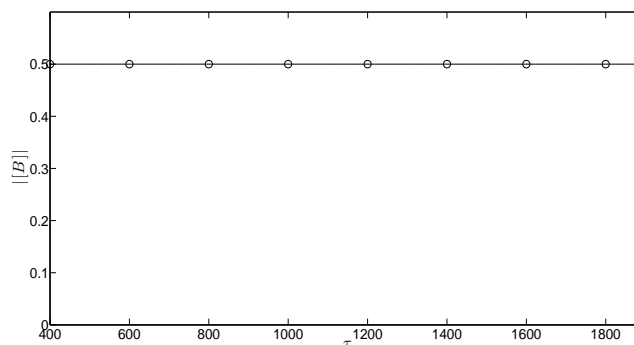
Figure 5.59: Comparison for the variations of the absolute value of jump, $|[B]|$ across the undular bore. Circles corresponds to the numerical data and the solid line to the analytical prediction.

5.5 Discussion

In this chapter, we have discussed the propagation of solitary waves and undular bores over different kinds of varying depth regions with the effects of weak dissipation induced by bottom friction or volume viscosity included. In our problem configuration, the dissipative terms only come into effect on the slope. Therefore, the evolution of solitary waves and undular bores on the slope are influenced by the effects of varying depth and dissipation simultaneously. After the slope, the evolution is affected only by dissipation.

For all the dissipative terms considered in this chapter, when a solitary wave propagates into a shoaling region, the outcome depends on the relative magnitude of the effects of the slope and dissipation. If the slope is stronger than dissipation, then the solitary wave will deform adiabatically with some growth in amplitude on the slope before it starts to decay after that. On the other hand, if the magnitude of the friction effect is greater than the slope, then the solitary wave dissipates once it encounters the sloping region despite the decreasing depth. When the solitary wave enters deeper region with friction, then the solitary wave decays almost instantaneously. The amplitude of the solitary wave decays faster than the case when friction is absent.

For undular bores, the evolution process is much more complicated than for solitary waves. When an undular bore propagates into a shallower region, the outcome also depends on the relative values of the slope and bottom friction. These two effects will compete with each other and this greatly influences the behaviour of the leading front of the bore. From our numerical results with $C_D = 0.0001$, a train of solitary waves is generated ahead of the bore when the bore interacts with the slowly decreasing depth region. However, for greater values of C_D, e.g. $C_D = 0.0005$ or 0.001, no solitary wavetrain or a fewer number of isolated solitary waves in the solitary wavetrain are generated. The increment in C_D apparently pushes the leading wave of the transformed bore to interact with the wavetrain behind it sooner and reduce the amount of time needed for the transition from the weak soliton interaction scenario to the strong soliton interaction scenario. The reduction of the transition time prevents the generation of more isolated solitary waves ahead of the bore. Moreover, with stronger effects of bottom friction, the undular bore collapses faster. However, for Burgers' friction term, the undular bore will not collapse at all and the time for the KdV undular bore to transform asymptotically into the viscous bore solution of the constant-coefficient KdVB equation is reduced greatly for greater values of C_D. On the other hand, when an undular bore propagates into a deeper region, then a weakly nonlinear trailing wavetrain is formed attached to the rear part of the transformed bore. This is

similar to our results in Chapter 4. At large time, the entire structure of the transformed bore after different types of varying topography will become a weakly nonlinear wavetrain due to the continuous effects of bottom friction after the slope, with an exception for Burgers' friction term, where a qualitatively steady undular bore solution of the constant-coefficient KdVB equation is formed.

Chapter 6

Conclusions and future work

In this thesis, we have studied the propagation of shallow-water undular bores over various types of variable topography, and also subject to different kinds of weak dissipation effects in the framework of the vKdV and vpKdV equations. The study was performed using a combination of analytical methods (multiple-scale expansions, Whitham modulation theory, method of characteristics) and detailed numerical simulations. The results obtained for undular bores have been compared with the respective results for isolated solitary waves propagating over variable topography and also subject to weak dissipation.

(a) Slowly varying depth

We have shown that the propagation of an undular bore over a slowly varying topography results in a number of new adiabatic and non-adiabatic effects depending on the geometry and magnitude of the topography variations. The classification of these effects was performed on the basis of a detailed analytical and numerical study of two general configurations: the propagation of an undular bore over (i) decreasing and (ii) increasing depth regions. In both cases, it was assumed that the bore eventually emerges onto a shelf with constant depth. One of the main objectives was a comparison of the behaviour of the leading solitary wave in the undular bore with the behaviour of an isolated solitary solitary wave of the (initially) same amplitude.

(i) *Slowly decreasing depth*

We have shown that, when the undular bore advances into a gradually decreasing depth region, its interaction with the varying topography results in the formation of a sequence of isolated solitary waves, an expanding modulated solitary wavetrain propagating ahead of the bore and having an amplitude greater than that of the leading solitary wave in the undular bore. Unlike other mechanisms for the soliton train generation for the vKdV equation, such as soliton fission (Madsen & Mei, 1969; Johnson, 1973*b*), soliton caustics (Malomed & Shrira, 1991) or the formation of secondary solitons in the trailing shelves (Kaup & Newell, 1979; Kivshar & Malomed, 1989; El & Grimshaw, 2002), the presented new mechanism is essentially related to non-adiabatic deformations of modulated cnoidal waves, rather than transformations/ decay of individual solitons.

160

Using several assumptions about the structure of the undular bore propagating over a sloping bottom, we have constructed an asymptotic modulation solution describing the generation and propagation of the solitary wavetrain ahead of the undular bore. Our analytical predictions were compared with the results of numerical simulations to validate the theoretical assumptions underlying our modulation analysis. In particular, we have shown that the leading solitary wave in the generated solitary wave train has an amplitude coinciding with that predicted by the well known adiabatic theory for isolated solitary waves. This has confirmed one of our key assumptions that decreasing depth propagation is governed by the "weak interaction scenario" (El *et al.*, 2007). Another key assumption that the undular bore itself retains its structure as a modulated periodic wavetrain while propagating over a gentle slope was investigated by a detailed study of the behaviour of certain parameters in the numerical solution, which play the role of the Riemann invariants in the corresponding modulation analysis (provided our assumptions were correct). The obtained behaviour of these parameters has fully confirmed our hypotheses. In a more general context, this can be viewed as a confirmation of the relevance of perturbed modulation theory (Forest & McLaughlin, 1984; Kamchatnov, 2004) for the description of a dispersive shock wave propagating in slowly varying media. We note that so far the perturbed modulation theory has been considered as a *formal* extension of the classical Whitham method and its applicability to problems of the type considered here was far from obvious due to the presence of several competing small parameters in the problem.

The adiabatic deformations of an undular bore propagating over variable topography are: (i) the change of the characteristic scale of the oscillations in the bore due to the change of the dispersion coefficient, β in the vKdV equation (4.4), and (ii) the occurrence of spatial shifts in the position of the trailing and leading edges of the transformed undular bore relative to the undular bore. Another non-adiabatic effect of the interaction of the undular bore with a gentle positive bottom slope observed in our numerical simulations was the occurrence of a transient multi-phase behaviour in the rear part of the bore during the evolution. We have proposed a simple theoretical explanation of this effect by studying the behaviour of the linear group velocity characteristic of the modulation system, defining the trailing edge of the undular bore.

(ii) *Slowly increasing depth*

When an undular bore propagates over a gently sloping bottom from one constant depth to another, deeper, shelf region, no advancing solitary wavetrain is formed. Instead, the main effect has been shown to be the generation of a small-amplitude weakly nonlinear wavetrain *behind* the undular bore. This wavetrain is not part of the bore and its generation

constitutes another non-adiabatic effect occurring in the propagation of undular bores over variable topography. The amplitude of the trailing wavetrain vanishes at its trailing edge and the train stretches up to the point where its amplitude will match with the amplitude of the undular bore at a certain point close to its own trailing edge determined by the Gurevich-Pitaevskii solution.

We have shown that the behaviour of the leading edge of the undular bore is now dominated by the nonlocal "strong interaction scenario" (El *et al.*, 2007) when the behaviour of the lead solitary wave is affected by its interaction with the remainder of the wavetrain in the bore. Due to the enhanced interaction of solitary waves near the leading edge, the lead solitary wave amplitude is expected to be somewhat larger than that of a "test" isolated soliton. Gradually, as time increases, modulation theory predicts that the lead solitary wave amplitude must restore its original value. Again, detailed numerical simulations have fully confirmed our theoretical description.

Using the descriptions of an undular bore propagating over decreasing and increasing depth regions as "building blocks", we were able to explain the complicated wave patterns occurring in the propagation of an undular bore over a smooth bump and a smooth hole.

(b) Rapidly varying depth

We then performed numerical simulations for undular bore propagation over rapidly changing depth regions – a counterpart of the classical "soliton fission" configuration. We have shown that, if the depth changes rapidly, all the non-adiabatic deformations mentioned above are also observed. In addition, a linear wave packet will be generated when an undular bore propagates over a rapidly decreasing depth region.

(c) Effects of weak dissipation

Then, the effect of bottom friction or dissipation was taken into account in the problem configuration. We have considered three kinds of dissipative or frictional terms, i.e. Chezy friction, linear friction and Burgers friction. In the problem setting, the bottom friction "switches on" only on the slope and the slope is assumed to be slowly varying. Generally, under the influence of weak dissipation, similar non-adiabatic effects as mentioned above were observed, provided the effect of varying depth is stronger than the bottom friction. After the slope, the undular bore is under the sole effect of the bottom friction, which then leads to the strong interaction scenario near the leading edge (El *et al.*, 2007). This contributes to some growth at the leading edge. If there is a solitary wavetrain ahead of the bore, then the bore would overtake the solitary wavetrain. The effect of the bottom

friction also caused the mean level across the bore to decrease over time. Consequently, the bore will become a nonlinear wavetrain and collapse at large time despite the nonlocal interaction at the leading edge. However, if one considers a Burgers friction term, it has no impact on the mean flow across the bore. Thus, the bore will transform into the solution of the constant-coefficient KdVB equation with the amplitude of the leading solitary wave remaining constant at $1.5U_0$, where U_0 is the size of the jump.

(d) Perspectives/ Future work

The approach described in this thesis is not confined to the dynamics of the KdV equation and it can be applied to other systems describing the propagation of undular bores (or dispersive shock waves in general) through nonuniform environments. For example, it could be used for the description of the generation of solitary wavetrains by internal undular bores in the ocean, where the waves typically are propagating on a background whose properties vary in the wave propagation direction. The relevant model here is the extended KdV (Gardner) equation, which is often used to model oceanic internal solitary waves over bottom shelves. A similar study can also be undertaken for systems where the initial evolution of the undular bore is described by a non-integrable dispersive equation, e.g. the propagation of a fully nonlinear shallow-water undular bore over a slope in the framework of the appropriate variable-coefficient Su-Gardner equation.

Appendix A

Numerical methods

A.1 The method of lines

Throughout our work, all our governing equations are solved using the method of lines (MOL). MOL is an alternative and powerful method to solve partial differential equations (PDEs). It involves making an approximation to the space derivatives and reducing the problem into a system of ordinary differential equations (ODEs). Then this system can be solved using a time integrator. In general, MOL can be divided into two steps:

- The spatial derivatives are first discretised using finite difference, finite volume, finite element or other algebraic approximations to reduce the problem to a system of ODEs.

- Next, the ODE system can be solved using a time integrator such as Runge-Kutta scheme.

The essence of MOL is to approximate PDEs by ODEs. Therefore, one of the advantages of MOL is that one can use all kinds of ODE solvers and techniques to solve the semi-discrete ODEs directly.

MOL has been used to solve many PDEs describing nonlinear wave phenomena, e.g. the KdV equation (Schiesser, 1991; Jiang, 1993; Schiesser, 1994) and the extended KdV equation (Marchant & Smyth, 1996).

A.2 Numerical scheme for the vKdV equation

All our numerical results illustrated in Chapters 3 and 4 are based on the vKdV equation

$$B_\tau + \frac{3}{2h^{5/4}}BB_X + \frac{h}{6}B_{XXX} = 0. \tag{A.1}$$

We rewrite equation (A.1) as

$$B_\tau = -\frac{3}{2h^{5/4}}BB_X - \frac{h}{6}B_{XXX}. \tag{A.2}$$

We then apply central finite difference formulae to discretise spatial derivatives

$$
\left.
\begin{aligned}
B &\approx \frac{B_{j+1} + B_j + B_{j-1}}{3}, \\
B_X &\approx \frac{B_{j+1} - B_{j-1}}{2\,\triangle X}, \\
B_{XXX} &\approx \frac{B_{j+2} - 2B_{j+1} + 2B_{j-1} - B_{j-2}}{2(\triangle X)^3},
\end{aligned}
\right\}
\tag{A.3}
$$

where j is the index denoting the position along X-axis and $\triangle X$ is the spacing along the axis. $X-$interval is divided into M points with $j = 0, 1, 2, \ldots, M-2, M-1$. Therefore, MOL approximation of (A.2) is given by

$$
\begin{aligned}
\frac{dB_j}{d\tau} = \ & -\frac{1}{4\,\triangle X h^{5/4}(\tau)} \left(B_{j+1} + B_j + B_{j-1}\right)\left(B_{j+1} - B_{j-1}\right) \\
& -\frac{h(\tau)}{12(\triangle X)^3}\left(B_{j+2} - 2B_{j+1} + 2B_{j-1} - B_{j-2}\right) \equiv f(B_j).
\end{aligned}
\tag{A.4}
$$

Notice that (A.4) is written as an ODE since there is only one independent variable, which is τ. Equation (A.4) also represents a system of M ODEs. The initial condition for (A.4) after discretisation is given by

$$
B(X_j, \tau = 0) = B_0(X_j), \qquad j = 0, 1, 2, \ldots, M-2, M-1.
\tag{A.5}
$$

For the time integration, we will use a fourth-order Runge-Kutta method. Thus, the numerical solution at time τ_{i+1} is

$$
B_{i+1,j} = B_{i,j} + \frac{1}{6}(a_{i,j} + 2b_{i,j} + 2c_{i,j} + d_{i,j}),
\tag{A.6}
$$

where

$$
\left.
\begin{aligned}
a_{i,j} &= \triangle\tau f(B_{i,j}), \\
b_{i,j} &= \triangle\tau f(B_{i,j} + \frac{1}{2}a_{i,j}), \\
c_{i,j} &= \triangle\tau f(B_{i,j} + \frac{1}{2}b_{i,j}), \\
d_{i,j} &= \triangle\tau f(B_{i,j} + c_{i,j}).
\end{aligned}
\right\}
$$

Here, $\triangle\tau$ is the stepsize of the temporal coordinate.

A.3 Testing numerical scheme

The constant-coefficient KdV equation has an infinite number of conserved quantities (Miura *et al.*, 1968). During numerical time integration, these quantities are not numerically conserved due to the unavoidable numerical errors (Grava & Klein, 2007). Thus, in

order to check the quality of our numerical results, we will examine to which extent these quantities are conserved numerically using our scheme. Here, we will only compare the conservations of mass and energy defined as (Schiesser, 1991)

$$M = \int_{-\infty}^{\infty} B \, dX \qquad \text{and} \qquad E = \int_{-\infty}^{\infty} B^2 \, dX. \qquad (A.7)$$

To test our numerical scheme, we let the depth, $h(\tau)$ in the vKdV equation (A.1) to be constant, $h = 1$. We consider three different types of initial conditions:

(a) one-soliton solution, $B(X,0) = \mathrm{sech}^2 \left(\frac{\sqrt{3}}{2} x \right)$,

(b) two-soliton interaction, $B(X,0)) = 3\mathrm{sech}^2 \left(\frac{3}{2}(x+50) \right) + \mathrm{sech}^2 \left(\frac{\sqrt{3}}{2} x \right)$, and

(c) humplike/ rectangular initial condition, $B(X,0) = \frac{1}{4}(1 - \tanh(x/10))(1 + \tanh((x + 100)/10))$.

Figure A.1 shows the propagation of one soliton described by (a). The comparison of mass and energy is shown in Table A.1 with different stepsize for spatial and temporal variables. From the table, clearly the numerical errors produced are small.
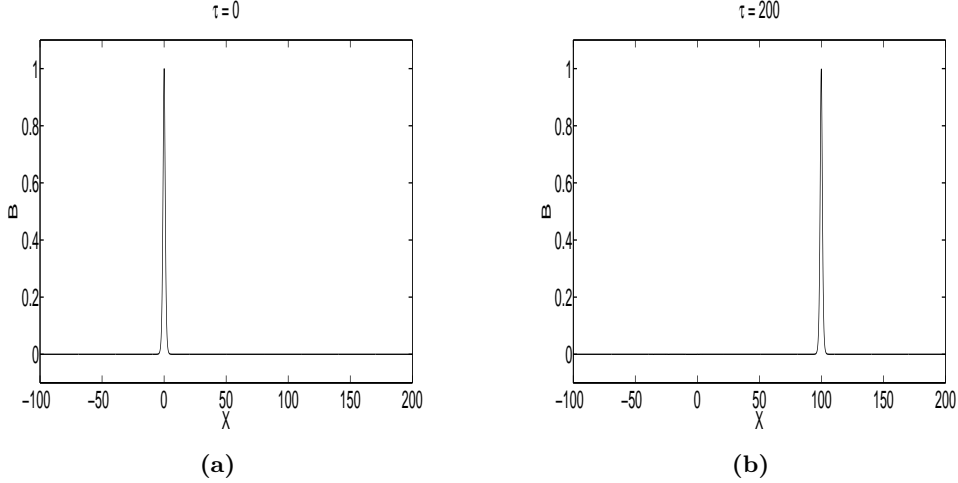
Figure A.1: Propagation of a soliton over a flat bottom. (a) $\tau = 0$, (b) $\tau = 200$.

Table A.1: Mass and energy conservation of the propagation of one-soliton

$\triangle X$	$\triangle \tau$	Before integration	After integration	Error
0.1	0.005	$M = 2.3094002$	$M = 2.3094291$	2.89×10^{-5}
		$E = 1.5396006$	$E = 1.5396008$	2.55×10^{-7}
0.2	0.005	$M = 2.3094004$	$M = 2.3095683$	1.68×10^{-4}
		$E = 1.5396008$	$E = 1.5396013$	4.53×10^{-7}
0.2	0.002	$M = 2.3094004$	$M = 2.3090927$	3.08×10^{-4}
		$E = 1.5396008$	$E = 1.5396012$	3.46×10^{-7}
0.2	0.002	$M = 2.3094002$	$M = 2.3094799$	7.96×10^{-5}
		$E = 1.5396006$	$E = 1.5396008$	2.48×10^{-7}
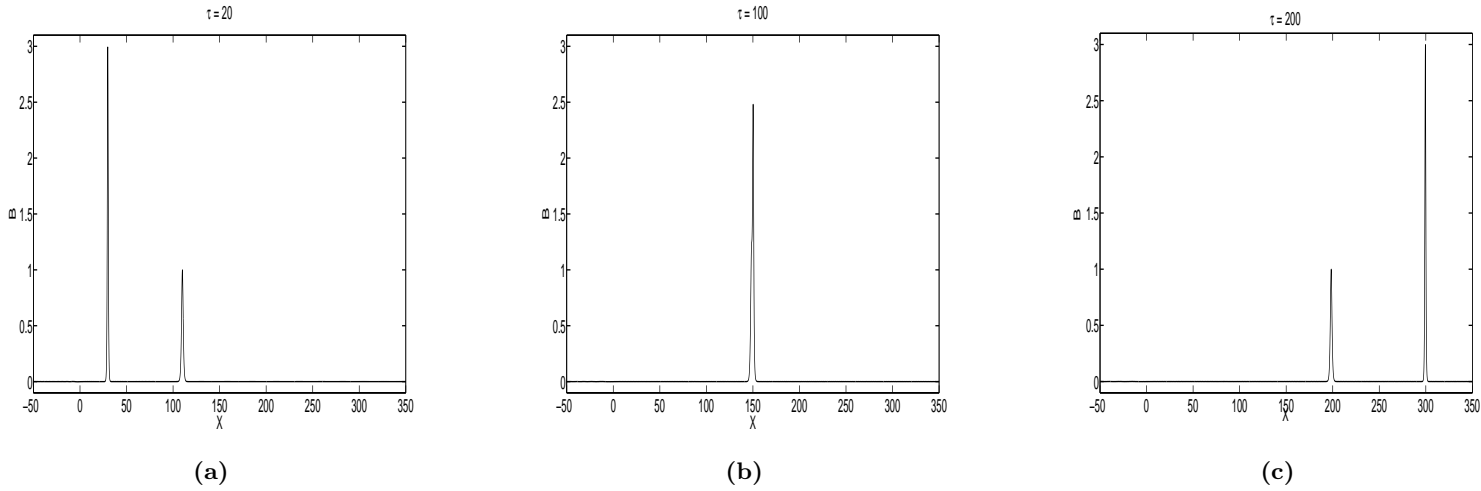
Figure A.2: Two-soliton interaction. (a) $\tau = 20$, (b) $\tau = 100$, (c) $\tau = 200$

For two-soliton interaction described by the initial condition (b), solitons will interacts with each other and regain its identity after the interaction (see Figure A.2). In this case, the total mass and energy should be conserved throughout the time integration. The comparison is shown in Table A.2. Again, the errors produced are small.

Table A.2: Mass and energy conservation of two-soliton interaction, $\triangle X = 0.1$, $\triangle\tau = 0.005$

Before integration, $\tau = 0$	After integration, $\tau = 20$	After integration, $\tau = 100$	After integration, $\tau = 200$
(Before interaction)	(Before interaction)	(During interaction)	(After interaction)
$M = 6.3093999$ $E = 9.5396007$	$M = 6.3091562$ $E = 9.5396003$	$M = 6.3093531$ $E = 9.5396013$	$M = 6.3087624$ $E = 9.5395997$
Error (After integration – Before integration)	$M = 2.44 \times 10^{-4}$ $E = 3.87 \times 10^{-7}$	$M = 4.69 \times 10^{-5}$ $E = 5.74 \times 10^{-7}$	$M = 6.38 \times 10^{-4}$ $E = 1.00 \times 10^{-6}$
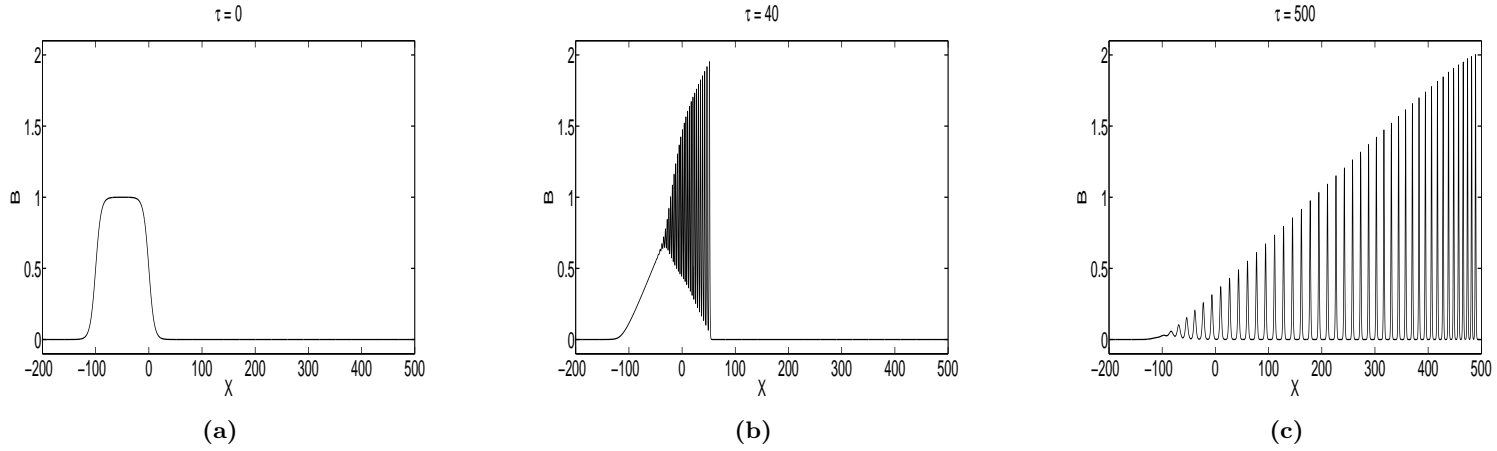
Figure A.3: Propagation of a humplike initial condition. (a) $\tau = 0$, (b) $\tau = 40$, (c) $\tau = 500$

Table A.3: Mass and energy conservation of the evolution of a humplike initial condition, $\triangle X = 0.1$, $\triangle \tau = 0.005$

Before integration, $\tau = 0$	After integration, $\tau = 40$	Error	After integration, $\tau = 500$	Error
$M = 99.9999949$	$M = 99.9999953$	4×10^{-7}	$M = 99.9999950$	1×10^{-7}
$E = 90.0000019$	$E = 89.9999974$	4.58×10^{-6}	$E = 89.9999991$	2.81×10^{-6}

Figure A.3 shows the evolution of a humplike initial data.The nonlinearity will cause the data to steepen up. Upon reaching breaking point, the dispersive effect would produce an oscillatory structure at the leading edge. As time increases, eventually we will have a train of solitons. This is shown in Figure A.3. Table A.3 shows the comparison of the mass and energy conservations. Similarly, the errors are small.

A.4 Numerical scheme for the vpKdV equation

A.4.1 Chezy friction

The governing equation is given by the vpKdV equation (5.3)

$$B_\tau + \frac{3}{2h^{5/4}}BB_X + \frac{h}{6}B_{XXX} = -\frac{C_D}{h^{7/4}}|B|B. \tag{A.8}$$

With the help of (A.3), after spatial discretisation yields

$$
\begin{aligned}
\frac{dB_j}{d\tau} &= -\frac{1}{4 \triangle X h^{5/4}(\tau)}(B_{j+1} + B_j + B_{j-1})(B_{j+1} - B_{j-1}) \\
&\quad -\frac{h(\tau)}{12(\triangle X)^3}(B_{j+2} - 2B_{j+1} + 2B_{j-1} - B_{j-2}) \\
&\quad -\frac{C_D}{9h^{7/4}(\tau)}|(B_{j+1} + B_j + B_{j-1})|(B_{j+1} + B_j + B_{j-1}) \equiv f(B_j) \quad \text{(A.9)}
\end{aligned}
$$

Thus, the numerical solution at time τ_{i+1} is given by (A.6) and (A.7).

A.4.2 Linear friction

The governing equation is given by the vpKdV equation (5.31)

$$B_\tau + \frac{3}{2h^{5/4}}BB_X + \frac{h}{6}B_{XXX} = -\frac{C_D}{h^{1/2}}B. \tag{A.10}$$

After spatial discretisation, we have

$$
\begin{aligned}
\frac{dB_j}{d\tau} &= -\frac{1}{4 \triangle X h^{5/4}(\tau)}(B_{j+1} + B_j + B_{j-1})(B_{j+1} - B_{j-1}) \\
&\quad -\frac{h(\tau)}{12(\triangle X)^3}(B_{j+2} - 2B_{j+1} + 2B_{j-1} - B_{j-2}) \\
&\quad -\frac{C_D}{3h^{7/4}(\tau)}(B_{j+1} + B_j + B_{j-1}) \equiv f(B_j) \quad \text{(A.11)}
\end{aligned}
$$

The numerical solution at time τ_{i+1} can be found from (A.6) and ((A.7)).

A.4.3 Burgers' friction

The governing equation is given by the vKdVB equation (5.44)

$$B_\tau + \frac{3}{2h^{5/4}}BB_X + \frac{h}{6}B_{XXX} = C_D h^{1/2}B_{XX}. \tag{A.12}$$

A.4.3 Burgers' friction

With the help of (A.3) and

$$B_{XX} \approx \frac{B_{j+1} - 2B_j + B_{j-1}}{(\triangle X)^2},$$ (A.13)

after spatial discretisation gives

$$
\begin{aligned}
\frac{dB_j}{d\tau} \;=\; & -\frac{1}{4 \triangle X h^{5/4}(\tau)} \left(B_{j+1} + B_j + B_{j-1}\right)\left(B_{j+1} - B_{j-1}\right) \\
& -\frac{h(\tau)}{12(\triangle X)^3} \left(B_{j+2} - 2B_{j+1} + 2B_{j-1} - B_{j-2}\right) \\
& +\frac{C_D h^{1/2}(\tau)}{(\triangle X)^2} \left(B_{j+1} - 2B_j + B_{j-1}\right) \equiv f(B_j)
\end{aligned}
$$ (A.14)

The numerical solution at time τ_{i+1} can be obtained through (A.6) and (A.7).

A.5   Numerical code

In order to compute the corresponding numerical data for equations (A.1), (A.8), (A.10) and (A.12), we use C programming. Here, we only include one example of the codes that we used throughout the entire work.

```c
/*
 *  vkdv_B.c
 *   Created by Wei King Tiong.
 *
 *       Solves the vKdV equation (A.1)
 */

#include <stdio.h>
#include <math.h>
#include <stdlib.h>

#define Xmin -9000                       // minimum value for X
#define Xmax 4000                        // maximum value for X
#define N 130000                         // number of X-subintervals
#define dx 0.1                           // stepsize in x
#define dt 0.005                         // stepsize in t
#define Tmin -400                        // minimum value for T
#define Tmax 4001                        // maximum value for T
#define M 880200                         // Tmax-Tmin/dt
#define Tm 600.00                        // end point for the slope
#define h0 1.0                           // local depth before the slope
#define h1 1.3                           // local depth after the slope
#define M1 80000                         // 0-Tmin/dt
#define M2 192140                        // Tm-Tmin/dt

double t, dummy;                         // variables declaration
double hh1;                              // variables declaration
int i,j;                                 // variables declaration

double f(double tt, double y[], int i,double h2);        //function for derivatives
double  f(double tt, double y[], int i,double h2)
{
        double b1=0.5;
        if (i==0) {return(-(((y[i+1]+y[i]+b1)*(y[i+1]-b1))/(4*dx*pow(h2,1.25)))-(h2*(y[i+2]-2*y[i+1]+2*b1-b1)/(12*pow(dx,3))));}
        if (i==1) {return(-(((y[i+1]+y[i]+y[i-1])*(y[i+1]-y[i-1]))/(4*dx*pow(h2,1.25)))-(h2*(y[i+2]-2*y[i+1]+2*y[i-1]-b1)/(12*pow(dx,3))));}
        if (i==N-2){return(-(((y[i+1]+y[i]+y[i-1])*(y[i+1]-y[i-1]))/(4*dx*pow(h2,1.25)))-(h2*(-2*y[i+1]+2*y[i-1]-y[i-2])/(12*pow(dx,3))));}
        if (i==N-1){return(-(((y[i]+y[i-1])*(-y[i-1]))/(4*dx*pow(h2,1.25)))-(h2*(2*y[i-1]-y[i-2])/(12*pow(dx,3))));}
        else {return (-(((y[i+1]+y[i]+y[i-1])*(y[i+1]-y[i-1]))/(4*dx*pow(h2,1.25)))-(h2*(y[i+2]-2*y[i+1]+2*y[i-1]-y[i-2])/(12*pow(dx,3))));}
```

```
}

double H(int j,double t);          // function for the slope
double H(int j,double t)
{
        double alpha=(h0-h1)/600;
        if (j<=M1) return(h0);
        if (j>=M1+1 && j<=M2) return(pow(sqrt(h0)-(0.5*alpha*t),2));
        if (j>=M2+1 && j<=M) return(h1);
}


int main(int argc,const char * argv[])
{
        double *x = malloc(N * sizeof (double));         // declaring pointer
        double *y = malloc(N * sizeof (double));         // declaring pointer
        double *yy = malloc(N1 * sizeof (double));       // declaring pointer
        double *xx = malloc(N1 * sizeof (double));       // declaring pointer

        FILE *output1, *output2, *fin;
        output1=fopen("vUB15May121.txt", "w");           // open file for saving numerical data
        output2=fopen("maxvUB15May121.txt","w");      // open file for saving the amplitude for the leading wave

        // Initial Condtions
        double b,w;
        b=0.5;w=10.0;
        gamma=sqrt((3*b)/(4*pow(h0,2.25)));
        for (i=0;i<N;i++)
        {
                x[i]=Xmin+i*dx;                                          // defining X-interval
                y[i]=b/pow(cosh(gamma*x[i]),2);          // initial condition for a solitary wave
                y[i]=0.5*b*(1-tanh(x[i]/w));               // initial condition for a step
        }

        for (i=0;i<N;i++)          fprintf(output1, "%f\t ",x[i]);          //saving X data
        fprintf(output1, "\n ");
        for (i=0;i<N;i++)          fprintf(output1, "%f\t ",y[i]);          // saving initial condition
        fprintf(output1, "\n ");

                t=Tmin+dt;
        j=1;
        //Runge-Kutta Integrator
        while (t<=Tmax)                              //time loop
        {

                double h=dt/2.0,m,m1;                              // the midpoint
                double *t1 = malloc(N * sizeof (double));       // temporary storage arrays for Runge-Kutta
```

```c
        double *t2 = malloc(N * sizeof (double));       // temporary storage arrays for Runge-Kutta
        double *t3 = malloc(N * sizeof (double));       // temporary storage arrays for Runge-Kutta
        double *k1 = malloc(N * sizeof (double));       // temporary storage arrays for Runge-Kutta
        double *k2 = malloc(N * sizeof (double));       // temporary storage arrays for Runge-Kutta
        double *k3 = malloc(N * sizeof (double));       // temporary storage arrays for Runge-Kutta
        double *k4 = malloc(N * sizeof (double));       // temporary storage arrays for Runge-Kutta


        //saving amplitude of the leading wave for the bore
        m=y[0];
        for (i=1;i<N-1;i++){
                if (y[i]-y[i-1]> 0.0 && y[i+1]-y[i]< 0.0 && y[i]>0.02){
                        m=y[i];
                }
        }
        fprintf(output2,"%f  %f \n",t,m);



        hh1=H(j,t);
        // Runge-Kutta integrator
        for (i=0;i<N;i++) t1[i]=y[i]+0.5*(k1[i]=dt*f(t,  y,  i,hh1));
        for (i=0;i<N;i++) t2[i]=y[i]+0.5*(k2[i]=dt*f(t+h,  t1,  i,hh1));
        for (i=0;i<N;i++) t3[i]=y[i]+    (k3[i]=dt*f(t+h,  t2,  i,hh1));
        for (i=0;i<N;i++) k4[i]=                 dt*f(t+dt,  t3,  i,hh1);
        for (i=0;i<N;i++) y[i]+=(k1[i]+2*k2[i]+2*k3[i]+k4[i])/6.0;
        //saving numerical data for every T=20
        if (j % 4000==0) {
                for (i=0;i<N;i++) fprintf(output1,"%f\t",y[i]);
                fprintf(output1,"\n");
        }


        // free pointer
        free(t1);free(t2);free(t3);free(k1);free(k2);free(k3);free(k4);
        t1=NULL;t2=NULL;t3=NULL;k1=NULL;k2=NULL;k3=NULL;k4=NULL;


        t+=dt;
        j+=1;
    }
    // free pointer
    free(x);free(y);free(xx);free(yy);
    x=NULL;y=NULL;xx=NULL;yy=NULL;


    // closing output files
    fclose(output1);
    fclose(output2);


    return(0);
}
```

References

ABLOWITZ, M. J., BALDWIN, D. E. & HOEFER, M. A. 2009 Soliton generation and multiple phases in dispersive shock and rarefaction wave interaction. *Physical Review E* **80**, 016603:1–5.

AVILOV, V. V., KRICHEVER, I. M. & NOVIKOV, S. P. 1987 Evolution of a Whitham zone in the Korteweg-de Vries theory. *Sov. Phys., Dokl.* **32** (7), 564–566.

BOUSSINESQ, J. 1872 Théorie des ondes et des remous qui se propagent le long d'un canal rectangulaire horizontal, en communiquant au liquide contenu dans ce canal des vitesses sensiblement pareilles de la surface au fond. *Journal de Mathmatique Pures et Appliques* **17**, 55–108.

BOUSSINESQ, J. 1877 Essai sur la théorie des eaux courantes. *Mémoires présentés par divers savants à l'Académie des Sciences* **23**, 1–660.

BRINK, K. H. 1988 On the effect of bottom friction on internal waves. *Continental Shelf Research* **4**, 397–403.

CLAEYS, T. & GRAVA, T. 2010 Solitonic asymptotics for the Korteweg-de Vries equation in the small dispersion limit. *SIAM Journal on Mathematical Analysis* **42**, 2132–2154.

DOBROKHOTOV, S. YU. & MASLOV, V. P. 1982 Multi-phase asymptotics of nonlinear partial differential equations with a small parameter. *Sov. Sci. Rev.: Math. Phys.* **3**, 221–280.

DRAZIN, P. G. & JOHNSON, R. S. 1989 *Solitons: An Introduction*. Cambridege University Press.

EL, G. A. & GRIMSHAW, R. H. J. 2002 Generation of undular bores in the shelves of slowly-varying solitary waves. *Chaos* **12**, 1015–1026.

EL, G. A., GRIMSHAW, R. H. J. & KAMCHATNOV, A. M. 2005 Wave breaking and the generation of undular bores in an integrable shallow-water system. *Studies in Applied Mathematics* **114**, 395–411.

EL, G. A., GRIMSHAW, R. H. J. & KAMCHATNOV, A. M. 2007 Evolution of solitary waves and undular bores in shallow-water flows over a gradual slope with bottom friction. *Journal of Fluid Mechanics* **585**, 213–244.

REFERENCES

EL, G. A., GRIMSHAW, R. H. J. & PAVLOV, M. V. 2001 Integrable shallow-water equations and undular bores. *Studies in Applied Mathematics* **106**, 157–186.

EL, G. A., GRIMSHAW, R. H. J. & SMYTH, N. F. 2006 Unsteady undular bores in fully nonlinear shallow-water theory. *Physics of Fluids* **18**, 027104:1–17.

EL, G. A., GRIMSHAW, R. H. J. & SMYTH, N. F. 2009 Transcritical shallow-water flow past topography: finite-amplitude theory. *Journal of Fluid Mechanics* **640**, 187–214.

EL, G. A., KHODOROVSKII, V. V. & LESZCZYSZYN, A. M. 2012 Refraction of dispersive shock waves. *Physica D* **241**, 1567–1587.

ESLER, J. G. & PEARCE, J. D. 2011 Dispersive dam-break and lock-exchange flows in a two-layer fluid. *Journal of Fluid Mechanics* **667**, 555–585.

FLASCHKA, H., FOREST, M. G. & MCLAUGHLIN, D. W. 1980 Multiphase averaging and the inverse spectral solution of the Korteweg-de Vries equation. *Communications on Pure and Applied Mathematics* **33**, 739–784.

FOREST, M. G. & MCLAUGHLIN, D. W. 1984 Modulations of perturbed KdV wavetrains. *SIAM Journal on Applied Mathematics* **44**, 287–300.

GARDNER, C. S., GREEN, J. M., KRUSKAL, M. D. & MIURA, R. M. 1967 Method for solving the Korteweg-de Vries equation. *Physical Review Letters* **19**, 1095–1097.

GRADSHTEYN, I. S. & RYZHIK, I. M. 2007 *Table of Integrals, Series and Products*. USA: Academic Press.

GRAVA, T. & KLEIN, C. 2007 Numerical solution of the small dispersion limit of Kortewegde Vries and Whitham equations. *Communications on Pure and Applied Mathematics* **60**, 1623–1664.

GRIMSHAW, R. 1970 The solitary wave in water of variable depth. *Journal of Fluid Mechanics* **42**, 639–656.

GRIMSHAW, R. 1971 The solitary wave in water of variable depth. Part 2. *Journal of Fluid Mechanics* **46**, 611–622.

GRIMSHAW, R. 1979 Slowly varying solitary waves. I Korteweg-de Vries equation. *Proc. Roy. Soc.* **368A**, 359–375.

GRIMSHAW, R. 2004 Korteweg-de Vries equation. In *Encyclopedia on Nonlinear Science* (ed. A.C. Scott), pp. 504–511. Taylor and Francis.

GRIMSHAW, R. 2005 Korteweg-de Vries equation. In *Nonlinear waves in fluids: Recent advances and modern applications* (ed. R. Grimshaw), pp. 1–28. SpringerWienNewYork.

GRIMSHAW, R. 2007*a* Solitary waves propagating over variable topography. In *Tsunami and Nonlinear Waves* (ed. A. Kundu), pp. 49–62. Springer.

GRIMSHAW, R., PELINOVSKY, E. & TALIPOVA, T. 2003 Damping of large-amplitude solitary waves. *Wave Motion* **37**, 351–364.

GRIMSHAW, R. H. J. 2007*b* Introduction. In *Solitary Waves in Fluids* (ed. R. H. J. Grimshaw), pp. 1–17. WIT Press.

GRIMSHAW, R. H. J. & PUDJAPRASETYA, S. R. 2004 Generation of secondary solitary waves in the variable-coefficient Kortewegcde Vries equation. *Studies in Applied Mathematics* **112**, 271–279.

GRIMSHAW, R. H. J. & SMYTH, N. 1986 Resonant flow of a stratified fluid over topography. *Journal of Fluid Mechanics* **169**, 429–464.

GRUE, J., PELINOVSKY, E. N., FRUCTUS, D., TALIPOVA, T. & KHARIF, C. 2008 Formation of undular bores and solitary waves in the Strait of Malacca caused by the 26 December 2004 Indian Ocean tsunami. *Journal of Geophysical Research C: Oceans* **113**, C05008.

GUREVICH, A. V. & PITAEVSKII, L. P. 1973 Decay of initial discontinuity in the Korteweg-de Vries equation. *JETP Letters* **17**, 193–195.

GUREVICH, A. V. & PITAEVSKII, L. P. 1974 Nonstationary structure of a collisionless shock wave. *Sov. Phys. JETP* **38**, 291–297.

GUREVICH, A. V. & PITAEVSKII, L. P. 1987 Averaged description of waves in the Korteweg-de Vries-Burgers equation. *Sov. Phys. JETP* **66**, 490–495.

HOEFER, M. A., ABLOWITZ, M. J., CODDINGTON, I., CORNELL, E. A., ENGELS, P. & SCHWEIKHARD, V. 2006 Dispersive and classical shock waves in Bose-Einstein condensates and gas dynamics. *Physical Review A* **74**, 023623.

IPPEN, A. T. & KULIN, G. 1954 The shoaling and breaking of the solitary wave. In *Proceedings of the Fifth Conference on Coastal Engineering*. Grenoble, France.

JIANG, C. J. 1993 A method for solving the KdV equation and some numerical experiments. *Tech. Rep.*. International Centre for Theoretical Physics, Trieste, Italy.

REFERENCES

JOHNSON, R. S. 1970 A nonlinear equation incorporating damping and dispersion. *Journal of Fluid Mechanics* **42**, 49–60.

JOHNSON, R. S. 1972 Shallow water waves on a viscous fluid − the undular bore. *Journal of Fluid Mechanics* **15**, 1693–1699.

JOHNSON, R. S. 1973*a* On an asymptotic solution of the Korteweg-de Vries equation with slowly varying coefficients. *Journal of Fluid Mechanics* **60**, 813–824.

JOHNSON, R. S. 1973*b* On the development of a solitary wave moving over an uneven bottom. *Mathematical Proceedings of the Cambridge Philosophical Society* **73**, 183–203.

JOHNSON, R. S. 1997 *A Modern Introduction to the Mathematical Theory of Water Waves.* Cambridge University Press.

KAKUTANI, T. 1971 Effect of an uneven bottom on gravity waves. *Journal of the Physical Society of Japan* **30**, 272–276.

KAMCHATNOV, A. M. 1997 New approach to periodic solutions of integrable equations and nonlinear theory of modulational instability. *Physics Reports* **286**, 199–270.

KAMCHATNOV, A. M. 2000 *Nonlinear periodic waves and their modulations: An introductory Course.* Singapore: World Scientific.

KAMCHATNOV, A. M. 2004 On Whitham theory for the perturbed integrable equations. *Physica D* **188**, 247–261.

KAMCHATNOV, A. M., KRAENKEL, R. A. & UMAROV, B. A. 2002 Asymptotic soliton train solutions of the defocusing nonlinear Schröedinger equation. *Physical Review E* **66**, 036609.

KAUP, D. J. & NEWELL, A. C. 1979 Solitons as particles, oscillators, and in slowly changing media : a singular perturbation theory. *Proc. Roy. Soc. London A* **361**, 413–446.

KAWAHARA, T. 1975 Derivative-expansion method for nonlinear waves on a liquid layer of slowly varying depth. *Journal of the Physical Society of Japan* **38**, 1200–1206.

KHRUSLOV, E. Y. 1976 Asymptotics of the solution of the Cauchy problem for the Korteweg-de Vries equation with initial data of step type. *Mathematics of the USSR-Sbornik* **28**, 229–248.

KIVSHAR, YU. S. & MALOMED, B. A. 1989 Dynamics of solitons in nearly integrable systems. *Rev. Mod. Phys.* **61**, 763–907.

REFERENCES

KNICKERBOCKER, C. J. & NEWELL, A. C. 1980 Shelves and the Korteweg-de Vries equation. *Journal of Fluid Mechanics* **98**, 803–818.

KNICKERBOCKER, C. J. & NEWELL, A. C. 1985 Propagation of solitary waves in channels of decreasing depth. *Journal of Statistical Physics* **39**, 653–674.

KORTEWEG, D. J. & DE VRIES, G. 1895 On the change of form of long waves advancing in a rectangular canal, and on a new type of long stationary waves. *Philosophical Magazine* **39**, 422–443.

LAX, P. D., LEVERMORE, C. D. & VENAKIDES, S. 1994 The generation and propagation of oscillations in dispersive initial value problems and their limiting behavior. In *Important Developments in Soliton Theory* (ed. A. S. Fokas & V. E. Zakharov), pp. 205–241. Springer-Verlag.

LUKE, J. C. 1966 A perturbation method for nonlinear dispersive wave problems. *Proceedings of the Royal Society A* **292**, 403–412.

MADSEN, O. S. & MEI, C. C. 1969 The transformation of a solitary wave over an uneven bottom. *Journal of Fluid Mechanics* **36**, 781–791.

MADSEN, P. A. 2010 On the evolution and run-up of tsunamis. *Journal of Hydrodynamics* **22**, 1–6.

MADSEN, P. A., FUHRMAN, D. R. & SCHÄFFER, H. A. 2008 On the solitary wave paradigm for tsunamis. *Journal of Geophysical Research* **113**, C12012:1–22.

MALOMED, B. A. & SHRIRA, V. I. 1991 Soliton caustics. *Physica D* **53**, 1–12.

MARCHANT, T. R. & SMYTH, N. F. 1996 Solitary wave interaction for the extended Korteweg-de Vries equation. *IMA Journal of Applied Mathematics* **56**, 157–176.

MILES, J. W. 1979 On the Korteweg-de Vries equation for a gradually varying channel. *Journal of Fluid Mechanics* **91**, 181–190.

MILES, J. W. 1980 Solitary waves. *Annual Review of Fluid Mechanics* **12**, 11– 43.

MILES, J. W. 1981 The Korteweg-de Vries equation: a historical essay. *Journal of Fluid Mechanics* **106**, 131–147.

MILES, J. W. 1983a Solitary wave evolution over a gradual slope with turbulent friction. *Journal of Physical Oceanography* **13**, 551–553.

REFERENCES

MILES, J. W. 1983*b* Wave evolution over a gradual slope with turbulent friction. *Journal of Fluid Mechanics* **133**, 207–216.

MIURA, R. M., GARDNER, C. S. & KRUSKAL, M. D. 1968 Korteweg-de Vries equation and generalizations II: existence of conservation laws and constants of motion. *Journal of Mathematical Physics* **9** (8), 1204–1209.

MYINT, S. & GRIMSHAW, R. 1995 The modulation of nonlinear periodic wavetrains by dissipative terms in the Korteweg-de Vries equation. *Wave Motion* **22**, 215–238.

NOVIKOV, S., MANAKOV, S. V., PITAEVSKII, L. P. & ZAKHAROV, V. E. 1984 *Theory of solitons: The inverse scattering method*. Springer.

PEREGRINE, D. H. 1967 Long waves on a beach. *Journal of Fluid Mechanics* **27**, 815–827.

PORTER, A. & SMYTH, N. F. 2002 Modelling the morning glory of the Gulf of Carpentaria. *Journal of Fluid Mechanics* **454**, 1–20.

RAYLEIGH, J. W. S. LORD 1876 On waves. *Phil. Mag.* **1**, 257–279.

REEDER, M. J., CHRISTIE, D. R., SMITH, R. K. & GRIMSHAW, R. H. J. 1995 Interacting Morning Glories over Northern Australia. *Bulletin of the American Meteorological Society* **76**, 1165–1171.

RUSSELL, J. S. 1845 Report on waves. In *Report of the 14th Meeting of the British Association for the Advancement of Science*, pp. 311–390. John Murray.

SCHIESSER, W. E. 1991 *The numerical method of lines: Integration of partial differential equations*. San Diego, California: Academic Press.

SCHIESSER, W. E. 1994 Method of lines solution of the Korteweg-de Vries equation. *Computers and Mathematics with Applications* **28**, 147–154.

SHUTO, N. 1985 Nihonkai-Chubu earthquake tsunami on the north Akita coast. *Coastal Engineering Journal* **28**, 255–264.

SMYTH, N. F. & HOLLOWAY, P. E. 1988 Hydraulic jump and undular bore formation on a shelf break. *Journal of Physical Oceanography* **18**, 947–962.

TAPPERT, F. D. & ZABUSKY, N. J. 1971 Gradient-induced fission of solitons. *Physical Review Letters* **27**, 1774 – 1776.

TAYLOR, R. J., BAKER, D. R. & IKEZI, H. 1970 Observation of collisionless electrostatic shocks. *Physical Review Letters* **24**, 206–209.

REFERENCES

Tsuji, Y., Yanuma, T., Murata, I. & Fujiwara, C. 1991 Tsunami ascending in rivers as an undular bore. *Natural Hazards* **4**, 257–266.

Wan, W., Jia, S. & Fleischer, J. W. 2007 Dispersive superfluid-like shock waves in nonlinear optics. *Nature Physics* **3**, 46–51.

Whitham, G. B. 1965 Non-linear dispersive waves. *Proceedings of the Royal Society A* **283**, 238–261.

Whitham, G. B. 1974 *Linear and Nonlinear Waves*. Wiley Interscience.

Zabusky, N. J. & Kruskal, M. D. 1965 Interactions of 'Solitons' in a collisionless plasma and the recurrence of intial states. *Physical Review Letters* **15**, 240–243.